Conseil national de recherches Canada
Institut de génie des matériaux
Boucherville (Québec)

National Research Council Canada
Industrial Materials Research Institute
Boucherville, Quebec

IGM85D-000-585-G
CNRC 27861

COMPOSITES 85

POLYMER COMPOSITES

VOLUME 7/NO. 5/OCTOBER 1986

Composites '85

National Research Council of Canada
Industrial Materials Research Institute

CONTENTS

261 L.A. UTRACKI and T. VU-KHANH/Preface

262 M. LAMBLA and V.C. VO/Optimization of Phenolic Resins for Friction Materials

274 L.A. UTRACKI/Flow and Flow Orientation of Composites Containing Anisometric Particles

283 A.T. MUTEL and M.R. KAMAL/Characterization of the Rheological Behavior of Fiber-Filled Polypropylene Melts Under Steady and Oscillatory Shear Using Cone-and-Plate and Rotational Parallel Plate Rheometry

295 M.Y. BOLUK and H.P. SCHREIBER/Interfacial Interactions and the Properties of Filled Polymers: I. Dynamic-Mechanical Responses

302 J. MARTINSSON and J.L. WHITE/Characteristics of Thermoplastics Containing Electrically Conducting Asymmetric Particles: Anisotropic Electrical Conductivity of Injection Molded Parts and Extrusion Behavior

315 T.M. MALIK, R.E. PRUD'HOMME, and B. RÊMILLARD/Determination of the Orientation of Mica in Composites

323 M.R. KAMAL, L. SONG, and P. SINGH/Measurement of Fiber and Matrix Orientations in Fiber Reinforced Composites

330 P.D. McLEAN, A. GARTON, W.T.K. STEVENSON, and K.E. MacPHEE/Improved Epoxy-Amine Matrices for Composites

337 B.V. KOKTA, C. DANEAULT, and A.D. BESHAY/Use of Grafted Aspen Fibers in Thermoplastic Composites: IV. Effect of Extreme Conditions on Mechanical Properties of Polyethylene Composites

349 Y.S. WANG, M.A. O'GURKIS, and J.T. LINDT/Electrical Properties of Exfoliated-Graphite Filled Polyethylene Composites

Continued on Back Cover

PUBLISHED BY SOCIETY OF PLASTICS ENGINEERS

POLYMER COMPOSITES

Published by the Society of Plastics Engineers

EDITOR—ROGER S. PORTER

% Polymer Science and Engineering
University of Massachusetts
Amherst, Mass 01003

ASSOCIATE EDITOR—RICHARD E. BALL

% Western New England College
Springfield, Mass 01119

GUEST EDITORS—L. A. UTRACKI and T. VU-KHANH

% Industrial Materials Research Institute
National Research Council of Canada
Boucherville, Quebec
Canada J4B 6YA

ADVISORY BOARD

LAWRENCE J. BROUTMAN
Illinois Institute of Technology

ANTHONY T. DI BENEDETTO
University of Connecticut

NIKOLAY ENIKOLOPYAN
USSR Academy of Sciences

DAVID H. KAELBLE
Arroyo Computer Center

JOHN L. KARDOS
Washington University

LON MATHIAS
University of Southern Mississipp

FREDERICK J. MCGARRY
Massachusetts Institute of Technology

L. NICOLAIS
University of Naples

R. BYRON PIPES
University of Delaware

N. S. SCHNEIDER
Army Materials and Mechanics Research Center

JAMES C. SEFERIS
University of Washington

J. G. WILLIAMS
Imperial College of Science & Technology

PUBLICATIONS COMMITTEE

E. W. ROWAN, JR., Chairman
Parkway Plastics, Inc

R. P. BRADDICKS, JR.
Plastics Consultant

LEONARD H. DREXLER
AT&T Consumer Products

R. D. FORGER
Society of Plastics Engineers

J. L. HULL
Hull Corporation

WILLIAM C. KUHLKE
DeWitt & Co., Inc

M. A. MENDELSOHN
Westinghouse Electric Corp

R. S. PORTER
University of Massachusetts

D. W. RILEY
Extrusion Engineers

A. A. SCHOENGOOD
Society of Plastics Engineers

A. E. WHITNEY, JR.
Plastics Consultant

Copyright by Society of Plastics Engineers, 1986. POSTMASTER: Send address changes to POLYMER COMPOSITES, 14 Fairfield Dr., Brookfield Center, CT 06805. Telephone (203) 775-0471, TELEX 643-712. Reproduction in whole or in part without written permission is strictly prohibited.

POLYMER COMPOSITES (ISSN 0272-8397) is published at Waverly Press, Easton, MD 21601. Address changes, undeliverable copies, and orders for subscriptions should be sent to Circulation Manager, Society of Plastics Engineers, 14 Fairfield Dr., Brookfield Center, CT 06805.

Published bimonthly (February, April, June, August, October, December). Second class postage paid at Brookfield Center, Conn., and additional entry offices. Accepted at special postal rate provided in P.M. Sec. 132.122.

Neither the Society of Plastics Engineers nor POLYMER COMPOSITES is responsible for the views expressed by individual contributors either in articles published in POLYMER COMPOSITES or in technical papers presented at meetings of the Society.

Subscription rates for 1986: SPE members, 1 year—$40. Nonmembers, 1 year—$100. Delivery outside North America, add $12 per year.

SOCIETY OF PLASTICS ENGINEERS

Business and Executive Offices, 14 Fairfield Dr., Brookfield Center, CT 06805

DANIEL J. DOMOFF
Managing Editor

MARIE J. BRUCKENTHAL
Production Manager

PAM ARSENAULT
Copy Editor

MICHAEL R. CAPPELLETTI
Circulation Manager

OFFICERS OF THE SOCIETY

GREG R. THOM
President

JOHN R. KRETZSCHMAR
President-elect

BRUCE A. PETERSEN
First Vice President

VIVIAN E. MALPASS
Second Vice President

JACQUES DE CRAENE
Vice President for International Affairs

LEONARD H. DREXLER
Secretary

KISHOR S. MEHTA
Treasurer

ROBERT D. FORGER
Executive Director and Publisher

POLYMER COMPOSITES is indexed by:—Chemical Abstracts—Engineering Index, Inc.

PREFACE

The present rate of increase in the use of reinforced plastics in America is about 20 percent/year. However, this seemingly large rate is severely depressed by reluctance & fear of the unknown on the part of designing engineers. To overcome this psychological obstacle, an effort is needed to disseminate information on the production, use, and properties of these materials.

The technology of polymer composites is continuously changing. New materials and new processing methods are being introduced. The use of thermoplastics such as nylons, polysulfones, PEEK, etc., is adding a new dimension to the current range of applicability of these materials. The solid-state formation of thermoplastics provides another vital development.

The symposium "Composites-'85" of November 19 and 20, 1985, was the fifth in a series on "Polymer Composites" and the fourteen organized and sponsored by the Industrial Materials Research Institute of the National Research Council of Canada. The remaining nine symposia are part of the two other series on "Mathematical Modeling of Plastics Processing and Properties," and on "Polymer Blends."

Proceedings of these symposia have been published in the technical journals of the Society of Plastics Engineers: "Modeling" and "Polyblends" in *Polymer Engineering and Science* (viz 22, Nos. 2 and 17 of 1982; 24, Nos. 2, 9, and 17 of 1984; 25, Nos. 11 and 17 of 1985; 26, No. 1 of 1986), "Composites" in *Polymer Composites* (viz 3, No. 4 of 1982; 5, Nos. 1 and 4 of 1984; 6, No. 4 of 1985). The proceedings of the entire symposia were recorded and the tapes are stored in the Institute library for two years, available to anyone interested in the subject.

Judging by the increasing number and the pertinence of papers as well as by the growing attendance at each symposium, they appear to be gaining an international recognition. The meetings provide a source of the most recent information, an open forum for discussion and consultation, and they facilitate contacts between the academic and commercial competence, as well as improve understanding, mutual respect, and cooperation between the participants.

As organizers of "Composites-'85," we thank all the participants for making the meeting a success.

L. A. Utracki and T. Vu-Khanh
Guest Editors

Optimization of Phenolic Resins for Friction Materials

M. LAMBLA *and* V. C. VO*

Ecole d'Application des Hauts Polymères
Institut Charles Sadron (CRM-EAHP)
F 67000 Strasbourg, France

The physicomechanical properties of phenolic composites containing a large amount of mineral fillers were enhanced through a chemical modification of the basic resin. Various phenolic compounds were first introduced in the condensation mixture leading to modified novolaks, but the final properties of the resulting composites were only slightly improved. Better results were obtained using an optimum content of epoxy-novolak or melamine in the last stage of processing as confirmed by static and dynamic mechanical analysis. The new procedure introduced recently by Halpin and Sendeckyj for fitting fatigue models was applied to our particle-filled material. The results confirm the reinforcement of the composite through the co-reactivity of phenolic resins with the introduced species in the final curing stage.

INTRODUCTION

The most widely used thermosets for friction materials are phenolic resins due to their high thermal stability and flame resistance. However, these composite materials contain a large amount of various fillers, and they may suffer from poor interfacial adhesion and related mechanical properties. The classical approach of fillers modification by chemical surface treatment (sizing) is not convenient in this case, as there are a large number of different fillers that have to be treated.

Moreover, a general survey of the literature shows that various chemical modifications of the phenolic binder have been introduced, based on esterification reactions (1) or complexing with transition metal (2). The thermal stability is increased but adhesion properties are reduced in these cases. Grafting reactions of thermoplastic copolymers (3) or blends with modified nitrile rubbers (4) are efficient to a limited extent for the improvement of the impact resistance. Thermal stability may also be increased by the introduction of caprolactam in the formulation (5), but further details of mechanical properties are not available. The main objective of the work presented here was to identify some of the chemical factors that influence the mechanical properties of the final composite materials.

In order to obtain improvement of the general mechanical properties of friction materials, the basic network was chemically modified in two different ways. First, the multiple possibilities of functional modifications were studied by introducing various amounts of substituted phenols in the condensation reaction leading to novolak oligomers. Secondly, the possibility of modification of the crosslinking system was studied by adding epoxy-novolak resins or amino reagents (e.g., melamine) in the molding mixture, thus leading to an interpenetrating network (IPN). Improvements of mechanical properties and fatigue resistance were studied on samples prepared from a model composite material containing only one type of filler: corundum or (preferably) glass beads.

MATERIALS AND METHODS

Phenolic Resins

A classical novolak resin, synthesized by condensation with formaldehyde in the presence of oxalic acid, was used for general reference. The molar ratio of phenol to formaldehyde was kept constant at 1.09. The reaction product softened at 60°C. The mean molecular weight was about 720 and the resin contained almost 3 percent free phenol by weight.

For the modified products prepared with substituted phenols by acidic condensation, the concentration of catalyst had to be adjusted according to the reactivity of the various products: cresols, resorcinol and p-hydroxy-benzoic acid. *Table 1* shows the general characteristics

* Present address: DOW Chemical, F67410 Drusenheim, France.

Table 1. General Characteristics of the Synthesis.

Sample Code	Modifier	[Mod]/[Ph]$_T$	[Oxa]/[Ph]$_T$	Time for Turbidity	Total Reaction Time (mn)	Apparent Rate Constant: K′ (mole l^{-1} s^{-1})
PF1	—	0	1.5	15	45	$8.9.10^{-2}$
PF2	—	0	0.5	35	50	
R10	Resorcinol	10	0.5	16	40	28.10^{-2}
R20		20	0.2	7	30	
Cr 10	m-cresol	10	0.5	20	45	26.10^{-2}
Cr 20		20	0.3	24	40	
PHB 10	p-hydroxy benzoic acid	10	0.5	40	50	$6.9.10^{-2}$
PHB 20		20	0.5	43	50	18.10^{-2}

[Ph]$_T$ = molar concentration of phenol and substituted products.
[Mod] = molar concentration of substituted phenol.
[Oxa] = molar concentration of oxalic acid.
K = experimental rate constant.
$K' = \frac{K}{[Oxa]^r}$.

of the synthesis. As expected, cresol and resorcinol, due to the favorable inductive effect of the substituents, seem to be more reactive than phenol. In the case of hydroxy-benzoic acid, characterized by a negative effect of the carboxylic group in the para position, first a decrease of reactivity is observed, but on further addition autocatalytic effect becomes evident.

As shown by Megson (6), the time necessary to obtain a turbid mixture is a primary approach to kinetic evaluation. These data have been confirmed here by the determination of apparent rate constant (k') assuming first order consumption of formaldehyde.

All these products were characterized by Size Exclusion Chromatography (SEC) (*Fig. 1*) and viscosity measurements in a Couette rheometer (*Fig. 2*). SEC was also used to establish the influence of acid concentration on molecular weight distribution and to confirm the specific behaviour of para-hydroxy-benzoic acid, which leads to further esterification during the last step (dehydration) of reaction. The increase in molecular weight of these oligomers appears in *Fig. 2*, describing the variation of viscosity, η, versus shear rate, $\dot{\gamma}$. It is also interesting to note the lower viscosity of the cresolic product.

Other Components

Various commercial epoxidized novolaks have been used, but finally a solid product was chosen from DOW Chemical: DEN 485, with density: 1.19 and epoxy equivalent weight: 190.

The melamine was supplied by Merck.

Hexamethylenetetramine (HMTA) supplied by Merck was used as the curing agent. Several catalysts, e.g., dimethylaniline (DMA) or N-methyl-imidazole (NMI), are suitable for pure epoxy systems; but in the mixed system used here, HMTA was generally sufficient.

Fillers

Glass microspheres, supplied by SOVITEC GLAVERBEL, Reference N°. 2530CP00, based on E glass, have density: 2.48 g/cm^3; diameter: 40 to 80 μm; Young's Modulus: 77 GPa; maximum filling is 62 percent by volume.

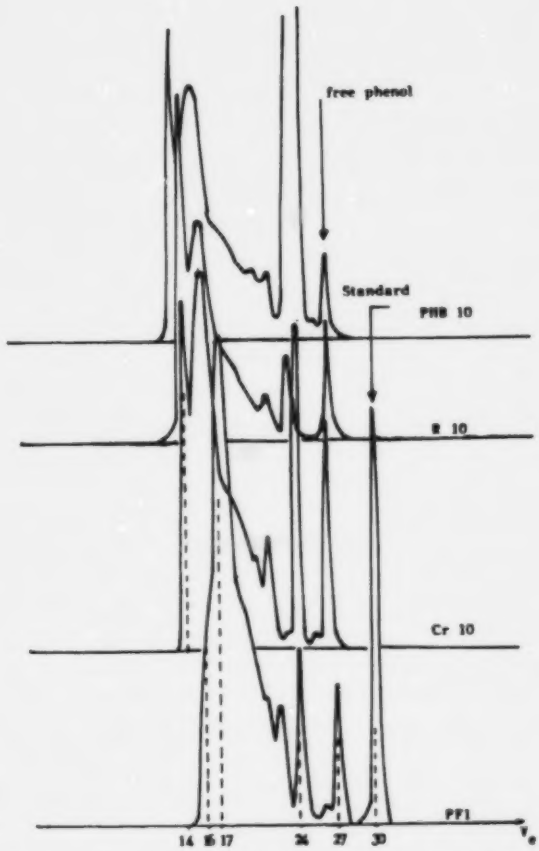

Fig. 1. SEC analysis of novolaks: PF1: standard phenolic resin; Cr 10: novolak containing 10% cresol; R 10: novolak containing 10% resorcinol; PHB10: novolak containing 10% para hydroxybenzoic acid.

Corundum mineral particles supplied by VALEO, Reference: CA 222, have density: 3.90 g/cm^3; shape: polygonal; dimension: 40 to 80 μm; Young's Modulus: 270 GPa; maximum filling is 52 percent (at 350 bars) by volume.

METHOD OF FABRICATION

The elaborated model composite material was based on phenolic binders (type PF1) generally

containing 5 percent HMTA as a curing agent. An homogeneous blend of the resin and filler with a well-defined composition, was obtained in a "turbula" mixer. The mixture was compression molded at 150°C, for the novolak systems; or 140°C for the IPN containing epoxy-novolak (DEN 485) and phenolic resin (PF1). Molding and curing conditions were defined by analysis of the crosslinking behavior in the Rheocord plastograph (*Figs. 3 a* to *c*). The molded composite plate was then heated (post-cured) for one hour at 270°C in order to complete the crosslinking reaction. Optimization of processing, especially the preheating and degassing conditions, was fundamental for the reproducibility of the samples. The specimens for mechanical testing had the following dimensions: 80 by 10 by 4.5 mm for static and 60 by 12 by 4 mm for dynamic mechanical testing.

MECHANICAL TESTING

Static Mechanical Properties

Static mechanical testing was performed on an hydraulic testing apparatus (INSTRON 8000). Sample elongation was followed under constant rate of load application (0.01 kN/s), using an extensional gauge of 25 mm.

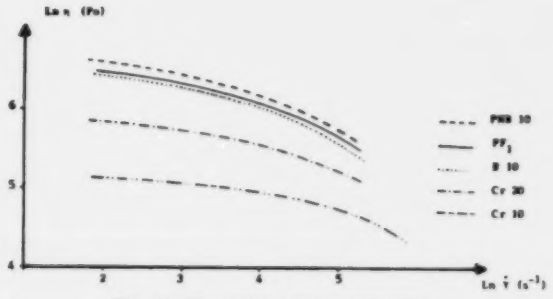

Fig. 2. Viscosity measurements.

Dynamic Mechanical Properties

Variations of G' and $\tan\delta$ with temperature were followed using a Rheometrics mechanical spectrometer, RMS 605. The rectangular sample was submitted to a sinusoidal torsional shearing with a strain of 0.6 percent at a frequency of 1 Hz. Measurements were made between 20°C and 200°C, taken in increasing steps of 5°C.

Fatigue Testing

The measurements were made on the INSTRON apparatus using a sinusoidal tension-tension procedure. The ratio R between minimal and maximal cyclic stress was fixed (R = 0.1) at the frequency of 10 Hz and temperature of 25°C.

Samples were subjected to a sinusoidal strain, with a maximal stress (σ_a) lower than static failure stress (σ_B). The value of (σ_a) was progressively reduced, and four or five samples were tested for each value. The number of cycles (N) corresponding to the rupture for a given value of (σ_a) was noted.

When the applied stress was too low to obtain rupture of the sample even if a high number of cycles were used, a classic tensile test was carried out with the same strain speed as that used to determine the static residual stress (σ_r). As it will be shown later, all the above results are necessary to analyze the fatigue behavior.

SCANNING ELECTRON MICROSCOPY

Fracture morphologies were studied in a Phillips CM 500 scanning electron microscope at

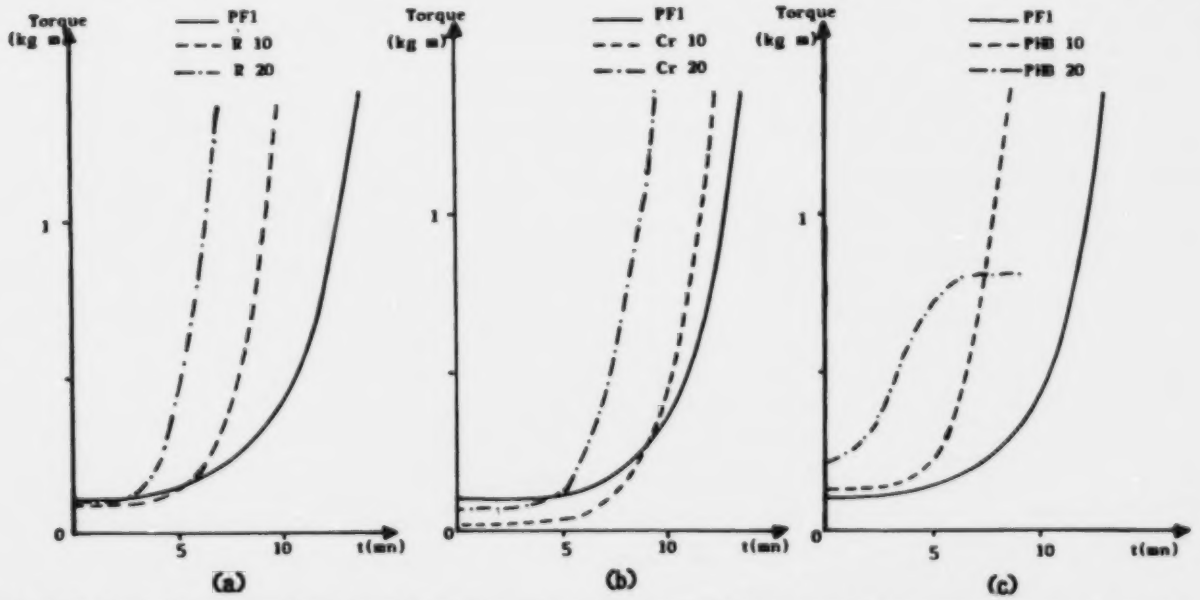

Fig. 3. Curing behavior of modified novolaks in Rheocord: (a) Resorcinol modified novolak; (b) m-cresol modified novolak; (c) para hydroxy benzoic acid modified novolak.

the VALEO Research Centre (Saint-Ouen, France).

POROSITY

These measurements were based on the following equation: $p = (1 - d_a/d_r)\ 100$, where d_r is the real density measured with a picnometer and d_a is the apparent density, defined as the ratio between sample weight in air and the weight difference between air and water.

RESULTS AND DISCUSSION

Adhesive bonding between the resin binder and filler plays the major role in a system containing such a large amount of fillers. However it is difficult to directly analyze this interfacial property. In order to correlate the chemical modifications of the crosslinked system with the final properties of the composite material, a range of static and dynamic mechanical properties were examined including the fatigue analysis. It was important to take into consideration the porosity of the material (7).

Phenolic Systems

First, the mechanical properties of pure phenolic resins (PF1) were compared using two filled materials containing 50 percent corundum by volume (CO) and 60 percent glass beads (BO) respectively. *Table 2* summarizes the main properties.

As expected, a large increase of modulus (E or G') was observed for filled materials, accompanied by a decrease of elongation at break, (ϵ_b). The composite filled with corundum (CO) seems to be slightly better than the corresponding product with glass beads. *Figure 4* shows the dynamic behavior of these three materials. Curves 2 and 3, showing variations of G' for the filled materials (CO and BO) are similar. However, the value of tanδ is altered in the case of the glass bead-filled system. Classical values of T_g are observed reaching approximately 160°C for CO.

Figures 5a and *5b* show fracture morphology of filled materials. It appears that the interfacial adhesion, poor for both fillers, is worse for corundum, even if due to irregular shape of the particles it is difficult to be certain.

Table 3 shows that the presence of resorcinol causes an increase of modulus and tensile strength of the materials filled with corundum. However, the high reactivity of the system seems to be accompanied by significant shrinkage leading to separation of matrix and filler, which is shown in *Figs. 6a* and *6b*. The para-hydroxy benzoic acid-modified product shows two drawbacks: high viscosity and premature gelling (*Fig. 3c*), thus augmenting the porosity of the material; therefore reducing the mechanical properties (*Tables 3* and *4*).

The binder modified with m-cresol shows better wetting properties related to low viscosity. Furthermore, the mechanical properties are also increased, especially with corundum-filled materials. *Figures 7a* and *7b* confirm the wetting efficiency for both kinds of fillers. Occasionally, an increase of porosity was observed (*Table 4*).

In general, it appears that glass bead-filled systems are more sensitive to chemical variations. Hence, only these geometrically well-defined particles were used in the rest of this work.

Epoxy-Novolak Modified Systems

First of all, the fact that molding composites based on pure epoxy-novolak systems cannot be used for thermally resistant friction materials was verified. However, it is easy to process a formulation containing a blend of novolak and epoxy-novolak—both solid products being prepared separately. These two resins are mixed thoroughly with glass beads and compression molded at 140°C. Curing behavior was analyzed in the mixing cell of the Rheocord plastograph, where large increase of the reactivity in comparison with pure phenolic systems was observed (*Fig. 8*). Molding conditions were adjusted in function of epoxy-novolak content. *Table 5* shows a comparison of the mechanical properties of the different formulations. An improvement of the maximum stress at break, σ_B and elongation at break (ϵ_B) was observed, while the modulus remained practically unchanged.

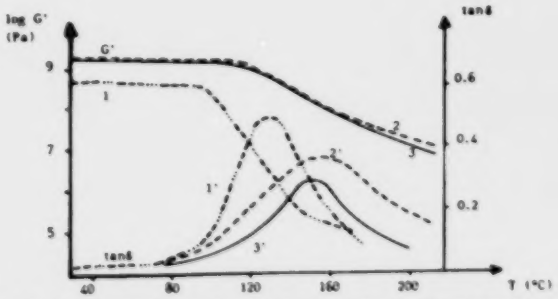

Fig. 4. Dynamic mechanical analysis: 1, 1': pure phenolic resin (PF_1); 2, 2': composite CO; 3, 3': composite BO.

Table 2. Mechanical Properties of Phenolic Materials.

Sample Code	Composition	E (GPa)	±s	σ_B (MPa)	±s	ϵ_B (%)	±s	G' (GPa)	T_g (°C)	tanδ	Porosity %
PF1	PF1 no filler	6.1	0.2	38	0.5	0.66	0.01	2.5	122	0.5	—
CO	PF1 + 50% Crd	19.8	2	36	1	0.24	0.02	6.9	157	0.37	2.6
BO	PF1 + 60% Bdv	16.2	0.5	34	1	0.21	0.01	6.6	149	0.33	2.4

The presence of holes indicated by the high level of porosity may affect these properties. It is interesting to note the higher value of T_g and the reduction of tanδ values. These observations may be connected with an increase in cohesion of this model composite. *Figure 9* demonstrates that there is an optimum in composition for the mechanical properties of this kind of IPN. Fracture morphology pictures (*Figs. 10a, b,* and *c*) show better wetting and interfacial adhesion and confirm an homogeneous distribution of particles in the matrix.

Dynamic measurements agree with previous results. This is shown in *Fig. 11*, where modulus and tanδ versus temperature dependencies of the classical phenolic reference BO (Curves 1, 1′) and the 15 percent epoxy modified product (Curves 2, 2′) are compared.

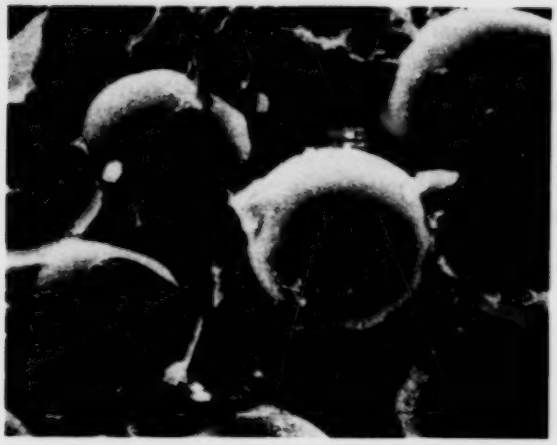

(a)

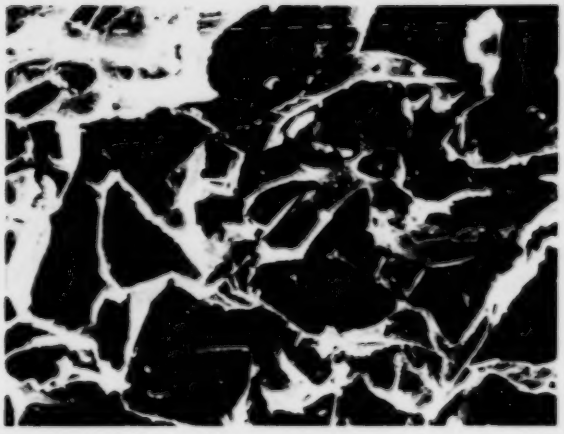

(b)

Fig. 5. Fracture morphology of composites: (a): composite BO; (b): composite CO.

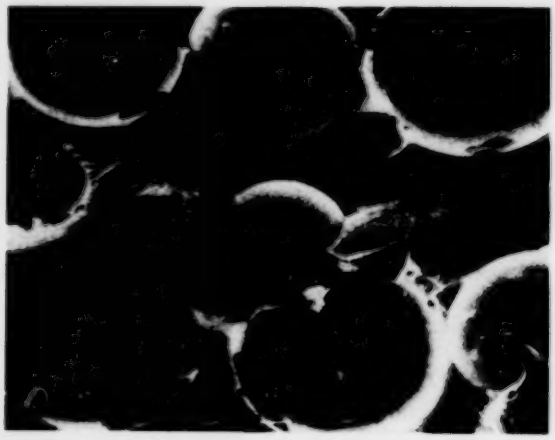

(a)

(b)

Fig. 6. Fracture morphology: (a): composite BR10; (b): composite CR20.

Table 3. Mechanical Properties of Corundum-filled Materials.

Sample Code	Composition	E (GPa)	σ_a (MPa)	ε_a (%)	G' (GPa)	Porosity (%)
O	PF1	6.1	38.0	0.66	2.5	—
CO	PF1 + 50% Corundum	19.8	35.8	0.24	6.9	2.6
CC_r 10	Cr10 + 50% Corundum	19.3	37.7	0.25	7.2	3.8
CC_r 20	Cr20 + 50% Corundum	21.3	50.3	0.27	7.9	2.1
CR 10	R10 + 50% Corundum	22.3	43.1	0.25	7.2	2.1
CR 20	R20 + 50% Corundum	23.2	41.0	0.21	7.9	1.0
$CPHB\ 10_a$	PHB10 + 50% Corundum	12.5	20.9	0.27	5.1	8.0
$CPHB\ 10_b$	PHB10 + 50% Corundum (4% HMTA)	11.6	19.3	0.21	4.8	6.0

Table 4. Mechanical Properties of Glass-bead-Filled Materials.

Sample Code	Composition	E (GPa)	σ_B (MPa)	ε_B (%)	G' (GPa)	Porosity (%)
O	PF1	6.1	38.0	0.66	2.5	—
BO	PF1 + 60% glass beads	16.2	34.0	0.21	6.6	2.4
BC_r 10	Cr10 + 60% glass beads	16.7	25.3	0.15	5.7	4.0
BR 10	R10 + 60% glass beads	14.5	26.0	0.19	5.2	1.5
BPHB 10	PHB10 + 60% glass beads	11.2	18.3	0.18	3.7	6.0

(a)

(b)

Fig. 7. Fracture morphology: (a): composite BC_r 10; (b): composite CC_r 10.

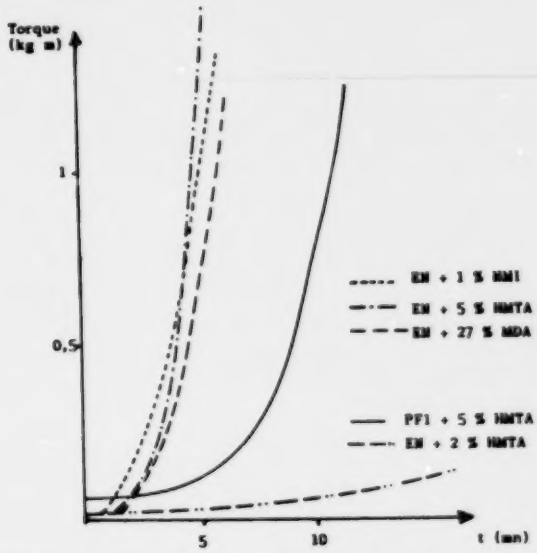

Fig. 8. Curing behavior of epoxidized novolaks (EN) with various catalysts.

Table 5. Mechanical Properties of Epoxy-Novolak Systems Molding Temperature T_m = 140°C.

Sample Code	E (GPa)	σ_B (MPa)	ε_B (%)	G' (GPa)	T_g (°C)	Tanδ	Porosity (%)
BO	16.5	34	0.21	6.9	149	0.33	1.9
BEN10	16.5	38	0.23	8.1	157	0.27	4.9
BEN15	17.0	41	0.25	8.1	160	0.24	3.5
BEN20	16.8	41	0.28	7.3	—	—	3.6

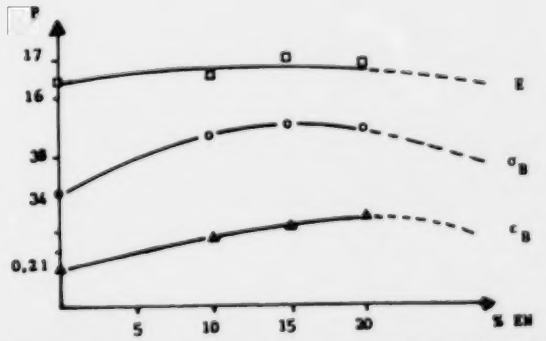

Fig. 9. Mechanical properties versus composition for epoxy-novolak systems. (Molding temperature: T_m = 140°C).

Melamine Modified Systems

Classically melamine-formaldehyde condensation products are characterized by their ability to allow coloration and by having fairly good mechanical properties. Condensation with phenolic products has been studied for laminated materials, showing good water resistance (8). In this work, various amounts of solid melamine were introduced in the molding formulation. There is no significant modification of the curing reaction, despite the general reactivity of the primary amino-groups (9). It is impossible to present in this paper the details of the chemical condensation reactions that may take place simultaneously in such a mixture. Undoubt-

(a)

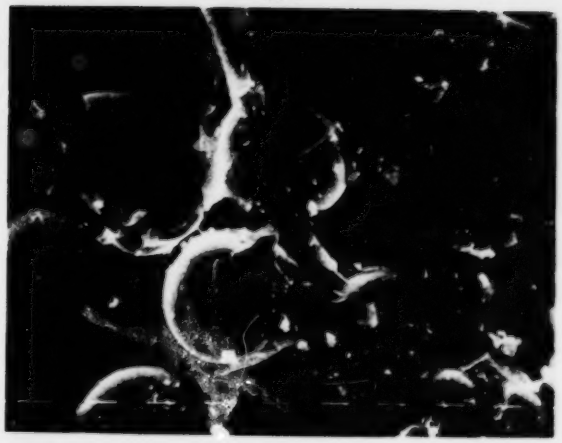

(b)

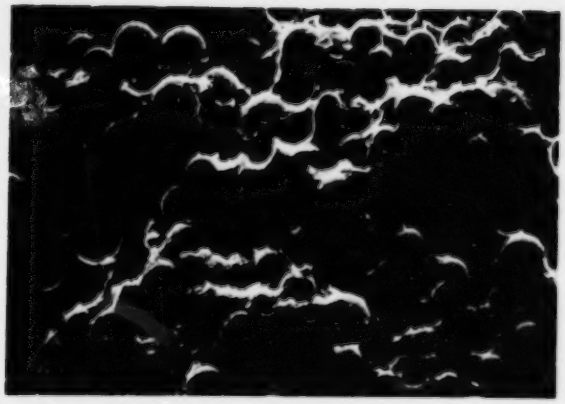

(c)

Fig. 10. Fracture morphology of epoxy-novolak systems: (a): 10% Epoxy-novolak (BEN 10); (b): 15% (BEN 15) × 640; (c): 15% (BEN 15, general view) × 160.

edly, post-curing at 270°C is of the greatest interest to enable the crosslinking reaction to be completed. *Table 6* shows the mechanical properties of three formulations containing melamine in comparison with the phenolic reference. An increase of both tensile strength and modulus is observed, whereas the elongation at break remains constant. These favorable properties were obtained despite the higher values of porosity, but they seem to be accompanied by a slight decrease of T_g. *Figure 12* shows that an optimum melamine composition is about 10 percent by weight in the blend. Results of dynamic mechanical analysis, shown in *Fig. 13*, confirm lower modulus of the modified material at temperatures above 120°C.

Fracture morphology analysis (*Figs. 14a* and *b*) shows the interfacial adhesion improve-

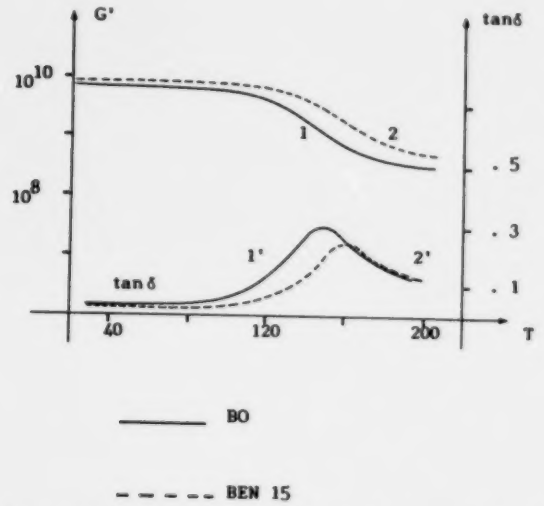

Fig. 11. Dynamic mechanical analysis: comparison between standard product (BO: curves 1 and 1') and composite modified with epoxy-novolak (BEN 15: dotted curves 2 and 2').

Table 6. Mechanical Properties of Melamine-modified Composites.

Sample Code	E (GPa)	σ_B (MPa)	ε_B (%)	G' (GPa)	T_g (°C)	Tanδ	Porosity (%)
BO	16.5	34	0.21	6.9	149	0.33	1.9
BM5	17.7	37	0.21	7.1	144	0.32	4.0
BM10	18.5	38	0.21	7.1	145	0.35	4.4
BM15	17.9	41.5	0.23	7.6	—	—	4.1

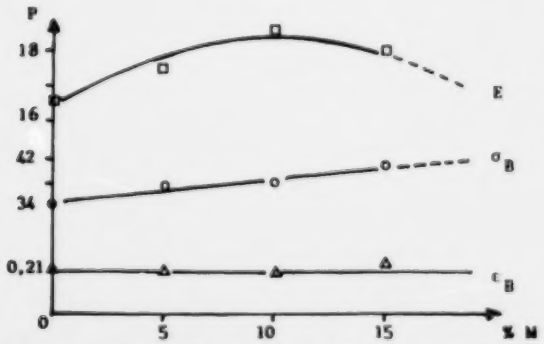

Fig. 12. Mechanical properties versus composition for melamine modified composites.

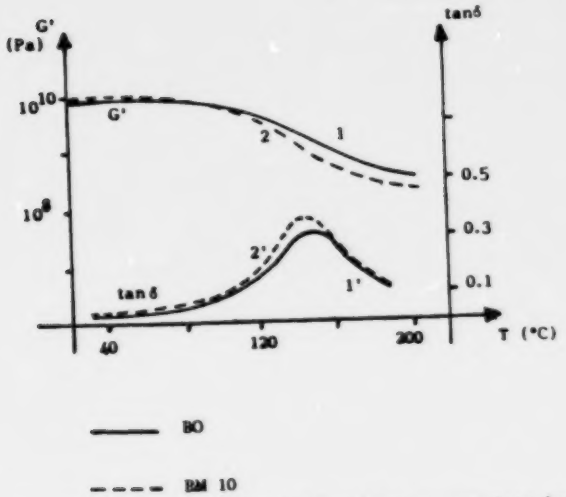

Fig. 13. Dynamic mechanical analysis: comparison between standard product (BO: curves 1 and 1') and melamine modified composite (BM: dotted curves 2 and 2').

ments obtained with melamine modified matrix, in accordance with the favorable mechanical properties observed at room temperature. However, it seems difficult to attribute the decrease observed at higher temperatures to thermal resistance of the crosslinked system or to interfacial adhesive bonding.

Preliminary Conclusions

Static and dynamic analysis of the mechanical properties and fracture morphology observations have shown that it is difficult to improve phenolic matrix properties with substituted phenols engaged in the primary condensation reaction. On the other hand, molding compositions modified with small amounts of epoxy-novolak and melamine may be optimized leading to substantial improvements of the mechanical properties. However, even though observations made by scanning electron microscopy confirm better interfacial wetting and adhesion, it is impossible to determine the influence of any specific chemical factor on binder efficiency and related mechanical properties.

FATIGUE DATA

Fatigue experiments are normally conducted in order to achieve specific objectives. The problem faced by the researcher is to prepare a large number of reproducible samples leading to efficient fatigue data analysis and interpretation procedures. This was done with four materials representative of the current research field:

- reference phenolic composite (BO);
- composite modified with 20 percent cresol (B, C_r 20);
- composite modified with 13 percent epoxy-novolak (BEN);
- composite modified with 5 percent melamine (BM).

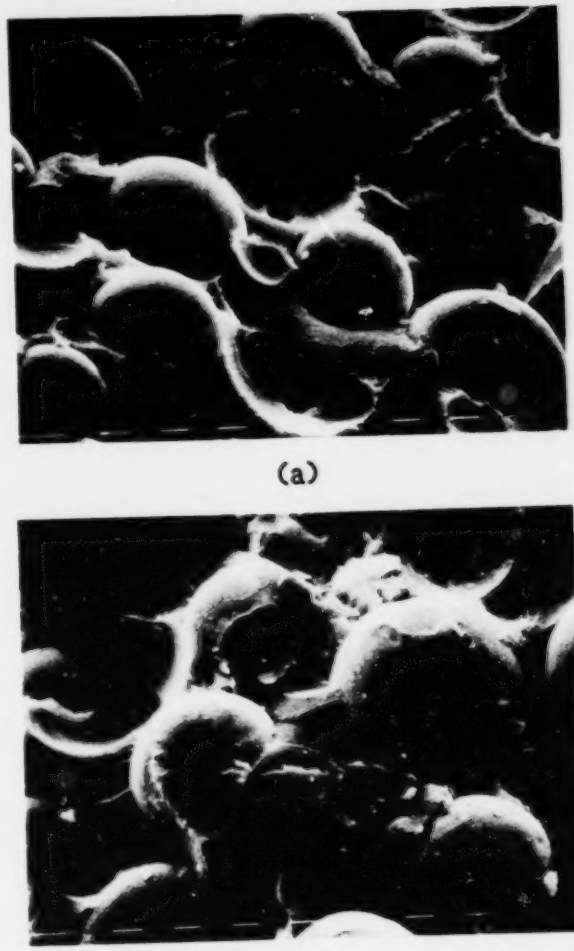

Fig. 14. Fracture morphology of melamine modified systems: (a): 5% melamine (BM 5); (b): 10% melamine (BM 10).

Figures 15a, b, c, and *d* show classical representations of S-N behavior, (applied cyclic stress, σ_a, versus fatigue life) obtained by tension-tension fatigue measurements on BO, B C_r 20, BM, and BNE composites. It is interesting to note that the epoxy-novolak modified material shows the highest value of cyclic stress, σ_a. These diagrams, characterized by large scatter of experimental values, show the limits of classical quantitative interpretation of these curves. Models proposed by Mandell and coworkers (10) based on a semi-logarithmic law may not be useful. This is also true for the power law generally introduced in mechanics (11). For this reason, the procedure for fitting fatigue models first introduced by Halpin and co-workers (12) and recently simplified by Sendeckyj (13), was used. The "wear-out" model of these workers is a direct application of metal crack growth concepts to composite materials. As cyclic loading is applied, the crack grows until the specimen can no longer support the applied cyclic load, resulting in a fatigue failure.

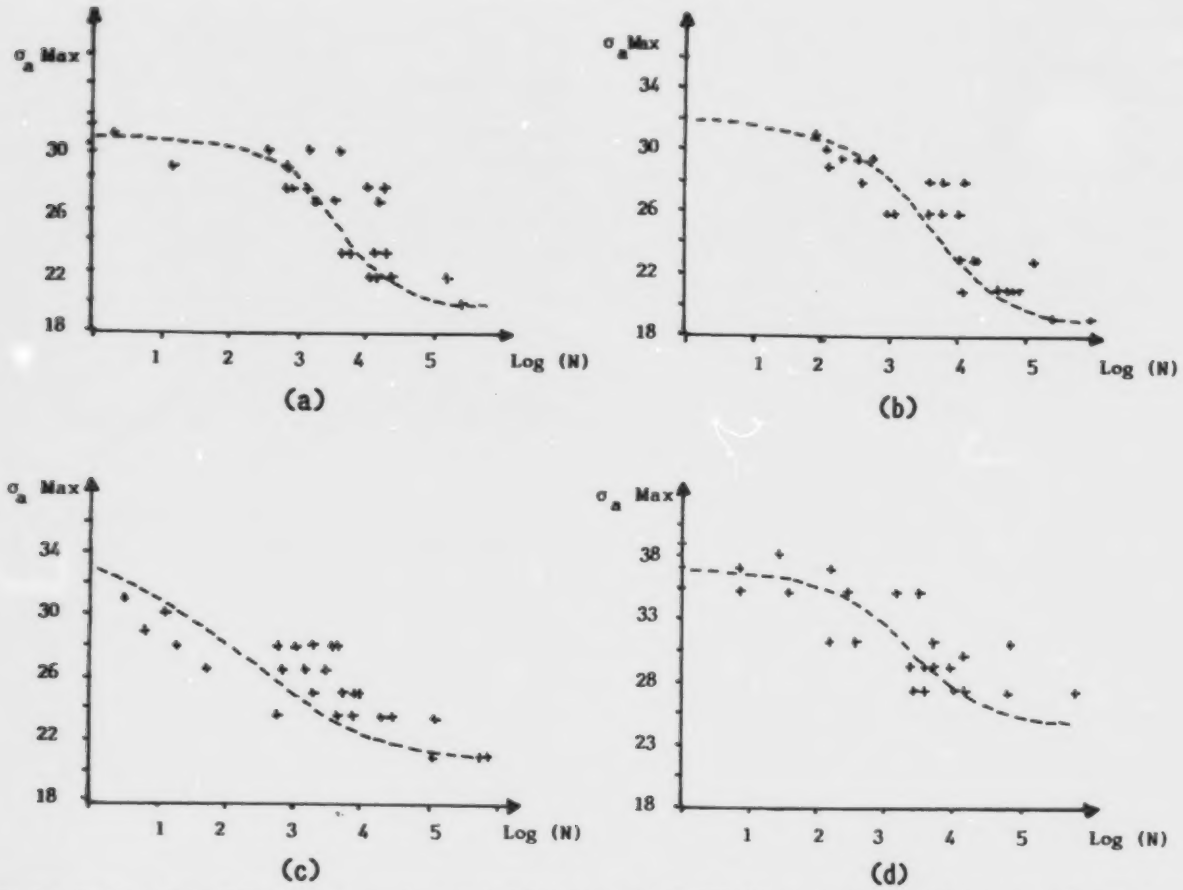

Fig. 15. Fatigue data: S-N curves for various materials: (a): composite BO; (b): composite BC, 20; (c): composite BM 5; (d): composite BEN 13.

If the cyclic stress is terminated prior to fatigue failure, the residual strength is related to the crack length through a fracture mechanics calculation.

The form of the resulting deterministic equation combining the residual strength (σ_r), applied cyclic load (σ_a), cycles (n), and equivalent static strength (σ_e) is the following:

$$\sigma_e = \sigma_a \left[\left(\frac{\sigma_r}{\sigma_a} \right)^{1/S} + (n-1)C\sigma_a^2 \right]^S \qquad (1)$$

The parameter S is the absolute value of the asymptotic slope at long life on a log-log plot of S-N curve. The parameter C is a measure of the extent of the "flat" region on the S-N curve at high applied cyclic stress levels. For fatigue failure, $\sigma_r = \sigma_a$ and $n = N$, thus *Eq 1* becomes:

$$\sigma_e = \sigma_a[1 + (N-1)C\sigma_a^2]^S \qquad (2)$$

From *Eqs 1* and *2* the Wöhler curve of the materials used here may be established. However, it is necessary to perform statistical calculations for efficient analysis. For this reason, the formulation of the wear-out model is completed by assuming that the equivalent static strength is two-parameter Weibull distributed, i.e.: the probability that the static strength is higher than σ_e is given by:

$$P_{(\sigma_e)} = \exp\left[-\left(\frac{\sigma_e}{\beta} \right)^{\alpha} \right] \qquad (3)$$

where α and β are the Weibull shape and scale parameters, respectively. The recommended procedure for determining the values of these two parameters is based on the maximum-likelihood method with progressive censoring (14).

Using the σ_e data corresponding to the best model parameters, the fatigue behavior for each material may be described by a probability of survival plot.

The survival distribution for the various composite materials was calculated using an analytical procedure (9). The results shown in *Fig. 16* represent the variations of survival probability versus equivalent static stress. These curves confirm previous results obtained by static and dynamic mechanical analysis. The composite containing epoxy-novolak (Curve 4) is superior to all other filled materials, especially in comparison with the unmodified standard product BO (Curve 1) and the cresol resin (Curve 2). The melamine co-crosslinked mate-

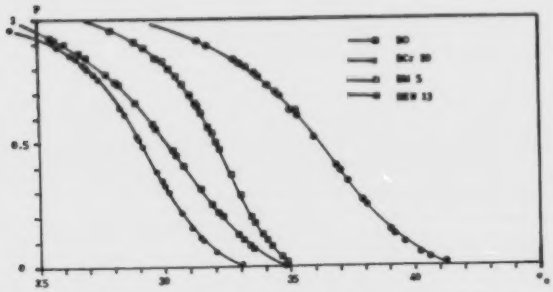

Fig. 16. Probability of survival for the equivalent static strength.

rials shows an intermediate behavior (Curve 3), providing further proof of the correct static properties.

From these observations and using the values of α, β, B, and C indicated in *Table 7*, the corresponding Wöhler curves for each material may be established, which matches the desired survival probability.

Equation 3 leads to:

$$\sigma_e = \beta(-\text{Ln } P_e)^{1/\alpha} \qquad (4)$$

and from *Eqs 4* and *2*, the following relation is obtained:

$$\beta(-\text{Ln } P_{s_e})^{1/\alpha} - \sigma_a[1 + (N - 1)C\sigma_a^2]^{1/S} = 0 \qquad (5)$$

Variations of σ_a versus log N are shown in *Fig. 17*. Each material is represented by two curves, corresponding to two survival probabilities: Po = 0.99 and Pd = 0.01. The diagram is thus divided into three zones:

zone I = rupture;
zone II = non-rupture;
zone III = intermediate, where rupture may take place.

This kind of representation may be very useful for the choice of composite materials for a well-defined application and the corresponding fatigue stress.

Fatigue behavior of cresolic and phenolic compounds are similar, whereas melamine modified composites are of some interest for applications where thermal resistance is not essential. As expected, epoxy-novolak binders lead to a high level of fatigue resistance, confirming the better cohesion of this filled model composite.

GENERAL CONCLUSIONS

Various chemical modifications of phenolic binders were studied based on model composite materials, using static and dynamic mechanical analysis and fatigue measurements.

Primary studies on co-condensates between phenol and substituted phenolic products do not lead to highly adhesive binding systems. The chemical modification performed in the last stage of processing, by co-reactivity with melamine or leading to an interpenetrated network

Table 7. "Wear-out" Model Parameters.

Sample Code	B	C	α	β
BO	$3.85\ 10^{-2}$	$1.56\ 10^{-2}$	12.80	30.9
BCr20	$7.86\ 10^{-2}$	$7.67\ 10^{-2}$	14.97	29.8
BM5	$1.80\ 10^{-2}$	$4.34\ 10^{-2}$	19.94	32.6
BEN13	$3.57\ 10^{-2}$	$2.39\ 10^{-5}$	13.83	37.1

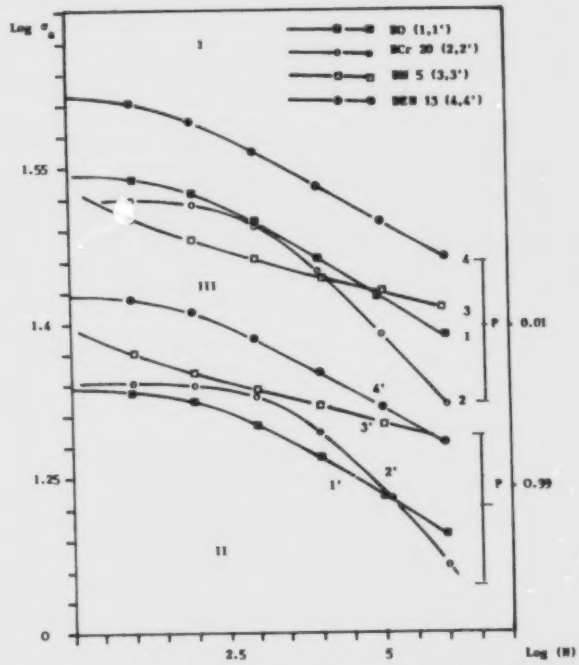

Fig. 17. S-N curves for two survival probabilities: P = 0.1 (curves 1, 2, 3, and 4); P = 0.99 (curves 1′, 2′, 3′, 4′).

with epoxy-novolak, seems to be of great interest for the enhancement of mechanical and fatigue properties. Applied to the working systems used here, which are characterized by a high level of mineral fillers, the new procedure introduced recently by Halpin (12) and Sendeckyj (13), for fitting fatigue models appears to be a useful tool for a quantitative comparison of cohesion properties in composite materials.

ACKNOWLEDGMENT

The authors wish to thank the VALEO Society for their financial support and close cooperation.

REFERENCES

1. A. Knop and W. Scheib, "Chemistry and Applications of Phenolic Resins," Ch. 8, Springer Verlag (1979).
2. A. Pizzi, *J. Appl. Polym. Sci.*, **24**, 1247 (1979).
3. T. Pith and M. Lambla, DGRST rep.n° 76.7.1566 (1978).
4. R. Kosfield and J. Borowitz, *Prepr.*, IUPAC, DUBLIN (1977).
5. H. Alaminov, R. Markova, and S. Slavova, *J. Appl. Polym. Sci.*, **20**, 1533 (1976).
6. S. Megson, *J. Soc. Chem. Ind.*, **57**, 189 (1938).
7. E. C. McLaughlin, *J. Mater. Sci.*, 15, 886 (1980).
8. H. P. Wohnsiedler, *Ind. Eng. Chem.*, 44, 2679 (1952).
9. V. C. Vo, Doctoral thesis, Univ. Strasbourg (1984).

10. J. F. Mandell, D. D. Huang, and F. J. McGarry, *Polym. Compos.*, **2**, 137 (1983).
11. J. M. Whitney, *ASTM STP 723*, 133 (1981).
12. T. C. Halpin, K. L. Jerina, and J. A. Johnson, *ASTM STP 521*, 5 (1973).
13. G. P. Sendeckyj, *ASTM STP 734*, 245 (1981).
14. R. Talreja, *ASTM STP 723*, 291 (1981).

DISCUSSION

G. Altounian: Do you think that the close packing structure of the polygonal corundum is higher or lower than that of the glass spheres? I am trying to understand why you have a better composite with glass.

M. Lambla: The structure of composites molded with polygonal particles is different than that with spheres. Glass beads are nice to mold. They pack in a regular structure without large voids. By contrast, the polygonal particles of corundum show highly mechanically entangled clusters with holes in their middle, which result in poor mechanical properties. With polygonal filler particles it is very difficult to get reproducible structure and properties.

G. Altounian: At the same volume loading is the viscosity with corundum higher or lower than that with E-glass?

M. Lambla: We do not have this information.

G. Altounian: Did you use any coupling agent?

M. Lambla: No. We pyrolized any coating the fillers may have had. We wanted to observe the effect of matrix directly on the filler without the usually irreproducible complication due to sizing.

M. R. Kamal: In the systems with epoxy and melamine, to which you referred as IPN, have you been able to look at the structure to see if you had any phase separation?

M. Lambla: Yes. On few micrographs the phase separation was clearly visible. On the glass beads we had epoxy-novolak and on the side the classical novolak resin. It was also clear that the systems co-react securing good adhesion between the domains.

M. R. Kamal: I guess that one cannot measure properties of the pure matrix materials without a filler.

M. Lambla: We looked at the properties of the classical phenolic resin without filler, but not at that of the epoxy-novolak modified one. We tried to prepare specimens of composite materials with only epoxy-novolak; in this case we observed a large decrease of thermal resistance and the mechanical properties were rather poor. This is the reason why we prefer to create the IPN.

C. Beatty: Did you do any dynamic study to look for relaxation processes? This would be particularly useful for IPN phase separated systems.

M. Lambla: No, we did not try to characterize the matrix by the dynamic mechanical means. You have to remember that we have only about 20 weight percent of the polymer. I doubt that dynamic mechanical analysis is sufficiently sensitive to provide information of phase separation in these systems. Were we able to work with oriented uniaxially glass fiber composites then, of course, the method could be used as demonstrated in our work with B. Schlund (*Polym. Compos.*, **6**, 272 (1985)). In that case we were able to characterize the special behavior of the viscoelastic material we coated the fibers with, as well as to see the behavior of the matrix. But this was a well defined geometrical system. Here, the low matrix concentration, lack of geometrical regularity, and high porosity make these methods very difficult to apply.

C. Beatty: Have you attempted to use vacuum compression molding to minimize the porosity?

M. Lambla: Yes. But the best procedure was to degas the system by opening the mold trice during the curing, after 1, 3, and 10 minutes. This gave the minimum porosity.

C. Beatty: I think that if you could pull a vacuum right during the compression molding you could reduce the porosity tremendously. In our experience, this is also an efficient way to reduce the scatter on fatigue data from about three decades to less than one.

M. Lambla: For this we would have to build a new mold, which was not possible during the period of time allowed for this PhD work.

C. Beatty: You reported that in some cases T_g went up, in some others, down. Was there any systematic correlation between the matric T_g and variation of the mechanical properties?

M. Lambla: In the case of melamine modified resin, we have a good example of simultaneous increase of mechanical properties and decrease of T_g. That was the reason why I have presented a slide with the chemical reactions. When you change the bridge between the aromatic rings you change the mobility of chain segments in the crosslinked product. This may reduce T_g. Melamine-modified systems had very good properties up to 120°C.

L. A. Utracki: I have been fascinated by the tanδ curves. This parameter being the ratio of the dissipated-to-stored energy in the system should correlate with the heating of the friction pads during the testing. One would expect the magnitude of the loss peak to correlate with amount of damage the material sustains during the abrasion test, i.e., it should be inversely proportional to the longevity. Have you observed any relation between the magnitude of tanδ and longevity?

M. Lambla: Yes, one of our products, which showed the lowest abrasion, had the highest tanδ; also in the melamine-modified material the abrasion was the worst and the loss peak

was the smallest. So, maybe there is a correlation between these two quantities.

L. A. Utracki: This is very interesting, especially since there are also numerous other influences on the longevity of the friction pads.

M. Lambla: Yes, but one has to be very careful. Both the T_g peak and abrasion change drastically during the post-curing operation. One must eliminate the methylene groups between the aromatic rings. These bridges are sensitive to oxydation which may affect the T_g value.

L. A. Utracki: Could you speculate why some of your materials have so much larger values of the loss modulus than the others?

M. Lambla: It is very difficult to do so for these very complex systems.

H. P. Schreiber: Apropos Utracki's last question, we managed to correlate the tanδ behavior with the quality of the interface between matrix and the filter. Part of this work will be presented later by Mr. Boluk. That was a thermoplastic system. I wonder if it could also be possible to relate the changes in tanδ to the quality of the interface in thermosets. Immobilization of macromolecules near the solid particles may cause a shift in tanδ.

M. Lambla: We tried to change the size of the glass beads to see the effect of the interface. However, we could not get very small beads, and the large ones gave very bad mechanical performance so I cannot be certain of the answer.

H. P. Schreiber: Could you say anything about the degree of dispersion of your particles in the matrix?

M. Lambla: I have shown several micrographs in which the dispersion of glass particles was not too bad. We think that the low molecular weight liquid generates a good wetting, which results in good dispersion even close to the maximum packing volume fraction of the filler.

C. Beatty: I noticed in the dynamic-mechanical data that you saw reduction in the magnitude of the relaxation strength as a function of filler loading. Does this scale in a linear manner with the reduction of the matrix volume in the system?

M. Lambla: No, we do not have further data on this.

Flow and Flow Orientation of Composites Containing Anisometric Particles

L. A. UTRACKI

National Research Council Canada
Industrial Materials Research Institute
Boucherville, Quebec, Canada J4B 6Y4

There is a growing commercial and academic interest in polymeric composites filled with short fibers and/or glass or mica flakes. Here, the properties depend strongly on the flow induced morphology and on the distribution of residual stresses. To optimize processing and properties, it is important to know both the melt rheology and the orientation of the dispersed phase. The industrial formulations are notoriously very complex. However, it is possible to understand, and sometimes predict, their behavior by a systematic comparison with simpler, better known systems, i.e., suspensions. This review concentrates on two main aspects of flow of polymer melts containing anisometric particles, namely yield phenomena and orientation.

INTRODUCTION

Under the term "polymer composites," only the polymeric systems containing discontinuous solid additives will be considered. However, such a definition allows discussion of carbon-black filled rubber as well as short fiber-filled poly(ether ether ketone). In this brief review of recent developments in the domain of flow of polymer composites containing anisometric particles the following aspects will be discussed: Newtonian flow, viscoelastic flow (in steady state, dynamic and elongational mode of deformation), and the orientational effects of flow.

In the plastics industry the isometric particulates are primarily used as fillers or pigments; calcium carbonate, carborundum, or rutile seldom provide reinforcing. By contrast, addition of anisometric particulates may lead to impressive enhancement of not only modulus but also of the strength and deformation at break. To achieve this, two conditions have to be met: there must be a good particle-matrix interaction, and the particles must be oriented to provide the maximum enhancement of properties in the direction critical for use of the finished product.

The use of interfacing or "sizing" agent is frequently crucial not only to achieve the desired mechanical performance, but also to prevent its rapid deterioration, e.g., due to moisture. The interfacial agent also may lead to differences in melt behavior: they may flow-segregate causing a die slip, they may change the degree of particulate aggregation resulting in a change of the viscous and elastic response, and/or they may significantly modify the apparent yielding of the composite melt. Due to inverse relation between the total interfacial area and the particulate diameter at constant loading, the effect of a sizing agent will be more important for finer particulates than the coarser ones.

For anisometric particle-filled plastics, the mechanical behavior depends on the degree of anisometry, i.e., the so called aspect ratio. Since higher aspect ratios can be achieved for rod-like particles (e.g., chopped glass, Kevlar, or steel fibers) it is natural that these materials have been primarily used. In addition, their orientation is relatively easy to understand, to control, and to use on the production line. The drawbacks of fiber reinforcement is the tendency to enhance the performance in a uniaxial direction, and to break or bend in processing, which drastically reduces the effective aspect ratio.

By contrast, the disk-like particles (e.g., mica, hammered glass, or sputtered aluminium flakes) are less prone to attrition at the same loading, show a smaller increases in melt viscosity than fibers, and provide a biaxial reinforcement. However, the rheology and processing of flake-filled composites are more complex. In particular the articulations of disk-like particles are more difficult to control. Recently, there has been significant progress in under-

standing the fiber flow and mechanism of orientation in flake-filled composites. This is why on the following pages a certain prominence will be given to these systems.

NEWTONIAN FLOWS

In the absence of interlayer slip, the addition of a second phase leads to an increase in zero-shear or Newtonian viscosity, η_o. The simplest system to consider is a hard sphere suspension. In the literature, there are many empirical or semi-empirical relations between η_o and the volume fraction of the filler, ϕ. Invariably they require knowledge of at least two parameters: the hydrodynamic volume of a statistical particle, expressed in terms of the zero shear intrinsic viscosity, $[\eta]_o$, and the maximum packing volume fraction, ϕ_m. The most successful relations between η_o and ϕ are those proposed by Simha (1) and by Mooney (2). Using empirical values of the parameters, the relations have been used far outside their theoretical limit, i.e., for polydisperse systems, non-spherical and/or non-rigid particle suspensions, etc. (3).

The Newtonian viscosity of non-spherical suspensions is more difficult to describe. At the onset of shearing, the particles begin to rotate with the period:

$$t_p = 2\pi(p + p^{-1})/\dot{\gamma} \qquad (1)$$

where p is the aspect ratio: $p \equiv a_{max}/a_{min}$ (a_{max} and a_{min} are respectively the maximum and minimum particle dimension) and $\dot{\gamma}$ is the rate of shear.

Here, all three parameters: $[\eta]_o$, ϕ_m, and t_p strongly depend on p, and the $\eta_o - \phi$ curve must be divided into two principal regions: the dilute suspensions, where the anisometric particle freely rotates with t_p given by *Eq 1*, and ϕ_m (defined in terms of the freely rotating particle encompassed volume), and the concentrated suspensions with $\phi > \phi_m$. In the latter region only a two-dimensional movement is possible. Rheologically this is equivalent to a decrease in the apparent hydrodynamic volume of the particles, evidenced by a decrease in the rate of the relative viscosity, η_{ro}, increase with ϕ. The phenomenon is illustrated in *Fig. 1* by results for mica-filled polyethylene (4). Surprisingly, even here the Simha and Mooney equation can be used provided the $[\eta]_o$ and ϕ_m are empirically described in terms of p (c.g., see *Fig. 2*). Alternatively, one can use a pragmatic approach and describe $\eta_o - \phi$ dependence in a wide range of concentrations by a simpler, Martin-type formula:

$$\ln \eta_r = k_M[\eta]_a\phi \qquad (2)$$

provided k_M and $[\eta]_a$ are taken as a ‡justable parameters.

NON-NEWTONIAN FLOWS

Theoretical treatment of suspension rheology is greatly complicated by structure formation.

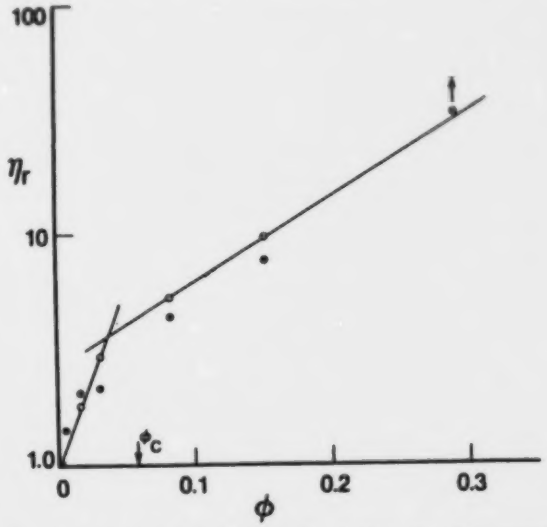

Fig. 1. Semi-log dependence of relative viscosity versus volume fraction for mica-filled polyethylene. The solid lines represent the behavior below and above ϕ_c with intrinsic viscosities of 51.6 and 8.5, respectively.

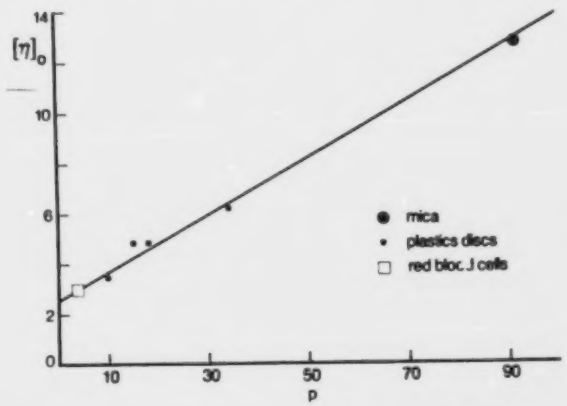

Fig. 2. The intrinsic viscosity, $[\eta]_o$, versus the aspect ratio p.

Two types can be distinguished, (a) introduced by the shear field (e.g., skin-core structures in long tube flows), and (b) formed by particle-particle interactions. The knowledge of structures (a) is important for proper measurement and interpretation of the flow phenomena, and that of structures (b) is the key for utilization of suspension rheology in processing (5).

Fundamentally, any mechanism that allows storage and recovery of energy must lead to some type of elasticity effect. Anisometry, either inherent (as in the case of rods) or created during the flow (e.g., by aggregation), may lead to the appearance of the first normal stress difference, N_1 (6). It follows that the anisometric particle suspensions can rarely be called "Newtonian." Two types of departure are distinguished: the time-dependent and the rate-of-deformation-dependent effects. Both of these enter into consideration when the viscoelastic

properties of suspensions are being discussed. The first of these effects, the thixotropy, was reviewed recently by Mewis (7).

Yield Stress

One aspect of the thixotropic system is the existence of the "apparent yield stress." If the mechanism responsible for thixotropy is the formation and destruction of bonds, then one must postulate that the stress required to break the bond must exceed the bond strength. The only difference between this and the definition of the true yield stress is the time factor.

The existence of the apparent (time scale of the experiment) or the true yield stress, τ_y, has a profound effect on the shape of flow curves and interpretation of data. There are several methods for determining τ_y. One of these, the modified Casson equation:

$$F^{1/2} = F_y^{1/2} + aF_m^{1/2} \qquad (3)$$

is the easiest and most frequently used. In *Eq 3*, F may stand for shear stress, τ_{12}, elongational stress, τ_{11}, shear loss modulus, G'', etc.; F_y indicate yield value of F; F_m is the F-value of pure matrix liquid at the same deformation rate as F; and a is a measure of the relative value of F (8). An example of the adequacy of *Eq 3* is given in *Fig. 3*. A strong correlation between τ_y and ϕ can be expressed as:

$$\tau_y = K(\phi - \phi_0)^n \qquad (4)$$

where K, $\phi_0 \simeq 0$ and n are adjustable parameters. Once the τ_y-values are known, the experimental stresses can be corrected, and the data can be analyzed using simple relations derived for systems without the yield.

Another method requires a simultaneous fit of experimental data to one or another constitutive equation in which a parameter or parameters are related to τ_y.

The yield stress can also be directly determined. Dzuy and Boger (9) proposed a specially constructed rotational vane viscometer. Yield stresses in compression and elongation have been directly measured for PP/mica and polyethylene/mica systems using standard rheological instruments. In the first case (10) $\tau_{y,c}$ was calculated from the unrelaxed stress value in parallel plate geometry using the Rheometrics Mechanical Spectrometer. In the second case (8), $\tau_{y,e}$, was taken as the critical stress value below which no sample deformation was observed during 30 min of straining in the Rheometrics Extensional Rheometer. When comparing $\tau_{y,c}$ with $\tau_{y,e}$, it was surprising to see their relative agreement.

The yield in dynamic tests is evidenced by the secondary plateau in G' versus ω or G'' versus ω plots (e.g., see *Fig. 4*). It is expected that the structure responsible for τ_y should be more apparent in G' than in G''. As mentioned before, *Eq 3* has been found to be reliable in calculating yield in shear stress, loss modulus, and extensional viscosity. Unexpectedly, it was found to work quite well for storage modulus (but it failed miserably when applied to complex modulus). In *Fig. 5* the values of the yield moduli G_y' and G_y'' are plotted versus mica content for the PP/mica system (10). Since the yield moduli are not equal, the "usual" way of examining the relative importance of the elastic component by plotting G' versus G'' for systems with yield may lead to wrong conclusions. In *Fig. 6* uncorrected data G' versus G'' for PP containing 0, 5, 10, 25, and 40 weight percent of mica are shown by solid lines. The data for the three lowest concentrations superimpose, while those for 25 and 40 weight percent fall below. Apparently the elasticity, at constant value of G'', decreases with loading. However, it seems that at low frequencies all concentrations collapse into a single

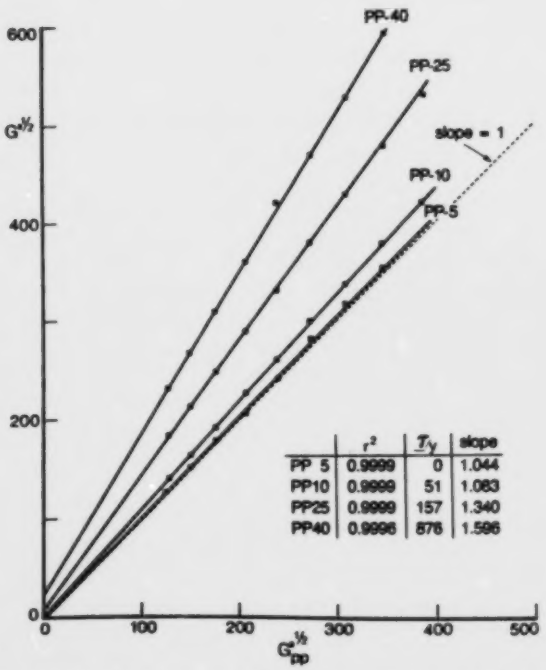

Fig. 3. Modified Casson plot for polypropylene/mica at 180°C.

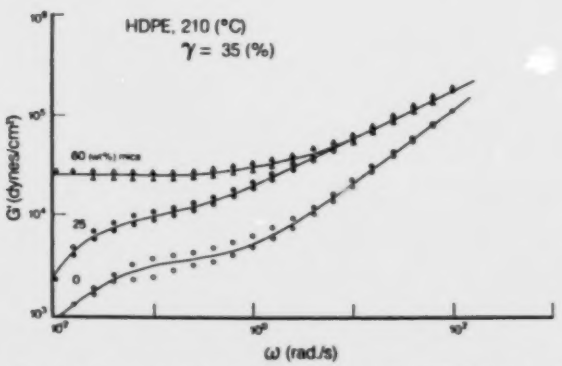

Fig. 4. Loss modulus versus frequency for HDPE-mica at 210°C.

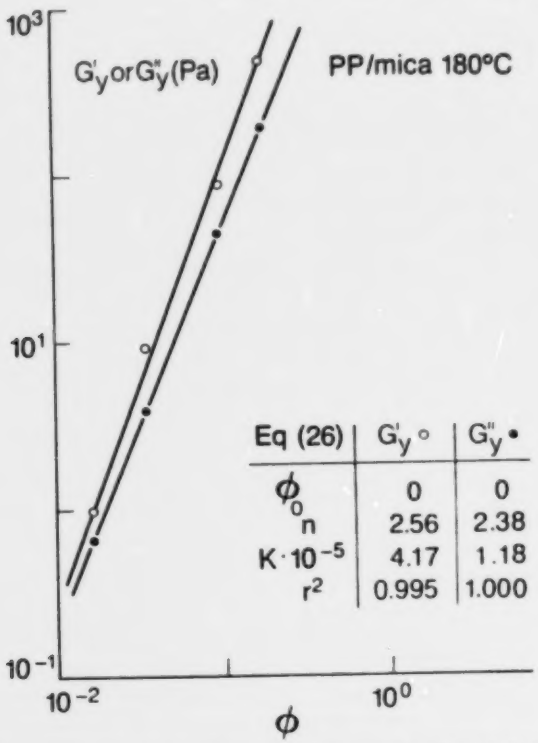

Fig. 5. Yield values of storage and loss shear moduli for PP/mica at 180°C, plotted versus volume fraction of the filler.

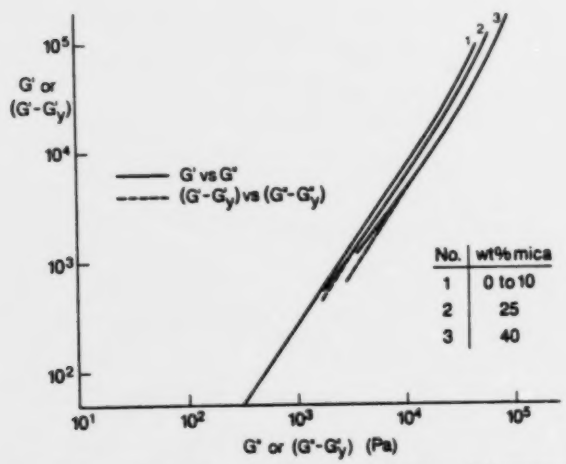

Fig. 6. G′ versus G″, solid lines, and (G′ − G'_y) versus (G″ − G''_y), broken lines, for PP with mica at 180°C.

dependence. This indicates that the relative importance of the elastic component depends differently on ω at low and high loading. The conclusion is quite different when instead of G' versus G'', the corrected for yield values $(G' - G'_y)$ versus $(G'' - G''_y)$ are considered. These are shown in *Fig. 6* by broken lines. It can be seen that three parallel curves are generated; top one for $w = 0$, 5, and 10; middle one for 25; and bottom one for 40 weight percent of mica. At low frequency the slope of the dependence is about 1.5, at high about 2. Note that all the data can be superimposed on the PP curve by a horizontal shift, i.e., empirically:

$$G'(\omega, T) = G'_y(T, \phi) + f[a_c(G'' - G''_y)] \quad (5)$$

where $a_c \leq 1$ is a concentration dependent shift factor.

The N_1 versus τ_{12} dependence should be similarly treated as that of G' versus G''. Plots of uncorrected for the yield data N_1 versus τ_{12} of composites give conflicting information; some authors reported that at constant τ_{12}, the N_1 of composites is smaller than that of the pure matrix polymer (11), other authors (12) reported that the reverse is true. It seems that here two effects superimpose: 1) addition of highly anisometric particles provides a mechanism for energy storage, which genuinely increases N_1; 2) at higher loading, the yield stress causes additional increase at low τ_{12} values, similar to that reported in *Fig. 6* for PP/mica.

Due to existence of τ_y in composites, the extrudate swelling ratio B, decreases with ϕ, to fall even below the swelling value for Newtonian liquids, $B_o = 1.13$. The phenomenon is well documented in the literature (12 to 16). It seems that the low extrudate swell originates in a flat flow profile and related to it yield stress. Plug flow at low filler content has been frequently reported (17, 18). When only a relatively thin annular layer of material undergoes deformation during the flow, the strain recovery can be expected to originate only in it. In addition, in material having a yield stress, only stresses $\tau > \tau_y$ can relax at the die exit.

In extensional flow yield stress, $\tau_{y,e}$, has been reported by White *et al.* (19 to 21); by Kamal and Mutel (22, 23); and by Utracki *et al.* (8, 10, 24). Yield stress is apparent in two (related) dependencies: (i) as a vertical displacement in the stress growth function at decreasing strain rates, and (ii) as a deviation from the Trouton rule at the extensional strain rate, $\dot{\epsilon} \to 0$. The second effect can be subtracted by means of *Eq 3*.

Over the years Kataoka *et al.* (25 to 30) published a series of lucid articles on rheologic behavior of suspensions and composites with iso- and anisometric filler particles. The steady state as well as dynamic data have been reported. Two methods of yield stress subtraction were used: (i) by means of modified Casson Equation (3), and (ii) by plotting η_r versus τ_{12}, where η_r is defined as the ratio of viscosity of suspension to that of medium at the same shear stress. Existence of high τ_{12} − plateau (see *Fig. 7*) was taken as evidence of the absence of the yield stress.

Dynamic Testing

For polymer composites, the dynamic testing is a convenient, rapid, and precise method of characterization. Since scanning can be done by either increasing or decreasing frequency,

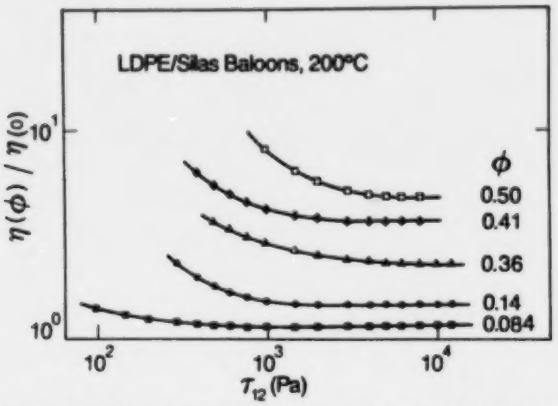

Fig. 7. Relative viscosity, $\eta_r(\tau_{12} = const)$, at 200°C as a function of shear stress for LDPE filled with ϕ = 0.084, 0.14, 0.36, 0.41, and 0.5 of silas balloons, 124 μm in diameter.

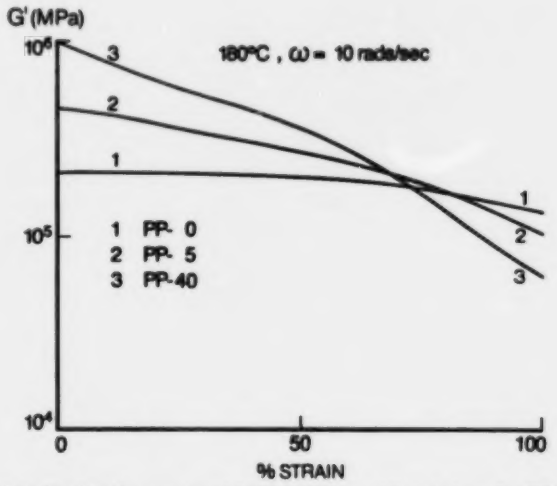

Fig. 8. Strain sweep at 180°C and ω = 10 rads/sec for PP/mica samples: γ = 0 to 100 percent with 2 percent per step.

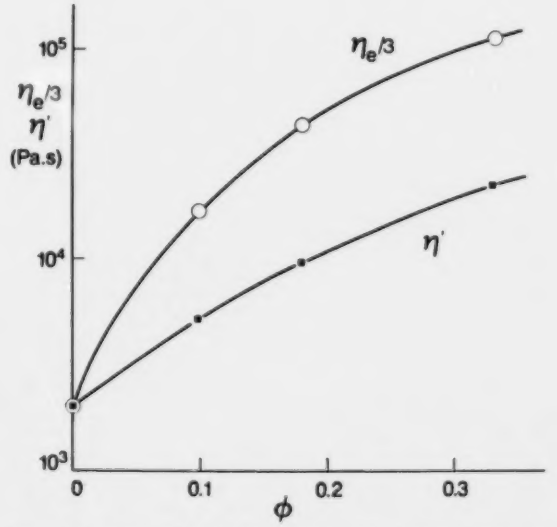

Fig. 9. Concentration dependence of elongational and dynamic viscosity of HDPE/mica system at 150°C.

one is able to verify effects of associated morphologic changes. By contrast, with the steady-state shearing and extensional flows, the dynamic mode offers the possibility to test the system under controllable, low strains, γ. The storage, G', and loss, G'', moduli depend on γ, ϕ, ω, time, t, temperature, T, method of preparation of the sample, and slip.

The effect of γ and ϕ on complex viscosity, η^*, and G' for glass fiber/LDPE were reported by Bigg (31), and on G' and G'' of mica filled HDPE ($\phi \leq 0.33$) by Fisa and Utracki (4).

The effect of γ and ω on glass fiber filled PP was discussed by Mutel and Kamal (22) and on mica filled PP by Utracki *et al.* (10). In highly filled systems, it is frequently impossible to find conditions for linear viscoelastic behavior. As shown in *Fig. 8* for PP containing 40 weight percent of mica at T = 180°C and ω = 1 rad/s, there is no strain–independent region. Even for 25 weight percent sample the region is reduced to $\gamma < 2$ percent. Since the theory for non-linear behavior is not available, the results can only be interpreted on a qualitative basis (32).

Extensional Flows

For hard sphere suspensions, Martischius (33) reported that due to morphologic rearrangements, the ratio of the extensional to shear viscosity at the same deformation rate $R_T = f(\dot{\epsilon})$ increases with ϕ. Similar conclusion can be drawn from the data presented in *Fig. 9* for HDPE/mica system (24). The extensional flow tests for glass fiber-filled polymer melts, reported by White *et al.* (34 to 36) gave similar results with even larger values of R_T = 7 to 10. These observations are in qualitative agreement with Bachelor's equation (37) for suspensions in Newtonian liquids:

$$R_T^0 = 1 + 4\phi p^2/9 \ln(\pi/\phi) \qquad (6)$$

where R_T^0 is the zero-deformation-rate Trouton ratio. This dependence was extended to non-Newtonian liquids with the "power-law" index, n, by Goddard (38):

$$\eta_{e,r} = \eta_e(\phi, \dot{\epsilon})/\eta_e(0, \dot{\epsilon}) = 1 + [2\phi R_T/3(n+2)]p^{n+1} \cdot \{(1-n)/n[1 - (\pi/\phi)^{(n-1)/2n}]\}^n \qquad (7)$$

Since elongational flow is irrotational, the particles should align themselves with the stress vector. For composites with initially random orientation of fibers or flakes, there must be a period of rearrangement. At higher loading this is accompanied with a very noisy stress signal observed for HDPE/mica (24) and PP/glass fiber (23) systems.

Unsuccessful efforts were made to study strain recovery and stress relaxation in systems

containing flakes and fibers. The phenomena seems to be complex, requiring multiple exponential decay functions and yield stresses.

ORIENTATION IN FLOW

The anisometric particles in shear flow rotate with the period given by *Eq 1*. Thus this flow was reported to have a disorienting effect on particles aligned in extensional flow field (39 to 42). However, in Couette flow of dilute fiber suspensions there is preferential orientation on the central surface of the annulus (17, 43, 44). At regular intervals fibers rapidly flip by 180°, i.e., statistically, as shown in *Fig. 10*, they are preferentially aligned within the narrow portion of the annular gap.

There is no doubt that the most powerful orientation fields are extensional. Using convergent and divergent flow channels, it is possible to control orientation of anisometric particles. Most of the work in this area has been done with fiber-filled materials (45, 46), but the effects are equally important for matrix polymers (47), neat resins (48 to 51), or liquid crystals (52).

Considering flow through a cone, Harris and Pittman (53) derived expressions for suspensions in Newtonian liquid, predicting that the alignment of rods should depend on the ratio of the initial and final position of the particle and should be independent of convergence angle, flow rate, viscosity, and aspect ratio. Takano reported (54) that for convergence angles larger than 120°, there are stagnation regions. For 60°, the alignment was observed to start upstream from the cone and achieve its limiting value, Ω_{min}. (Ω is the average angle between the particle and cone axes) upstream from the cone end (55).

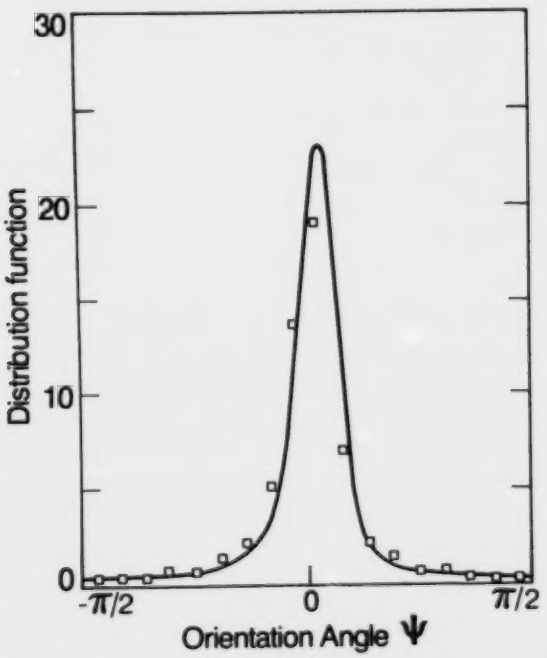

Fig. 10. Steady state orientation of Nylon fibers, p = 16, in silicone oil, ϕ = 0.01. Points = experimental, line = best fit to theoretical relation (after Folgar and Tucker).

According to Goettler (45, 46), plug flow may occur at $\phi \geq 0.05$ with the sheared layer less than 0.5 mm thick. The alignment is possible through the extensional flow in converging (or diverging) channels, Goettler's equation:

$$\frac{\tan\psi}{\tan\psi_o} = \left(\frac{A}{A_o}\right)^{3\theta/2} \qquad (8)$$

was recently rederived by Vincent (43). In *Eq 8*, ψ is the angle between fiber axis and its local streamline, $\theta \equiv (p^2 - 1)/(p^2 + 1)$, A is the cross-sectional area of the channel, and subscript "o" indicates the initial position. For small values of the convergence ratio, *Eq 8* gives an excellent agreement with the experimental results. However, for very large strains, or convergence ratios, the angle ψ tended towards a minimum value of 10 to 15°, instead the predicted zero. The discrepancy is primarily due to shear flow on the wall, not considered in derivation of *Eq 8*.

There is less information on the orientation of platelets. In converging flow these particles are less susceptible to orientation. In fact, there is conflicting information on alignment of mica particles in the extruded strands. Okuno and Woodhams (56) reported that near the center line, mica flakes in polypropylene are aligned perpendicularly to the flow direction with a progressive change toward parallel orientation near the surface. More recently (3, 4, 10) the orientation of mica in HDPE or PP was shown to be uniform throughout the full cross section of the extrudate; it seems that in this case the platelets aligned themselves in concentric circles, parallel to the capillary wall and to the direction of flow. The orientation improved with increase of γ. Recent experiments on flow orientation of mica flakes in PP during extrusion (57) point out a surprisingly large effect of vapors and gases adsorbed on the filler surface.

It is apparent that by contrast with rods, platelets undergo a two-stage orientation. Upstream from the die they are randomly oriented. During the convergent flow to die they orient with the flow axis. However, at that stage a cut perpendicular to the flow direction reveals a near-random orientation of the platelet in respect to the die wall. Thus, the second stage of orientation can only be accomplished during the residence time flow through a die (long die or slow flow).

CONCLUSION

At the present time the most important subject is the development, stabilization and characterization of particle orientation. Optimization of the processing conditions must lead to the desired morphology and amelioration of ul-

timate properties. Fibrillar, lamellar structures in polymer composites lead to substantial reinforcement, modification of permeability, electrical or thermal conductivity, etc.

NOMENCLATURE

a_c = concentration shift factor in *Eq 5*.
a = relative measure of F in *Eq 3*.
a_{max}, a_{min} = maximum and minimum particle dimension, respectively.
A, A_o = cross sectional area in convergent flow and its initial value, respectively; *Eq 8*.
B = extrudate swell.
F, F_m, F_y = stress in composite, in the matrix, and in its yield value, respectively, *Eq 3*.
G', G'' = storage and loss shear moduli.
G'_y, G''_y = yield values of G' and G''.
K_M = Martin constant; *Eq 2*.
K, n = parameters of *Eq 4*.
N_1 = the first normal stress difference.
p = a_{max}/a_{min}.
t = time.
R^0_T = zero-deformation rate Trouton ratio; *Eq 6*.
t_p = particle period of rotation; *Eq 1*.
T = temperature.
w = weight fraction.
$\dot{\epsilon}$ = elongational strain rate.
γ = strain (%).
$\dot{\gamma}$ = strain rate (s^{-1}).
η, η_o = viscosity and zero shear viscosity, respectively (Pa.s).
η_r, η_{ro} = relative viscosity and zero-shear relative viscosity, respectively.
η', η^* = dynamic and complex viscosity, respectively (Pa.s).
η_e = elongational viscosity.
$[\eta]$, $[\eta]_o$, $[\eta]_a$ = intrinsic viscosity, its value at zero $\dot{\gamma}$, and its apparent value, respectively.
ρ = density (kg/m^3).
θ = $(p^2 - 1)/(p^2 + 1)$ shape factor in *Eq 8*.
τ_y, $\tau_{y,e}$, $\tau_{y,c}$ = yield stress in shear, elongation, and compression, respectively (Pa).
τ_{11} = elongational stress.
τ_{12} = shear stress.
ϕ, ϕ_o, ϕ_m = volume fraction, its value at F_y = 0, and its value at the maximum packing, respectively.
ω = frequency in dynamic tests, (radians/s).

REFERENCES

1. R. Simha, *J. Appl. Phys.*, **23**, 1020 (1952).
2. M. Mooney, *J. Colloid Sci.*, **6**, 162 (1951).
3. L. A. Utracki and B. Fisa, *Polym. Compos.*, **3**, 193 (1982).
4. B. Fisa and L. A. Utracki, *Polym. Compos.*, **5**, 36 (1984).
5. L. A. Utracki, *J. Colloid Interf. Sci.*, **42**, 185 (1973).
6. O. L. Forgacs and S. G. Mason, *J. Colloid Sci.*, **14**, 473 (1959).
7. J. Mewis, *J. Non-Newtonian Fluid Mech.*, **6**, 1 (1979).
8. L. A. Utracki, *Rubber Chem. Technol.*, **57**, 507 (1984).
9. N. Q. Dzuy and D. V. Boger, *J. Rheol.*, **27**, 321 (1983); ibid. **29**, 335 (1985).
10. L. A. Utracki, B. D. Favis, and B. Fisa, *Polym. Compos.*, **5**, 227 (1984).
11. J. L. White, L. Czarnecki, and H. Tanaka, *Rubber Chem. Technol.*, **53**, 823 (1980).
12. B. A. Knutsson, J. L. White, and K. B. Abbas, in "Rheology," G. Astarita, G. Marrucci, and L. Nicolais, eds., Plenum, N.Y., Vol. 3, 83 (1980).
13. P. K. Agarwal, E. B. Bagley, and C. T. Hill, *Polym. Eng. Sci.*, **18**, 282 (1978).
14. D. C. Goel, *Polym. Eng. Sci.*, **20**, 198 (1980).
15. L. A. Utracki, in "Advances in Rheology," B. Mena, A. Garcia-Rejon, and C. Rangel-Nafaile, eds., Univ. Nation. Auton. Mexico, **3**, 467 (1984).
16. R. J. Crowson and M. J. Folkes, *Polym. Eng. Sci.*, **20**, 934 (1980).
17. H. L. Goldsmith and S. G. Mason, in "Rheology," F. R. Eirich, ed., Vol. 4, Academic Press, New York (1967).
18. W.-K. Lee and H. H. George, *Polym. Eng. Sci.*, **18**, 146 (1978).
19. J. L. White and H. Tanaka, *J. Appl. Polym. Sci.*, **26**, 579 (1981).
20. Y. Suetsugu and J. L. White, "The Influence of Particle Size and Surface Coating of Calcium Carbonate on the Rheological Properties of its Suspensions in Molten Polystyrene," PATRA Report No. 186, June 1982.
21. V. M. Lobe and J. L. White, *Polym. Eng. Sci.*, **19**, 617 (1979).
22. A. T. Mutel and M. R. Kamal, NRCC/IMRI symposium "Composites-'82," Montreal, Que., Canada, November 30, 1982; *Polym. Compos.*, **5**, 29 (1984).
23. M. R. Kamal, A. T. Mutel, and L. A. Utracki, NRCC/IMRI symposium "Composites-'83", Boucherville, Que., Canada, November 29, 1983; *Polym. Compos.*, **5**, 289 (1984).
24. L. A. Utracki and J. Lara, *Polym. Compos.*, **5**, 44 (1984).
25. T. Kataoka, T. Kitano, and T. Nishimura, *Rheol. Acta*, **17**, 626 (1978).
26. T. Kitano, T. Nishimura, T. Kataoka, and T. Sakai, *Rheol. Acta*, **19**, 671 (1980).
27. T. Kitano and T. Kataoka, *Rheol. Acta*, **19**, 753 (1980); ibid., **20**, 390, 403 (1981).
28. T. Kitano, T. Kataoka, T. Nishimura, and T. Sakai, *Rheol. Acta*, **19**, 764 (1980).
29. T. Kitano, T. Kataoka, and T. Shirota, *Rheol. Acta*, **20**, 207 (1981).
30. T. Kitano, T. Kataoka, and Y. Nagatsuka, *Rheol. Acta*, **23**, 20 (1984).
31. D. M. Bigg, *Polym. Eng. Sci.*, **22**, 512 (1982); ibid., **23**, 206 (1983).
32. S. Onogi and T. Matsumoto, *Polym. Eng. Rev.*, **1**, 45 (1981).
33. F.-D. Martischius, *Rheol. Acta*, **21**, 311 (1982).
34. J. L. White and H. Tanaka, *J. Appl. Polym. Sci.*, **26**, 579 (1981).
35. H. Tanaka and J. L. White, *Polym. Eng. Sci.*, **20**, 949 (1980).
36. Yu Chan, J. L. White, and Y. Oyanagi, *J. Rheol.*, **22**, 507 (1978); ibid., **24**, 500 (1980).
37. G. K. Batchelor, *J. Fluid Mech.*, **46**, 813 (1971).
38. J. D. Goddard, *J. Rheol.*, **22**, 615 (1978).
39. P. F. Bright, R. J. Crowson, and M. J. Folkes, *J. Mater. Sci.*, **13**, 2497 (1978).
40. R. J. Crowson, M. J. Folkes, and P. F. Bright, *Polym. Eng. Sci.*, **20**, 925 (1980).
41. R. J. Crowson and M. J. Folkes, *Polym. Eng. Sci.*, **20**, 934 (1980).
42. R. J. Crowson, A. J. Scott, and D. W. Saunders, *Polym. Eng. Sci.*, **21**, 1014 (1981).
43. M. Vincent, Dr. Eng. thesis, L'École National Supérieure des Mines de Paris, Sophia Antipolis, France (1984).

44. F. Folgar and C. L. Tucker III, *J. Reinf. Plast. Compos.*, **3**, 98 (1984).
45. L. A. Goettler and K. S. Shen, *Rubb. Chem. Technol.*, **56**, 619 (1983).
46. L. A. Goettler, NRCC/IMRI symposium "Composites-'82," Montreal, Que., Canada, Nov. 30, 1982; *Polym. Compos.*, **5**, 60 (1984).
47. P. D. Patel and D. C. Bogue, *Polym. Eng. Sci.*, **21**, 449 (1981).
48. M. R. Kamal and F. H. Moy, *J. Appl. Polym. Sci.*, **28**, 1787 (1983).
49. M. R. Kamal and V. Tan, *Polym. Eng. Sci.*, **19**, 558 (1979).
50. J. L. White and J. E. Spruiell, *Polym. Eng. Sci.*, **23**, 247 (1983).
51. A. I. Isayev, *Polym. Eng. Sci.*, **23**, 271 (1983).
52. M. Mansuripur, *Int. J. Multiphase Flow*, **9**, 299 (1983).
53. J. B. Harris and J. F. T. Pittman, *Trans. Inst. Chem. Eng.*, **54**, 73 (1977).
54. M. Takano, A.R.P.A. Report HPC-73-165.
55. K. N. Murty and G. F. Modlen, *Polym. Eng. Sci.*, **17**, 848 (1977).
56. K. Okuno and R. T. Woodhams, *Polym. Eng. Sci.*, **15**, 308 (1975).
57. B. Remillard and B. Fisa, presented during the 68th Canadian Chemical Conference, 2–5 June 1985, Kingston, Ont., Canada.

DISCUSSION

J. L. White: I very much like your talk, especially the part related to the evolution of the orientation of mica particles along the length of the tube. I am concerned about certain parts. There are many separate effects existing in the flow of particle-filled melts which should be clearly separated. There is the effect of anisotropy, another of inter-particle forces accentuated as the particles become smaller. The yield is rather the effect of the latter than the former. I am concerned about the yield value of the glass fiber filled melts. Your report is in difference to our observation on that same system. In regards to the effect of filler on the stability of extentional flow. Our observation shows that putting small particles into polymer melts destabilizes elongational flow whether as far as pulling filament in the bath or the draw resonance are concerned. This was true for both small particles and fibers. In fiber-filled systems it was difficult to even get uniform diameter filaments outside the extrusion die. Regarding the orientation in shear flow, it is at least one order of magnitude less effective than the elongational flow. In viscoelastic fluids, as shown by the work of Giesekus and others, it is specially effective because normal stresses are involved. The final comment deals with orientation and the need there to develop quantitative methods for the characterization of orientation of particulates in solids as well as in the melts.

L. A. Utracki: Thank you for the kind words and comments. As the period of rotation of anisometric particle indicates, at low stress level the relaxation occurs slowly and the testing is seldom done under the equilibrium conditions. The observed unrelaxed stresses may not be due to the true yield stress but rather to the apparent one, related to the time scale of the measurements or processing. However, the proposed treatment to consider them as apparent yield simplifies the description. The yield stress does depend on the interface properties. This has been demonstrated by Onogi *et al.* for large spheres—depending on the ionic change the yield was observed or not. The difference in the type of sizing agent may explain the difference between your observation of the absence of yield stress in polypropylene glass fiber system and that observed by Kamal and Mutel, who noted yield in extensional flow for the same system. Regarding the effect of particulates on flow stability, it very well may be that the improved stability in shear flow observed for polyethylene/silica by Schreiber and that in extensional flow for polyethylene/mica by us, as contrasted with decreased stability in fiber spinning and draw resonance, show a fundamental difference between these types of flow.

It is well known that the shear flow has a significantly lower orientational effect than extentional one. As a matter of fact, it has also been reported that the orientation of fibers in the melt, imposed by the converging flow, worsens as the capillary length increases. However, in dilute suspensions there is an orientational effect as both the theory and the experiments demonstrated. As the concentration increases, the interparticle interactions prevent their free rotation and the effect diminishes.

J. L. White: I agree that the shear flow can give a moderate amount of orientation but not necessarily where you want it. My interpretation of Goettler's patent was that if you set up a shear flow die, you always end up with axial orientation. If you need another orientation you have to redesign the die so as to give orientation in another direction.

L. A. Goettler: I think that another problem with shear orientation in tubular flow is that shear field is not homogenous. As a result the orientation is pretty much relegated to the region near the wall where the shearing takes place. On another subject, I wonder, Leszek, if the creep rheometer could not resolve the issue White brought up, if there is a true yield stress at very low rates, say down to 10^{-6} s^{-1}. One could put a low stress on the sample and see if it flows or not.

L. A. Utracki: This is a good idea. As a matter of fact we tried something similar to check the value of the yield stress in polyethylene/mica system. We placed the samples in the extensional rheometer and observed at which minimum value of tensile stress the sample would deform. Due to possible degradation and silicon oil effects, the test time at each stress was limited to 30 min. The creep rheometer probably can extend this to a few hours. However, there is already information in the literature that for many filled systems, tested at long

times, the flow occurs at below yield stress value determined within the "usual" laboratory time scale. This, as White indicated, is particularly true for large particle size filler systems. That is why we have to be careful to distinguish the true and the apparent yield stress.

L. A. Goettler: Yes, I agree. You also mentioned that you treated G' and G'' data separately subtracting the yield values. I wonder if you tried to correlate the steady data and dynamic data to see if the Cox-Mertz rule holds or not.

L. A. Utracki: We published several papers indicating that in multiphase systems rarely the low strain dynamic data agree with the large strain capillary flow results. The disparity obviously increases with the orientational effect of the filler. However, even for pure matrix materials I do not believe that the Cox-Mertz rule holds. Recently with Bruno Schlund we have looked into this problem. What we found is that the coincidence of η with η^* was observed for systems with large pressure gradient of viscosity. When the data were corrected for pressure effect, the η coincided with η', as it should.

M. R. Kamal: Our observation on fiber reinforced melts is that this is an apparent yield. When you do the Casson plot and subtract the calculated yield stress, the viscosity does not level off. We still see a yielding behavior, maybe resulting from a decreasing amount of orientation.

Characterization of the Rheological Behavior of Fiber-Filled Polypropylene Melts Under Steady and Oscillatory Shear Using Cone-and-Plate and Rotational Parallel Plate Rheometry

A. T. MUTEL *and* M. R. KAMAL*

Department of Chemical Engineering
McGill University
Montreal, Canada, H3A 2A7

Utilization of cone-and-plate and rotational parallel plate rheometry to characterize the rheological behavior of fiber-filled polymer melts at low shear rates was evaluated. The effect of flow geometry and dimensions on the viscoelastic and viscometric functions was considered. Stress growth functions were found to be dependent on the dimensions of the flow channel. However, viscometric functions were not affected by the dimensions or the geometry of the flow channel. The initial state of orientation was found to be an important factor in determining the flow behavior. Oscillatory shear tests yielded highly strain-dependent loss and storage moduli even at very small strain amplitudes. However, the stress response was found to be sinusoidal in most cases, although the properties were strain dependent.

INTRODUCTION

Interest in understanding the rheological behavior of fiber-filled viscoelastic fluids has increased substantially in recent years. The interest is mainly due to increased utilization of fiber-reinforced polymer products, due to enhancement achieved in the mechanical and thermal performance of the product. Fiber-filled polymer melts, which are highly anisotropic, are characterized by an internal structure, associated with the state of orientation and distribution of the fibers. Bulk rheological properties are determined by the internal structure as well as by the base polymer properties. Hence, the rheological properties of filled polymer melts are quite complex in nature, and the interrelation between the internal structure and the bulk properties is not well established yet. Cone-and-plate, capillary, and slit devices are the most commonly used rheometers to study the shear flow properties of fiber-filled polymer melts. Under steady shear conditions, the addition of fibers increases the viscosity, as in all suspensions, and there is a positive correlation between the concentration of fibers and the increase in viscosity. The effect of fibers on the steady shear viscosity at any concentration is higher at low shear rates, and the relative viscosity decreases with increasing shear rate. A pronounced effect of fibers on the steady shear viscosity is observed at low shear rates. The increased pseudoplasticity is usually related to the change in fiber orientation towards shear planes with increasing shear rate, which causes less disturbance of the flow by the fibers. Yield behavior has not been observed for fiber-filled polymer melts (1 to 6), unlike melts filled with small particles, except at high concentrations of the former (~30 percent by volume) or in the case of long non-rigid fibers (3, 7, 8). The rheological properties of fiber filled melts under oscillatory shear has been studied by Onogi and coworkers (9), and Kitano and coworkers (10). Onogi *et al.* evaluated the effect of preshearing on subsequent oscillatory shear response and attempted to relate the behavior under oscillatory shear to the reformation process of fiber structure. However, the strain amplitude was not given, and the authors did not indicate whether the stress response was harmonic. Kitano *et al.* used a cone-and-plate type rheometer at a constant strain amplitude of

* To whom all correspondence should be addressed.

0.035 and studied the effect of frequency on the viscoelastic functions G' and G'' for polyethylene melts filled with fibers. They observed a harmonic stress response. The effect of fibers on the ratio of moduli of the filled to unfilled melts changed markedly with frequency. Strain dependency was not studied. G' and G'' were found to be sensitive not only to fiber concentration but also to the fiber length and length distribution.

In the characterization of the rheological behavior of polymer melts filled with fibers, by employing methods generally applied to homogeneous unfilled melts, two factors should not be overlooked:

- The fiber size is comparable to the characteristic flow dimensions, which may result in considerable wall effects. Steady shear viscosities for fiber-filled polymer melts were found to be different for different capillary diameters keeping all the other parameters constant (11).
- Change in fiber orientation distribution during flow is mainly determined by the flow type.

Cone-and-plate and rotational parallel plate rheometers are extensively used to characterize some rheological properties of unfilled homogeneous melts at low shear rates. The major purpose of the present study is to evaluate the utilization of these rheometers to characterize some rheological properties of fiber-filled polymer melts. The effect of flow geometry and dimensions on the viscoelastic and viscometric functions is considered. Another aspect studied is the rheological behavior of filled melts under oscillatory shear as a function of strain amplitude and frequency. Oscillatory shear experiments can yield valuable information regarding the internal structure and they can permit the separation of time and strain effects.

EXPERIMENTAL

A Rheometrics Mechanical Spectrometer was used with cone-and-plate and rotational parallel plate fixtures. Stress growth at constant shear rate and oscillatory shear tests were performed with unfilled polypropylene and 10 percent by weight glass fiber-filled polypropylene melts. Base polymer was Hercules Pro-Fax 6501 polypropylene, which had a weight average molecular weight between 340,000 and 400,000, and a number average molecular weight between 60,000 and 73,000. Cones used were 25 mm in radius and had cone angles of 0.04 and 0.1 radian. The gap used in parallel plate geometry was 1 mm, and the radius of the plates was 25 mm. The diameter of the fibers used was 12 microns and the average length was 600 microns, which is the same order of magnitude compared to flow dimensions. All tests were performed under nitrogen atmosphere at 200°C. The possibility of degradation was checked by performing an oscillatory shear experiment using unfilled polymer at 0.15 strain amplitude and at a frequency of 3 rad/s. Loss and storage moduli were followed as a function of time. There was practically no change in either moduli for 75 min, which was much longer than the longest test performed. This indicates that there was no severe degradation to the extent that would affect the rheological properties sought.

RESULTS AND DISCUSSION

Steady Shear Results

Stress growth tests were made using both filled and unfilled polypropylene melts at shear rates between 0.02 and 0.3 s^{-1}. The lower limit was due to the machine limitations and the higher limit was determined by the surface deformations at the free edge, which were reflected by a continuous decrease in torque measured.

The effect of flow geometry on transient behavior is shown in *Fig. 1*. A small stress overshoot was observed with unfilled polypropylene and the equilibrium stress was reached in a relatively short time. The stress growth function for unfilled polymer melt was not affected by the geometry. However, a very large peak in stress was observed with filled melts initially, and the equilibrium stress was achieved in a much longer time scale compared to unfilled polymer melt. The peak stress was found to be a strong function of the flow dimensions, although the equilibrium value was virtually the same in the three different geometries studied.

The stress growth curve for parallel plates was corrected for the uneven shear rate distribution by using the method proposed by Ganani and Powell (12). Torque values measured for transient and steady shear were corrected using the well known equation

$$T = \frac{3T}{2\pi R^3}\left(1 + \frac{1}{3}\frac{d\ln}{d\ln\gamma_R}\right) \qquad (1)$$

at each time.

Fluctuations in torque between 5 and 10 percent of the mean value were observed with fiber-filled melts. Comparison with the stress signal obtained for unfilled melts at the same mean stress value showed that this is not a noise problem related to the instrument, but is a characteristic response associated with the fiber-filled melts. Similar observations had been made with similar materials in uniaxial extension (13), and the fluctuations were thought to be reflections of fiber interactions on the stress signal. The amplitude of the fluctuations observed with cone-and-plate and parallel plates was also a function of the dimensions of the flow channel.

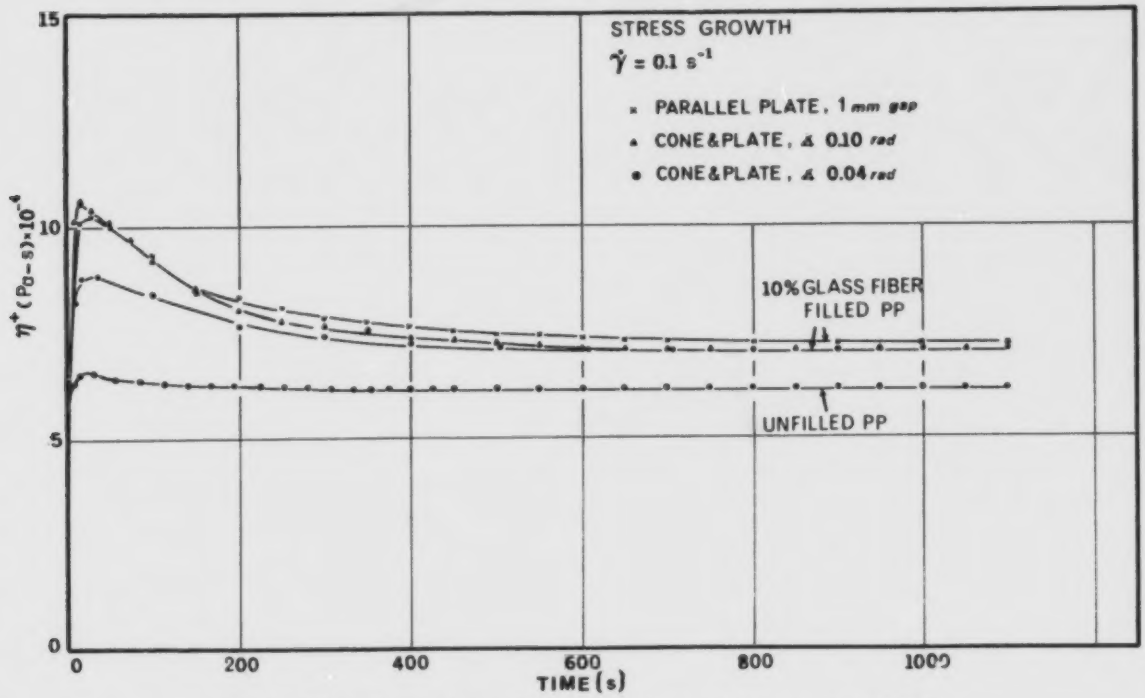

Fig. 1. Effect of geometry and flow dimension on stress growth at 200°C.

The dependency on the geometric constraints supports the hypothesis that the fluctuations were a result of the fiber motions. The effect of flow dimensions on transient response can also be seen clearly in *Fig. 2*, where the stress growth functions for fiber-filled melt are given as a function of gap dimension keeping all other parameters the same. The stress peak increased with increasing gap dimension. However, in all cases, including cone-and-plate geometry, the final equilibrium value was virtually the same. This phenomenon is thought to be a reflection of the orientation process of fibers and fiber interactions. With flow, fibers rotate and drift to equilibrium orientations in shear planes, which produce lower resistance to flow. Initially, most fibers are not oriented in shear planes, and their rotation results in enhanced viscous dissipation and a larger number of fiber-wall and fiber-fiber interactions. When the dimensions of the flow channel are decreased, free rotations of the fibers are obstructed, and the energy dissipated, due to the rotation of fibers, is diminished, resulting in smaller stress peaks for smaller gap sizes. Another factor diminishing the peak stress in smaller dimensions is the pre-orientation of fibers during sample loading. However, the rotation orbits drift in time toward equilibrium orientations, in which the angle between the shear planes and the fibers becomes much smaller, and the fibers spend most of the rotation period in the shear planes, resulting in less resistance to flow. Fiber-wall interactions decrease considerably,

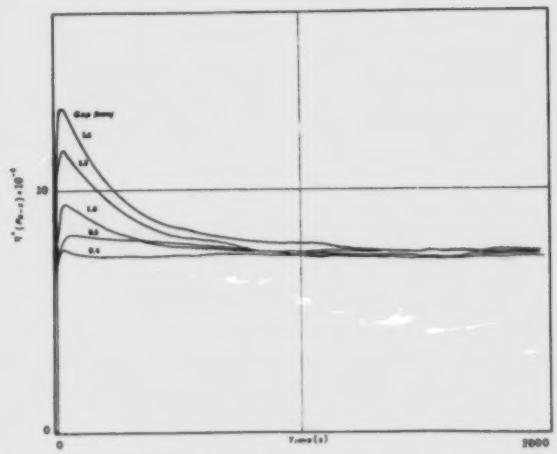

Fig. 2. Effect of gap size on the stress growth function for 10 percent glass fiber filled polypropylene melt at 200°C with rotational parallel plates.

and the effect of geometry diminishes, resulting in virtually the same equilibrium stresses for different geometries. These results show that although the viscometric functions measured were not particularly affected by the geometry or gap size, the transient behavior was highly dependent on the size of the flow channel. Hence, these materials cannot be treated as homogeneous fluids under these conditions. Measured properties are not solely material properties but are also a function of the geometrical constraints. The effect of geometrical constraints on the bulk behavior of filled materials is an important phenomenon, consider-

ing that most flow channels in commercial processes include dimensions comparable to the geometrical dimensions used in this study.

Transient first normal stress difference results for fiber-filled polypropylene with 0.1 radian cone angle are given in *Fig. 3*. Ambiguous stress fluctuations were observed with the 0.04 radian cone angle; hence this cone was not further utilized. Measurable first normal stress differences were observed with fiber-filled melts at shear rates as low as 0.03 s^{-1}, while no measurable first normal stress differences were observed up to 0.08 s^{-1} with unfilled melts. A small stress overshoot was observed with unfilled polymer melt at a shear rate of 0.1 s^{-1}, and the equilibrium stress was reached within 5 min. In contrast, a large stress overshoot was observed with fiber-filled melts, which decreased to an equilibrium stress in relatively long time scales. Equilibrium first normal stress differences for filled melts at shear rates below 0.1 s^{-1} were practically the same, within the range of accuracy. For shear rates above 0.1 s^{-1}, normal stress differences increased with increasing shear rate. Steady state first normal stress differences were increased by up to 30 percent with the addition of 10 percent by weight fibers. Large stress peaks and subsequent decrease are attributed to the change in orientation distribution of fibers with flow.

Another important factor that should be considered in studying the rheological behavior of fiber-filled melts is the initial state of orientation distribution. Fiber dimensions are too large for an appreciable effect of Brownian motions. Hence, there are no significant restoring forces to return to an original state after the cessation of flow. In this case, equilibrium fiber orientation could also be a function of the initial orientation. Since the orientation distribution of fibers is one of the major factors determining the bulk rheological behavior of filled melts, the bulk flow behavior will be affected by the initial state of orientation in a similar way. A step test was conducted to evaluate the effect of the initial state of fiber orientation, as shown in *Fig. 4*. Three samples prepared under identical conditions were subjected to different shear histories both for unfilled and filled melts. One sample was sheared at 0.06 s^{-1} for 1000 s. The second sample was first sheared at a lower shear rate (0.04 s^{-1}) for 500 s in order to establish a steady state, and then the shear rate was increased to the same shear rate as in the first test (0.06 s^{-1}), and shearing was continued for another 500 s to reestablish the new steady state. The third sample was first subjected to a higher shear rate (0.2 s^{-1}) for 500 s, and subsequently the shear rate was reduced to 0.06 s^{-1} and maintained at this shear rate shearing for another 500 s. Again, steady state was reached in both steps.

In the case of unfilled melts, in all three tests the same steady state stresses were observed within the reproducibility limits. For fiber-filled melts, in the first two cases, the steady state stresses were the same. When the melt was first sheared at 0.2 s^{-1}, the equilibrium stress at the end of the second stage was lower than the equilibrium stresses observed in the first two cases. The average orientation of fibers at the end of the first stage is a function of shear rate applied. The maximum angle between the fibers and shear planes decreases with increasing shear rate. Once the melt is sheared at a higher shear rate, the average orientation angle of fibers is already smaller than the final equilibrium orientation angles of fibers in the first two tests. Since there is no randomizing mechanism to restore the orientation, the final orientation at the end of the third test is different from that at the end of the first two tests. The final steady state stresses are strongly affected by the orientation of fibers and hence are different.

The subsequent stress growth experiments, from which the equilibrium stresses and steady shear viscosity values were extracted, were carried out using a new sample prepared under the

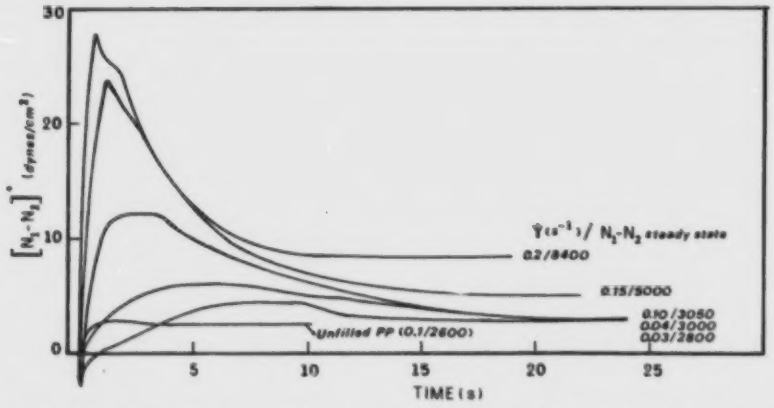

Fig. 3. First normal stress difference growth function for 10 percent fiber filled polypropylene melt at 200°C.

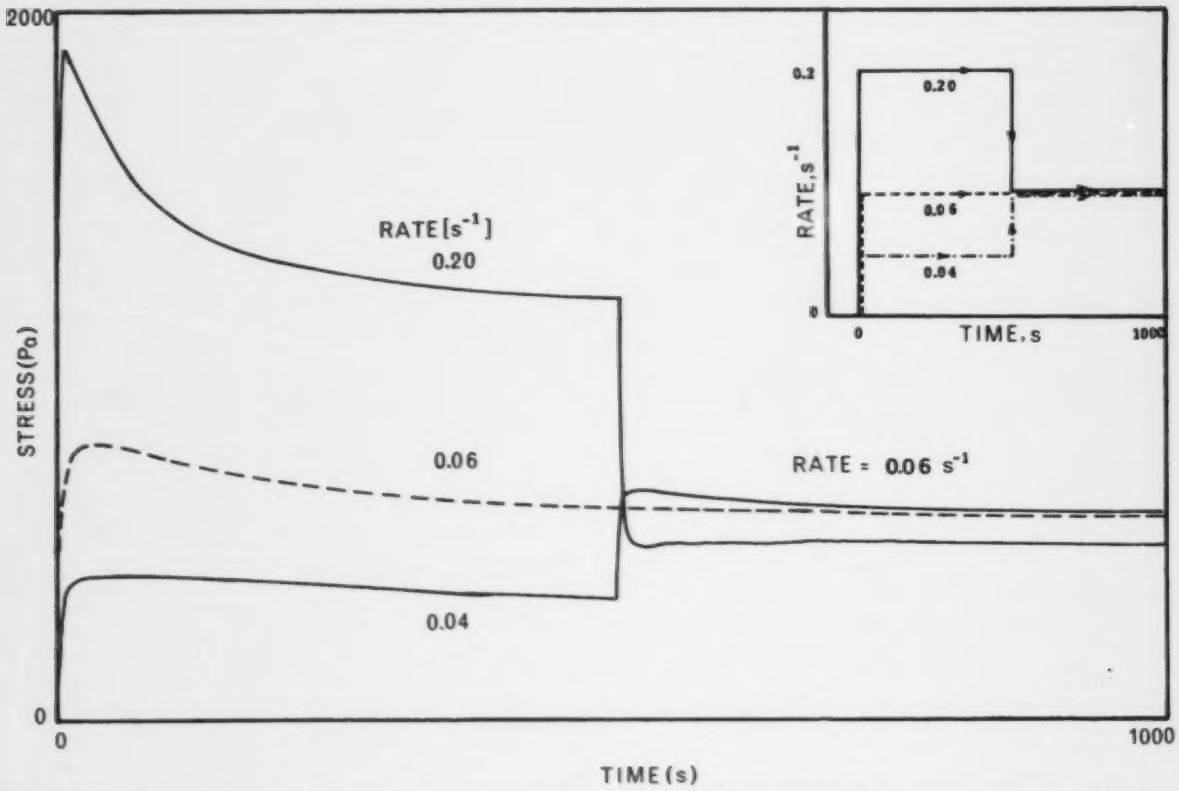

Fig. 4. Effect of shear history on steady shear viscosity for 10 percent glass fiber filled polypropylene melt at 200°C.

same conditions for each shear rate, considering the effect of the initial orientation state. Steady shear viscosity curves for filled and unfilled melts, extracted from single stress growth experiments, are given in *Fig. 5* for three different geometries. Parallel plate results were corrected using *Eq 1* for uneven shear rate distribution. Steady shear viscosities for both filled and unfilled melts were not affected by geometry. Viscosity values obtained with different geometries agreed with each other within the reproducibility limits at all shear rates.

Addition of fibers increased the steady shear viscosities 15 to 20 percent within the shear rate range covered. The viscosity of fiber-filled melts continued to increase with decreasing shear rate at low shear rates, although unfilled melt viscosity approached a zero shear viscosity. Casson plots were prepared to check whether there were yield stresses associated with fiber-filled melts. A yield stress value of 100 Pa was obtained with the fiber filled melt, which was only 4 percent of the minimum stress obtained at the lowest shear rate. The viscosities obtained by subtracting the yield stress from the stresses obtained at different shear rates still showed an increasing trend with decreasing shear rate. This indicates that there is no yield stress associated with the fiber-filled melts at this level of filling. Pseudoplastic behavior of fiber-filled melts at low shear rates, where the unfilled melt exhibits a shear rate independent viscosity, can be attributed to the change in equilibrium orientations of fibers with the shear rates applied. A structural change is implied by the shear thinning behavior of filled melts in this shear rate range; an increase in shear rate causes a decrease in the angle between the axis of the fiber and the shear planes, and hence the energy dissipation due to fibers.

The effect of fibers on bulk properties can be better illustrated using relative viscosities. Two different definitions were used for the relative viscosity curves given in *Fig. 6*. The first relative viscosity was defined as the ratio of the difference between filled and unfilled melt viscosities at the same shear rate to the viscosity of the unfilled melt at this shear rate. The relative viscosity showed a sharp decline at low shear rates and reached an equilibrium value around 0.08 s^{-1}. The equilibrium fiber orientation at low shear rates, and hence, the contribution of fibers to total stress is a strong function of shear rate. However, at higher shear rates, fibers are almost oriented within the shear planes, and further increase in shear rate practically has no effect on orientation. The other definition of relative viscosity used was based on the stress, considering the base poly-

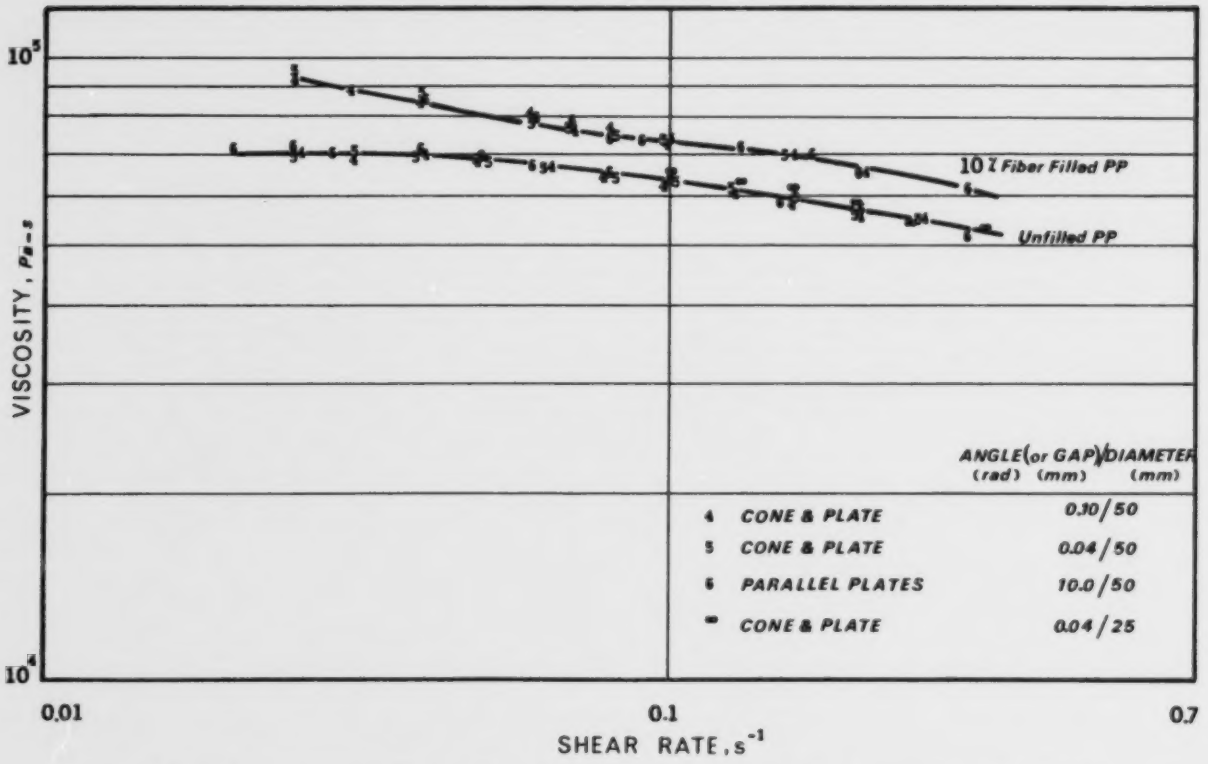

Fig. 5. Steady shear viscosity for unfilled and 10 percent glass fiber filled polypropylene melt at 200°C.

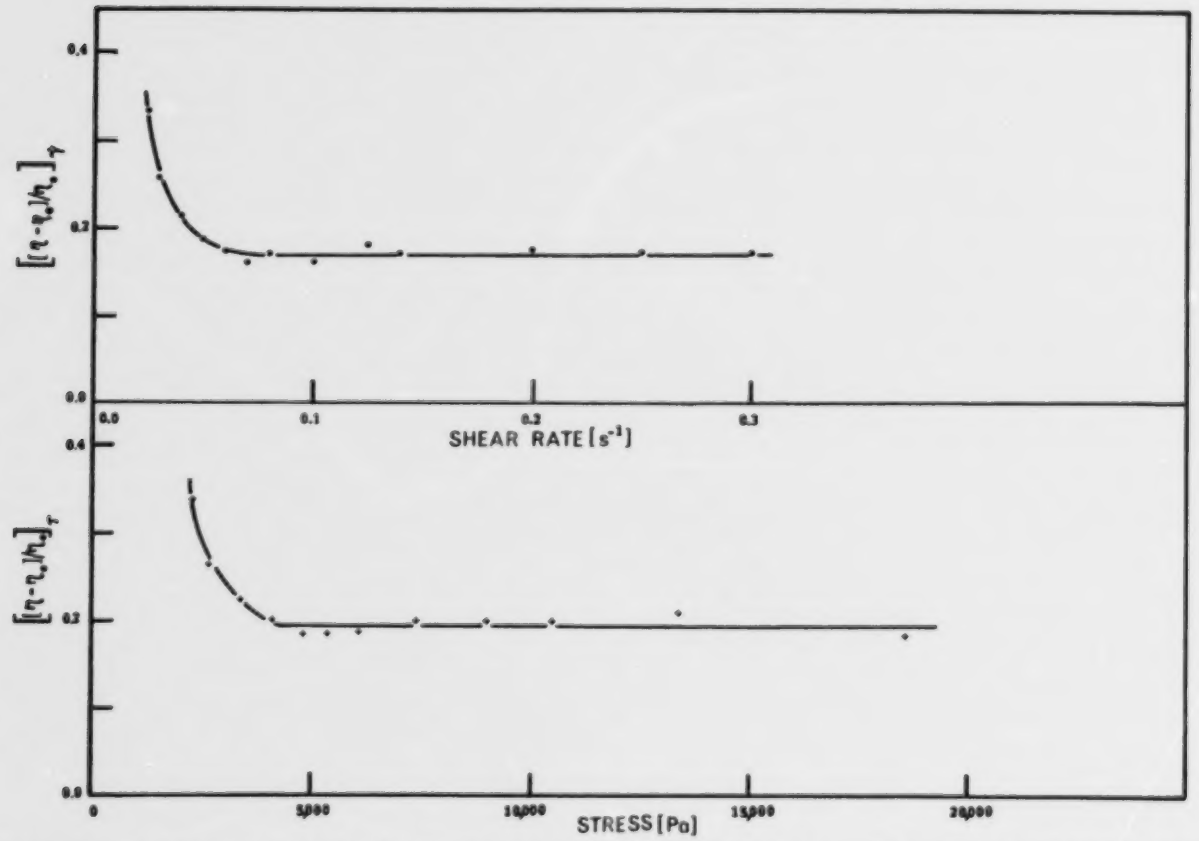

Fig. 6. Relative viscosity based on both stress and strain rate respectively for 10 percent glass fiber filled polypropylene melt at 200°C.

mer would also be subjected to the bulk stress. The relative viscosity here was defined as the ratio between the filled melt viscosity and the unfilled melt viscosity at the same bulk shear stress. The relative viscosity decreased with increasing stress at low stress levels, but it reached an equilibrium value at higher stress levels. The contribution of energy dissipation caused by fibers to total stress was not affected by the total stress at high stress levels.

Oscillatory Shear Results

Unfilled and filled melts were also tested under oscillatory shear using cone-and-plate geometry. A strain sweep test was made, in which the strain was changed from 0.01 to 0.95 keeping frequency and all other parameters constant.

A region, at low strain levels, was observed with the unfilled melt where loss modulus, G'', and storage modulus, G', were independent of strain amplitudes applied. G' and G'' started to decrease with increasing strain at strain amplitudes larger than 0.3 to 0.4. The storage and loss moduli for the filled melt were found to be a strong function of the strain amplitude even at strain levels as small as 1 to 2 percent, as shown in *Fig. 7*. Onogi and Matsumoto (14) observed a similar strain dependency of viscoelastic functions at strain levels as small as 0.5 to 1 percent for small particle filled viscoelastic fluids. This strain-dependent, nonlinear behavior is usually accompanied by an anharmonic stress response for unfilled melts. Anharmonicity in stress response was also observed with small particle filled viscoelastic fluids. However, Parker and Hibbard (15, 16) have observed highly strain dependent viscoelastic functions but a harmonic stress response with wheat flour doughs at large strain amplitudes, using a concentric cylinder rheometer. The viscoelastic functions observed were independent of the strain amplitude at very low strain amplitudes (below 10^{-3}). Loss and storage moduli started to decrease with increasing strain amplitude at strains above 10^{-3}, but the stress response was found to be harmonic. This shows that there is an envelope of strain amplitudes and frequency combinations where the material response is nonlinear in terms of strain dependency but the stress signal is harmonic and the material response can be described by only two parameters, $G'(\omega, \gamma_0)$ and $G''(\omega, \gamma_0)$. Parker and Hibbard attributed this behavior to the fact that if the

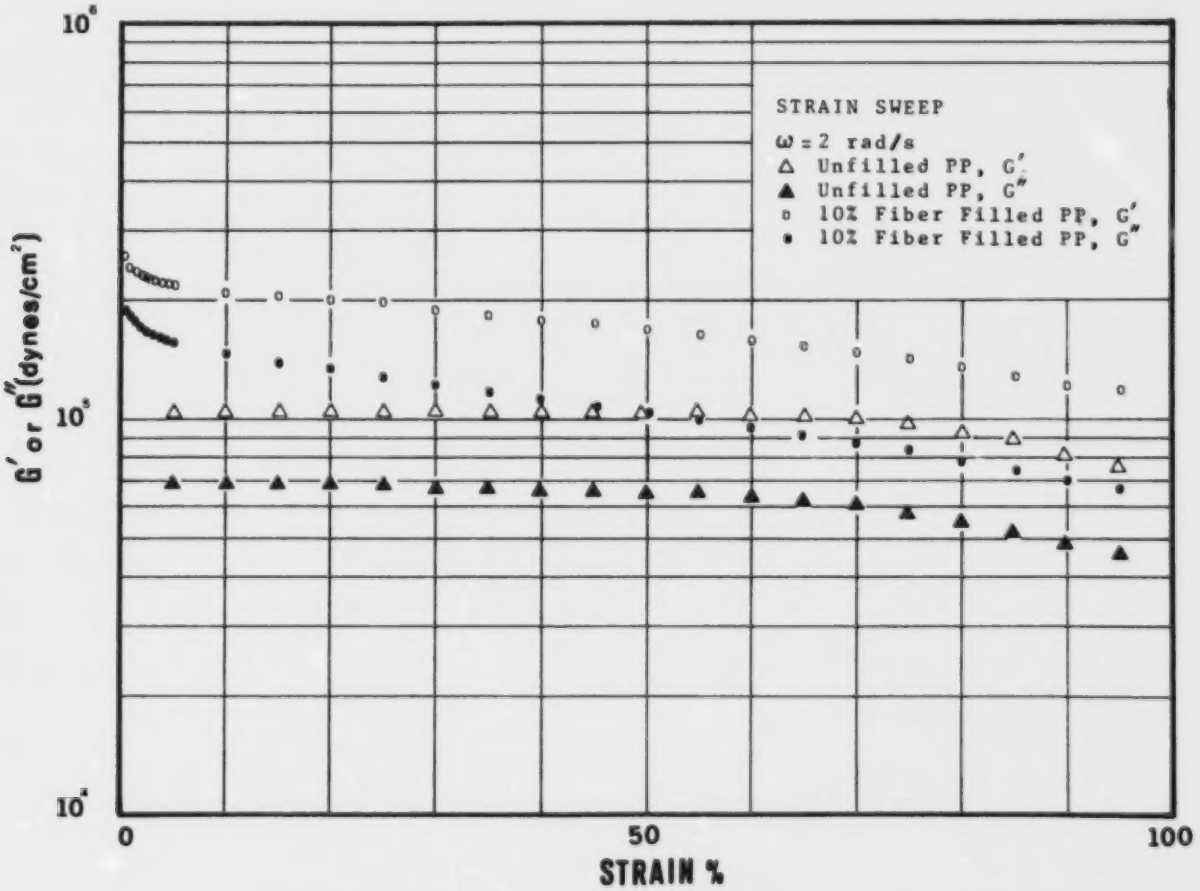

Fig. 7. Strain sweep for unfilled and 10 percent glass fiber filled polypropylene melt at a frequency of 2 rad/s and 200°C.

frequency applied was such that the time constant for changes in the mechanical properties of the material, after a change in the strain, is long compared with the forced vibrations, the deformation in response to a sinusoidal force would also be sinusoidal. Hence, three regions can be distinguishable in material response to sinusoidal deformations: 1) A strain independent and harmonic stress response at low strain amplitudes; 2) A strain dependent and anharmonic stress response at large strain amplitudes and intermediate frequencies; 3) A strain dependent but harmonic stress response at large strain amplitudes and high frequencies. Both types of stress response were observed at large strain amplitudes with polyisobutylene by Giacomin and Dealy (17).

The stress signal was followed, using an oscilloscope, for both filled and unfilled melts. When the stress response is plotted against shear rate, an ellipse should be obtained if the stress is harmonic.

Torque (stress)—shear rate loops are given in *Fig. 8* at a frequency of 0.3 rad/s and strain amplitudes between 0.4 and 1.6 for unfilled melt. The stress-shear rate loops were compared with an ellipse, which had the same axis ratio at 0.4 and 1.6 strain amplitudes. At a strain amplitude of 0.4, the torque—shear rate loop was a perfect ellipse, showing that the stress signal was harmonic. At higher strain amplitudes, the strain response became anharmonic, as clearly seen in the case of 1.6 strain amplitude, and G' and G'' decreased with increasing strain. A transition from the region, where the stress is harmonic and the viscoelastic properties are independent of strain, to the region where the stress is anharmonic and the properties are strain dependent, is exhibited by the deviation in shape from an ellipse and the values of $G'(\omega, \gamma_0)$ and $G''(\omega, \gamma_0)$ listed on the figure.

In the case of fiber-filled melts, the stress response was found to be harmonic, in most cases, as shown in *Fig. 9*. The stress was found to be harmonic up to 2.4 strain amplitude at a frequency of 0.5 rad/s, although the viscoelastic functions G' and G'' were strongly strain-dependent. The phase angle increased with increasing strain, indicating that the viscous dissipation was increased with increasing strain.

Stored elastic energy in unit volume in one-half of a deformation cycle, W, and the work done per cycle of oscillations per unit time, A,

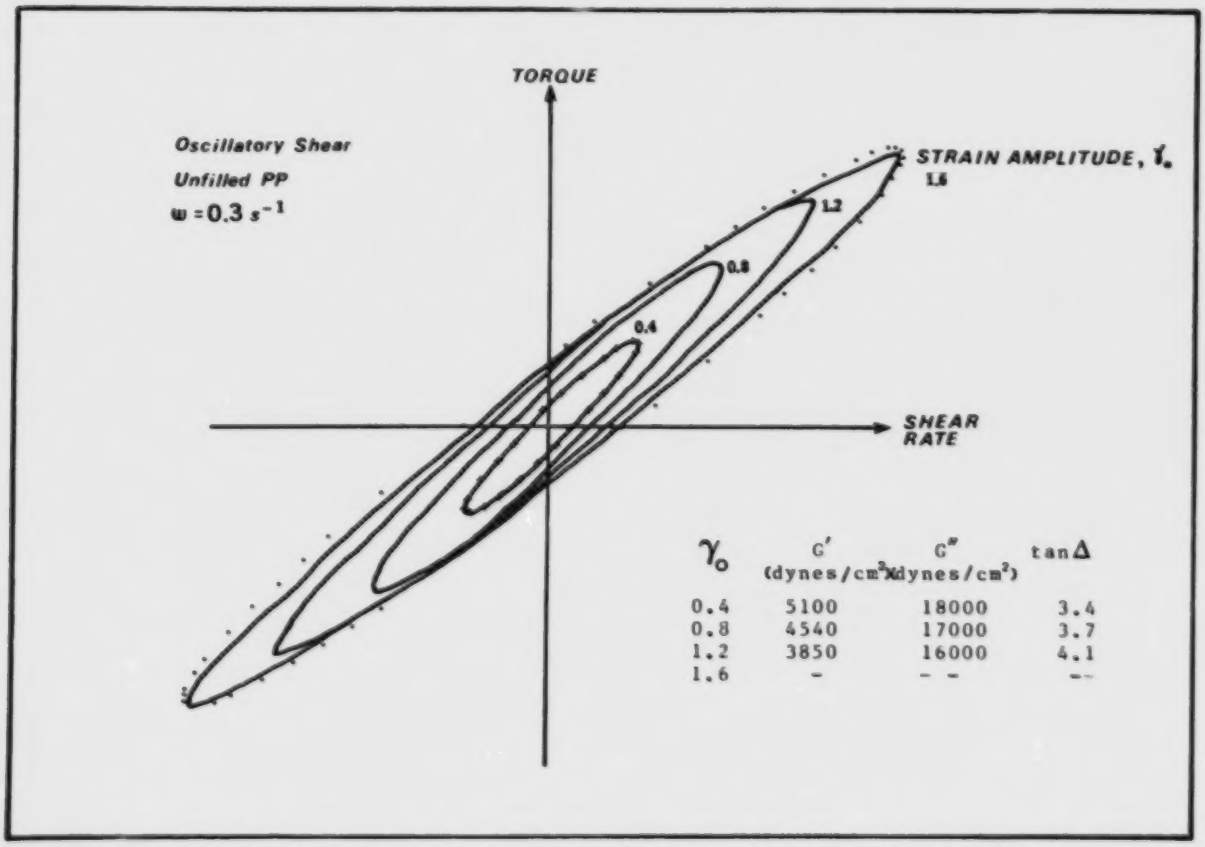

γ_0	G' (dynes/cm²)	G'' (dynes/cm²)	tanΔ
0.4	5100	18000	3.4
0.8	4540	17000	3.7
1.2	3850	16000	4.1
1.6	-	- -	--

Fig. 8. Oscillatory shear results for unfilled polypropylene melt at a frequency of 0.3 rad/s and 200°C. Points correspond to an ellipse with the same axis ratio.

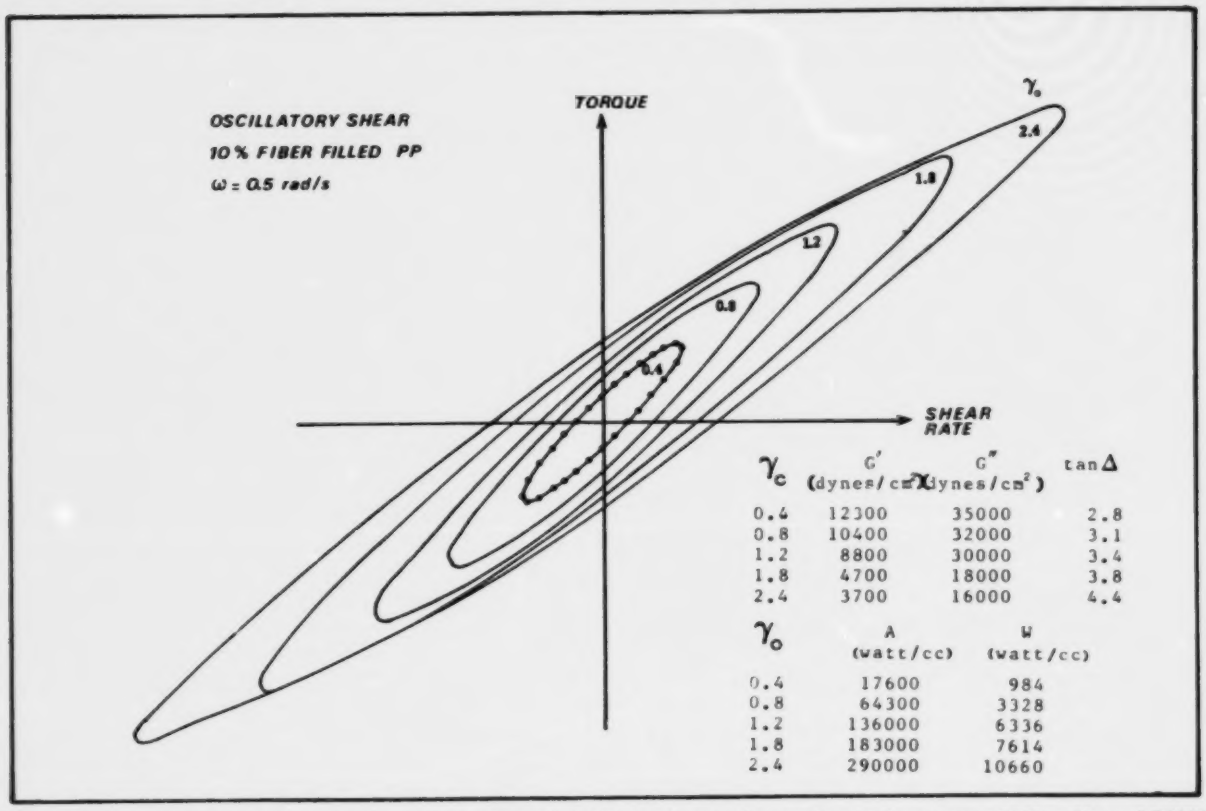

γ_c	G′ (dynes/cm²)	G″ (dynes/cm²)	tan Δ
0.4	12300	35000	2.8
0.8	10400	32000	3.1
1.2	8800	30000	3.4
1.8	4700	18000	3.8
2.4	3700	16000	4.4

γ_o	A (watt/cc)	W (watt/cc)
0.4	17600	984
0.8	64300	3328
1.2	136000	6336
1.8	183000	7614
2.4	290000	10660

Fig. 9. Oscillatory shear results for 10 percent glass fiber filled polypropylene melt at a frequency of 0.5 rad/s and 200°C. Points correspond to an ellipse with the same axis ratio.

were calculated using the well known equations (18):

$$A = \pi\gamma_0^2 G'' \qquad (2)$$
$$W = \gamma_0^2 G'/2$$

The effect of strain amplitude at a frequency of 0.3 rad/s is shown in *Fig. 10*. The stress response was harmonic up to a strain amplitude of 1.8, and became anharmonic at strain amplitudes of 2.4 and 3.0, only one of which is shown to avoid congestion of the figure. A similar behavior, as in the case of 0.5 rad/s, was observed in terms of strain dependence of viscoelastic properties. Transition from the harmonic stress region to the anharmonic region occurred at a strain amplitude of 2.4 for a frequency of 0.3 rad/s, although stress was harmonic at the same strain at a frequency of 0.5 rad/s. The material was given sufficient time to partly relax in one cycle when the frequency was lowered and the stress became anharmonic. At similar strain amplitude-frequency combinations, only a transition from the strain-independent harmonic region to the strain dependent anharmonic region was observed with the unfilled melt.

The effect of frequency on transition is clearly demonstrated in *Figs. 11* and *12*. At a strain amplitude of 1.2 and the three frequencies studied, the stress response was harmonic

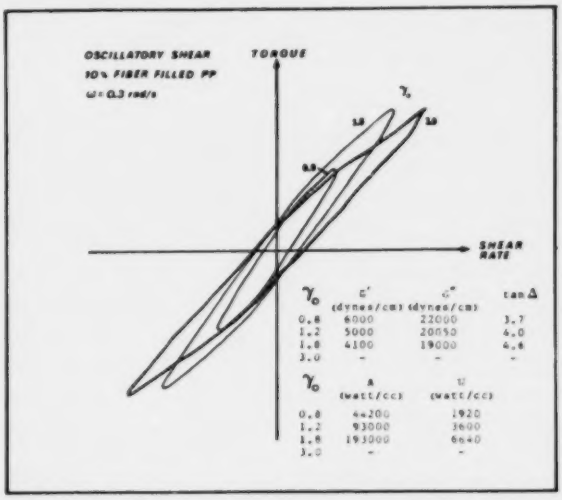

Fig. 10. Oscillatory shear results for 10 percent glass fiber filled polypropylene melt at a frequency of 0.3 rad/s and 200°C.

in all cases, as can be seen from the comparison with an ellipse with the same axes. The frequencies used are apparently above the transition limit at this strain amplitude. If the strain amplitude is increased, the material is forced further from equilibrium and the relaxation process becomes faster. The transition to anharmonicity occurs at a frequency of 0.3 rad/s

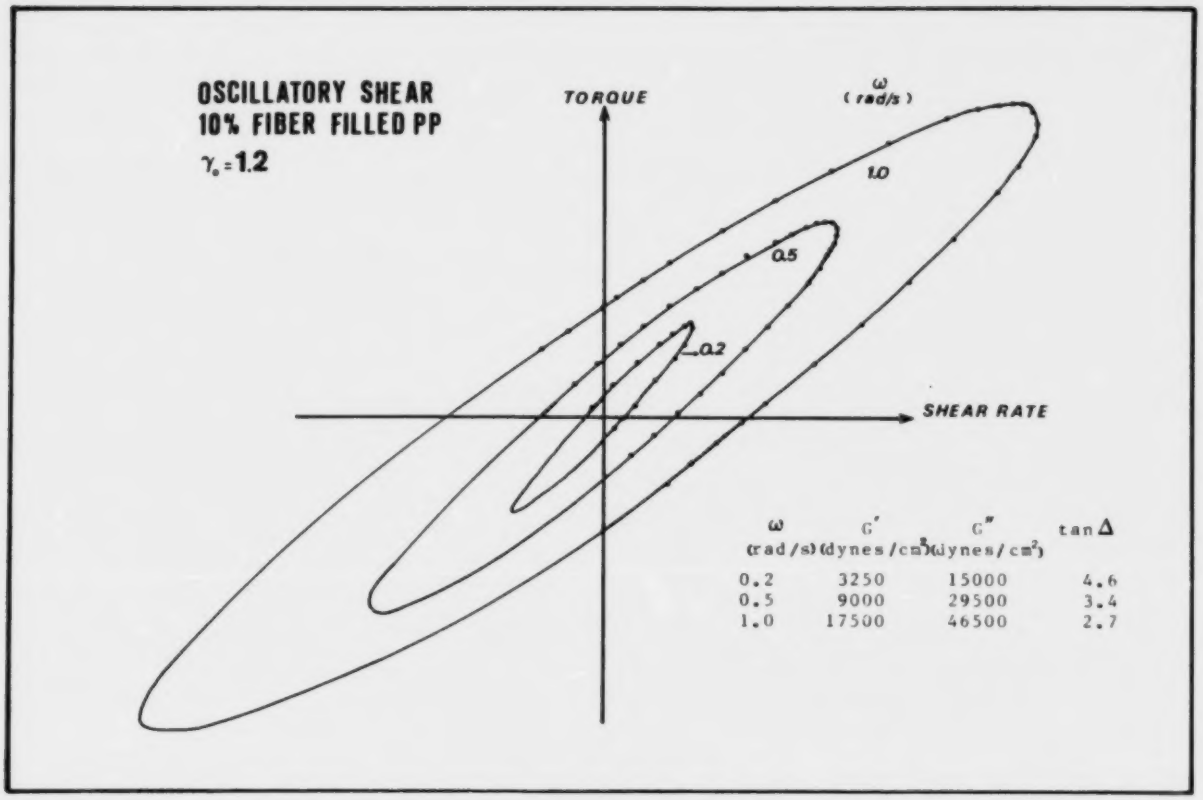

Fig. 11. Oscillatory shear results for 10 percent glass fiber filled polypropylene melt at a strain amplitude of 120 percent and 200°C. Points correspond to an ellipse with the same axis ratio.

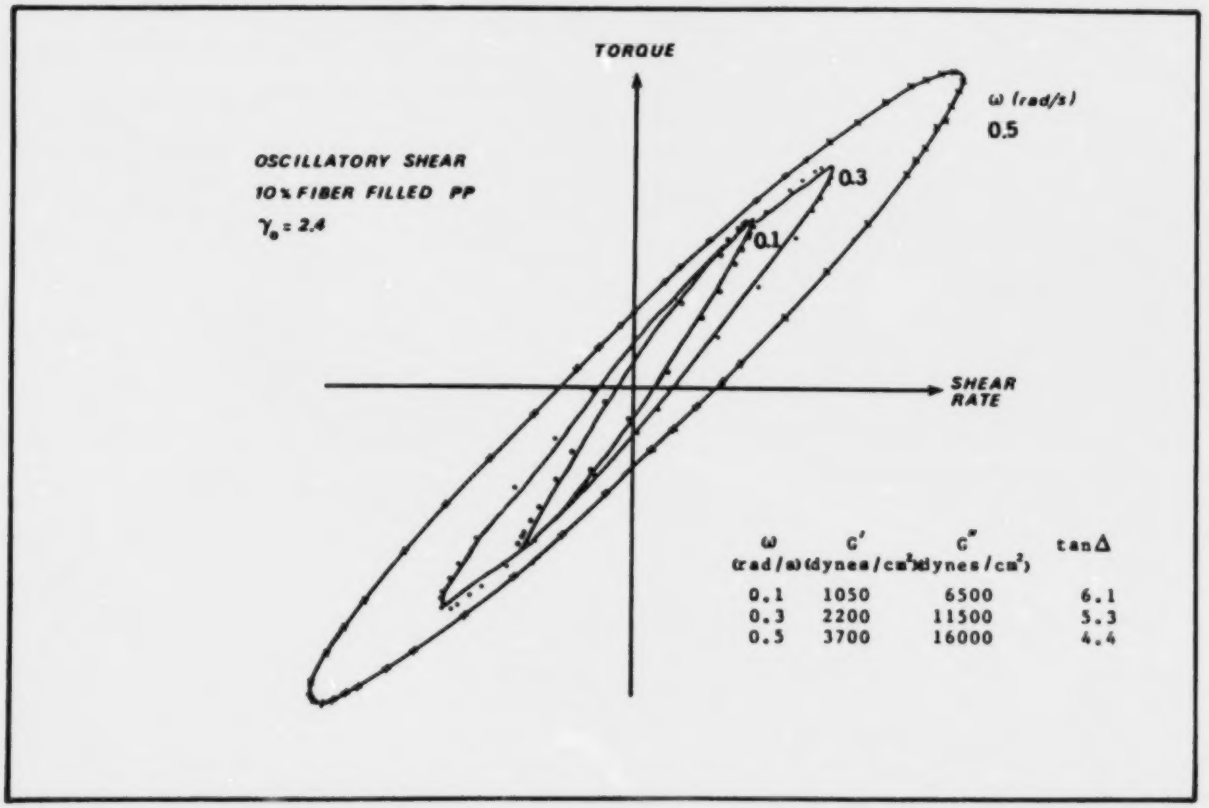

Fig. 12. Oscillatory shear results for 10 percent glass fiber filled polypropylene melt at a strain amplitude of 240 percent and 200°C. Points correspond to an ellipse with the same axis ratio.

for a strain amplitude of 2.4, while the stress is harmonic at 0.5 rad/s, as shown in *Fig. 11*.

In conclusion, viscoelastic functions measured for fiber-filled polypropylene melts are dependent on the dimensions of the flow channel. However, filled melts exhibit geometry- and dimension-independent viscometric properties due to development of steady state orientations within the shear planes. Large stress overshoots are observed in stress growth followed by a thixotropic behavior, which is attributed to the slow change in fiber orientation. The fluid is highly anisotropic, and fiber-wall interactions contribute significantly to the stress during transient flows. The initial state of orientation is an important factor in determining the flow behavior.

A strain dependent but harmonic stress region was observed for filled melts in oscillatory shear as well as an anharmonic stress region at low frequencies and large strain amplitudes. The strain-dependent harmonic stress region is thought to be the result of the much longer time scales for the relaxation of fluid compared to the period of oscillations. In this region, the fluid response can be represented by two parameters, $G'(\omega, \gamma_0)$ and $G''(\omega, \gamma_0)$, and oscillatory shear tests permit the separation of the time and strain dependence of the fiber orientation development.

ACKNOWLEDGMENTS

The authors would like to acknowledge financial support from the following organizations: Engineering Mechanics Department of General Motors Corporation, Natural Sciences and Engineering Research Council of Canada, and Ministère de l'Education of the Government of Quebec.

The following companies supplied the materials and helped in the preparation of the compounds: Himone Canada Inc., Wilson-Fiberfill Canada and Certain Teed Corporation.

REFERENCES

1. T. Kitano, T. Kataoka, M. Sasahara, and K. Nishijima, *Rheol. Acta*, **17**, 149 (1978).
2. T. Kitano, T. Kataoka, and Y. Nagatsuka, *Rheol. Acta*, **23**, 20 (1984).
3. T. Kitano and T. Kataoka, *Rheol. Acta*, **19**, 753 (1980).
4. Y. Chan, J. L. White, and Y. Oyanagi, *J. Rheol.*, **22**, 507 (1978).
5. L. Czarnecki and J. L. White, *J. Appl. Polym. Sci.*, **25**, 1217 (1980).
6. A. T. Mutel and M. R. Kamal, *Polym. Compos.*, **5**, 29 (1984).
7. N. J. Millis, *J. Appl. Polym. Sci.*, **15**, 2791 (1971).
8. T. Kitano and T. Kataoka, *Rheol. Acta*, **20**, 403 (1981).
9. S. Onogi, Y. Mikami, and T. Matsumoto, *Polym. Eng. Sci.*, **17**, 1 (1977).
10. T. Kitano, T. Kataoka, and Y. Nagatsuka, *Rheol. Acta*, **23**, 408 (1984).
11. K. K. Wang, S. F. Shen, C. Cohen, C. A. Hieber, and A. I. Isayev, Computer Aided Injection Molding System Progress Report #8, Cornell Univ. (1981).
12. E. Ganani and R. L. Powell, Abs. 55th Ann. Meeting Soc. Rheol., Knoxville, Tenn. (Oct. 17–20, 1983), *J. Rheol.*, **28**, 479 (1984).
13. M. R. Kamal, A. T. Mutel, and L. A. Utracki, *Polym. Compos.*, **5**, 289 (1984).
14. S. Onogi and T. Matsumoto, *Polym. Eng. Rev.*, **1**, 46 (1981).
15. N. S. Parker and G. E. Hibbard, *Rheol. Acta*, **13**, 910 (1974).
16. G. E. Hibbard and N. S. Parker, *Rheol. Acta*, **14**, 151 (1975).
17. A. J. Giacomin and J. M. Dealy, unpublished data.
18. G. V. Vinogradov and A. Ya. Malkin, 'Rheology of Polymers', p. 61, Mir Publishers (1980).

DISCUSSION

J. L. White: This was an excellent, though provoking paper. When you say "viscometric" and "viscoelastic," what do you mean? Are you including shear viscosity in viscometric? The normal stresses do you include in viscometric are viscoelastic?

A. T. Mutel: This is a matter of definition. The steady state normal stresses are included in viscometric. Anything which is time dependent, I place into viscoelastic.

J. L. White: Often the word "viscoelastic" is meant to represent the behavior of the material which obeys Boltzman's superposition principle. You may have more complicated situation than that because you have particle orientation and matrix effects. The matrix may obey Boltzman principle, but your suspension certainly does not.

A. T. Mutel: But even matrix can obey the Boltzman principle only in a very limited range.

J. L. White: Yes, yes, but your system will not be even asymptotic.

L. A. Utracki: I do not understand your conclusions. In the strain sweep tests both G' and G'' fell very rapidly. Your time sweep results show that the stress growth function varies both with time and geometry. But at the same time, your constant strain torque-rate of shear loops are eliptical and, as you said, without a sign of unharmonicity. Are you saying that these loops were run for a several cycles without any degeneration of the ellipticity?

A. T. Mutel: Each experiment started with new sample. Ten to fifteen cycles were run at high, and three or four at low frequency. No degeneration of the signal was observed. It does not take long to run these tests.

L. A. Utracki: The time scale of these three types of tests is comparable. I do believe the samples to be thermally stable; my concern is related to the stress-strain-time dependent orientation of fiber particles, which is very apparent in the first two tests but absent in the third. It is possible that the method of analysis of your figures is not precise enough?

A. T. Mutel: Although you have strain dependent properties, the stress signal is harmonic. The reason for this is long relaxation time for these materials. The response of the material to the strain is very slow compared to the frequency of the experiment. The result seems to be perfectly harmonic signal.

C. E. Chaffey: How were the samples made before testing? Did you prepare discs and then loaded into the rheometer? Was the disc pre-oriented?

A. T. Mutel: The discs were prepared by compression molding. Only a small degree of orientation was imposed by the process.

Interfacial Interactions and the Properties of Filled Polymers: I. Dynamic-Mechanical Responses

M. Y. BOLUK *and* H. P. SCHREIBER

Department of Chemical Engineering
Ecole Polytechnique de Montréal
Montréal, Québec H3C 3A7

The dynamic mechanical responses of rutile-filled, chlorinated polyethylene (CPE) were studied as a function of temperature, of filler loading, and of filler surface condition. An objective was to establish the influence of matrix-filler interactions on mechanical properties. Necessary information on potential interactions between matrix and filler was obtained from inverse gas chromatographic data, in the form of an acid-base interaction parameter, Ω. The damping peak in filled CPE compounds was depressed by the pigment, as called for by theoretical models. The magnitude of the effect exceeded expectations, however, and clearly depended on the strength of interfacial interactions. These were consistent with the acid-base ranking of CPE and the various rutiles, as given by Ω. It has been postulated that in the presence of acid-base interactions, an immobilized layer of polymer in the vicinity of solid particles increases the effective particle dimension, thereby accounting for the observed variations in relative damping. Additional effects of matrix-filler interaction were noted in the variation of storage moduli with loading and temperature. Again, the effects tend to be more pronounced when significant specific interactions between matrix and solid are operative. These observations point to the inadequacy of existing models as interpretative bases for dynamic mechanical properties in systems with significant specific interactions among their components.

INTRODUCTION

Properties of filled polymer compositions depend on the properties of the individual constituents, adjusted to their volume fractions in the compound. Additional, and more subtle property dependencies involve the degree of dispersion of the filler in the polymer matrix and the nature of the interface between the continuous and dispersed phases. Many surface treatments are applied to fillers and pigments to benefit from interfacial effects and to reduce the cost of compounding operations. A quantitative understanding of interfacial phenomena, however, capable of rationalizing such procedures, remains an important goal in the basic and applied development of filled polymer systems.

In this paper the viscoelastic, dynamic-mechanical properties of filled polymers have been studied by way of contributing to the stated goal. The sensitivity of these properties to the condition of the interface has been documented frequently: In rubbery matrices, fillers tend to increase relative damping (1 to 3), but conversely, the damping peak is decreased in the glassy region (4 to 6). The glass transition temperature, T_g, shifts to a higher temperature as a combined result of the high surface area in fillers and of strong polymer-filler interactions (7, 8). Nielsen (9) and Manson and Sperling (10) briefly reviewed studies on dynamic mechanical properties of composites, but in none of these studies was the issue of treating polymer-filler interactions considered analytically. Guidelines for the preferred design of filler surface treatments in different polymer systems therefore are still needed.

An experimentally accessible route to the quantification of interfacial interactions in polymer compounds involves the use of acid-base

interactions. This route, based on the proton donor/acceptor theories of Drago *et al.* (11), has been developed by Fowkes and coworkers (12, 13), and has recently been extended in these laboratories (14, 15) using the technique of inverse gas chromatography (IGC). This provides a convenient relative ranking of acid-base interactions in polymers and in the solid components of polymer systems. Chlorinated polyethylene (CPE), and polyethylene (PE) have been chosen as polymer matrices for this work. The former is an acidic matrix, capable of strong specific interactions, while in PE interactions may be assumed to arise predominantly from dispersion (Van der Waals) forces. Rutile TiO_2 has been used as the filler, both because of its many applications in plastics and paints and because of its availability in various surface modified forms. The present paper is concerned with CPE-based systems. The behavior of PE systems will be discussed in a forthcoming paper.

EXPERIMENTAL

Materials

The polymer used in this study is a commercially supplied sample of amorphous CPE. The polymer was compounded with 0.5 phr stearic acid and 2 phr calcium stearate stabilizers prior to further use. The rutile pigments were commercially available samples, supplied by Tioxide Canada Ltd. Their B.E.T. surface areas (from N_2 adsorption) were in the range of 7 to 9 $m^2 \cdot g^{-1}$ as shown in *Table 1*.

IGC determinations of acid-base interaction indexes involved the use of a Perkin-Elmer dual column gas chromatograph. Techniques for determining specific retention volumes (Vg^0) of polymers have been discussed previously in detail (16). Pigment samples were supported on glass beads, 10^{-2} cm in diameter. Glass beads and pigments were tumble blended, giving a thin pigment coating to the substrate. Specific retention volumes are given in *Table 1*. The probes, selected for their specific interaction potential (17), were n-butanol (acidic vapor) and n-butylamine (basic vapor). The tabled Vg^0 data are averages of quadruplicate determinations of retention times, corrected for the minor retention characteristics of uncoated glass, obtained from a "dummy" column of glass beads. For present purposes, IGC data were restricted to 90°C. The acid-base interaction potential of polymers and rutiles is expressed in terms of the ratio

$$(Vg^0)_a/(Vg^0)_b \qquad (1)$$

where $(Vg^0)_a$ and $(Vg^0)_b$ are the retention volumes for butanol and butylamine, respectively. The values quoted in *Table 1* introduce the parameter, Ω; for basic subtrates where $(Vg^0)_a > (Vg^0)_b$,

$$\Omega = [(Vg^0)_a/(Vg^0)_b] - 1 \qquad (2a)$$

while for acidic substrates, $(Vg^0)_b > (Vg^0)_a$, and

$$\Omega = 1 - [(Vg^0)_b/(Vg^0)_a] \qquad (2b)$$

Table 1. Material Characterization.

Material	Surface Area ($m^2 \cdot g^{-1}$)	IGC Characteristics $(Vg^0)_a$ ($ml \cdot g^{-1}$)	$(Vg^0)_b$ ($ml \cdot g^{-1}$)	Ω
CPE	—	9.1	24.7	−1.71
TiO_2-1	7.32	688	677	0.02
TiO_2-2	8.55	988	940	0.06
TiO_2-3	7.55	285	106	1.69
TiO_2-4	9.05	200	32	5.25
TiO_2-5	8.52	343	151	1.27
TiO_2-6	7.68	109	18	5.05
TiO_2-7	8.70	1047	1071	−0.02
TiO_2-8	8.98	96	136	−0.42
TiO_2-9	8.64	38	57	−0.50

Blend Preparation and Evaluation

Rutile-filled polymer blends were prepared using a Brabender Plasticorder at 180°C. Pigment content ranged from 3–20 volume percent. In all cases, materials were blended at a rotational speed of 50 r.p.m. Blending was continued for the time needed to attain a steady state torque plus an additional 2 min. This procedure results in the maximum degree of dispersion attainable at the given temperature and by the chosen shearing conditions.

Rutile-filled CPE was compression molded at 180°C to produce plaques 0.05 cm thick. These were quenched in running cold water, and then stored at room temperature for several days prior to further use. The plaques were used to cut test specimens 6.0 cm long with an average cross-sectional area of 0.010 cm^2.

Dynamic mechanical properties were measured over the temperature range, 160°C to −50°C, at a frequency of 100 Hz using the Rheovibron Model DDV-IIB viscoelastometer. The heating rate was $1°C \cdot min^{-1}$. The suggestions of Seferis *et al.* (18) were followed to improve data reproducibility. Measurements included storage and loss moduli, E' and E'', and the mechanical damping tan δ calculated from

$$\tan \delta = \frac{E''}{E'} \qquad (3)$$

RESULTS AND DISCUSSION

Acid-Base Indexes

The values of Ω in *Table 1* show the wide range of acid-base interaction characteristics that can be attained through the surface modification of pigment grade TiO_2. In the group, TiO_2-1 can be regarded as a reference material, no surface treatment having been applied to this calciner discharge sample. The proton donor-acceptor sites in this reference pigment appear to be very closely balanced, nearly equal $(Vg^0)_a$ and $(Vg^0)_b$ resulting in an Ω very close to

the "neutrality" point of zero. Specific surface treatment can produce highly acidic pigment surfaces, as exemplified by TiO_2-8 and TiO_2-9, and also strongly basic surfaces, particularly exemplified by rutiles-4 and -6. Previously determined Ω values indicate strong acidity in the CPE matrix. More detailed analysis of the interaction characteristics of pigments, reinforcing materials, and polymers is in preparation.

Damping Characteristics

The temperature dependence of the loss tangent, and its response to the presence of filler is illustrated for the CPE matrix in *Figs. 1* and *2*. The untreated rutile (-1) is represented in *Fig. 1*, while the effect of the highly basic pigment (-4) is shown in *Fig. 2*. The tan δ peak at 297 K corresponds to the T_g of the polymer (19). It is not affected by the presence of rutile, at any of the loading levels used.

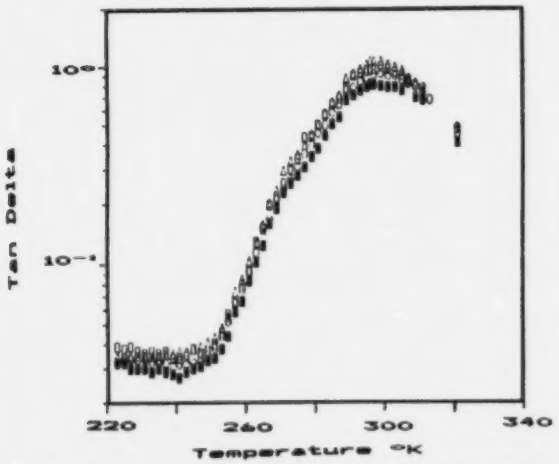

Fig. 1. Loss tangent versus temperature for system CPE-TiO_2-1: volume percent filler: 0 ..... Δ; 3 ..... □; 10 ..... ○; 20 ..... ■

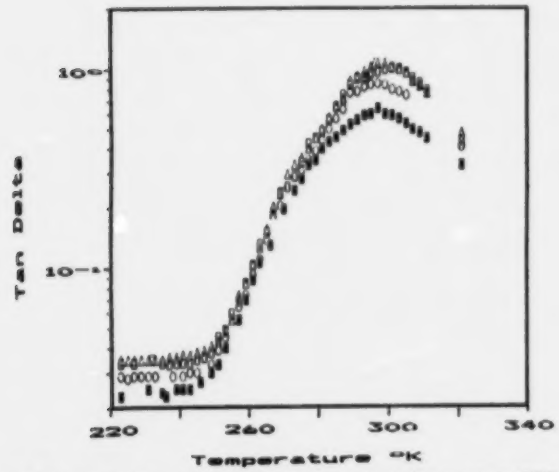

Fig. 2. Loss tangent versus temperature for system CPE-TiO_2-4: volume percent filler: 0 ..... Δ; 3 ..... □; 10 ..... ○; 20 ..... ■

The relative damping of filled polymers, $\tan \delta_c/\tan \delta_p$ (the subscrips c and p referring to compounded and pure polymer, respectively), however, is influenced by the pigment over the entire temperature range. As shown in *Figs. 1* and *2*, the magnitude of the change in $\tan \delta_c/\tan \delta_p$ is also sensitive to the surface coating applied to the rutiles, and therefore appears to be responding to interfacial conditions in the filled compounds.

An interpretation of data such as those shown is possible, taking as a starting point concepts due to Nielsen (20). If damping in filled and unfilled polymers has common origins, then, as shown by Nielsen (20),

$$\tan \delta_c = \tan \delta_p(1 - \phi_f) \qquad (4)$$

where ϕ_f is the volume fraction of the filler. This equation is valid for an agglomerate—free composite, based on rigid solid particles, and excluding interactions (e.g., adhesion) at the polymer—particle interface. The general temperature dependence of relative damping in an amorphous model polymer system is illustrated in *Fig. 3*. As temperature decreases below T_g, relative damping increases since, driven by differences between relevant thermal expansion coefficients, the polymer molecules contract around filler particles (21). This "squeezing" phenomenon will simulate the effects of specific interfacial interactions, even when these are absent.

The damping performance becomes particularly interesting around the T_g; here the matrix phase will not, in general, deform filler particles. Damping, therefore, is due primarily to the polymer phase, and the relative damping should be related simply to the polymer volume fraction, as indicated in *Eq 4*. If there is significant physico-chemical (dispersion force) or specific (e.g., acid-base) interaction between polymer and filler, this will tend to immobilize a layer of polymer around each solid particle. Assuming

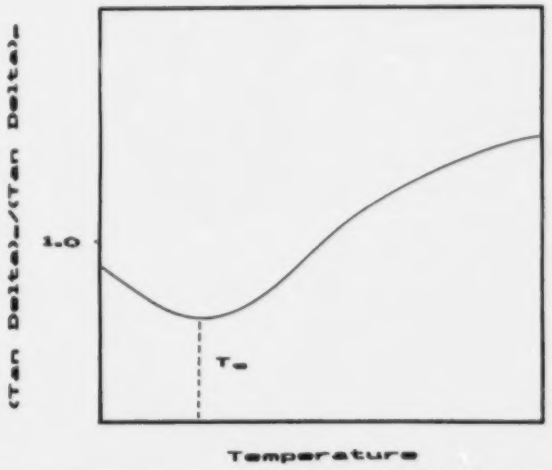

Fig. 3. Typical temperature variation of relative damping in filled, amorphous polymers, following Nielsen (Ref. 20).

the dispersed pigment particles to be rigid spheres, the immobilized polymer layer will contribute to the effective filler volume fraction in the compound. As a result of such polymer-filler interaction, *Eq 4* then can be re-written, with the introduction of a correction parameter B, as shown recently by Iisaka and Shibayama (7),

$$\tan \delta_c = \tan \delta_p(1 - B\phi_f) \quad (5)$$

and applied particularly in the region around T_g. The correction parameter, B, is related to the effective thickness of the particle—matrix *interphase*, through

$$B = (1 + \Delta R/R)^3 \quad (6)$$

where R is the radius of dispersed particles, and ΔR is the thickness of the immobilized polymer layer.

In cases where strong polymer-filler interactions are coupled with high surface area solids, it may be expected that the T_g itself will increase. This effect has been reported, for example, for polyethylene glycol filled with high surface area silica (8). In the rutile-filled polymers, however, as already noted, no significant change takes place in T_g.

The contribution of specific interactions to dynamic mechanical properties is, of course, to be expected in a matrix such as CPE, and is readily apparent in the CPE systems. The interaction potential of the polymer stems from the electron deficiency in hydrogens associated with halogenated carbons, the ensuing electron acceptor sites placing the polymer in the Lewis acid category. Particularly strong interfacial forces should therefore exist when the basic rutiles (e.g., TiO_2-4 and -6) are used as fillers. As shown in *Fig. 4*, the expected trend is clearly established by the relative damping data. For convenience, *Fig. 4* shows only a selection of results. The behavior of polymers using the "neutral" TiO_2-1 is essentially identical to the ideal represented by the Nielsen model (*Eq 4*). This filler evidently satisfies the condition of spherical particle dispersions without adhesion at the solid-matrix interface.

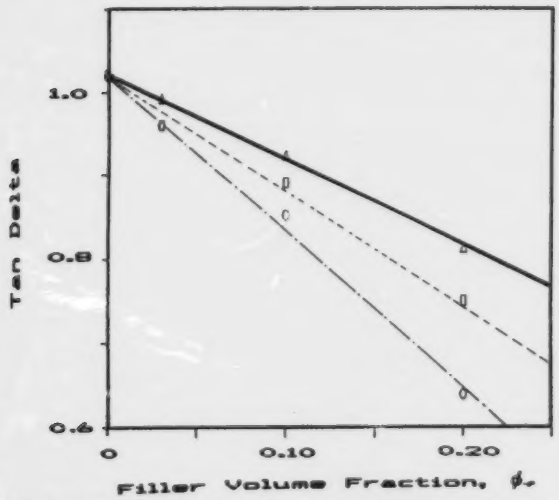

Fig. 4. Loss tangent, δ, as function of filler volume fraction. System CPE-TiO_2 at 297 K; △ TiO_2-1; □ TiO_2-2; ○ TiO_2-4; — Calculated relationship from model for rigid, non-interacting filler.

Deviations from the ideal become manifest with TiO_2-2 and particularly with TiO_2-4. In these cases the deviations from ideality suggest increasing strength of acid-base interactions and thus the formation of appreciable layers of immobilized polymer in the vicinity of dispersed particles, as expressed by the B parameter in *Eq 5*.

The correction parameter, B, can be evaluated from the slope of tan δ versus ϕ_f plots for each CPE-rutile system. The immobilized polymer layer, ΔR, due to specific interactions, was calculated from B values using *Eq 6*. An overview of the relationship between the correction parameter, B, the apparent thickness of the polymer interphase, ΔR, and the acid-base parameter, Ω, is given in *Table 2*. The ΔR values, falling in a range up to about 200 Å, appear to be in good agreement with estimates of immobilized polymer layers reported in the literature (7, 22). In our view, however, their significance is primarily relative. In that context the thick layers built around TiO_2-6, -4, -3, and -5 are clearly consistent with expectations founded on the noted acid-base interaction concepts. The more acidic pigments produce ΔR values of less than 100 Å, but still somewhat greater than the datum for the "neutral," control pigment TiO_2-1. Evidently specific, acid-base interactions at the polymer-filler interface do not entirely rationalize the damping performance of the filled polymer. Further discussion of this matter is planned for a forthcoming publication.

Finally, in this connection, the inferred relationship between B, ΔR, and acid-base concepts, is made explicit in the representation of *Fig. 5*. Evidently, the influence of acid-base interactions is particularly noted in the Ω region between −1 and +1; that is, in the transition between electron donor and acceptor capabilities. An increase in surface basicity beyond the level represented by $\Omega \approx 1$, produces only relatively minor additional increases in polymer immobilization. It seems reasonable that the curve

Table 2. Values of Interaction Parameters in CPE-Rutile Compounds.

Sample	B	ΔR(Å)	Ω
TiO_2-1	1.03	10	0.02
TiO_2-2	1.27	70	0.06
TiO_2-3	1.74	195	1.69
TiO_2-4	1.84	190	5.25
TiO_2-5	1.70	170	1.27
TiO_2-6	1.76	200	5.05
TiO_2-7	1.37	90	−0.02
TiO_2-8	1.23	60	−0.42
TiO_2-9	1.23	60	−0.50

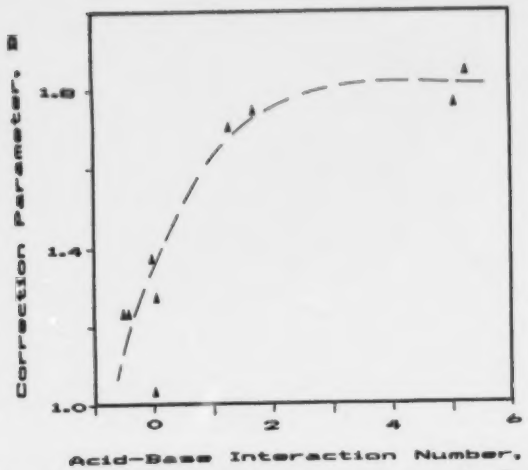

Fig. 5. Correlation between correction parameter, B, and acid-base interaction number, Ω, for CPE-rutile compounds.

in *Fig. 5*, should be "symmetric" about $\Omega = 0$, and that analogously, at increasingly negative Ω values, the parameters B and ΔR would tend to 1.0 and 0, respectively. This point will be clarified when additional, more strongly acidic filler samples become available.

The results of this study, though emphasizing the importance of specific interactions to the development of composite properties, are not intended to overstress that point. Contributions from a variety of other factors should not be neglected in a comprehensive approach to the question of property development in filled polymer compounds. These include among others, the fineness of dispersion attained in the filled compound, interparticle friction, preferential adsorption of matrix components at the filler surface, and an ensuing compositional heterogeneity in the vicinity of the particles. Some of these factors are under continuing study in our laboratory.

Modulus Characteristics

The storage and loss moduli, E' and E'', of composites also appear to be sensitive to conditions at the filler—matrix interface. The present discussion is limited to a consideration of E', and the dependence of the storage modulus on filler content is shown for rutile TiO_2-1 and TiO-4, in *Figs. 6* and *7* respectively. The tendency of the filler to increase the storage modulus is particularly evident at temperatures near and above T_g, as might be expected intuitively.

No truly satisfactory model appears to fit the behavior of moduli in filled polymer compounds. Several empirical expressions for elastic moduli have been proposed (10), but these are not broadly applicable. Perhaps the best known approach, the Kerner expression (23), is based on the concept of a rigid particle suspended in a rubbery matrix. The model does not take in account the contribution of interfacial forces to the elastic modulus of composites, and it is restricted to very low concentrations of the reinforcing component. These limitations notwithstanding, the Kerner model, in modified form, provides a convenient starting point for rationalizing behavior such as that shown in *Figs. 6* and *7*.

In order to modify and simplify the complex Kerner equation, we restrict its applicability to the rubbery state of filled compounds (i.e., $T > T_g$), and assume that the shear modulus of the filler greatly exceeds that of the polymer (i.e., $G_p \gg G_p$). If now the Poisson ratio for the polymer equals 0.5, then at given filler volume fraction, ϕ_f, the Kerner equation may be written as

$$\frac{E_c}{E_p} = \frac{1 + 1.5\phi_f}{1 - \phi_f} \tag{7}$$

Since G_f and ν do not appear explicitly, then

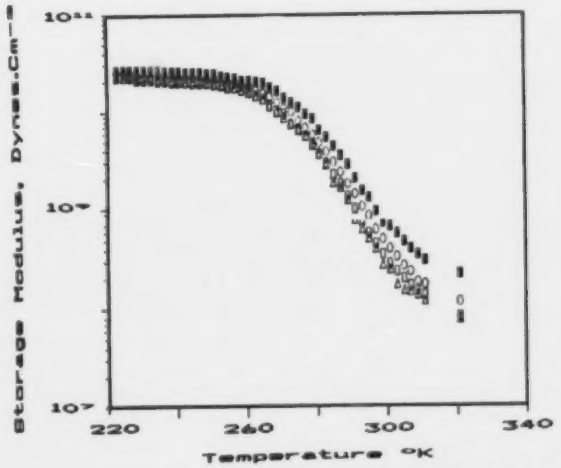

Fig. 6. Temperature dependence of storage modulus for CPE-TiO_2-1. Volume percent filler: 0 ..... Δ: 3 ..... □: 10 ..... ○: 20 ..... ■.

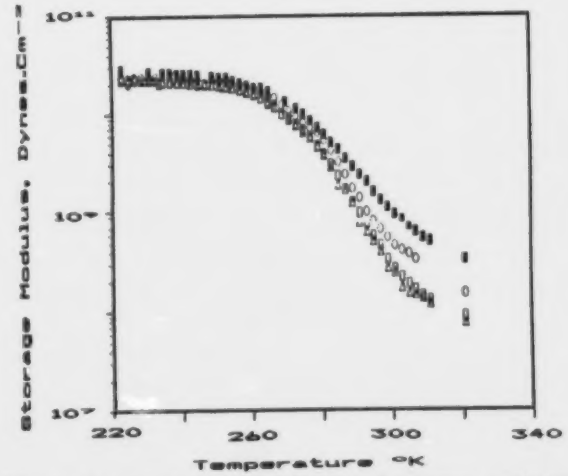

Fig. 7. Temperature dependence of storage modulus for CPE-TiO_2-4. Volume percent filler: 0 ..... Δ: 3 ..... □: 10 ..... ○: 20 ..... ■.

following Hashin (24), the principle of viscoelastic correspondence permits the substitution of storage or complex moduli in *Eq 7*. Not surprisingly, however, the suitably altered *Eq 7* did not describe the E' versus ϕ_f relationship for any of the fillers used. An interaction parameter, A, was therefore introduced to account for the contribution, particularly, of specific (acid-base) polymer-filler interactions. To counteract the limitation of very dilute filler concentrations inherent in the Kerner model, a reduced concentration term, ψ, was also introduced. Following Nielsen (20), the reduced concentration term is defined

$$\psi = 1 + [(1 - \phi_m)/\phi_m^2]\phi_f \qquad (8)$$

where ϕ_m is the maximum packing fraction of the filler and ϕ_f is the filler volume fraction. *Equation 7* is then rewritten in the form

$$\frac{E'_c}{E'_p} = \frac{1 + 1.5A\phi_f}{1 - \psi A\phi_f} \qquad (9)$$

As shown in *Fig. 8*, *Eq 9* is quite successful in describing the filler load dependence of the relative modulus in CPE compounds. The solid lines in the figure have been generated for A = 2.0, 2.5, and 2.7 and for an assumed maximum packing fraction $\phi_m = 0.7$. The general conclusion from this representation is that a close relationship exists between the A parameter and the B parameter introduced earlier in connection with the relative damping properties of filled polymers. Thus, the data for compounds with basic rutiles (TiO_2-4, -5, -6) fit calculations using high A values. However, in contrast with the damping data, from which the Nielsen model permitted calculation of the thickness of the immobilized polymer layer, a similar estimate from the A parameter would call for the assumption that the modulus of the immobilized polymer layer was equal to that of the filler. Such an assumption seems unwarranted, and therefore the thickness of the immobilized polymer layer has not been calculated from this data base.

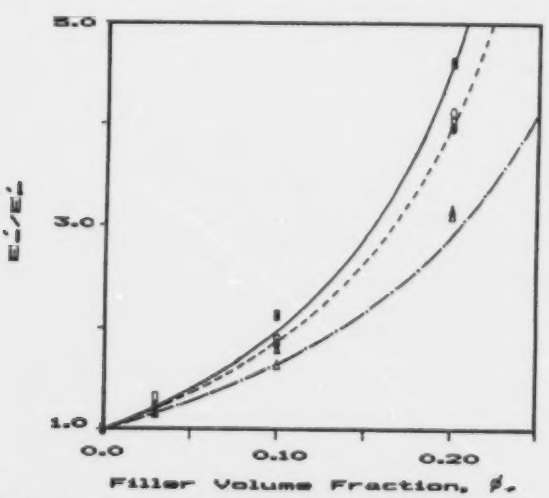

Fig. 8. Comparison of predicted relative modulus with experiments at T = 321 K: △ CPE-TiO_2-1; □ CPE-TiO_2-3; ■ CPE-TiO_2-4; ○ CPE-TiO_2-5; ● CPE-TiO_2-6; ▲ CPE-TiO_2-9; (——) A = 2.7, ϕ_m = 0.70; (– – – –) A = 2.5, ϕ_m = 0.70; (—··) A = 2.0, ϕ_m = 0.70.

ACKNOWLEDGMENT

We thank Tioxide Canada Ltd, Sorel, Québec, for material support of this work and for many helpful discussions. Portions of this research were supported by operating grants from the Natural Sciences and Engineering Research Council, Canada.

REFERENCES

1. R. D. Bohme, J. Appl. Polym. Sci., **13**, 1097 (1968).
2. K. D. Ziegel and A. Romanov, J. Appl. Polym. Sci., **17**, 1119 (1973).
3. G. Kraus, *Adv. Polym. Sci.*, **8**, 155 (1971).
4. I. Galperin and T. K. Kwei, J. Appl. Polym. Sci., **10**, 673 (1966).
5. V. P. Chacko, F. E. Karasz, and R. J. Farris, *Polym. Eng. Sci.*, **22**, 968 (1982).
6. D. R. Saini, A. V. Shenoy, and V. M. Nadkarni, J. Appl. Polym. Sci., **29**, 4123 (1984).
7. K. Iisaka and K. Shibayama, J. Appl. Polym. Sci., **22**, 3135 (1978).
8. A. Yim, R. S. Chahal, and L. E. St-Pierre, *J. Colloid Interf. Sci.*, **43**, 583 (1973).
9. L. E. Nielsen, "Mechanical Properties of Polymers and Composites," Vol. 2, Dekker, New York (1974).
10. J. A. Manson and L. H. Sperling, "Polymer Blends and Composites," Plenum, New York (1976).
11. R. S. Drago, G. G. Vogel, and T. E. Needham, *J. Am. Chem. Soc.*, **93**, 6014 (1971).
12. F. W. Fowkes and S. Maruchi, *Prepr. Am. Chem. Soc., Div. Polym. Chem.*, **37**, 606 (1977).
13. M. J. Marmo, M. A. Mostafa, H. Jennal, F. W. Fowkes, and J. A. Mason, *Ind. Eng. Chem. Prod. Res. Dev.*, **15**, 206 (1976).
14. H. P. Schreiber, M. R. Wertheimer, and M. Lambla, J. Appl. Polym. Sci., **27**, 2269 (1982).
15. H. P. Schreiber, C. Richard, and M. R. Wertheimer, in "Physicochemical Aspects of Polymer Surfaces," Vol. 2, K. L. Mittal, ed., Plenum, New York (1983).
16. C. S. Su, D. Patterson, and H. P. Schreiber, J. Appl. Polym. Sci., **20**, 1025 (1976).
17. V. Gutmann, "The Donor-Acceptor Approach to Molecular Interactions," Plenum, New York (1978).
18. A. R. Wedgewood and J. C. Seferis, *Polymer*, **22**, 966 (1981).
19. C. E. Locke and D. R. Paul, *Polym. Eng. Sci.*, **13**, 308 (1973).
20. L. E. Nielsen, *J. Polym. Sci., Polym. Phys. Ed.*, **17**, 1897 (1979).
21. L. E. Nielsen and T. B. Lewis, *J. Polym. Sci., A-2*, **7**, 1705 (1969).
22. A. Yim and L. E. St-Pierre, *Polym. Lett.*, **37**, 237 (1967).
23. E. Kerner, *Proc. R. Soc.*, **69B**, 808 (1956).
24. Z. Hashin, *J. Solid Structures*, **6**, 539 (1970).

DISCUSSION

C. L. Beatty: I want to congratulate you for an excellent piece of work and the presentation. Were both polyethylene samples semicrystalline?

M. Y. Boluk: The chlorinated polyethylenes we used as matrix material were amorphous. They were chlorinated in solution. The low density

polyethylene was semicrystalline. It would be interesting to examine the effect of filler on the morphological changes of the crystal.

C. L. Beatty: Yes, this is what I was about to ask.

M. Lambla: Did you use frequencies other than 100 Hz to characterize the immobilized layer?

M. Y. Boluk: No. We used only one frequency, 100 Hz.

M. Lambla: Would you expect that by changing the frequency you could see different thicknesses of the immobilized layer?

M. Y. Boluk: I think that frequency change would be equivalent to temperature variation.

M. Lambla: I am not certain if this is true for your system. In effect you are not measuring a thickness but the extent of interaction. In your table there were several products with different levels of acid-base interaction but the thickness was about the same.

M. Y. Boluk: What is important is not the absolute value of the acid-base level of the filler but the balance with the matrix material.

H. P. Schreiber: These figures on the immobilized polymer layer are only relative. I am quite convinced that changing the frequency would produce another set of values. But, the point is that in the absence of strong acid-base coupling you do get categoric differences in the total amount of immobilized layer.

Characteristics of Thermoplastics Containing Electrically Conducting Asymmetric Particles: Anisotropic Electrical Conductivity of Injection Molded Parts and Extrusion Behavior

JAN MARTINSSON* *and* JAMES L. WHITE

Polymer Engineering Center
University of Akron
Akron, Ohio 44325

The characteristics of compounds of acrylonitrile-butadiene-styrene and high impact polystyrene resins, filled with carbon fibers, steel fibers, carbon black, and aluminum flakes have been investigated with special emphasis on electrical conductivity and flow behavior in a capillary rheometer. Compression and injection molded compounds were found to be highly electrically anisotropic. The components of the electrical conductivity tensor, κ_{11}, κ_{22} and κ_{33}, were measured. Generally κ_{11}, the flow direction conductivity, has the highest value and the thickness direction, and κ_{33} has the lowest. The injection molded parts were usually electrically heterogeneous with the conductivities highest at the greatest distances from the gate. The results were interpreted in terms of particle orientation and distribution. Shear viscosities were measurable for all but the aluminum flake compounds which exhibited fluctuating pressure drops. The flow of these compounds through dies was investigated. Examination of material from the die entrance indicated streamline flow without entrance vortices. Sometimes high entrance concentration of particulates were observed especially for the aluminum flakes. Extrudates were found to contain oriented particles.

INTRODUCTION

Electrically conducting particles are being commercially compounded into thermoplastics to produce compounds that may be molded into products suitable as electromagnetic wave interference (EMI) shielding (1 to 5). The types of particles used include steel and carbon fibers and aluminum flakes as well as carbon black. The EMI shielding phenomenon is complex in nature and is associated with both (i) reflection of waves by the particles and (ii) the electrical conductivity of the filled plastic, which causes dissipation of the electromagnetic waves. The two phenomena are well known in electromagnetic theory (6, 7). This makes the study of electrical conductivity of compounds of great importance (8 to 11).

The literature on EMI shielding treats it as electrically isotropic. It is well known that fiber and flakes orient during the processing of particle filled thermoplastics (12 to 17), and the level of orientation varies with process history. As the electrical conductivity of the compounds is due to the presence of the particles, it should be expected that the electrical conductivity has anisotropic characteristics and differs with direction. It is the purpose of this paper to investigate the extrusion and injection molding characteristics of EMI compounds and to study the anisotropy of electrical conductivity of molded products.

EXPERIMENTAL

Materials

The materials used in this study were high impact polystyrene (HIPS) and acrylonitrile-butadiene styrene (ABS), resins compounded with aluminum flakes, carbon fibers, steel fibers,

* Permanent Address: *LM Ericsson, Box 2072, 29102 Kirstianstad, Sweden.*

and carbon black. The HIPS was supplied by BASF (Polystyrole 475). The ABS resins were obtained from two suppliers. These were BASF (Teluran 967) and CdF Chimie (Ugikral SN). We designate these as ABS-1 and ABS-2, respectively. The characteristics of the particulates used are summarized in *Table 1*. The compositions of the compounds are contained in *Table 2*.

Compounding

The carbon black, steel fiber, carbon fiber, and aluminum flake compounds were primarily made by Buss AG (Switzerland) using a Buss-kneader MDE 46-11D. The ABS samples with 6 and 8 weight percent steel fiber and the HIPS with 6 weight percent steel fibers were made by Bakaert AG, (Belgium) using a single screw extruder.

Capillary Extrusion Pressure Studies and Viscosity

The extrusion of the compounds through a capillary die was investigated using an Instron Capillary Rheometer. Measurements for the HIPS compounds were carried out at 200°C and for the ABS compounds at 230°C. Capillaries with diameters of 1.5 and 2 mm were used with most studies involving the former set. The 1.5 mm dies had length-diameter (L/D) ratios of 10, 20, and 30. The 2.0 mm dies, which were also used with the aluminum flake compounds, had L/D ratios of 7.5, 15, and 22.5.

The data was used to compute shear viscosities where possible (14, 15, 18, 19). This involved making ends pressure loss corrections using the various length-diameter ratio dies and the Weissenberg shear rate correction (18,19). Specifically the pressure, p_T, was expressed as

$$p_T = \Delta p_{ends} + 4(\sigma_{12})_w \frac{L}{D} \qquad (1)$$

where Δp_{ends} is the ends pressure loss and $(\sigma_{12})_w$ is the die wall shear stress. The die wall shear rate, $\dot{\gamma}_w$, was determined from

$$\dot{\gamma}_w = \left(\frac{3n' + 1}{4n'}\right) \frac{32Q}{\pi D^3} \qquad (2a)$$

where

$$n' = \frac{d \log(\sigma_{12})_w}{d \log 32Q/\pi D^3} \qquad (2a)$$

Q is the volumetric extrusion rate.

Die Entrance Flow

The flow patterns in the rheometer near the die entrance were examined in more detail in a number of compounds. Following extrusion, the rheometer was cooled, and the solidified rods were pushed from the reservoir and longitudinally sectioned. This procedure is essentially that used by Ma, *et al.* (20 to 22) for small particle-filled compounds.

Fabrication of Molded Products

Parts were fabricated from the compounds by both compression and injection molding. A Wabash compression molding press was used to prepare sheets of dimensions 200 x 200 x 1.5 mm. The HIPS sheets were molded at 200°C and the ABS at 230°C.

Tensile bars and circular plaques were injection molded on a Boy 155 screw injection molding machine. The dimensions of the bars and plaques are shown in *Fig. 1*. The HIPS was injection molded at 200°C and the ABS com-

Table 2. Compounds Used in this Study.

Polymer	Particulates	Weight Percent	Volume Percent
HIPS	Steel Fiber	4, 6, 8	0.5, 0.8, 1.1
	Carbon Fiber	10, 20, 30	5.8, 11.6, 17.5
	Aluminum Flakes	20, 30, 40	7.8, 11.7, 15.6
	Carbon Black	5, 10, 16.3	2.9, 5.8, 9.5
ABS-1	Steel Fiber	4, 6, 8	0.5, 0.8, 1.1
	Carbon Fiber	10, 20, 30	5.8, 11.6, 17.5
	Aluminum Flakes	20, 30, 40	7.8, 11.7, 15.6
	Carbon Black	5, 10, 14.3	2.9, 5.8, 8.3
ABS-II	Steel Fiber	4, 6, 8	0.5, 0.8, 1.1
	Carbon Fiber	10, 20, 30	5.8, 11.6, 17.5
	Aluminum Flakes	20, 30, 40	7.8, 11.7, 15.6
	Carbon Black	5, 10	2.9, 5.8, 8.3

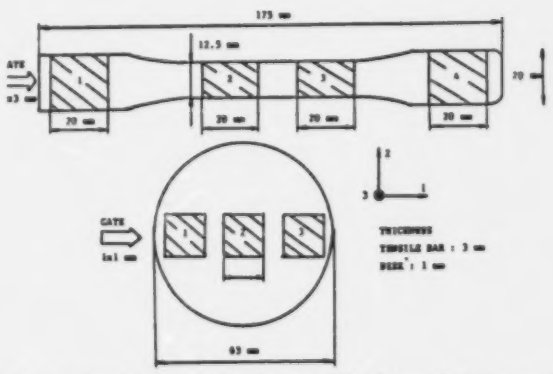

Fig. 1. Dimensions of injection molded tensile bars and discs.

Table 1. Characteristics of Particulates Used.

Particle	Supplier	Type	Specific Gravity	Smallest Dimension	Aspect Ratio
Steel Fiber (SF)	Bakaert	1-4B-610-6	7.85	7 μm	860
Carbon Fiber (CF)	Courtaulds	Hysol Grafic FSD	1.89	7 μm	860
Aluminum Flake (AF)	Transmet	K102-HE	2.7	25 μm	40–55
Carbon Black (CB)	Cabot	Black Pearls 2000	1.89	0.015 μm	—

pounds at 230°C. Two different injection speeds were used.

Electrical Conductivity

The electrical conductivity was measured at various positions in molded specimens. In studies of injection-molded plaques and bars, samples were removed as indicated in *Fig. 1*. Generally four samples were removed from the tensile bars and three from the plaques. The conductivities were measured in three perpendicular directions. These include the flow direction (1), the direction transversed to flow (2), and the perpendicular or neutral direction (3).

The arrangements for measurements are shown in *Fig. 2*. Silver wires were attached to the sample on opposite sides. These sides were then painted with silver paint, minimizing the contact resistance between wire and sample. The voltage E was measured as a function of current I using an ampere and a voltage meter; and the resistance, R, was calculated using Ohm's Law. The conductivity, κ, and resistivity, r, were calculated from

$$\frac{E}{I} = R = \frac{A}{\kappa d} = \frac{rA}{d} \qquad (3)$$

where A is the painted area, and d the distance between the wires/electrodes.

Scanning Electron Microscopy

A JEOL Model U3 scanning electron microscope was used to characterize the state of some of the fabricated products.

EXTRUSION

Pressure and Viscosity Measurements

The compounds containing steel fibers, carbon fibers, and carbon black extruded uniformly through the capillary dies with smooth pressure time traces. Addition of particulates generally increased pressure gradients at specific extrusion rates. The compound with aluminum flakes exhibited a rather different response. The pressure traces exhibited random large amplitude pressure fluctuations. This is discussed in *Fig. 3*.

The uniform pressure traces for dies of varying L/D were converted into shear viscosity. The results of the shear viscosity measurements are shown in *Figs. 4* to *7*. The base resins are exhibited in *Fig. 4*. They show viscosity functions decreasing with increasing shear rate.

Figure 5 compares the various compounds of HIPS. It may be seen that increasing weight or volume loading increases the shear viscosity and this is most pronounced at low shear rates. At equivalent weight fractions (i.e., 0.05 carbon black, 0.04 or 0.08 steel fibers or 0.10 carbon black, 0.10 carbon fibers, 0.08 steel fibers), it may be seen that the viscosities order as

Lower weight percent carbon black
> steel fibers (4a)

Higher weight percent carbon black
> carbon fibers > steel fibers (4b)

The data would order in the same manner if comparisons were made at the same volume fraction.

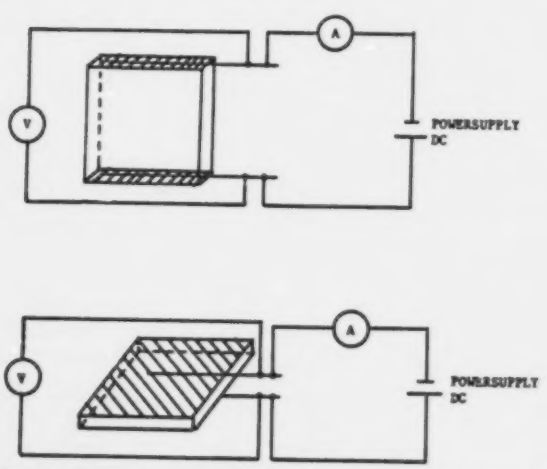

Fig. 2. Arrangement for electrical conductivity measurements.

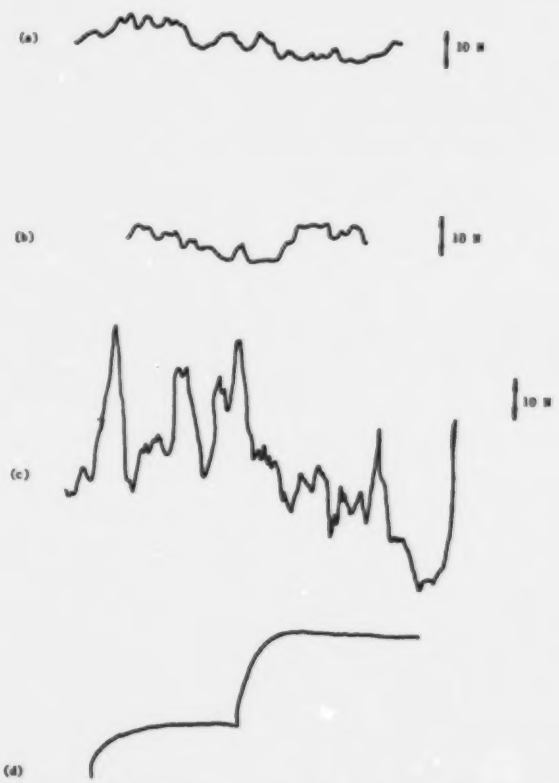

Fig. 3. Typical pressure traces for (a) steel fiber, (b) carbon fiber, (c) aluminum flake, and (d) carbon black compounds.

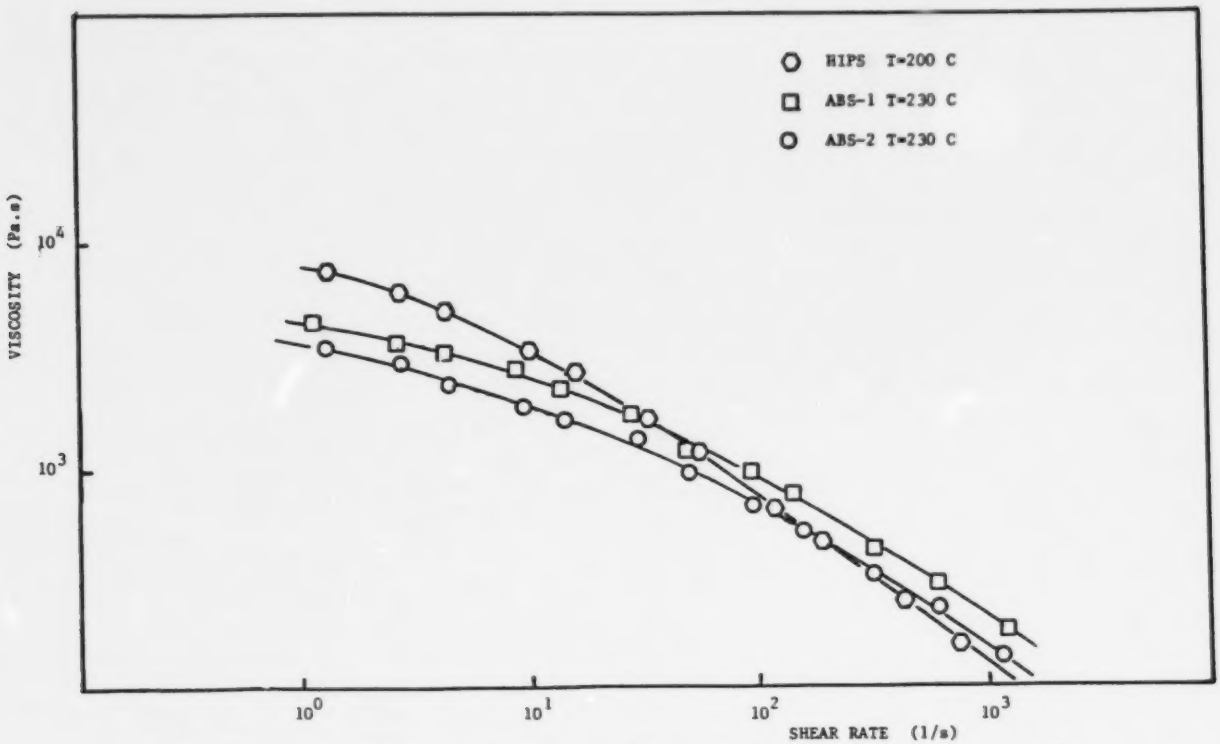

Fig. 4. Shear viscosity of base resins of this study HIPS (200°C), ABS-1 (230°C), ABS-2 (230°C).

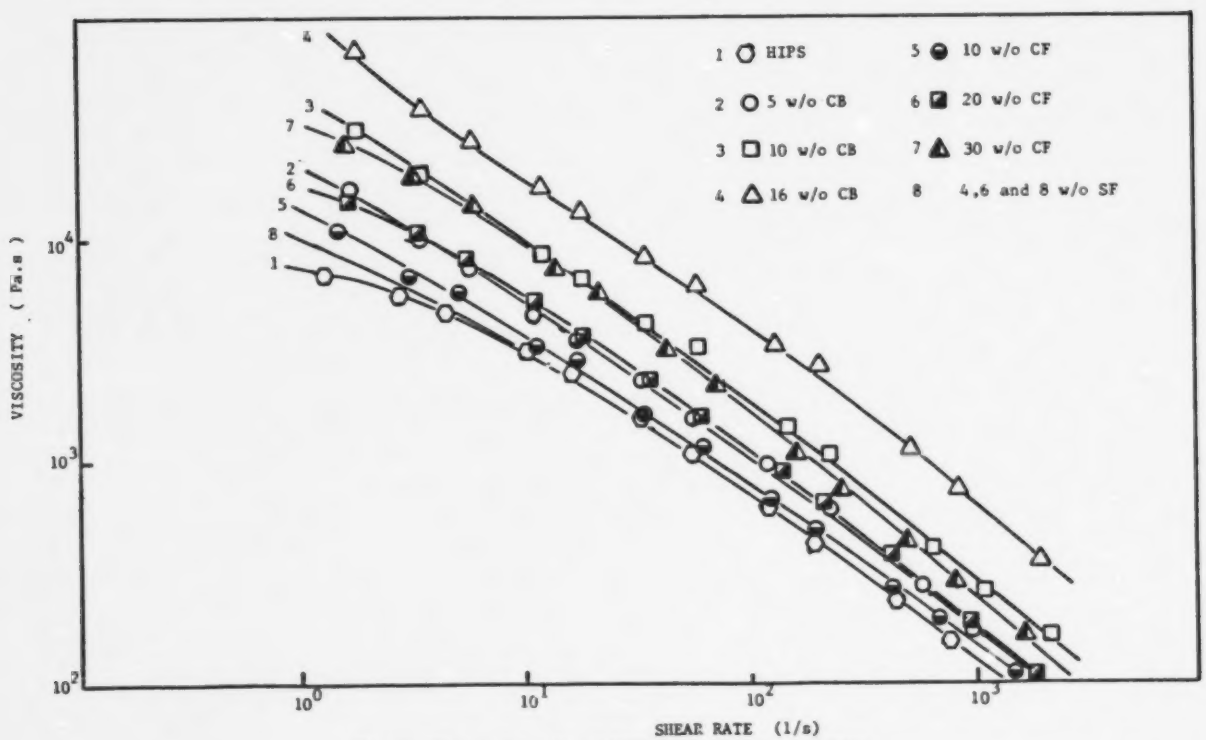

Fig. 5. Shear viscosity of HIPS compounds at 200°C.

The behavior of the ABS compounds are shown in *Figs. 6* and 7. The behavior at the lower loadings is the same as for HIPS and is indicated in *Eq 4a*. For ABS-1, it appears that the carbon fiber compounds have at the higher loading

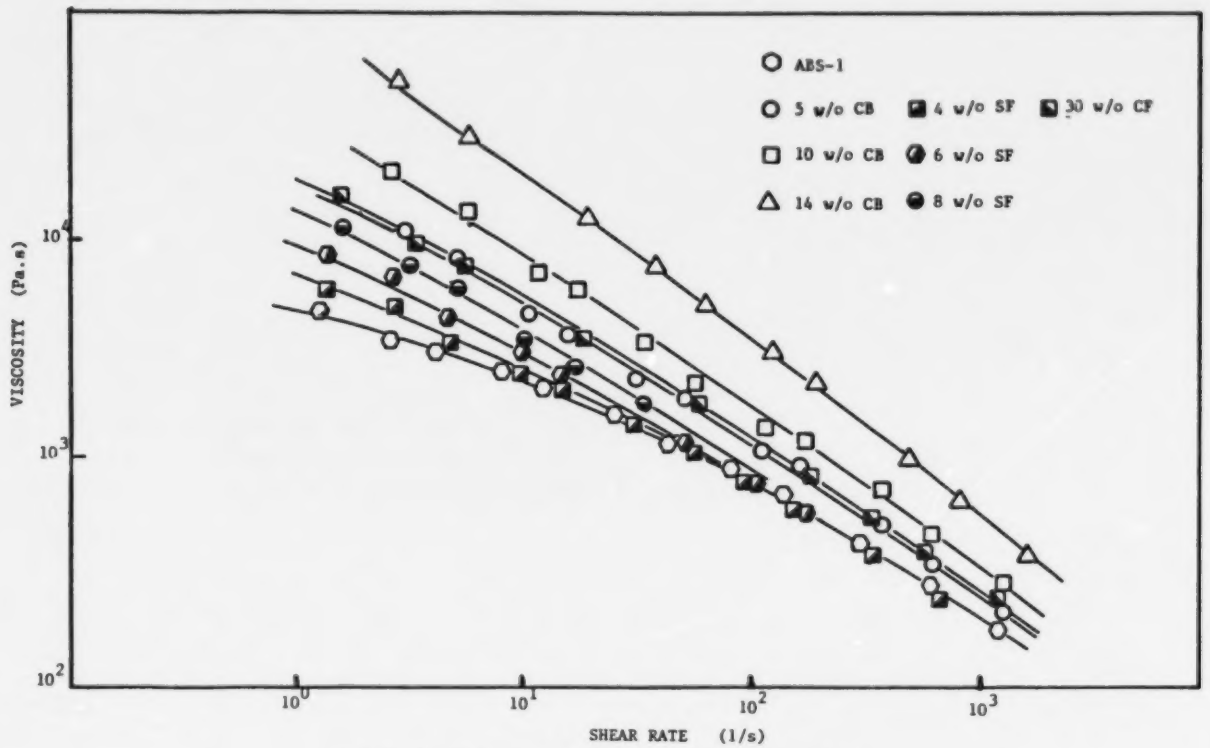

Fig. 6. Shear viscosity of ABS-1 compounds at 230°C.

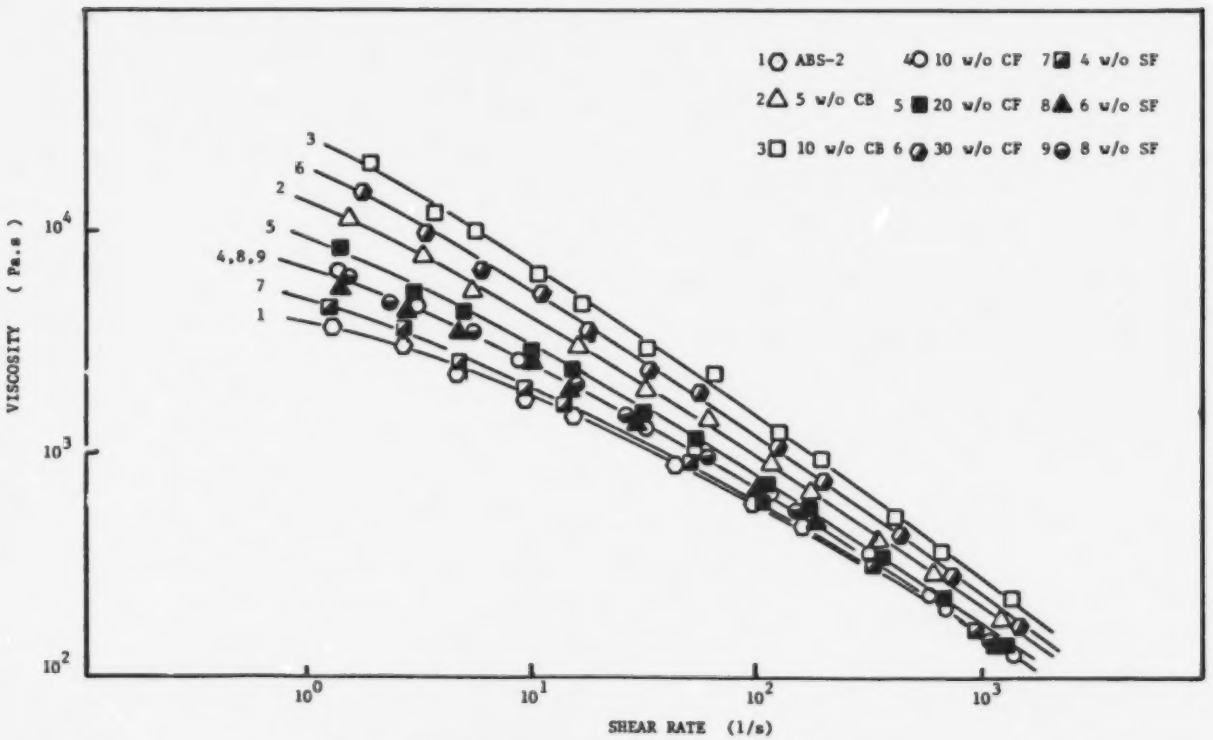

Fig. 7. Shear viscosity of ABS-2 compounds at 230°C.

carbon black > carbon fiber ~ steel fiber (5)

The different behavior of the aluminum flake compound is surely due to its disc shape. The pressure oscillations are associated with forcing the aluminum flakes from the reservoir into the die. The lateral dimensions of the flake are of the same order as the diameter of the capillary. The flakes must enter the capillary is such a way that at least one of the diameters of the flake must be parallel to a capillary diameter.

The levels of the shear viscosities of the compounds are essentially as would be expected from earlier investigations of the rheological properties of filled polymer melts (14, 15, 23, 24). Increasing volume loading of particulates elevates shear viscosity. At the same volume loading, the magnitude of the increase depends upon the size and interaction of the particles. Thus the small carbon black particles exhibit much higher shear viscosities than the compounds with steel or carbon fibers. The steel fiber compounds involve large particles at low leadings.

Die Entrance Flow Patterns

The flow streamlines have been observed in the die entrance region for several compounds. Typical results for aluminum flake compounds are shown in *Fig. 8*. Carbon fiber compounds are shown in *Fig. 9* and steel fiber compounds in *Fig. 10*. Generally the melt appears to converge uniformly into the die entrance and there is no presence of vortices indicated. In the case of the compound with aluminum flakes, the neighborhood of the die entrance is seen to possess unusually high particulate conditions.

The flow patterns in the die entrance region exhibit a uniform radially inward flow and no vortices. Only three studies (20 to 22) have previously appeared for particle filled polymer melts. These indicate that carbon black suppresses vortices exhibited by low density polyethylene. There is nothing inconsistent in the observations.

The abnormally high concentrations of aluminum flakes near the die entrance is consistent with the mechanism of the observed pressure fluctuations described in the first paragraph of this section.

Extrudate Characteristics

We have examined extrudates in the scanning electron microscope. Typical results are shown in *Figs. 11* through *14*. These indicate that the fibers tend to orient in the direction of flow. A similar situation exists for the aluminum flakes. Flow lines are observed for the carbon black compounds.

The orientation of suspended fibers in extrudates of plastics has been remarked on by various earlier investigators (13 to 15). Indeed Menendez and White (15) have quantified this using wide angle x-ray diffraction for the case of Kevlar fibers in polymethyl methacrylate.

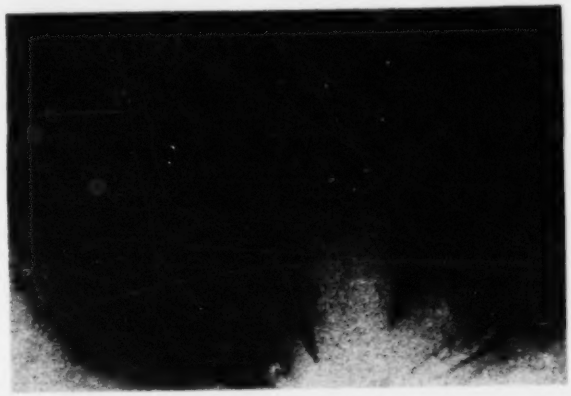

No filler
$\dot{\gamma}_{app} = 444.6\ sec^{-1}$

15.6 volume percent aluminum flakes
$\dot{\gamma}_{app} = 14.8\ sec^{-1}$

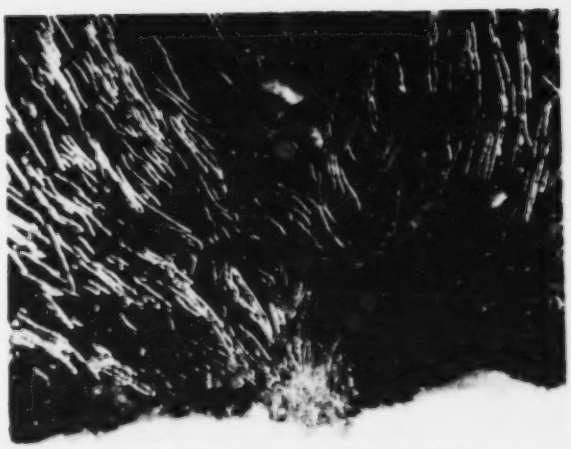

15.6 volume percent aluminum flakes
$\dot{\gamma}_{app} = 444.6\ sec^{-1}$

Fig. 8. Die entrance flow patterns of ABS-2 compounds with aluminum flakes.

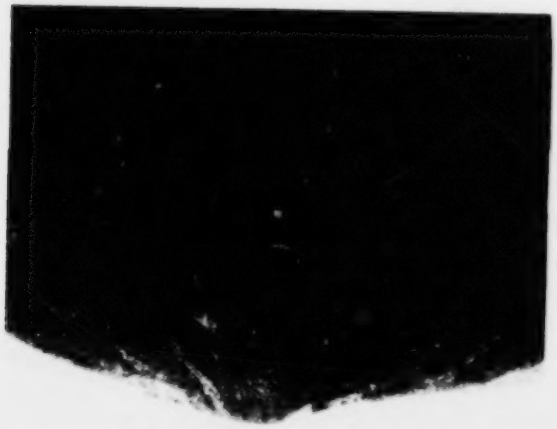

17.5 volume percent carbon fiber
$\dot{\gamma}_{app} = 14.8\ sec^{-1}$

1.1 volume percent steel fiber
$\dot{\gamma}_{app} = 14.8\ sec^{-1}$

17.5 Volume percent carbon fiber
$\dot{\gamma}_{app} = 444.6\ sec^{-1}$

Fig. 9. Die entrance flow patterns of HIPS compounds with carbon fiber.

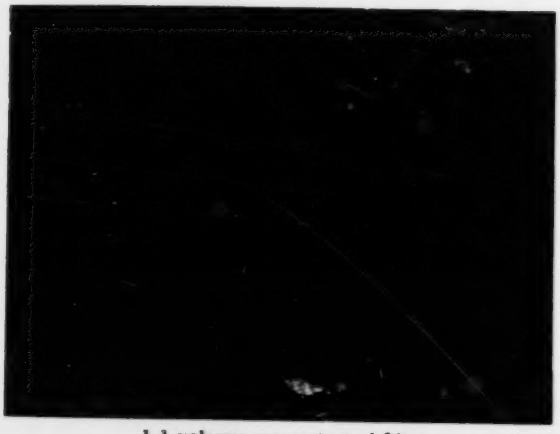

1.1 volume percent steel fiber
$\dot{\gamma}_{app} = 444.6\ sec^{-1}$

Fig. 10. Die entrance flow patterns of HIPS compounds with steel fibers.

ELECTRICAL CONDUCTIVITY OF MOLDED PARTS

General

The electrical conductivities of the various molded compounds are found to differ substantially with direction. This is shown for injection-molded bars containing steel and carbon fibers in *Figs. 15* and *16*. these results suggest that electrical conductivity should be treated as a second order tensor and we should seem to determine its components. Consider the electrical flux vector J_i

$$J_i = \sum_j \kappa_{ij} E_j \tag{6}$$

The components of κ_{ij} are

$$\underline{\kappa} = \|\kappa_{ij}\| = \begin{vmatrix} \kappa_{11} & \kappa_{12} & \kappa_{13} \\ \kappa_{12} & \kappa_{22} & \kappa_{13} \\ \kappa_{13} & \kappa_{23} & \kappa_{33} \end{vmatrix} \tag{7a}$$

where we note

$$\kappa_{ij} = \kappa_{ji} \tag{7b}$$

The electrical flux in any direction i will be influenced by all the components of the electrical field strength vector $\underline{E}$. This is described by *Eq 6*. Our experimental measurements determine J_i as a function of E_i only. This yields the diagonal components κ_{ii}.

It is possible to define a mean compound conductivity. This should be based on the sum of the diagonal components being a scalar. Specifically

$$\bar{\kappa} = \frac{1}{3} \text{tr } \underline{\kappa} = \frac{1}{3} (\kappa_{11} + \kappa_{22} + \kappa_{33}) \tag{8}$$

Carbon Black Compounds

The behavior of compression molded samples is summarized in *Fig. 17*. One finds that the conductivity of the 0.029 volume fraction is too low to measure, i.e., κ is less than $10^{-6}\ \Omega\ cm^{-1}$. At higher loadings, κ_{11} increases with loading. The data for the 0.058 volume fraction compound are anisotropic with

$$\kappa_{11} = \kappa_{22} > \kappa_{33} \tag{9}$$

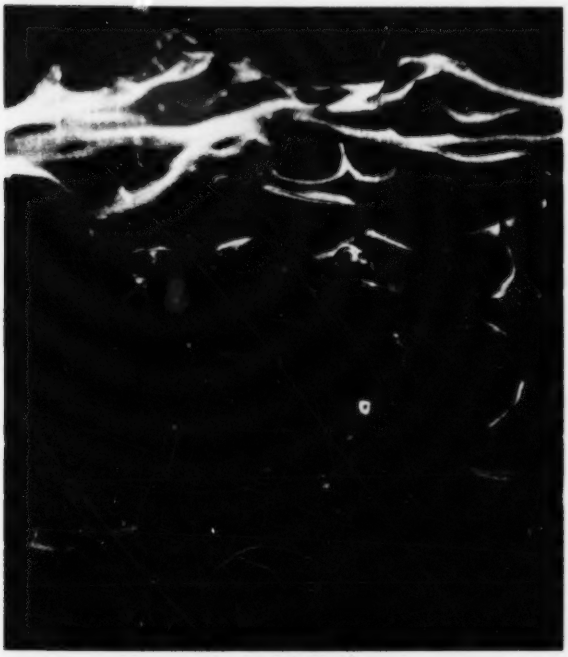

$\dot{\gamma}_{app} = 1.4\ sec^{-1}$

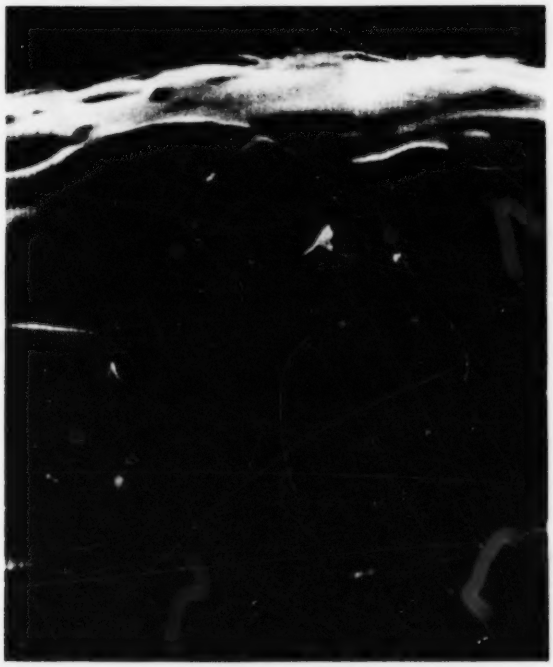

$\dot{\gamma}_{app} = 912.9\ sec^{-1}$

Fig. 11. SEM photomicrographs of extrudates of ABS-2 compound with 1.1 volume percent steel fiber.

$\dot{\gamma}_{app} = 1.4\ sec^{-1}$

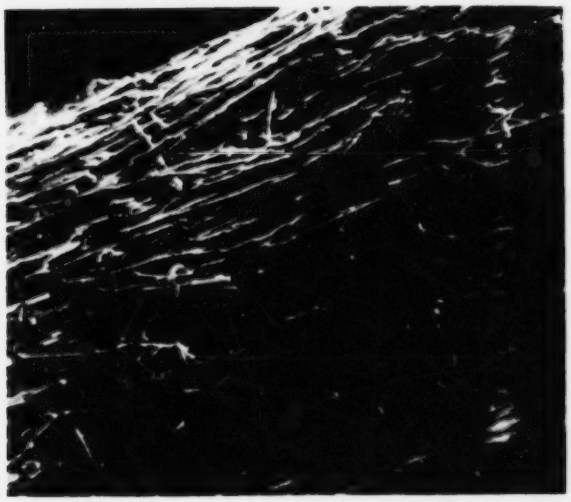

$\dot{\gamma}_{app} = 912.9\ sec^{-1}$

Fig. 12. SEM photomicrographs of extrudates of ABS-2 with 17.5 volume percent carbon fiber.

where '3' is the thickness direction and '1' and '2' is in the plane. This is also the case for the higher 0.083 volume loading, but the behavior is more isotropic here. The HIPS and two ABS samples behave similarly.

We now turn to injection molding. We display the experimental results for κ_{11}, κ_{22}, and κ_{33} as a function of position in *Fig. 18*. Here 1 is the machine direction, 2 is the transverse direction, and 3 is the thickness direction. The data are much more anisotropic than the compression-molded sample results, with

$$\kappa_{11} > \kappa_{22} > \kappa_{33} \tag{10}$$

The 0.029 volume fraction data is again not measurable. The 0.058 compound exhibits higher κ_{11} and κ_{22}, and lower κ_{33}. The 0.083 compound has higher conductivities and is more isotropic than the 0.058 compound.

The comparison to the compression molded compound is striking. For the 0.083 compound, all three components, κ_{11}, κ_{22}, and κ_{33}, for the injection molded compound are higher than for the compression molded compound. For the

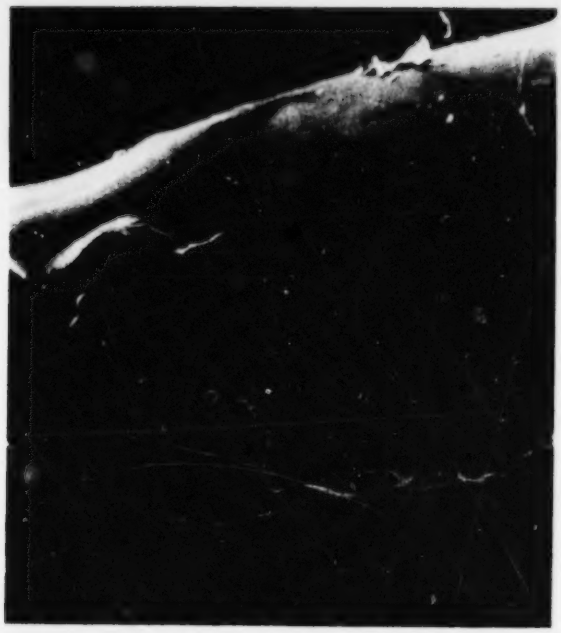

($\dot{\gamma}_{app}$ = 114.1 sec^{-1}

Fig. 13. SEM photomicrographs of extrudate of ABS-2 with 15.6 volume percent aluminum flakes.

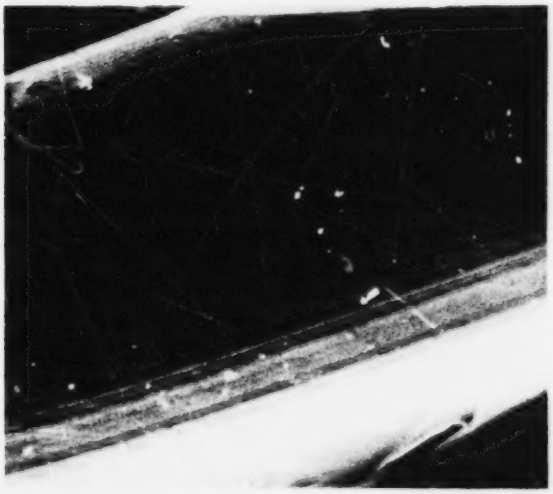

$\dot{\gamma}_{app}$ = 273.9 sec^{-1}

Fig. 14. SEM Photographs of ABS-1 extrudate with 8.3 volume percent carbon black.

0.058 compound, κ_{11} and κ_{22} are higher for the injection molded compound, but κ_{33} is lower.

Carbon Fiber Compounds

The compression molded carbon fiber compounds are electrically anisotropic with

$$\kappa_{11} = \kappa_{22} > \kappa_{33} \quad (11)$$

The injection molded bars are more highly electrically anisotropic with

$$\kappa_{11} > \kappa_{22} > \kappa_{33} \quad (12)$$

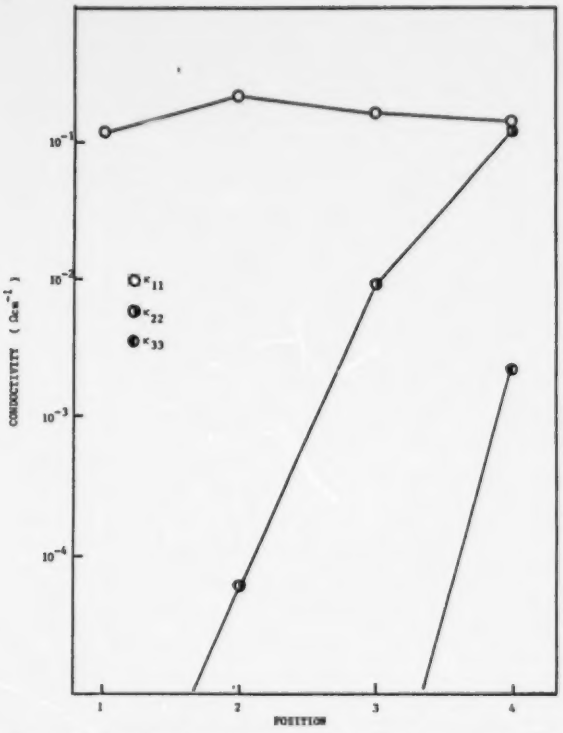

Fig. 15. Electrical conductivity of ABS-2 compound with 1.1 volume percent steel fibers of tensile bars as a function of position from the edge.

This behavior is shown in *Figs. 16* and *19*. The conductivities tend to be higher for compression molded as compared to injection molded compounds at any loading. This conductivity increases with volume loading of carbon fibers.

Steel Fiber Compounds

Conductivities for compounds with 0.5 volume percent steel fibers are too low to be measured (i.e., $>10^{-6}\ \Omega\ cm^{-1}$). The conductivities for compression and injection molded bars are summarized in *Figs. 15* and *20*. For the compression molded bars

$$\kappa_{11} = \kappa_{22} > \kappa_{33} \quad (13)$$

At the two higher loadings (0.8 and 1.1 volume percent), the conductivities for the injection molded bars are highly anisotropic with

$$\kappa_{11} > \kappa_{22} > \kappa_{33} \quad (14)$$

Figure 20 shows how conductivity varies with position along the tensile bar. The variation for κ_{11} is negligible, but it is large for κ_{22} and κ_{33}.

Aluminum Flake Compounds

The aluminum flake compounds are also electrically anisotropic. The level of anisotropy is displayed in *Figs. 21* and *22*. The compression molded bars are anisotropic with

$$\kappa_{11} = \kappa_{22} > \kappa_{33} \quad (15)$$

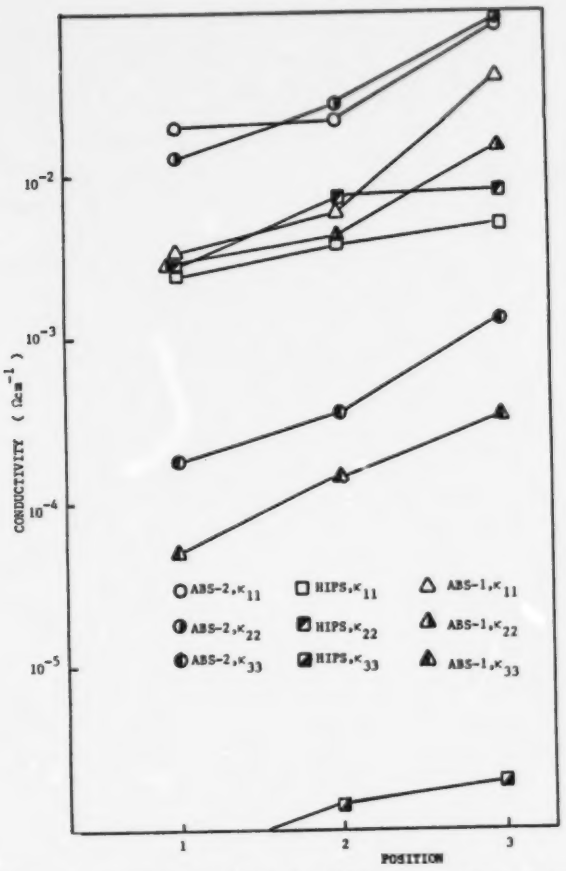

Fig. 16. Electrical conductivity of injection molded discs for ABS and HIPS compounds filled with 5.8 volume percent carbon fiber as a function of distance from the gate.

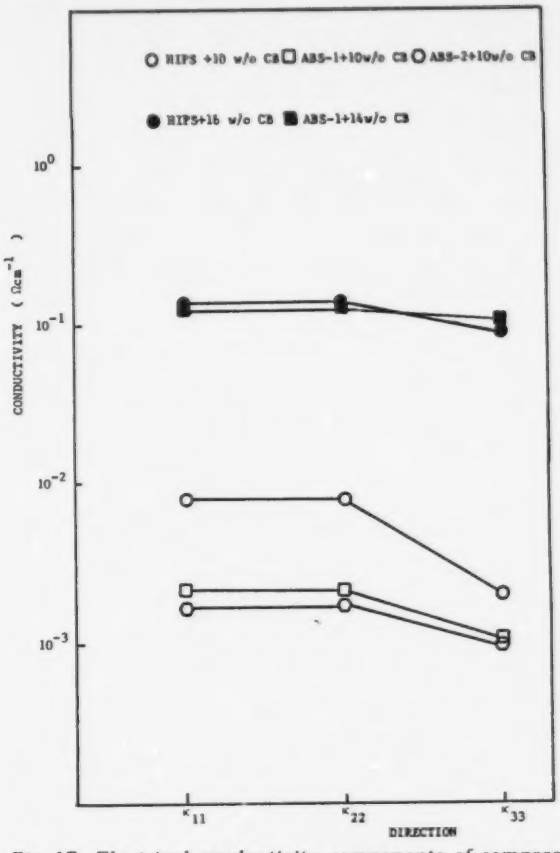

Fig. 17. Electrical conductivity components of compression molded carbon black compounds of HIPS and ABS.

For the injection molded bars we again have

$$\kappa_{11} > \kappa_{22} > \kappa_{33} \qquad (16)$$

The differences become smaller with increasing amounts of aluminum flakes. Conductivities for injection molded tensile bars are generally higher than for compression molded sheets.

For the lowest (7.8 volume percent) loading we also have a large difference in conductivities (κ_{22} and κ_{33}) as a function of position on the injection molded parts, with lower conductivities close to the gate.

DISCUSSION

Some of the experimental results require some consideration. These are the electrical anisotropy of many of the parts and the disappearance of the anisotropy at higher volume loadings. What are the structural mechanisms of this behavior? We also need to consider the source of the electrical heterogeneity of the parts.

The electrical anisotropy of fiber filled compounds (steel and carbon fiber) must be due to orientation of fibers when molded. Fibers and flakes generally orient with their major axis in the direction of flow. The anisotropy does not disappear at higher loadings. The anisotropy of the thermal conductivity associated with orientation of fiber filled compounds has also been discussed in the literature (25).

Aluminum flakes and carbon black compounds show different behavior with decreasing anisotropy with increasing loading. It would appear that electrical conductivity is determined by the number of conductive paths formed by the particles. The conductivity suddenly rises when these paths are created and then levels off with necessary concentration. With oriented particle systems, the level of electrical conductivity increases with concentration in an anisotropic manner. The level of electrical conductivity in oriented systems will thus tend to be higher in the direction of the greatest particle axis. This would tend to level off at higher concentration where contact paths become large in numbers. The difference in absolute conductivity between compression molded sheets and injection molded parts is probably due to more severe breakage of fillers in injection molding.

The electrical heterogeneity of the injection molded parts usually shows higher conductivity at large distance from the gate. *Figure 23* shows

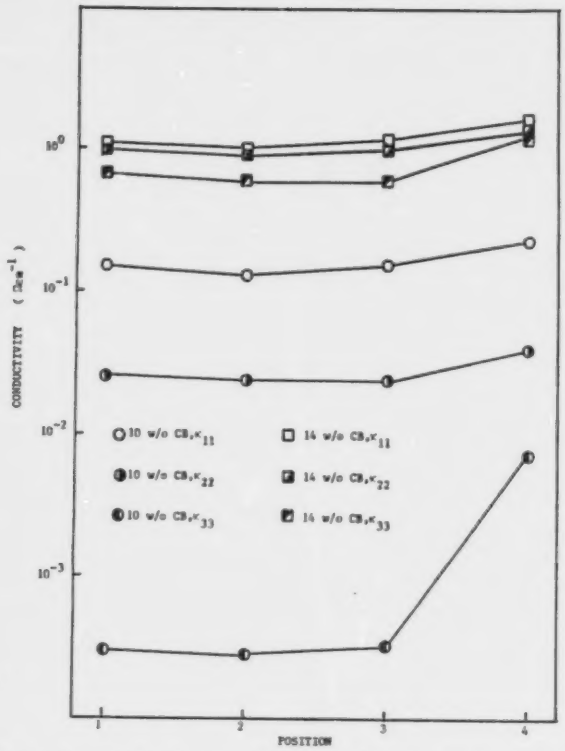

Fig. 18. Electrical conductivity components for injection molded carbon black compounds.

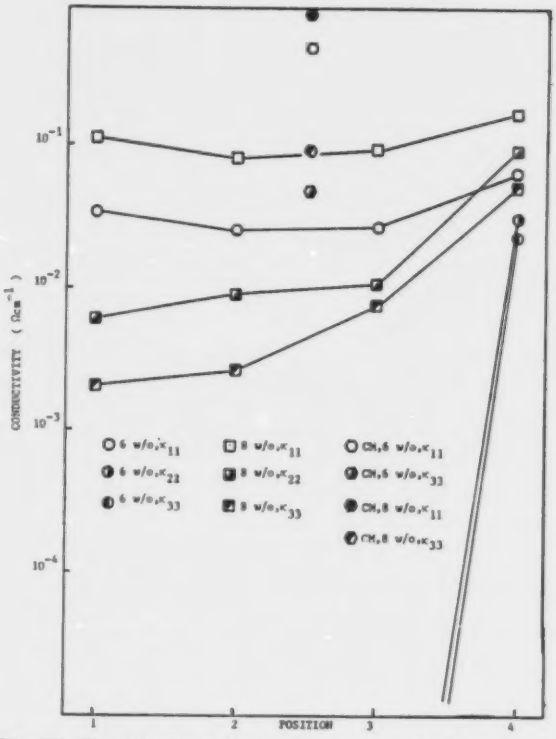

Fig. 20. Electrical conductivity components of compression and injection molded tensile bars containing steel fibers.

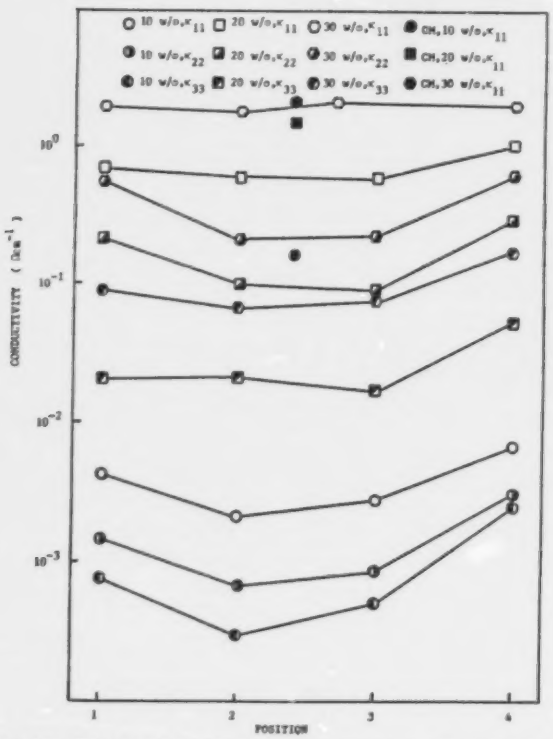

Fig. 19. Electrical conductivity components for compression and injection molded carbon fiber compounds at different volume fractions.

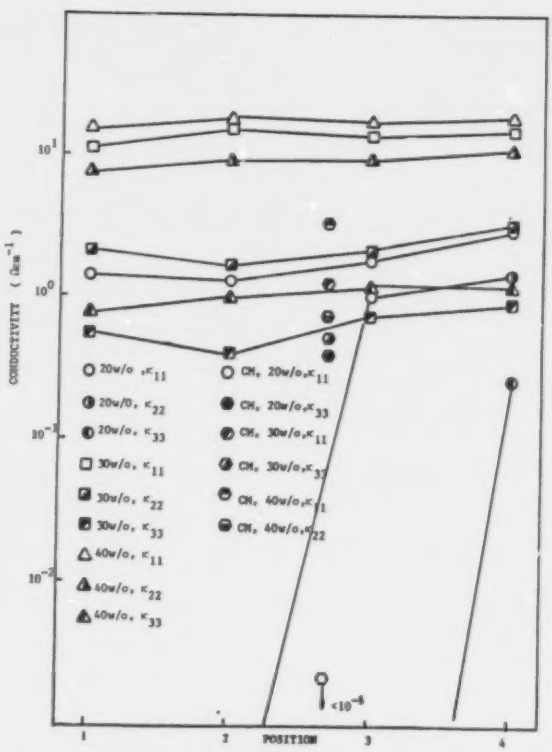

Fig. 21. Electrical conductivity components of compression and injection molded bar for aluminum flake compounds.

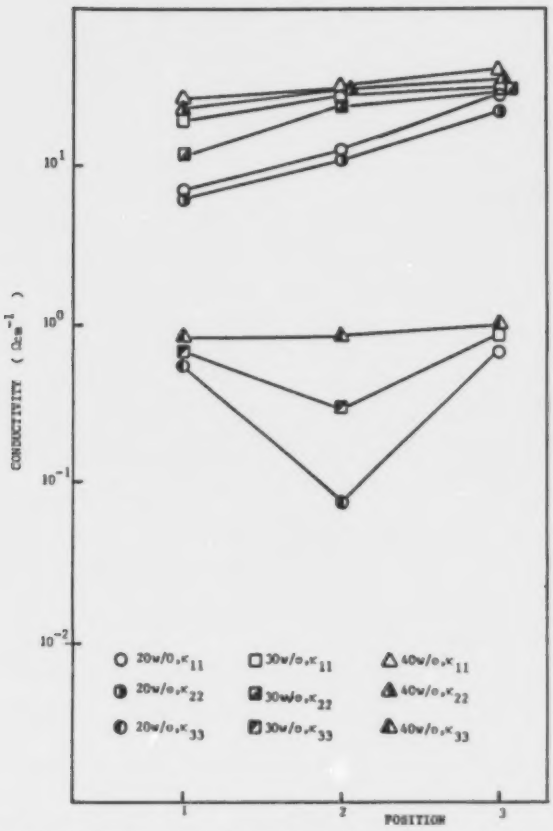

Fig. 22. Electrical conductivity components of injection molded disk with aluminum flake compounds.

(a)

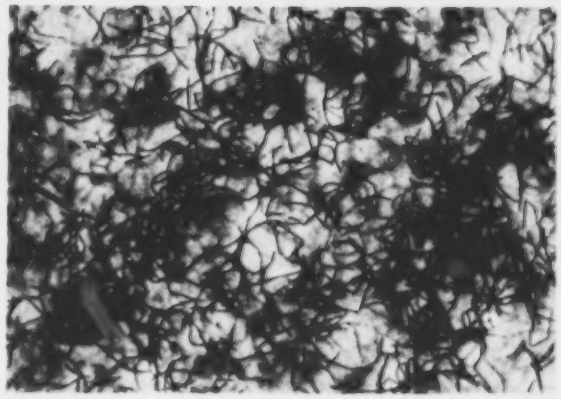

(b)

Fig. 23. Photomicrographs of ABS-1 with 1.1 volume percent steel fiber: (a) Far from the gate, (b) Close to the gate. Magnification: 60×.

the distribution of steel fibers in an injection molded disc. The concentration of steel fiber is much higher far from the gate. This behavior is also more striking for disks compared to tensile bars, which is probably due to gate size. A small gate (relative to sizes of fillers) means that the filler will concentrate in the gate entrance. In the early stages of mold filling, the compounds with lower filler loading will enter the mold. This material will be largely deposited on the mold wall near the gate. As the pressure increases, the more concentrated compound will be forced into the mold. This material will flow through the mold and deposit at a large distance from the gate. This may be envisaged to occur through a 'fountain' motion in the melt front where material on the mold walls originates in melt surging through the mold center.

ACKNOWLEDGMENT

J. Martinsson would like to thank the Marcus Wallenberg Foundation and Telefon A8 LM Ericsson for financial support during his stay at the University of Akron. We also would like to thank BASF and CDF Chimie for supplying material and Buss AG and Bakaert AG for the compounding.

REFERENCES

1. J. McDermott, EDN, **5**, 165 (1979).
2. D. R. Dreger, *Machine Design* (July) **26**, 114 (1979).
3. R. M. Simon, *Ind. Res. Dev.*, 104 (1982).
4. D. M. Bigg and D. E. Stutz, *Polym. Compos.*, **4**, 40 (1983).
5. K. Nangrani and S. Gentelsen, *Research and Development*, **60**, (July 1985).
6. J. A. Stratton, "Electromagnetic Theory," McGraw-Hill, New York (1941).
7. M. Born and E. Wolf "Principles of Optics," 4th ed. Pergamon, London (1970).
8. D. M. Bigg, *Polym. Eng. Sci.*, **17**, 842 (1977).
9. D. M. Bigg, *Polym. Eng. Sci.*, **19**, 1188 (1979).
10. D. M. Bigg, *Adv. Polym. Technol.*, **4**, 255 (1984).
11. T. Katsura, M. R. Kamal, and L. A. Utracki, *Polym. Compos.*, **6**, 282 (1985).
12. M. W. Darlington and P. L. McGinley, *J. Mater. Sci.*, **10**, 906 (1975).
13. L. A. Goettler, R. I. Leib, and A. J. Lambright, *Rubber Chem. Technol.*, **52**, 838 (1979).
14. B. A. Knutsson, J. L. White, and K. A. Abbas, *J. Appl. Polym. Sci.*, **26**, 2347 (1981).
15. H. Menendez and J. L. White, *Polym. Eng. Sci.*, **24**, 1051 (1984).
16. S. H. McGee and R. L. McCullough, *J. Appl. Phys.*, **55**, 1394 (1984).
17. S. Fakirov and C. Fakirova, *Polym. Compos.*, **6**, 41 (1985).
18. K. Walters, "Rheometry," Wiley, New York (1975).

19. J. L. White in "Rheometry:s Industrial Applications," K. Walters, ed., Wiley, New York (1981).
20. C. Y. Ma, J. L. White, F. C. Weissert, and K. Min, *J. Non-Newt. Fluid Mech.*, **17**, 275 (1985).
21. C. Y. Ma, J. L. White, F. C. Weissert, and K. Min, *Polym. Compos.*, **6**, 215 (1985).
22. C. Y. Ma, J. L. White, F. C. Weissert, A. I. Isayev, N. Nakajima, and K. Min, *Rubber Chem. Technol.*, **58**, 815 (1985).
23. J. L. White, L. Czarnecki, and H. Tanaka, *Rubber Chem. Technol.*, **53**, 823 (1980).
24. Y. Suetsugu and J. L. White, *J. Appl. Polym. Sci.*, **28**, 1481 (1983).
25. J. L. White and B. A. Knutsson, *Polym. Eng. Rev.*, **2**, 71 (1982).

DISCUSSION

L. A. Utracki: I have been intrigued by the changes in fiber orientation you reported for the injection molded specimens. As I understand, there is a definite loss of orientation along the length: the most oriented specimens were near the gate, the least at the end. The orientation is responsible for very large variations of conductivity in the transverse direction. However, if the fiber loading is near the percolation concentration, a very minute change of concentration may cause a drastic, many orders of magnitude change of conductivity. In short, there are two different mechanisms which may lead to increases in transverse conductivity near the end of the specimens: change or orientation or increase in fiber concentration. Would you please comment on which of these two mechanisms is responsible for the conductivity changes, and why the concentration at the specimen end should be higher.

J. L. White: Due to the fact that the compound goes through the gate, there is a separation. Some of the steel fiber is retained in the reservoir in front of the gate and the compound which actually goes through has initially lower concentration of fibers. But since we are dealing with a batch process, in the end all the materials has to be injected. In terms of the mechanism of the fountain flow, the last part of the mold to be filled is in the end. So, you tend to end up with a higher concentration of particulates at the rear wall of the mold. The other difference of conductivity is clearly associated with distribution of particulates orientation. But it is true that conductivity is not a clear and simple measure of orientation. To interpret these data one would have to use formalism such as of the percolation theory, looking at the number of paths which go through the sample. We are now working with percolation theory, trying to see what we can extract from the data—Not only worrying about things like orientation but, as in the case of carbon black, about dispersion.

Ch. L. Beatty: Do you think that the viscosity of the polymer matrix, the rate of filling the mold, and the temperature of the mold may have an effect on the segregation of the filler in the different parts of the experiment?

J. L. White: It is hard to answer with regard to the segregation effect. At first, this seems to be the geometric one. But it is certainly true as far as orientation of the fibers is concerned. The orientation most probably is controlled by the stresses, so the effect may be more pronounced at lower than at higher temperatures, at higher injection pressures rather than at lower, etc.

Determination of the Orientation of Mica in Composites

T. M. MALIK *and* R. E. PRUD'HOMME

Chemistry Department
Laval University
Ste-Foy, Quebec, Canada G1K 7P4

and

B. RÉMILLARD

Industrial Materials Research Institute
National Research Council Canada
Boucherville, Quebec, Canada J4B 6Y4

A wide angle x-ray diffraction technique has been used to determine the orientation of mica flakes in composites. The mica used was a fine grade Phlogopite, and the polymers were polystyrene, polycarbonate and poly(vinyl chloride). Composite samples of varying mica contents and orientations were prepared. The x-ray method can give the orientation distribution function of mica flakes across and parallel to the surface of the sample. From this function, an average orientation parameter was calculated. The results show that there is no orientation of mica across the surface of the sample (the x-ray beam is normal to the surface), but that there is a strong orientation in a direction parallel to this surface, the average orientation parameter being strongly dependent upon the particle size of mica and mode of preparation.

INTRODUCTION

Composite materials are used extensively in engineering applications (1 to 5). A composite material is made of a reinforcing substance (fibers or fillers) embedded in a polymer matrix. By carefully selecting the reinforcing material and resin system, composites can achieve strength and modulus values that are competitive with those of most other materials, including metals (6). Such composites are highly attractive to designers for applications where weight is of prime importance.

In principle, a large number of fibrous materials can be used to reinforce polymers, depending of course on their physical and mechanical properties, thermal resistance, cost, and strength. Traditionally, glass fibers have been extensively used. Recently, other reinforcing materials such as wool, rayon, sisal, cotton, synthetic polymer fibers, and asbestos have also found increasing applications in the preparation of high strength/high modulus composites (6).

More recently, mica composites have been used, particularly in the automotive industry. The high strength and rigidity of mica, along with its low density and low cost, make it an ideal candidate as an alternate reinforcing agent in composites where strength, modulus, dimensional stability, and strength to weight ratio are necessary requirements (7, 8).

Mica, a silicate mineral found abundantly in nature in the form of flakes, consists of potassium aluminum substituted pyrophyllite (9). The potassium atoms form weak bridges between silica layers resulting in a thin sheet structure. These sheets exhibit excellent dielectric strength, high modulus, low thermal conductivity, and good flexibility (6).

In order to use mica, or any other reinforcing agents in a composite material for engineering purposes, it is important to know the orientation of the reinforcing agent in the polymer matrix. Composites are often anisotropic materials whose properties, unlike those of isotropic materials, depend greatly upon the alignment of the fibers or flakes.

Due to an increasing interest in mica reinforced composites, a number of investigators have reported on their mechanical and rheological properties and on the effect of coupling agents on mica (10 to 17). In the composites, the mica flakes have a tendency to orient parallel to the surface of the film, but not perpen-

dicular to it. However, this phenomenon of orientation has never been studied quantitatively even if the mechanical properties of the composite depend upon it.

The commonly used techniques for measuring the orientation of crystals in polymers and/or reinforcing materials in composites involve x-ray diffraction (4, 18 to 21), light scattering (22, 23), optical anisotropy and birefringence (24), zero span (25) and sonic velocity tests (24). Most of these techniques are either qualitative in nature or very tedious for quantitative measurements. Prud'homme *et al.* (26) have proposed a wide angle x-ray diffraction method for a rapid and quantitative measurement of the orientation distribution of cellulose fibers in composites.

In the present study, we use the same method to determine the orientation of mica flakes in composites. The method permits quantitative measurement of the orientation distribution function of mica flakes not only in a direction normal (across) but also in a direction parallel to the surface of the film. From this function, an average orientation parameter is calculated. Effects of particle size of mica, variation of the pressure of the press during the preparation of composites, and different polymer matrices on the orientation parameter are discussed.

THEORY

In this section, we will recall briefly the method proposed by Prud'homme *et al.* (26) for the x-ray analysis of the orientation of fibers in composites. It has been demonstrated that the intensity of the diffracted beam as a function of the azimuthal angle, ϕ, is proportional to the density of the reciprocal lattice points on the reciprocal lattice sphere (26, 27):

$$I(\phi) = KP(\beta, \omega) \tag{1}$$

where $I(\phi)$ is the x-ray intensity at ϕ, $P(\beta, \omega)$ is the density of the reciprocal lattice points, and K is a proportionality constant. As the density of reciprocal lattice points is identical to the distribution of orientation of the crystal planes, *Eq 1* becomes

$$I(\phi) = KN(\epsilon) \tag{2}$$

where the function $N(\epsilon)$ describes the distribution of orientation of crystals, and ϵ is the tilt angle of the crystals.

The function $N(\epsilon)$, to a first approximation, is assumed to be given by

$$N(\epsilon) = \frac{C}{C^2 \sin^2\epsilon + \cos^2\epsilon} \tag{3}$$

where C is an orientation parameter. When C is equal to unity, a random distribution is generated; when C is larger than unity, the crystals are preferentially aligned with respect to $\epsilon = 0$. The function $N(\epsilon)$ is given in *Fig. 1* for several values of C. All the curves are arbitrarily normalized to unity $\epsilon = 0$ for comparison purposes.

In order to obtain the orientation function of a given sample for a given (hkl) plane at a fixed Bragg angle, one must rotate the sample in the YZ plane (around the X axis) while holding the incident x-ray beam and detector fixed (*Fig. 2*). Then by superposing the experimental azimuthal intensity curve, after all necessary corrections, to the corresponding theoretical curve (*Fig. 1*), one determines the orientation parameter, C, that best describes the sample.

The method described above was suggested for the quantitative measurement of cellulose fiber orientation in composites. However, the method can be used equally well to determine the orientation of mica flakes in composites as demonstrated in this article.

EXPERIMENTAL

The mica used in this study was a Phlogopite mica of the Suzorite variety supplied by Marietta Resources Int. Ltd. Details about the physical properties of this mica can be found in Refs. 28 and 29. Three mica samples of different mesh sizes were used, i.e., 60 HK, 200 HK and 325 HK; the numerical values correspond to the average mesh size of the flakes and the letters HK refer to a mica which has not received any surface treatment. The polymers were polystyrene (PS, 667-26 Clair from Dow Chemicals), polycarbonate (PC, Merlon M40F from Mobay), and polyvinyl chloride (PVC, 85791/021 from BF Goodrich).

The composites were prepared by blending the polymer resin and the mica in a roll mill blender at 200°C for PS and PVC, and at 230°C for PC. The components were mixed until the mica was homogeneously distributed into the polymer matrix. The mixture was then granulated and introduced into a flat plate mold, which was placed in a hydraulic press. The mold was heated up to the desired temperature (160 to 180°C for PS and PVC, and 200 to 245°C for PC), maintained at that temperature 5 min, and the pressure applied slowly to the desired value and held for 2 min. The mold was then cooled to room temperature, keeping the pressure constant. By this procedure, sheets having

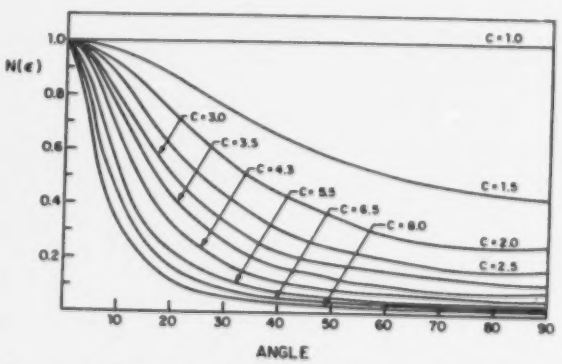

Fig. 1. Orientation function N(ε) plotted as a function of ε for different values of the orientation parameter C.

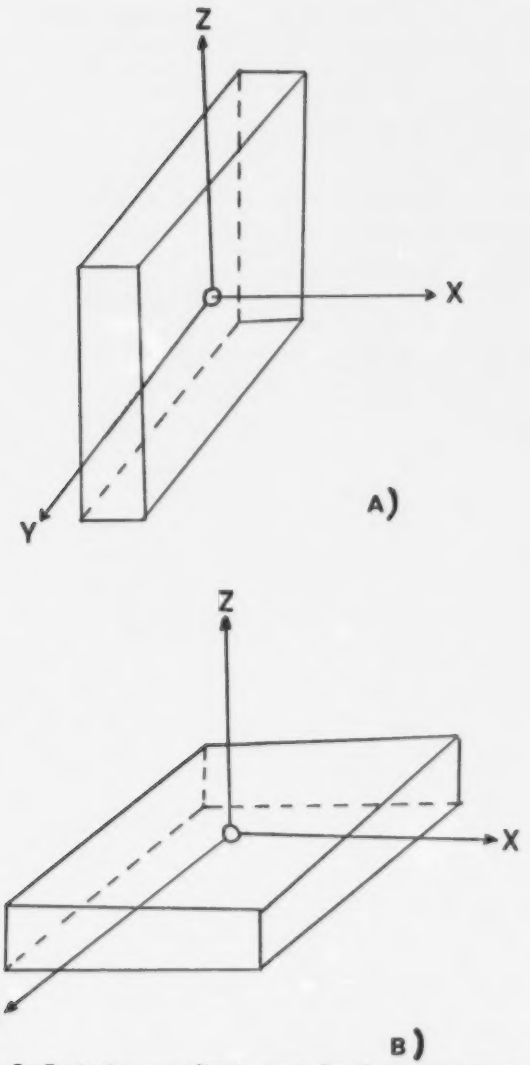

Fig. 2. Cartesian coordinate axes for the x-ray experiment. The x-ray beam travels along the x axis: a) measurement across the surface of the sample; b) measurement parallel to the surface of the sample.

a thickness of 2 to 3 mm were prepared and used for the x-ray diffraction measurements; for x-ray measurements in a direction parallel to the surface (*Fig. 2b*), the samples were cut with a saw making sure that the edge was smooth and uniform. Some samples were cut in pieces of about 10 by 5 cm^2, two layers were superposed, and the samples were then reheated and repressed once or twice (two or three presses).

X-ray measurements were performed with a Philips generator, model PW-1009, using a Ni filtered Cu$k\alpha$ radiation with $\lambda = 0.154$ nm, operated at 40 kV and 25 mA. X-ray patterns were obtained with Warhus-Statton cameras using Kodak DEF5 x-ray films. The cameras were calibrated with NaCl.

X-ray intensities were recorded using an automatic x-ray diffractometer constructed in our own laboratory (30). The scattering intensities were recorded by a scintillation counter set at a particular 2θ Bragg angle. The sample was mounted in the sample holder and rotated at a rate of 4°/min for azimuthal scans. For 2θ scans, the sample was held fixed and the detector moved at a rate of 1°/min. For each sample, between 20 and 30 scans were made. The intensity data were then corrected for background and diffuse scatterings. The corrections for incoherent scattering, polarization, and Lorentz factor were not made since they affect only the 2θ scan and are azimuthally independent (19).

In this study, the orientation of mica flakes in composites is determined using the azimuthal x-ray intensity dependence. A complete analysis of a sample required between 3 and 5 hours depending upon the number of scans made.

RESULTS AND DISCUSSION

Figure 3 shows the x-ray diffraction pattern of 325 HK mica, which is made of sharp and uniform rings, each one representing the diffraction from a particular lattice plane. Other grade micas give the same x-ray pattern, but it is then more diffused because of the bigger size of the flakes. The position of the diffracted rings of *Fig. 3* was measured and, by applying Bragg's equation, values of 2θ and interplanar spacings, d, were calculated (*Table 1*).

The Phlogopite mica is known to have a monoclinic unit cell structure with cell parameters a = 0.532 nm, b = 0.921 nm, c = 1.024 nm and $\beta = 100.2°$ (9). The relation between d spacings and unit cell parameters for different (hkl) Miller indices is

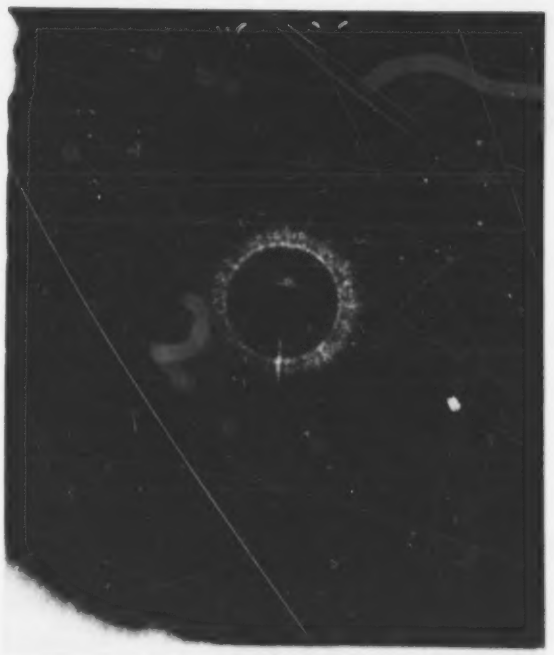

Fig. 3. Wide angle x-ray pattern of 325 HK mica.

$$\frac{1}{d^2} = \frac{h^2}{a^2\sin^2\beta} + \frac{k^2}{b^2\sin^2\beta} + \frac{l^2}{c^2} + \frac{2hk}{ab\sin^2\beta}[\cos(180-\beta)] \quad (4)$$

The d values of mica were then calculated and compared with the experimental ones: hkl indices were allocated if a sufficiently good match was obtained, of course taking measurement errors into account. *Table 1* shows that there is a good agreement between the d spacings measured in this study [d(exp)] and those reported in the literature [d(lit)] or calculated from the unit cell parameters [d(unit cell)].

Figure 4 shows the x-ray diffraction pattern of a 50/50 325 HK mica/PS composite with the incident x-ray beam across (normal to) the surface of the sample (*Fig. 2a*). Each ring shows a uniform distribution of intensity with no indication of orientation of the mica flakes. It is worth noting that these rings still remain as sharp in *Fig. 4* as they were in *Fig. 3* for a pure mica sample. However, a diffuse halo from the amorphous PS matrix is superposed in the center of the pattern upon the rings due to crystalline mica. To verify this, the specimen was extracted with toluene so as to dissolve most of the PS, assuming that the random distribution of mica flakes was preserved. *Figure 5* shows the x-ray diffraction pattern of such an extracted specimen where it is seen that the amorphous halo has disappeared to a large extent. This observation indicates that the accurate determination of mica orientation in composites requires a correction for the diffraction by the polymer matrix.

Figure 6 shows the x-ray diffraction pattern of a 50/50 325 HK mica/PS composite with the incident x-ray beam parallel to the surface of the film (see *Fig. 2b*). It exhibits a moderate to high degree of flake orientation since the x-ray reflections corresponding to mica no longer appear as rings but as narrow arcs (see for example the (001) plane). This figure also shows that the PS matrix is oriented; this orientation was developed during the processing of the polymer in the molten form and it is not present when the x-ray beam is passing across the sample (see *Fig. 4*). It is not seen either for an unfilled compression molded PS sample, indicating that the orientation of PS develops only in the presence of oriented mica flakes. With the x-ray beam parallel to the surface of the sample, it appears that the (001) plane is the most suitable one for the analysis of the orientation of mica in composites because of its high intensity and because it gives directly the orientation of the mica crystal *c* axis contrary to some other intense rings listed in *Table 1*.

Figure 7 shows the azimuthal scan of the x-ray (001) plane of the sample analyzed in *Fig. 6*, the 2θ angle being fixed at 9.0°. The intensity distribution curve is quite symmetrical with respect to ϕ = 0, 90, 180, or 270° indicating an

Table 1. X-Ray Data for Mica, Including 325 HK Mica (exp).

Ring	2θ	I(exp)*	d(exp) nm	d(unit cell) nm	d[lit](9) nm	hkl
1	9.0	100	1.005	1.023	0.997	001
2	19.5	70	0.456	0.453	0.458	020, 110
5	26.6	10	0.332	0.339	0.334	112, 003
8	34.5	80	0.263	0.260	0.260	116
9	37.0	40	0.241	0.239	0.249	113, 201

* Intensities expressed on an arbitrary scale going from 0 to 100 for the most intense ring.

Fig. 4. X-ray diffraction pattern of 50/50 325 HK mica/PS composite. The x-ray beam is passing across the sample (Fig. 2a).

Fig. 5. X-ray diffraction pattern of a 50/50 325 HK mica/PS composite after the extraction of PS. The x-ray beam is passing across the sample (Fig. 2a).

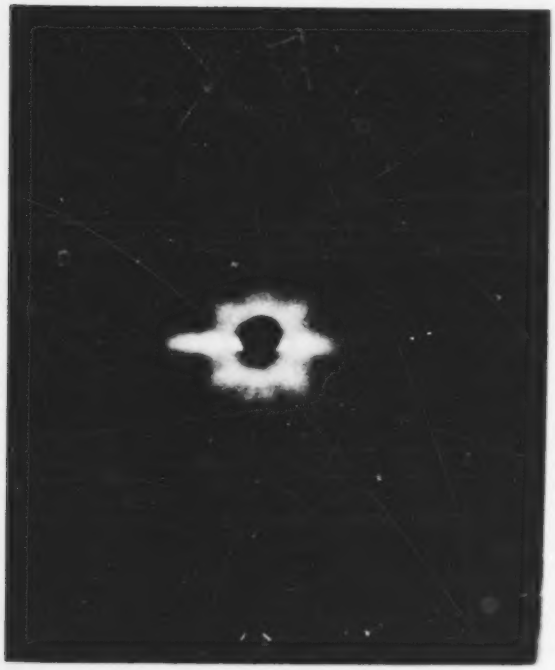

Fig. 6. X-ray diffraction pattern of a 50/50 325 HK mica/PS composite. The x-ray beam is parallel to the surface of the sample (Fig. 2b).

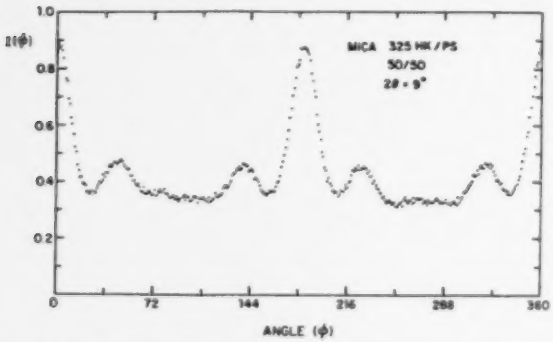

Fig. 7. Variation of the x-ray (001) plane intensity as a function of azimuthal angle for a 50/50 325 HK mica/PS composite.

appropriate alignment of the sample with respect to the incident beam. Therefore, it suffices to analyze the curve from 0 to 90°. In that angular range, the intensity curve drops rapidly from $\phi = 0$ to 25°, but then a small maximum appears at about 45°. This is due to the PS amorphous fraction, which has been oriented as seen in *Fig. 6*. In order to get rid of this contribution, and to simultaneously isolate the mica contribution, a straight line was drawn on each azimuthal scan from $\phi = 30$ to 60°, the intensity above this line was discarded and the resulting curve was used in the calculations.

To calculate the orientation parameter C, the intensity curve of *Fig. 7* was set at unity at $\phi = 0°$ and is replotted in *Fig. 8* (upper curve) in a 0 to 90° angular range. C values were then calculated, using *Eqs 2* and *3* and the experimental intensities. An average C value was computed

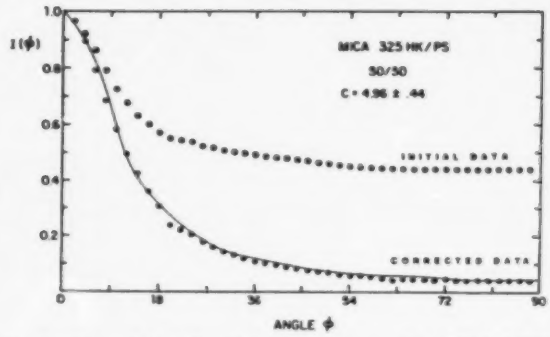

Fig. 8. X-ray intensity distribution curve for a 50/50 325 HK mica/PS composite. The continuous line through the corrected experimental points is obtained with Eq 3 considering an orientation parameter of 4.96.

with its standard deviation "S". By inserting this average C value in *Eqs 2* and *3*, theoretical intensities were calculated and compared with the experimental ones. It was found that these two curves do not agree with each other, indicating that an additional correction must be made for diffuse scattering originating from PS amorphous fraction, the background, etc. For that matter, the following approach was adopted assuming that this correction is independent of the azimuthal angle. Half of the intensity of the experimental curve at $\phi = 90°$ was subtracted from the entire intensity distribution curve, and the curve was then re-set at unity at $\phi = 0°$. A C parameter was again calculated along with an S value. This procedure was repeated several times, generating a series of C values. With each subtraction, the S values decrease until they reach a minimum value. With further subtraction, the S values start increasing. The parameter C was then selected to correspond to the lowest S value. In the example of *Fig. 8*, the value of 4.96 ± 0.44 was selected as the orientation parameter for that particular sample. Using this C parameter, a theoretical intensity curve was calculated using *Eqs 2* and *3* and compared with the experimental one (*Fig. 8*, bottom curve). A good agreement between the theoretical and experimental curves is then found.

To check the validity of this procedure, different subtraction parameters were used for the same data. Again, S values decrease with each subtraction, before reaching a minimum; with further subtraction, they start increasing. Within experimental error, it was verified that the C values obtained by this procedure are independent of the subtraction parameters used.

The same method of correction was used to calculate C parameters for all the composites studied. *Table 2* gives average orientation parameters C of mica/PS composites prepared at a pressure of 10^4 psi. Reported values are the average of six to eight independent analyses. It is seen that the C values are greatly influenced by the mica particle size (*Fig. 9*). For 50/50 mica/PS composites, C = 4.4, 5.2, and 6.3 for 325 HK, 200 HK, and 60 HK micas, respectively, which shows that an increase of flake size leads to an increase of orientation. In other words,

Table 2. Average Orientation Parameter of Mica/Polymer Composites Prepared at a Pressure of 10^4 psi.

Mica/Polymer	Composite	Number of Presses*	C ± S**
325 HK/PS	50/50	3	4.4 ± 0.3
	50/50	1	3.4 ± 0.2
	25/75	3	4.9 ± 0.3
	25/75	1	3.5 ± 0.3
200 HK/PS	50/50	3	5.2 ± 0.5
	50/50	1	3.5 ± 0.3
	25/75	3	5.7 ± 0.6
	25/75	1	3.3 ± 0.2
60 HK/PS	50/50	3	6.3 ± 0.7
	25/75	3	7.0 ± 0.5
	25/75	1	5.6 ± 0.4
325 HK/PC	50/50	3	4.0 ± 0.4
325 HK/PVC	50/50	3	4.5 ± 0.4

* Number of presses indicates how many times the composite was pressed at constant pressure.
** Standard deviation on the six to eight C (average) values obtained for each sample.

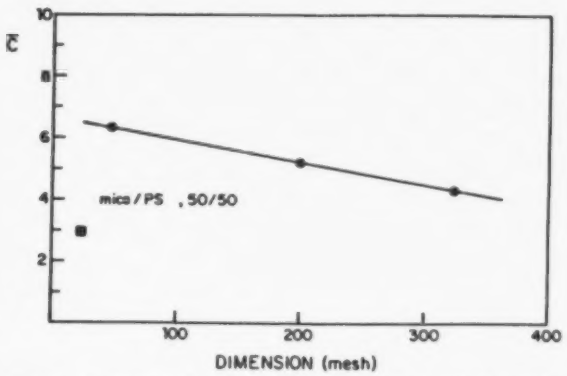

Fig. 9. Variation of orientation parameter with the flake dimensions for the 50/50 mica/PS composites.

the bigger the flakes, the higher the tendency to be oriented. This behavior is mainly related to the thickness of the samples. For thin samples where the flake size is comparable to the thickness of the sample, the flakes must be oriented parallel to the surface, at least near the surface. The larger the flakes, the thicker the skin layer, and the greater the average orientation of mica. However, orientation is also favored in the core of the sample because the flakes tend to orient parallel to each others and parallel to the flakes in the skin layer.

Table 2 also gives data for composites with two other polymer resins, i.e., PC and PVC. The C values of 50/50 mica composites with PS, PC, and PVC are almost identical. In other words, there is no matrix effect on the mica orientation in composites.

Figure 10 finally shows the dependence of the orientation parameter on the pressure of the press during the preparation of the composites. It is seen that the higher the pressure, the greater the tendency of the mica flakes to become oriented parallel to the film surface because the use of high pressures decreases the thickness of the sample and favors orientation of the flakes.

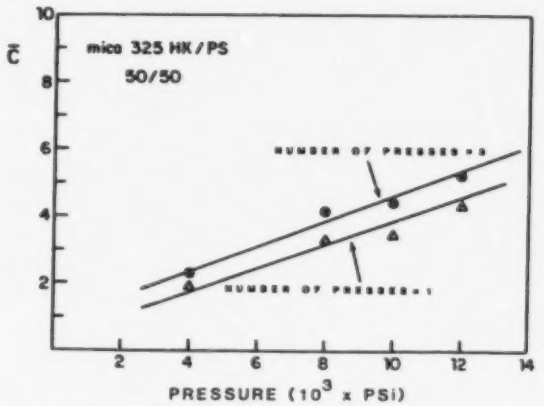

Fig. 10. Pressure dependence of the orientation parameter for the mica/PS composites.

CONCLUSIONS

The x-ray method initially proposed to quantitatively determine the distribution of fiber orientation of cellulosic composites has been successfully applied to mica/PS composites. For each composite investigated, we have been able to determine an orientation parameter, which indicates that the micas flakes are oriented parallel to the surface of the sample. This orientation parameter describes, in turn, an orientation distribution function for the mica flakes.

With the proposed method, it is assumed that the orientation distribution function is given by *Eq 3*. It was found that this function satisfactorily explains the orientation data of various mica/polymer composites. However, this function may not be universal, and other orientation functions may be more appropriate for different composites. In addition, it is assumed that the sample shows uniaxial orientation. This assumption is certainly valid with the compression molded specimens investigated in this study. It may not be applied equally well to injection molded and extruded specimens which can give, in some instances, biaxial orientation. For biaxially oriented samples, a more sophisticated x-ray analysis method needs to be used.

The experimental results indicate that the major factors controlling the orientation of mica in composites are the processing conditions (pressure of the press, number of presses) and the size of the flakes. The change of polymer matrix has little effect on the degree of orientation.

The mica flakes in the composites are preferentially oriented parallel to the surface of the film as shown in *Fig. 11*. However, in this study, the x-ray experiments were carried out using the whole sample thickness. Therefore, it was not possible to verify the presence of changes in orientation through the thickness of the sample. Such variations may occur, particularly when the sample is much thicker than the size of the mica flakes. If this happens, it is expected that the flakes will be more highly oriented near

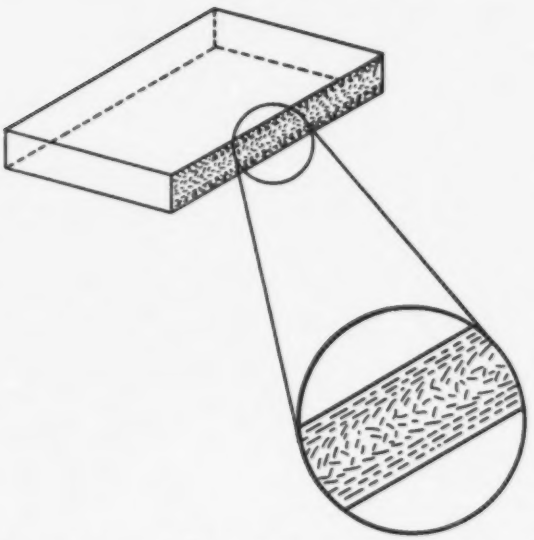

Fig. 11. Schematic illustration of the orientation of mica flakes in a thick composite.

the surface of the sample than in its core, as shown schematically in *Fig. 11*.

In this study, the orientation of mica flakes could be determined without too much interference from PS, PC, and PVC matrices. In principle, the same method could be used with semi-crystalline matrices. In practice, this would imply that the semi-crystalline polymer matrix does not diffract at $2\theta = 9°$ (001 ring of mica) or using another diffraction ring of mica for the analysis of its orientation.

ACKNOWLEDGMENT

Funding for this project was granted by the Industrial Materials Research Institute of the National Research Council of Canada under contract #12SD.31950-4-0015.

REFERENCES

1. I. Crivelli-Visconti, *Polym. Eng. Sci.*, **15**, 167 (1975).
2. L. Nicolas, *Polym. Eng. Sci.*, **15**, 137 (1975).
3. A. Youngs, *SPE ANTEC Tech. Pap.*, **31**, 1181 (1985).
4. H. Menendez and J. L. White, *Polym. Eng. Sci.*, **24**, 1051 (1984).
5. M. Xanthos, G. C. Hawley, and J. Antonacci, *Proc. 33rd Ann. Tech. Conf., Reinforced Plastics/Composites Div., SPI*, Section 2-D (1978).
6. R. G. Weatherhead, "FRP Technology: Fiber Reinforced Resin Systems," Applied Sciences, London (1980).
7. C. Busigin, G. M. Martinez, R. T. Woodhams, and R. Lahtinen, *Polym. Eng. Sci.*, **23**, 766 (1983).
8. S. Newman and F. J. Meyer, *Polym. Compos.*, **1**, 37 (1980).
9. G. W. Brindey and G. Brown, "Crystal Structures of Clay Minerals and their X-Ray Identification," Mineralogical Society, London (1980).
10. B. D. Favis, L. P. Blanchard, J. Léonard, and R. E. Prud'homme, *Polym. Compos.*, **5**, 11 (1984).
11. B. Fisa and L. A. Utracki, *Polym. Compos.*, **5**, 36 (1984).
12. K. Okuno and R. T. Woodhams, *Polym. Eng. Sci.*, **15**, 308 (1975).
13. M. S. Boaira and C. E. Chaffey, *Polym. Eng. Sci.*, **17**, 715 (1977).
14. A. Garton, S. W. Kim, and D. M. Wiles, *J. Polym. Sci., Polym. Letters*, **20**, 273 (1982).
15. P. Bataille, S. Boisse, and H. P. Schrieber, *J. Vinyl Technol.* **6**, 147 (1984).
16. T. Vu-Khanh, B. Sanschagrin, and B. Fisa, *Polym. Compos.*, **6**, 299 (1985).
17. I. Chun and R. T. Woodhams, *Polym. Compos.*, **5**, 250 (1984).
18. N. W. Darlington and P. L. McGinley, *J. Mater. Sci.*, **10**, 906 (1975).
19. M. Kakudo and N. Kasai, "X-Ray Diffraction by Polymers," Elsevier, New York (1972).
20. R. G. Schierding, *J. Compos. Mater.*, **2**, 104 (1968).
21. K. Yoshida, G. Budiman, Y. Okayama, and T. Kitao, *Sen-i-Gakkaishi*, **31**, T-335 (1975).
22. L. Rudstrom and U. Sjolin, *Svensk. Papperst.*, **73**, 117 (1970).
23. M. B. Rhodes and R. S. Stein, *J. Polym. Sci., A2*, **1**, 1539 (1969).
24. R. S. Stein and G. L. Wilkes, "Structure and Properties of Oriented Polymers," I. M. Ward, ed., Wiley, New York (1975).
25. O. J. Kallmes, *Tappi*, **52**, 482 (1969).
26. R. E. Prud'homme, N. V. Hien, J. Noah, and R. H. Marchessault, *J. Appl. Polym. Sci.*, **19**, 2609 (1975).
27. K. C. Ellis and J. O. Warwicker, *J. Polym.Sci.*, **A1**, 1185 (1963).
28. J. Lusis, R. T. Woodhams, and M. Xanthos, *Polym. Eng. Sci.*, **13**, 139 (1973).
29. *Technical Information*, Marietta Resources Int. Ltd., Boucherville (Québec), Canada.
30. D. M. Lévesque, *M. Sc. Thesis*, Université Laval (1982).

DISCUSSION

J. L. White: I wanted to note that the experimental technique to determine the orientation of suspended particles in a polymer matrix using X-ray diffraction is due to Schierding of Monsanto and later to Kitao *et al.* of the Kyoto Institute of Technology. One case was with mineral fibers in a polymer matrix, another with carbon fibers in polystyrene. Other people have used this technique as well. In my view, the way you orient your specimens and interpret the data means that you are interpreting the results in terms of a crystallographic axis which runs normal to the surface of the mica platelets. You are presuming that when you compression mold the samples you have uniaxial orientation developed, so the normal to the flakes are like fibrils. Yes?

T. M. Malik: Yes, we assume that we have uniaxial orientation.

J. L. White: Okay, I just wanted to be sure of that. In the case of the compression molding at any particular point, this may be true. However, if you were to look at injection molded specimens, the orientation would be much more complicated and you would need another method of data analysis—pole figures or whatever.

T. M. Malik: In the analysis of compression molded specimens, we assume that we have uniaxial orientation of the mica flakes and this seems to be a good assumption. For some injection molded and extruded specimens, biaxial orientations can develop. If this occurs, then you are right, a more sophisticated method of analysis of the x-ray data should be used.

J. L. White: Yes. We did that with extrusion through dies (Ref. 4).

L. A. Utracki: You mentioned that there is a significant amount of orientation in the polystyrene matrix, indicating that your specimens were not annealed.

T. M. Malik: The samples were prepared by blending the polymer with different amounts of mica on a roll mill and then compressed at 160 to 180°C. They were not annealed. I cannot tell you if annealing would reduce the matrix orientation or not.

L. A. Utracki: The way you described the correction of the X-ray intensity data seems to be arbitrary. First of all, you eliminated the shoulder peak by a handwaving argument that it does not reflect the particulate orientation; then you assumed that the theory must be correct and that your data must fit the theoretical curve. You justified this by saying that they do not agree due to matrix orientation, background scattering and so on. I did not detect in your exposé any attempt to justify this treatment. Why did you subtract half the intensity not 10 percent or 90 percent? Why the correction is assumed to be independent of the angle? Why do you think the theory has to be valid?

T. M. Malik: First of all, the shoulder observed is clearly due to the matrix orientation. This can be seen from the X-ray photograph and a comparison with the X-ray diffraction patterns of pure mica and pure PS. The elimination of this peak is not a problem at all and similar data are obtained by analyzing the full curve after elimination of the PS peak or by analyzing the portions of the curve where the PS peak is not seen. Second, the data have to be corrected for background scattering, diffuse scattering, etc. In principle, as you said, these contributions could be measured. In practice, they cannot because the PS matrix is oriented whereas the reference sample is not. However, the orientation function and the orientation parameter obtained for each sample are independent upon the intensity subtracted initially. The amount subtracted is determined by the standard deviation between the intensity curve and the orientation function. However, if by mistake 90 percent of the intensity was subtracted, no agreement could be reached between the intensity curve and the orientation function. Third, we admit that there is some arbitrariness in the choice of the orientation function. However, if the real function was very different from the one chosen, it would be impossible, as we have checked with other functions, to get the agreement that we reported.

L. A. Utracki: Don't you think, if you are postulating that the correction is due to the matrix, that the matrix behavior and the background scattering should be measured and subtracted, that to minimize the need for correction the specimens should be annealed?

T. M. Malik: The matrix behavior could not be measured and subtracted because it is oriented in the composite, whereas the reference matrix is non-oriented. Annealing could help in reducing this orientation, but this is something that we have not checked.

C. L. Beatty: I have a similar type of question. What would happen if you take mica flakes and mix them into a thermoset polymer, compress that, and allow the cure to take place? Would you see that the same correction effects are required?

T. M. Malik: I expect that yes, but to what extent, I do not know.

J. L. White: This technique is more potentially powerful that anything said so far has indicated. What you could do is not to use an amorphous but a crystalline polymer. By just looking at different Bragg angles in the diffractometer scan, you could pick up the orientation of the matrix as well as that of the particles.

T. M. Malik: I agree that if we use a semicrystalline polymer like polyethylene or polypropylene, then we can observe orientation of the matrix too, if the crystalline peaks of the polymer do not superimpose on those of mica.

J. L. White: In the earlier works involving this technique, organic-based materials, like carbon fibers of Kevlar, were used. There you could have trouble with the crystalline polymer in that the diffraction peaks tend to be in the same range as those of the filler and you could get peak overlap. However, with inorganic particles like mica, you can probably see that since the structures are quite different, so are the Bragg angles. The technique may be more powerful here.

T. M. Malik: Yes, that is right.

Measurement of Fiber and Matrix Orientations in Fiber Reinforced Composites

MUSA R. KAMAL,* LI SONG, *and* PETER SINGH

Department of Chemical Engineering
McGill University
Montreal, Canada H3A 2A7

Short glass fiber reinforced polypropylene was employed in a study to determine the effect of molding and mold design variables on the distribution of fibers and their orientations, and consequently, on the distributions of mechanical properties in the molded article. In this paper, a variety of experimental techniques were employed to evaluate the distributions of fibers and their orientations. Moreover, techniques were developed to evaluate the orientation and crystallization of the matrix. The results yield significant information regarding the development and control of both the microstructure and the properties of short fiber reinforced composites.

INTRODUCTION

In injection fiber reinforced molded articles, the distributions of fiber concentration, size and orientation are governed by a variety of factors. These include the original size and concentration of fibers, the gate design, and the processing conditions. These factors also have a strong influence on the orientation and crystallinity of the polymer matrix.

A number of techniques have been developed in recent years for investigating the matrix orientation in injection molded articles (1 to 9). These include x-ray diffraction, birefringence, sonic modulus, infrared dichroism, small angle light scattering, and electron microscopy. Considerable success has been achieved with these techniques in the measurement of orientation in pure polypropylene. However, there are many problems in employing them to study matrix orientation in short fiber reinforced composites. Birefringence and x-ray diffraction are not suitable measures of the matrix orientation because of light diffusion by the glass fibers. The glass fibers also affect the sound propagation speed in the composites, thus the sonic modulus is not a suitable measure of the matrix orientation.

The technique of a contact micro-radiography (CMR) (8) has been described as a means to study fiber reinforced thermoplastics. The fibers have to be made of high lead content glass to absorb the radiation, so that they are easily distinguished in the radiograph.

A semi-quantitative measure of fiber orientation has been developed by McGee and McCullough (10). This representative fiber distribution, for example, is a negative of a micrograph. Diffraction patterns characteristic of the fiber orientation are produced using diffraction masks in a Fraunhafer diffractometer.

A more rapid technique for analyzing a fiber micrograph has been developed by Lovrich and Tucker (11). The micrograph is digitized by a computer that utilizes a video camera and special digitizing hardware. The images of the fibers are then stored in the memory. Subsequently, a Fourier transformation is computed on the stored image, and the distribution is extracted from the transform.

In this study, a variety of techniques have been developed to study the fiber and matrix orientation in short glass fiber reinforced polypropylene samples that were injection molded under controlled conditions. The techniques employed include thermogravimetric analysis, Fourier transform infrared analysis (FTIR), pyrolysis, and polarized light microscopy.

SAMPLE PREPARATION

The materials used in this study were pure polypropylene (Pro-Fax 6501), which was supplied by Hercules Canada Ltd., and a fiber filled polypropylene, which utilized the Pro-Fax 6501 as the matrix material. The fiber filled material contained 10 percent by weight fibers of 10 microns diameter and an average length of 710 microns.

A reciprocating screw 2½ oz. metalmec injection molding machine was used. A center-gated

* To whom all correspondence should be addressed.

rectangular mold cavity of dimensions 10 cm x 6 cm x 3 mm was used. The gate width was 7.8 mm. The moldings were produced under the following conditions: 1. A melt temperature of 208°C for pure polypropylene and 232°C for fiber filled polypropylene; 2. An injection time of 3 s; and 3. A mold temperature of 30 to 35°C.

ANALYTICAL TECHNIQUES

Rectangular samples of dimensions 10 mm x 4 mm x 3 mm were cut from the different moldings at positions indicated in *Fig. 1*. The samples were located at 0.5 cm, 5 cm, and 8.5 cm from the gate at the center positions, and 0.5 cm from the gate at the off-center position. Microtomed layers of required thickness were then removed from the sections in the transverse, longitudinal, and depth directions of the moldings. These were then used for the various measurements.

Fiber Length Measurements

Samples from the moldings were placed in a crucible and heated to 500°C to burn off the resin. After cooling, the remaining glass fibers were placed on a glass slide. The slide was placed on a Reichert microscope and a photograph was taken to be used for obtaining a digitized fiber micrograph. The ends of the fibers in the photograph were manually digitized onto a graphics database. The computer then generated the angle and the length distribution based on the end point coordinates of the fibers.

Fiber Concentration Measurements

A thermogravimetric analysis system (TGA) model Cahin DC113 was used. Samples approximately 100 micron thick, were weighed in the TGA at room temperature. The temperature was then increased to 600°C at a scan rate of 20 C/min to burn off all the resin. The sample was then weighed again to obtain the fiber concentration.

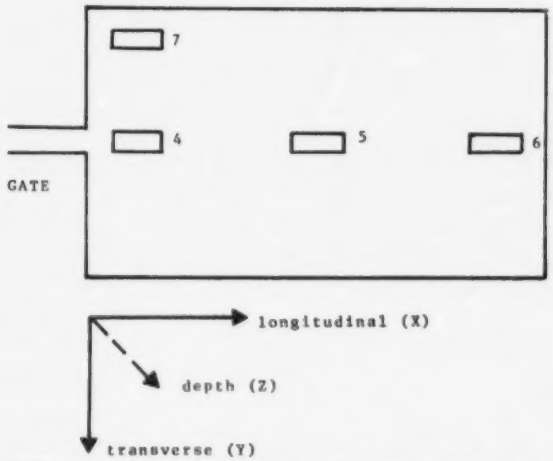

Fig. 1. Designated positions for monostructural studies in the depth direction of molding.

Fourier Transform Infrared Spectroscopy

Absorption spectra were obtained using a Nicolet model 7199 FTIS. A sample space wire grid polarizer was utilized. Thirty-one scans at 0.5 cm-1 resolution were a signaled, averaged and stored on disk for each sample. All measurements were made at room temperature. Samples were obtained by immersing microtomed layers in hydrofluoric acid for 24 h to remove glass fibers. Eventually, it was found out that the spectra in the region of interest could be obtained with the glass fibers intact, providing that the samples were sufficiently thin.

Fiber Orientation Measurements

Microtomed layers approximately 30 microns in thickness were placed on microscope slides and covered with glass covers. The slides were heated to 5 to 10°C above the melt temperature of the resin for 5 s to eliminate the knife traces. The slides were then placed on the rotating stage of a polarization microscope and a photograph was taken. The photograph was used to obtain a digitized fiber micrograph.

RESULTS AND DISCUSSIONS

Fiber Length Distribution

In composites, the length distribution is affected by the shape of the gate as well as by the injection molding conditions. The fiber length distribution influences the mechanical properties of the composite articles. Thus, the average fiber length and fiber length distribution provide a reliable method of characterizing some of the mechanical properties of composites. The fiber length distribution of the pellet and the molded articles are shown in *Fig. 2*. After processing, the average fiber length decreases from 0.710 mm in the pellet to 0.274 mm in the molding. The length distribution curve was also shifted towards the lower length direction. Thus, it can be seen that the fiber length distribution is drastically changed by processing. The

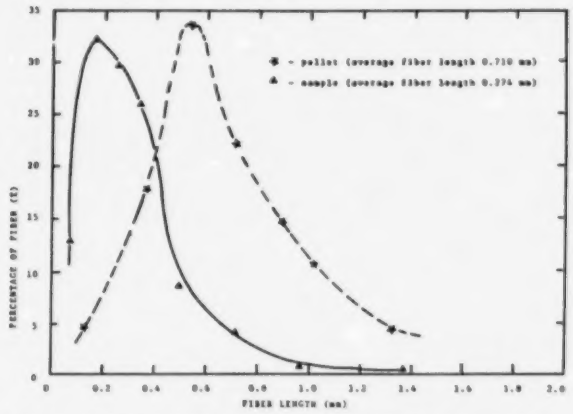

Fig. 2. Fiber length distribution in the pellet and the processed material.

length distribution appears normal in the pellet, but is skewed towards the shorter lengths in the molding. This phenomenon is due mainly to the screw action and partly to fiber-fiber interactions and hydrostatic forces.

Fiber Concentration Distribution

Figure 3 shows the variation of fiber concentration in the depth direction at position 6. The fiber concentration changes only slightly in the higher fiber concentration than in the surface region. This behavior is expected and is due to the fiber migration from the walls because of the discontinuity effect.

Matrix Orientation

Dichroic measurements corresponding to 1220 cm-1 and 1256 cm-1 absorption peaks were made and used to quantify the matrix orientation. Isotatic polypropylene can be considered as a two-phase system consisting of type I (monoclinic) crystals, type II (hexagonal) crystals, or a mixture of both. For partially crystalline polymer, infrared peaks can arise from vibrations either within the crystalline phase, within the amorphous phase, or within both.

For a uniaxially oriented polymer sample, the absorbence ($A1$), measured with radiation polarized in the stretched or flow direction, may differ from the absorbence (At) measured for the radiation polarized perpendicular to this direction. The dichroic ratio (D) is given by $D = A1/At$.

In polypropylene, it is generally agreed that the 1220 cm-1 band is due to absorption by the crystalline phase only (9). The 1256 cm-1 band results from absorption in both the crystalline and the amorphous regions, and its infrared dichroism is expected to correlate with an average orientation function (9). The transition moment angle for the 1220 cm-1 band is 72°. This is linked to the fact that isotatic polypropylene has a helical conformation in the crystalline phase, and each band makes an angle of 72°C with the helical axis (9). The transitional moment angle for the 1256 cm-1 band has no

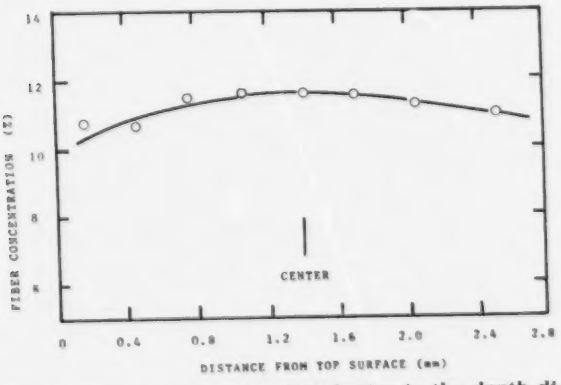

Fig. 3. Fiber concentration distribution in the depth direction at position 6.

structural significance. A value of dichroic ratio lower than 1.0 will give an orientation function fp that is positive, signifying that the C axis of the polymer is preferentially oriented in the longitudinal direction. This means that the a and b axis are oriented in the transverse direction. A dichroic ratio greater than 1.0 signifies that the C axis is preferentially oriented in the transverse direction, while a and b are in the longitudinal direction.

In this paper, the direction perpendicular to the C axis (i.e., the molecular chain axis) will be referred to as the orientation direction. This direction corresponds to the radial fibril direction in the crystalline phase.

Figure 4 shows the variation of the dichroic ratio in the depth direction for the 1220 cm-1 band. The results show that the dichroic ratio is always less than one, implying that the crystalline phase has a preferred orientation in the transverse direction. The crystalline phase in the composite shows more preferred orientation than that of the pure polypropylene. In both samples, the crystalline phase is highly oriented at the surface and becomes more randomly oriented at the core. The greatest orientation in the transverse direction for the crystalline phase is obtained near the gate position. This behavior has been explained by the longer cooling times, higher packing pressure and shear rate gradient that prevail near the gate (1). At the core, the dichroic ratio for the pure polypropylene sample is close to one. This means that the crystalline phase is randomly oriented at the core for the pure sample. However, the crystalline phase at the core in the composite sample shows some degree of transverse orientation. At position 7, the orientation is random throughout the depth direction for the pure polypropylene. This is expected since the flow characteristics in that region would be random. However, there is still some orientation in the crystalline phase for the composite sample. It appears that the presence of fibers has an effect on the orientation of the crystalline phase of the matrix.

Figure 5 shows the dichroic ratio for the 1256 cm-1 band. These results provide information on the combined orientation of both the amorphous and the crystalline phase. Since the crystalline phase orientation is known, then some conclusions can be drawn regarding the orientation of the amorphous phase. In both samples, the dichroic ratio is greater than one, implying that the orientation of the amorphous phase is in the longitudinal direction or in the direction of flow. The variation of the amorphous phase orientation in the depth direction is very similar to that for the crystalline phase. The difference lies in the direction of orientation. The amorphous phase is more highly oriented in the composite, at the surface, and near to the gate. It is oriented randomly at the core for the pure polypropylene but shows some orientation in

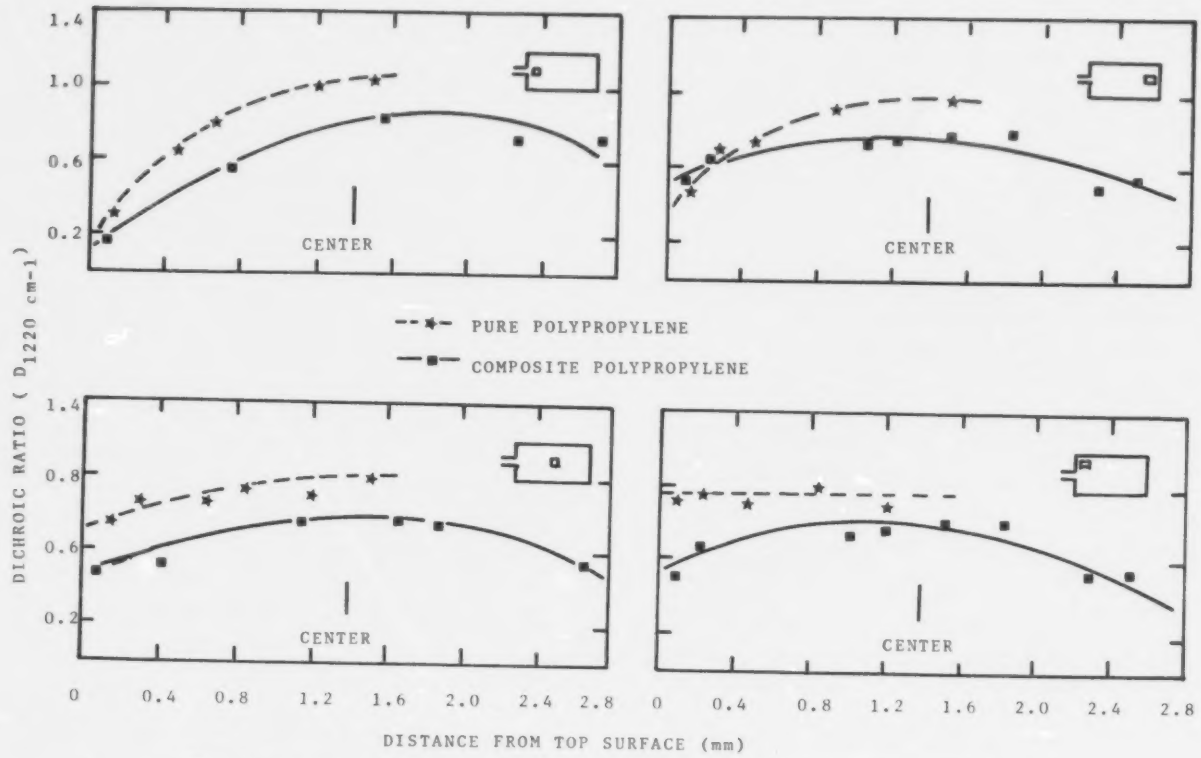

Fig. 4. Variation of dichroic ratio in the depth direction for crystalling phase (D_{1220}).

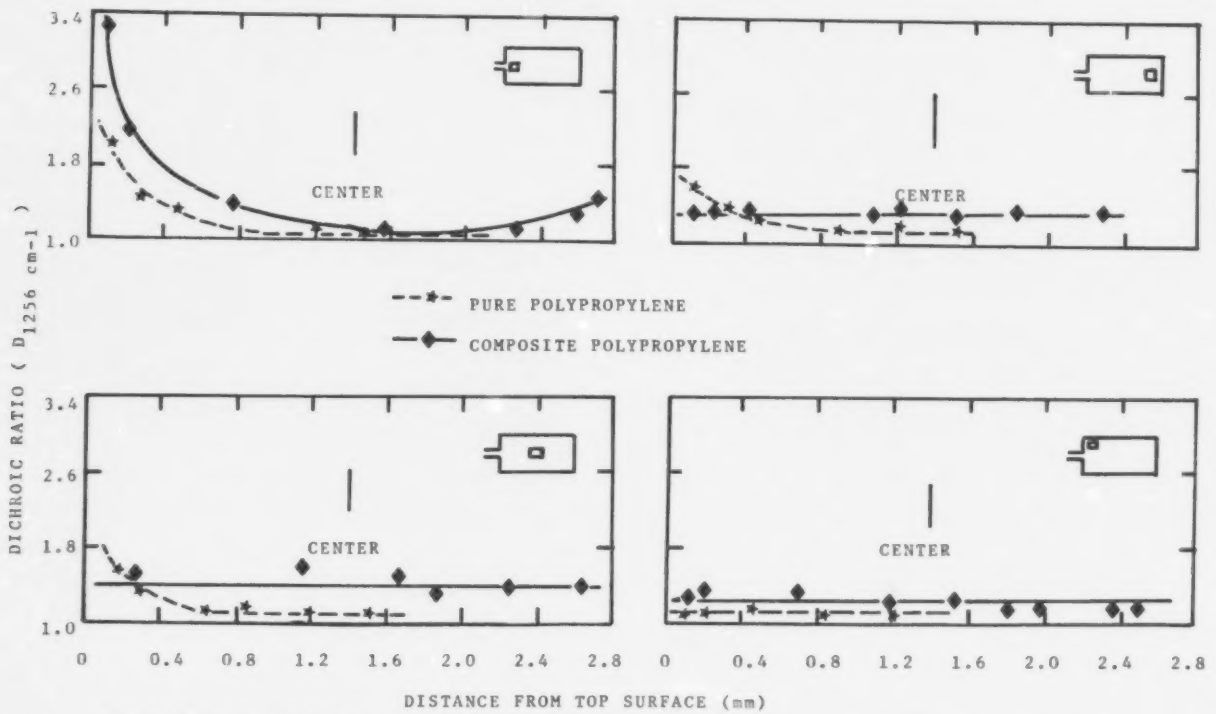

Fig. 5. Variation of dichroic ratio in the depth direction for crystalline and amorphous phases (D_{1256}).

the composite. At position 7, the orientation is random throughout the depth for the composite and the pure polypropylene.

Fiber Orientation

During the molding process, the fibers may become oriented in a complex manner to form

layers of different orientation (4). This can produce marked anisotropy of the mechanical properties. The flow geometry has a major effect on fiber orientation. The shear rate and melt viscosity can also significantly alter the size of the oriented regions.

The fiber orientation with the designated positions in the depth direction of the molding are shown in *Figs. 6* and *7*. The orientation shows a layered structure. The central region contains fibers aligned mainly transversely to the flow direction. This behavior has been explained by Bright (4). When the material enters the mold, the fibers are already strongly aligned in the injection direction. At the gate, the sudden increase in the dimensions of the channel produce a deceleration in the material flow, which is accompanied by a compressive force along the flow direction. A fiber that is slightly inclined away from the axis will tend to rotate into an orientation transverse to the flow direction under the action of the compressive force. It has been shown that fiber orientation in the cavity can be controlled using extensional fields in converging or diverging flow channels (12, 13). The flow of the composite melt through the gate and into the cavity represents diverging flow. This produces transverse fiber orientation. It is only near the walls where shear deformation recurs, that there is a tendency for the fibers to orient in the longitudinal direction.

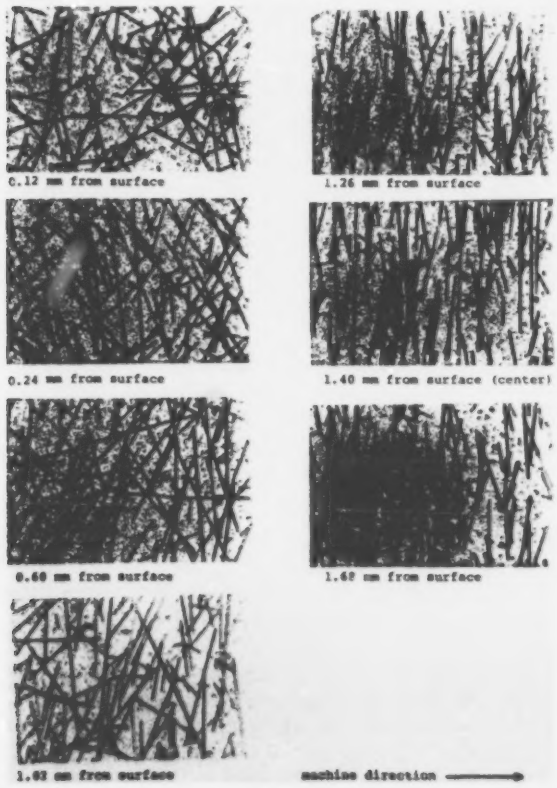

Fig. 6. Fiber micrographs in the depth direction at position 6.

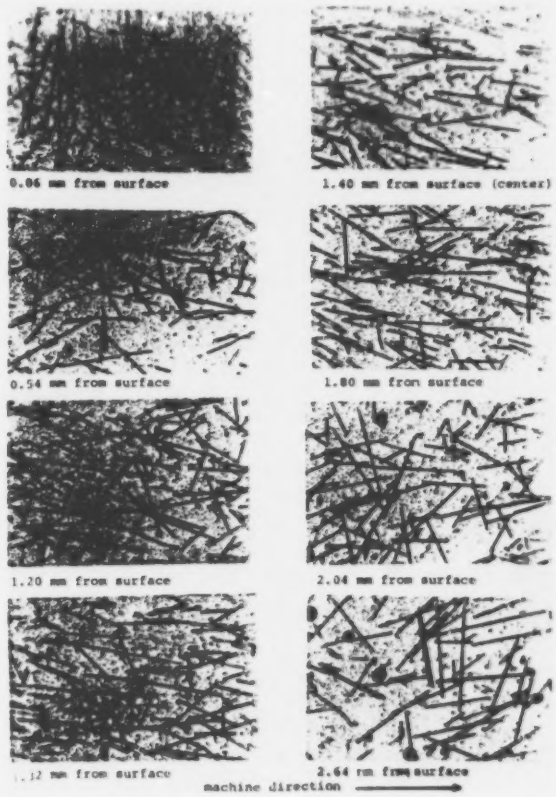

Fig. 7. Fiber micrographs in the depth direction at position 7.

The fiber orientation histograms at positions 6 and 7 are shown in *Fig. 8*. The figures show that, in the central region, fibers were highly aligned, and in the surface regions, the fibers were arranged randomly. At position 6, the direction of orientation of the fibers in the core is transverse to the machine direction and transverse to the flow direction. At position 7, the preferred orientation is parallel to the machine direction but also transverse to the flow direction. In both cases, the fibers are oriented transverse to the flow direction.

The histograms properly normalized are experimental measurements of the orientation distribution function. The accuracy of the distribution function provided by this method depends on the number of fibers sampled (10).

CONCLUSIONS

This study has used some techniques to characterize matrix orientation, fiber orientation, fiber length distribution, and fiber concentration in a semi-transparent matrix of a short glass fiber reinforced polypropylene. For the measurement of fiber orientation, the most important factor is to obtain good quality fiber micrographs. A polarization microscope was employed to obtain the fiber micrograph in the clear matrix. In this case, care must be taken to eliminate the knife traces. TGA was used to

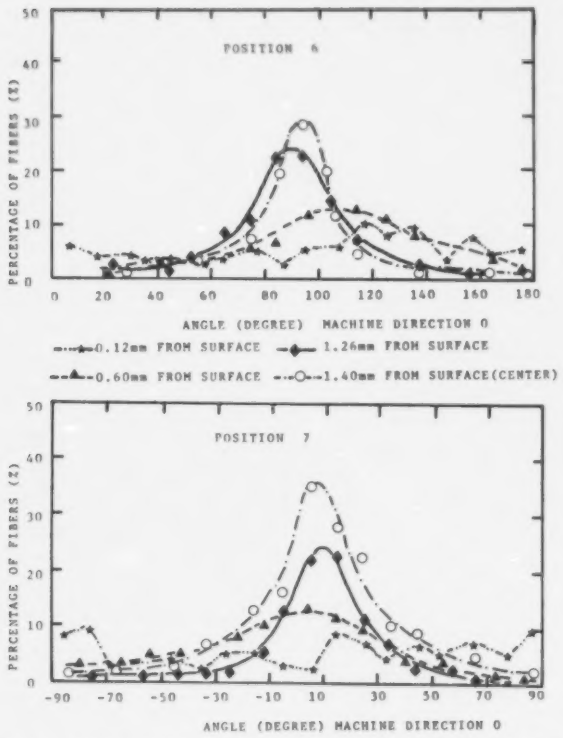

Fig. 8. Fiber orientation histograms for positions 6 and 7.

measure fiber concentration distribution. This method is convenient, accurate, and a small sample is needed. The method of burning off all the resin and using a polarization microscope can be used with most thermoplastic composites. From the results obtained, it is seen that the fibers in the central regions are oriented transverse to the flow direction, while the surface layers show no preferred orientation. The fiber length distribution is seen to be drastically shifted and skewed in the direction of the shorter lengths after processing due mainly to the screw action. The fiber concentration is slightly higher in the center regions than in the surface regions.

FTIR was used to measure dichroic ratio. The dichroic ratio at 1220 cm-1 is used to yield information concerning the crystalline orientation. The dichroic ratio at 1256 cm-1 results from absorption in both the crystalline and the amorphous regions, and it can be related to an average orientation function. The degree of matrix orientation is highest at the surface in both the pure and composite matrix, and decreases to a minimum in the core for both. The degree of orientation is also highest near the gate. The preferred direction of the orientation of the crystalline phase is transverse to the flow direction in both the unfilled and the filled polypropylene. The direction of the orientation of the amorphous phase is parallel to the flow direction.

ACKNOWLEDGMENTS

The authors would like to acknowledge financial support from the following organizations: Engineering Mechanics Department of General Motors Corporation, Natural Sciences and Engineering Research Council of Canada, and Ministère de l'Education of the Government of Quebec.

The following companies supplied the materials and helped in the preparation of the compounds: Himont Canada Inc., Wilson-Fiberfill Canada and, Certain Teed Corporation.

REFERENCES

1. M. R. Kamal and F. H. Moy, *J. Appl. Polym. Sci.*, **28**, 1787 (1983).
2. W. W. Moseley Jr., *J. Appl. Polym. Sci.*, **III**, 266 (1960).
3. P. F. Bright, M. W. Darlington, *Plast. Rubb. Proc. Appl.*, **12**, 139 (1981).
4. P. F. Bright, R. J. Crowser, and M. J. Folkes, *J. Mater. Sci.*, **13**, 2479 (1978).
5. Z. W. Wilchinsky, *J. Appl. Phys. 31*, **11**, 1969 (1960).
6. S. S. Katti and M. Schultz, *Polym. Eng. Sci.*, **22**, 1001, (1982).
7. R. Zbinden, "Infrared Spectroscopy of High Polymers," New York (1964).
8. M. W. Darlington and P. L. McGinley, *J. Mater. Sci.*, **10**, 906 (1975).
9. R. J. Samuels, *J. Polym. Sci., A*, **31**, 1741 (1965).
10. S. H. McGee and R. L. McCullough, *J. Appl. Phys.*, **65**, 1394 (1984).
11. M. L. Lovrich and C. LO. Tucker III, *SPE ANTEC Tech. Paper*, **31**, 1119 (1985).
12. L. A. Goettler and K. S. Shen, *Rubber Chem. Technol.*, **56**, 619 (1983).
13. L. A. Goettler, NRCC/IMRI Symposium "Composites-'82," Montreal, Quebec, Canada, Nov. 30, 1982; *Polym. Compos.*, 60 (1984).

DISCUSSION

J. L. White: In the calculations of molecular orientation using infrared dichroism one needs to have the transition moment angle as well as the dichroic ratio. Basically, what this represents is that the absorbing group is oriented along the axis or perpendicular. If you just take polypropylene or any other sample and stretch it, and you look at all different absorption bands, some ratios become more than one, some less than one, depending on this transition moment. So, you need to know the transition moment to make such calculations. Also, don't you implicitly presume that you have a uniaxial type molecular orientation with regard to certain direction in it. You can measure two dichroic ratios, say by cutting sample in different directions and check that.

M. R. Kamal: We did not calculate the orientation function, but showed only the dichroic ratios. This is really the beginning of the study, and we are simply trying to get a feel what is going on there. However, your point is well taken. We did a lot of work on virgin, nonreinforced polythylene. We found through a variety of tests that if one looks at the microtomed specimens, one approaches the uniaxial symmetry. We did not check this carefully in the

case of either polypropylene or reinforced polymer moldings.

M. Y. Boluk: You have reported higher orientation near the surface and gate, which is reasonable because you decreased the entanglement density. When you reported higher orientation in the composites, again is it the same mechanism. It is possible that when you mix fiber with polymer you decrease the entanglement density, specially near the fibers due to high shear rate and increase orientation. Was the effect of entanglement density decrease responsible for the increase of orientation?

P. Singh: Could you rephrase the question? I did not get it.

M. Y. Boluk: You said that you have near the surface high shear rate and higher orientation. Can we say that when there is a high shear rate the entanglement density decreases and makes higher orientation possible? Can you agree on that first?

P. Singh: That is possible.

M. Y. Boluk: In the second phase, I want to ask you if you can make the same reasoning as far as preparation of polymer composites go. When you mix polymer with fibers, is it possible to decrease entanglement, specially around fibers and increase the orientation?

P. Singh: I would not know how to answer this question. But we are doing the studies which may allow us to answer quantitatively your point in the near future.

C. L. Beatty: In the semicrystalline polymer composites did you take note of the morphology, in particular of any change in transcrystalline layer versus spherulitic character of the sample from location to location within the mold as well as far as the filler concentration is concerned?

P. Singh: We did not measure crystallinity in this study. This is only a preliminary report.

C. L. Beatty: Do you plan to use nucleating agents or vary temperature of the mold to change the crystallization characteristics?

P. Singh: We plan to change a number of processing conditions and study all these effects.

M. R. Kamal: This is again a very good question and in studies of morphologies all the way through it is something that we would look into. But I presume you appreciate how difficult it is to get into this. When one looks into composites, considering the effects of nucleating agents, sizing agents, and other variables, one can think of a lot of issues which may arise. But each of these is between three and five years long. This is why we will probably not do it in the next few years. To start this work we had to get a few tonnes of resin, large volume of fiber, clearly identified for us and prepared according to our specification, to send this material to a commercial compounder. Now, effectively for the next few years we have to freeze on that. If we want to introduce other variables we can, but it is a major task.

C. L. Beatty: I can appreciate that. We are doing a similar study with glass beads. One thing which we are doing is to use a statistically designed experiment to accomplish what we want without unduly increasing the number of required experiments.

M. R. Kamal: Actually, we know that we are not working in the vacuum, that people like you, White, Utracki are doing work in the field and another way to minimize our effects is to draw on what these people can teach us.

L. A. Utracki: I am truly amazed how much information you can get on both fiber and matrix orientation using these minute microtomed samples. How do you microtome these microscopic specimens without modifying the original structure?

P. Singh: First, we cut the molding in strips of a suitable dimension, say one millimeter, and then use Crazy glue and glue it onto something else. Then you can microtome across.

L. A. Utracki: At the liquid nitrogen temperature?

P. Singh: No, at ambient temperature.

L. A. Utracki: Don't you distort the polymeric matrix? We observed a ductile deformation during freeze fracturing of polyethylene rod immersed in liquid nitrogen.

P. Singh: No, there is no distortion. This is why we glue it onto another material and cut it perpendicularly. If you try to microtome it across a broad surface, then you will get distortion.

Improved Epoxy-Amine Matrices for Composites

P. D. McLEAN, A. GARTON,* *and* W. T. K. STEVENSON

National Research Council of Canada
Ottawa, Ontario, K1A OR6

and

K. E. MacPHEE

Uniroyal Ltd.
Guelph, Ontario

The physical and mechanical properties of epoxy-amine matrices can be improved by the use of additives known as epoxy fortifiers. The tensile strength of a typical amine-cured epoxy increased from 82 MPa to 123 MPa, the tensile modulus from 2.5 GPa to 4.1 GPa, and the tensile test specimens also failed in a ductile fashion. The improvements in matrix properties translated into improved performance for filament-wound and cloth-reinforced composites. For example, the transverse moduli and compression strengths of carbon fiber/epoxy filament-wound tubes and plates increased at least 20 percent with the addition of fortifiers, while the compression strength of glass cloth/epoxy laminates increased by up to 41 percent.

INTRODUCTION

Epoxy resins are best known to the general public as adhesives, but this application accounts for only about 5 percent of epoxy resin consumption. A much larger market (60 million lb. p.a. in 1980, 290 million lb. p.a. predicted in 1995) involves the use of epoxy resins as one component of fiber-reinforced composite materials. Such composites typically are used in transportation or structural applications, where their high specific stiffness and strength, as well as ease of fabrication, offer unique advantages over traditional materials.

At first sight, the mechanical properties of the resin matrix component of a composite may appear to be unimportant because of the presence of the reinforcing fibers. Experience has shown, however, that composites frequently will be subjected to tensile stresses perpendicular to the fiber direction as well as compression, fatigue, or impact stresses. Under such conditions, the response of the matrix will strongly influence the performance of the composite. Therefore, there is considerable interest in the development of resins or additives that improve the physical and mechanical properties of the matrix material.

We report here on the successful development of a range of additives that improve the strength (up to 60 percent) and stiffness (up to 70 percent) of amine cured epoxy resins, as well as improving the ability of the samples to yield before fracture (ductility), which has important consequences for the damage tolerance and machinability of the plastic (1 to 3). One particular additive formation (designated EPPHAA) is described in detail here. This formulation may be considered as representative of the series in terms of its effect on the mechanical properties of the plastics and composites, although because of the depression it produces in the glass transition temperature (T_g), has only moderate elevated temperature performance. Several other additive formulations are described in less detail. These additives, known as epoxy fortifiers, are produced by Uniroyal Limited, Chemical Division of Elmira, Ontario, and are identified only by their commercial nomenclature, (e.g., Fortifier A).

EXPERIMENTAL

1,2-Epoxy-3-phenoxypropane (EPP) was of reagent grade and 98 percent pure by liquid chromatography. 4-Hydroxyacetanilide (HAA, Eastman) had a melting point of 170°C and contained no detectable impurities by liquid chromatography. The product EPPHAA was prepared by heating EPP and HAA at a 1.05:1 mole ratio to 160°C for 60 min. Standard analytical techniques showed that the product was

* To whom correspondence should be addressed.

largely of structure A, with the starting materials as the major impurities (3).

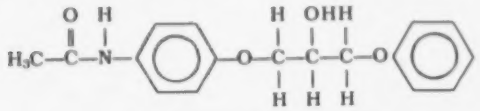

Structure A

Details of the nomenclature of resins, curing agents, and additives are given in *Table 1*. The mixing and casting of epoxy resin plaques followed standard industrial practice (3, 4). Unless stated otherwise, the cure cycle for unreinforced specimens was 100°C (1 h), then 125°C (2 h), and 175°C (4 h). Filament wound carbon/epoxy tubes and plates were made with Thornel 300 carbon fiber (Union Carbide) and the DER 383/Ancamine 1482 resin system, then cured at 100°C (2 h), 130°C (2 h), and 160°C (2 h). Similarly, filament-wound glass/epoxy tubes were made from Fiberglas Canada ECR 3709 roving with XC181 finish. Glass/epoxy laminates for compression testing were made from 8 plies of 137-style fabric (Bay Mills) with 139 finish. The glass was impregnated with the hot resin system [Epon 828 + 19 phr (parts per hundred of resin) Ancamine 1482], with and without additives, vacuum bagged and cured for 1 h at 100°C then 4 h at 150°C.

Tensile testing of the unreinforced plastics was carried out on dumbbell-shaped specimens according to ASTM D638 (type II), using an Instron tensile tester at 2 mm/min crosshead speed (3). Changes in transverse dimensions during the tensile test were determined using glue-on strain gauges (Macro-Measurements EA-06-062TT-120) at low strains (5) (≤1.5 percent) and clip-on Instron strain gauges at higher strains (up to 7 percent).

Fracture toughness determinations were made in a controlled environment (65 percent) relative humidity, 23°C), using rectangular compact tension specimens (6). A Rheometrics mechanical spectrometer (RMS-605) with a forced-torsion test fixture was used to measure the shear modulus (G'), loss modulus (G'') and loss tangent ($\tan \delta$) as a function of temperature and frequency. Tensile fracture surfaces were examined by scanning electron microscopy (SEM) with an AMR-1000 microscope (3).

The glass/epoxy laminates (7.5 × 1.9 × 0.16 cm) were tested in compression at 2 mm/min.

Table 1. Nomenclature of Epoxy Resin Formulations.

Epon 828	A diglycidyl-type epoxy resin (Shell)
DER 383	A diglycidyl-type epoxy resin (Dow)
DEN 431	A novolac epoxy resin (Dow)
CY 179	A cycloaliphatic epoxy resin (Ciba-Geigy)
DDM	Diaminodiphenylmethane (Ciba-Geigy)
DDS	Diaminodiphenylsulphone (Ciba-Geigy)
Ancamine 1482	A proprietary amine curative (Pacific Anchor)
Fortifiers I, A, C, K, G	Proprietary fortifier formulations (Uniroyal)

The hoop-wound glass and carbon-reinforced tubes were tested in tension and compression using a friction clamp fixture and a crosshead speed of 5 mm/min. Samples cut from filament-wound carbon/epoxy flat plates were tested for compressive strength (ASTM D3410), flexural strength and modulus (ASTM D790), and short beam shear strength (ASTM D2344) at a crosshead speed of 5 mm/min.

RESULTS

Properties of the Unreinforced Plastic

Figure 1 shows the stress-strain curves for Epon 828 + 30 phr DDM, as well as for samples containing 15 and 30 phr EPPHAA. Clearly, the tensile modulus is increased by the presence of EPPHAA, as is the maximum engineering stress. Note also that the slope of the stress-strain curve becomes negative before failure for EPPHAA-containing samples, indicating that some localized yielding occurs before fracture.

The changes in transverse dimensions of the tensile-test specimens are shown in *Fig. 2*. The increase in volume with tensile strain (the Poisson effect) for Epon 828/DDM, with and without EPPHAA, is shown in *Fig. 2a*. The data are expressed as volume expansion, not as Poisson's ratio as is conventional in metals technology, because the plastic samples respond to stress in a viscoelastic fashion, which therefore makes Poisson's ratio a time dependent variable. *Figure 2a* shows that the tensile test is accompanied by a significant volume increase, and that the rate of volume increase, at least at low strains, is about 35 percent higher for EPPHAA-containing samples than the control.

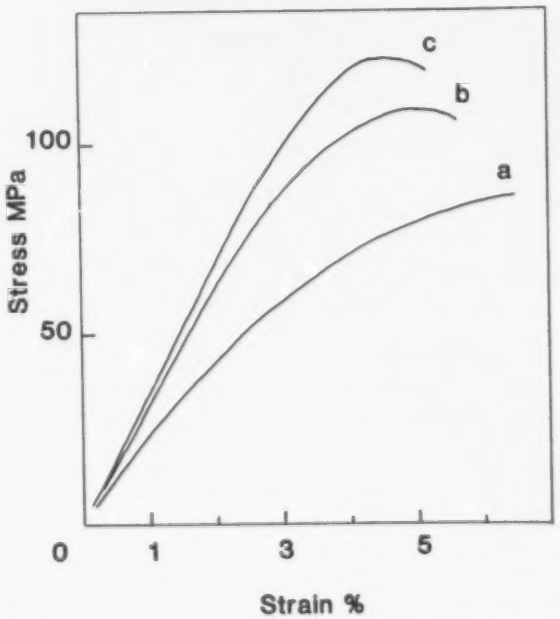

Fig. 1. Stress-strain curves for Epon 828/DDM. (a) Epon 828/DDM control; (b) +15 phr EPPHAA; (c) +30 phr EPPHAA.

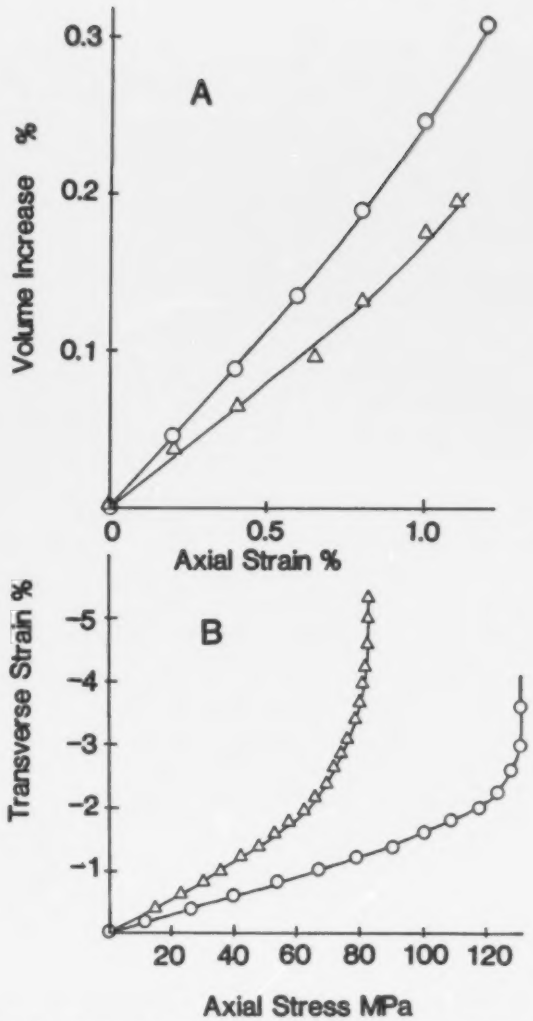

Fig. 2. Changes in transverse dimensions that occur during tensile testing. (A) Low-strain data obtained from glue-on strain gauges mounted parallel and perpendicular to the tensile stress. (B) High strain data obtained with clip-on strain gauge. —Δ—Δ— Epon 828/DDM control; —O—O— + 30 phr fortifier I.

Figure 2b demonstrates that the axial yielding which occurs in EPPHAA-containing samples at high stresses (*Fig. 1*), is accompanied by a similar yielding in the transverse direction. This behavior is characteristic of a material passing through a generalized glass-to-rubber transition, rather than simply yielding by a crazing mechanism, when the transverse dimensions would remain constant. It should be noted that the clip-on strain gauges exert a significant compressive force (~0.8 MPa) and so *Fig. 2b* cannot be considered as a measure of volume change with tensile strain, as is shown in *Fig. 2a*.

Figure 3 shows the SEM micrographs of the tensile fracture surfaces. The control sample (*Fig. 3b*) shows conventional brittle epoxy failure (7), with a smooth region of slow initial crack growth, surrounded by a large area of

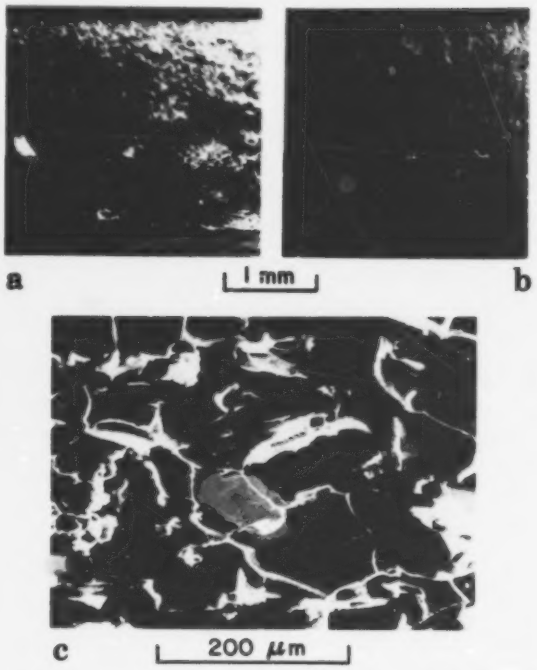

Fig. 3. SEM of fracture surfaces of tensile test specimens. (a), (c) Epon 828/DDM + 30 phr EPPHAA; (b) Epon 828/DDM control.

catastrophic crack growth. The EPPHAA-containing sample has a fracture topography characterized by a series of shallow cavities, about 100 μm diameter, surrounded by ridges of material which clearly had undergone extensive plastic deformation (*Fig. 3a, 3c*).

The fracture toughness values for EPPHAA-containing samples were strongly strain-rate dependent (*Fig. 4*). At low testing speeds, the toughness was increased significantly by the presence of EPPHAA, while at higher speeds the toughness was reduced to a value close to that of the control. Note that these data were obtained from samples which had been dried at 120°C, then stored for several days at 23°C and 65 percent R.H. Studies of the effect of long-term aging on the fracture process are in progress.

The temperature dependence of the shear modulus is shown in *Fig. 5*, for the control and for samples containing EPPHAA and proprietary fortifier A. Room temperature moduli were increased up to 60 percent by the additives. At low temperatures, the stiffening effect diminishes, although the moduli of the additive-containing samples exceeded the control even at −100°C. At elevated temperatures, the moduli in *Fig. 5* drop below that of the control as their T_g is approached. The depression of T_g caused by the additives varied from about 50°C for 30 phr EPPHAA to about 15°C for proprietary formulation A. Other proprietary formulations can produce a small increase in T_g (1, 2).

As well as having good high temperature per-

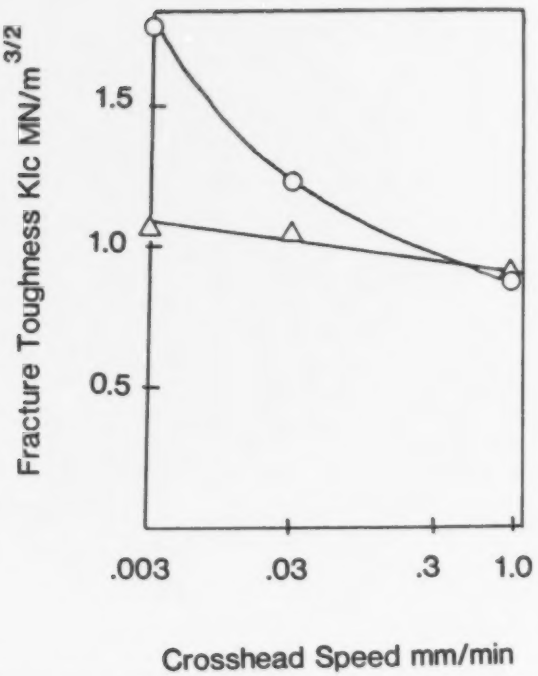

Fig. 4. Fracture toughness of compact tension specimens as a function of testing rate. —△—△— Epon 828/DDM control; —○—○— + 30 phr EPPHAA.

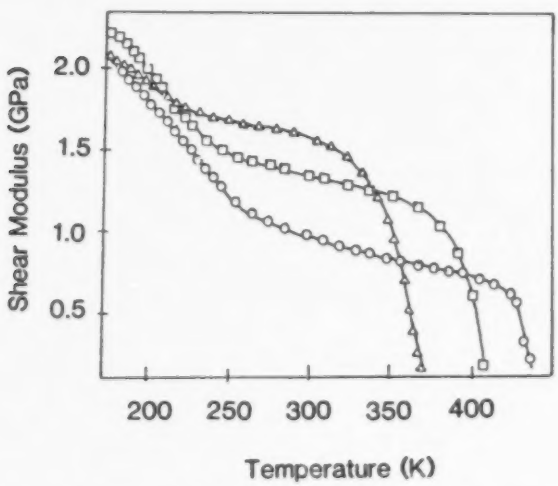

Fig. 5. Shear modulus at 1 Hz as a function of temperature. —○—○— Epon 828/DDM control; —△—△— + 30 phr EPPHAA; □—□—□— 30 phr fortifier A.

formance, epoxy matrices should also be unaffected by aggressive environments. *Figure 6* shows that fortifier formulation C retained its enhancing properties even after prolonged humid-aging. Eight days of aging at 70°C and 95 percent relative humidity produced a constant ~10 MPa decrease in strength for both the control and the additive-containing samples. Drying the humid-aged samples returned their strengths close to the original values. A gravimetric determination of water uptake at 23°C and 100 percent relative humidity (*Fig. 7*)

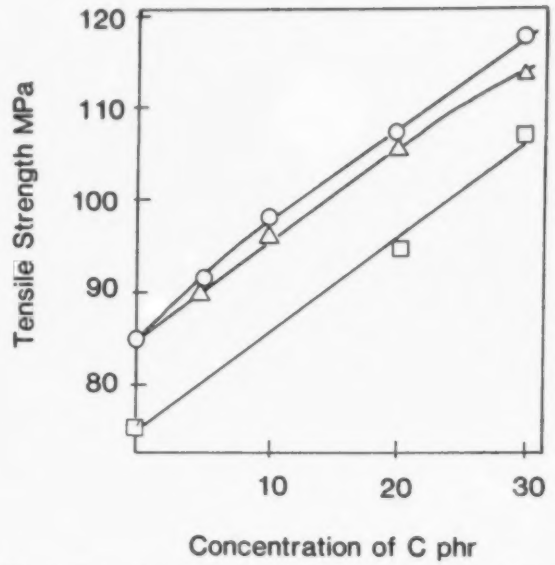

Fig. 6. Retention of properties on exposure to moisture Epon 828/DDM with various concentrations of fortifier C. —○—○— Original plastic; —△—△— Boiled 15 min.; □—□—□— 8 days, 75°C, 95 percent R.H.

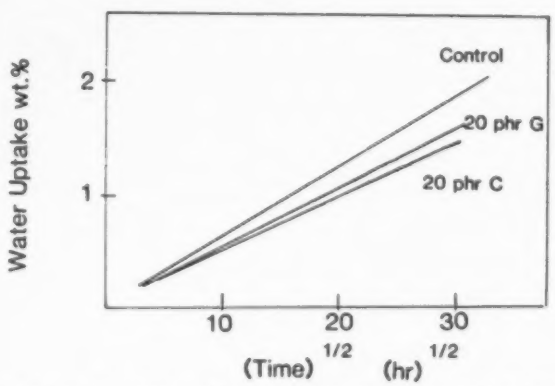

Fig. 7. Gravimetric determination of water uptake as a function of the square root of time of exposure to 100 percent relative humidity air at 23°C.

shows that, under these conditions, fortifiers G and C caused a reduction in water uptake of the cured plastic. It was noted, however, that as with the moduli (*Fig. 4*), the water-uptake characteristics were temperature dependent. For example, at 100°C (2 h in boiling water), the water uptake of the additive-containing samples became similar to that of the control (0.89 weight percent for 30 phr C, 0.85 weight percent for control).

Another benefit of the fortifiers is their catalytic effect on the cure process. This allows the production of high modulus, high strength matrices at relatively low cure temperatures. Curing the Epon 828-DDM system at less than 100°C produces a frail B-stage material (*Fig. 8*). The addition of 20 phr of Fortifier I produced excellent matrix properties at a cure temperature of only 60°C.

Finally, these additives have been used successfully with a variety of epoxy resins and curing agents. *Table 2* shows that DEN 431 (a novolac resin) responded favorably to the addition of fortifier C. Alicyclic resins (e.g., CY179), which are normally considered difficult to cure with amines, were also responsive to a range of additives. The curing agent diaminodiphenylsulphone (DDS) is well known to enhance the high temperature performance of epoxy resins, but it is difficult to process by conventional casting techniques. The addition of fortifier A improves the processability of the Epon 828-DDS system by making the DDS more readily soluble and also produced a relatively high strength material.

Properties of Reinforced Systems

Although the enhancement of the properties of the plastic by the additive is demonstrated clearly in the previous section, predictive theories of composite properties are not yet sufficiently developed to allow confident calculation of what effect matrix enhancement will have on composite properties. Therefore, a series of composites was fabricated to demonstrate practically the benefits of matrix enhancement.

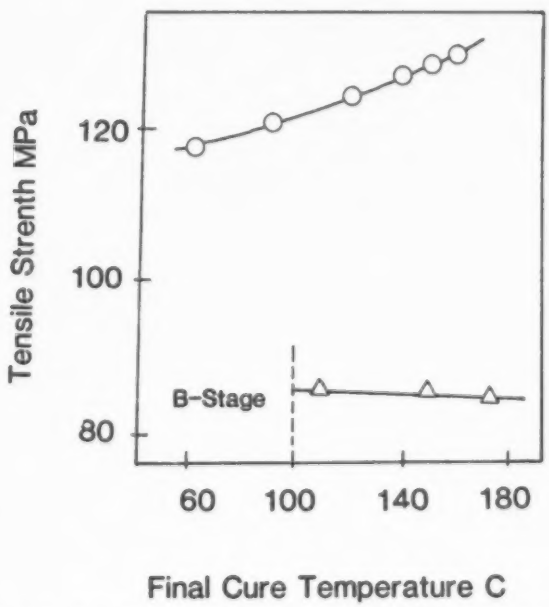

Fig. 8. Tensile strength as a function of cure temperature for Epon 828/DDM. —Δ—Δ— Control; —O—O— + 30 phr fortifier I.

Table 2. Use of Additives in Other Resin Systems.

Resin	Curative	Additive	Strength
DEN 431	DDM	—	96 MPa
DEN 431	DDM	20 phr C	122 MPa
DEN 431	DDM	30 phr C	128 MPa
CY 179	DDM	10 phr A	103 MPa
CY 179	DDM	10 phr G	107 MPa
Epon 828	DDS	10 phr A	98 MPa
Epon 828	DDS	20 phr A	106 MPa
Epon 828	DDS	30 phr A	116 MPa

Glass Cloth Laminates

Table 3 shows that matrix dominated composite properties, such as compression strength, were enhanced by the use of a stronger, stiffer matrix. An additional parameter, which appeared to influence the composite properties, was the viscosity of the resin/curing agent/additive mixture. This indicated that wetting of the glass fabric by the resin must be satisfactory for the enhanced matrix properties to translate into improved composite properties.

Filament-Wound Glass Composites

Table 4 shows representative test data for glass/epoxy composites. The addition of 15 phr of fortifier I produced a significant improvement in the transverse properties of the tube specimens.

Filament-Wound Carbon Composites

Table 5 shows a comprehensive listing of the properties obtained with carbon/epoxy tubes and plates. As expected, the major benefits of fortifier addition (15 phr fortifier K) were in transverse and compression properties. The reported values generally are the average of 8–10 measurements, and for all properties but the transverse flex strength (plate) the percentage improvement exceeds the coefficient of variation.

DISCUSSION

The mechanism by which these additives stiffen and strengthen the plastic is described in detail elsewhere (3). Briefly, for the model system EPPHAA, it was demonstrated that the

Table 3. Compression Testing of Glass Cloth Laminates.

Sample	Average Strength, MPa	% Variance
Control	360	—
20 phr C	466	5.0
30 phr C	509	7.8
20 phr I	439	7.8

Table 4. Transverse Tensile and Compression Data for Glass/Epoxy Filament-Wound Tubes.

	Control	+ 15 phr I
Transverse tensile strength		
No. of samples	15	12
Average strength MPa	51.0	57.1
% variation	14	7.3
Improvement		12%
Transverse compressive strength		
No. of samples	12	12
Average strength MPa	166	187
% variation	4.6	4.3
Improvement		13%

Table 5. Filament Wound Carbon Fiber Composites.

Test	Control	+ 15 phr K	Improvement
Transverse tensile strength (tube)	54.8 MPa	59.5 MPa	9%
Transverse tensile modulus (tube)	8.5 GPa	10.3 GPa	21%
Transverse compression strength (tube)	181 MPa	199 MPa	10%
Transverse compression strength (plate)	136 MPa	170 MPa	25%
Longitudinal compression strength (plate)	930 MPa	1270 MPa	37%
Longitudinal flex strength (plate)	1140 MPa	1310 MPa	15%
Longitudinal flex modulus (plate)	73.3 GPa	76.8 GPa	5%
Transverse flex strength (plate)	53.2 MPa	53.9 MPa	1%
Transverse flex modulus (plate)	6.36 GPa	7.78 GPa	22%
Short team shear (plate)	66.5 MPa	73.3 MPa	10%

major stiffening effect was a result of the decrease in free volume which occurred when the additive was present. The decrease in free volume was demonstrated through an anomalous increase in density and the suppression of the low temperature molecular relaxations of the polymer. The free volume decrease is a result of strong intermolecular interactions between the stiff polar polymer and the stiff polar additive. When a small molecule (volume fraction V_1, fractional free volume f_1) is added to a polymer (volume fraction V_2, fractional free volume f_2) the free volume of the mixture (f) is given by (8):

$$f = V_1 f_1 + V_2 f_2 + K V_1 V_2 \qquad (1)$$

where K is an interaction parameter. For most polymer/additive systems, K is negative but small (~ -0.01) so that the free volume of a polymer (low f) is generally increased by the addition of a small (high f) molecule; hence plasticization occurs. The principle of antiplasticization (9, 10) is that the interaction parameter between the polymer and the additive is negative and large. The resultant decrease in free volume hinders polymer molecular motion, and so stiffens the plastic. The fortified epoxy systems, therefore, have the attractive engineering properties of a high stiffness, yet they also exhibit a ductile failure mode (*Fig. 1*). Such a combination of properties makes them particularly suitable for load-bearing engineering applications, such as in composites.

The additive formulations described here are only a fraction of the total that have been tested. The reason for proceeding with several additive formulations is the loosely-defined term processability. Epoxy matrices have a wide range of applications, and each application requires specific processing characteristics. For filament winding, for example of pipe, major considerations are low viscosity and long pot life. For prepreg applications, a high T_g is important, while viscosity is of lesser importance because the resin mixture frequently is applied in a solvent. Reaction-Injection-Molding (RIM) requires a rapid cure and a low exotherm, and may, therefore, have its own optimum additive.

As well as a variety of processing requirements, an epoxy matrix must also satisfy a range of end-use requirements. The emphasis in this paper has been on the mechanical performance of the matrix and how it contributes to composite properties. For many engineering applications, this may be the dominant requirement, but other factors such as long-term resistance to thermal and hydrolytic degradation or exposure to extremes of heat or cold may also need to be considered. For these reasons, there is not likely to be one ideal epoxy matrix or one ideal additive. Most of the attention in the composites field in recent years has been on the development of improved reinforcements, but, as is demonstrated here, the performance of the matrix material is equally important in determining composite properties.

REFERENCES

1. P. D. McLean, A. Garton, R. F. Scott, and S. Gransden, U.S. Pat. 4,480,082.
2. P. D. McLean, R. F. Scott, and A. Garton, *British Polym. J.*, **15**, 66 (1983).
3. J. Daly, A. Britten, A. Garton, and P. D. McLean, *J. Appl. Polym. Sci.*, **29**, 1403 (1984).
4. H. Lee and K. Neville, "Handbook of Epoxy Resins," McGraw Hill, New York (1967).
5. R. F. Scott, private communication.
6. R. Y. Ting and R. L. Cottington, *J. Appl. Polym. Sci.*, **25**, 1815 (1980).
7. R. J. Morgan and J. E. O'Neal, *Polym. Plast. Technol. Eng.*, **10**, 49 (1978).
8. J. D. Ferry, "Viscoelastic Properties of Polymers," Wiley, New York (1970).
9. W. J. Jackson Jr., and J. R. Caldwell, *J. Appl. Polym. Sci.* **11**, 227 (1967).
10. L. M. Robeson and J. A. Faucher, *J. Polym. Sci., Polym. Letters Ed.*, **7**, 35 (1969).

DISCUSSION

M. Y. Boluk: In one of your slides you showed the stress-strain curves. The materials containing the fortifier exhibited the yield. Did you try to see if the material obeys the Nicolais-Narkis model? Can you explain this behavior by a wetting function?

A. Garton: Yes, we have theories as to why the yield happens, but I have been asked not to say anything on the subject.

M. Y. Boluk: What sort of plasma treatment did you apply?

A. Garton: Plasma treatment involved placing the samples in an air-plasma at 10^{-3} torr with a RF power of about 5 watts for a period of approximately 15 hours.

M. Lambla: You have shown that you have a difference in the fracture morphology between the standard and modified products. I am really surprised that while you have an increase in stiffness, which may be related to the fortifier, you have a ductile rather than a brittle fracture. How can you explain this?

A. Garton: I admit that normally materials with higher stiffness ought to be brittle. Our materials are not and I am afraid that I will not be able to comment on this.

M. Lambla: Do you think that you may have a premature gelling of your product?

A. Garton: We see no link between the rate of cure and the type of fracture. We have some additive formulations, like the ones I have mentioned here, where gelling does happen rather quickly. We have other formulations where there is no change in the gel time yet we see the ductile mode of failure. Therefore, I would conclude that there is no link between these two.

M. Lambla: You have also mentioned a decrease of T_g of the product, which may indicate that you create a lot of pendant chains. This may explain the ductile behavior of your material.

A. Garton: You could certainly for this system. But the fact is that we also see ductile failure in the system where there is no decrease in T_g. Again, these two cannot be linked.

C. L. Beatty: Have you measured densities of the standard and modified epoxy systems?

A. Garton: Yes, we do see a rise in density. There is obviously some decrease in the free volume associated with the use of the fortifiers.

C. L. Beatty: Have you done dynamic-mechanical spectroscopy?

A. Garton: Yes, we have. We see a higher modulus and suppression of the low temperature relaxation.

C. L. Beatty: So, you see a difference in the sub-T_g behavior?

A. Garton: Yes, there is a substantial difference in the sub-T_g behavior.

C. L. Beatty: This rings a bell in terms of phenomenon observed in polycarbonates, the so-called antiplasticization.

A. Garton: You said it, not me.

Use of Grafted Aspen Fibers in Thermoplastic Composites: IV. Effect of Extreme Conditions on Mechanical Properties of Polyethylene Composites

BOHUSLAV V. KOKTA *and* CLAUDE DANEAULT

Centre de recherche en pâtes et papiers
Université du Québec à Trois-Rivières
Trois-Rivières, Québec, Canada G9A 5H7

and

ALPHONS D. BESHAY

The Faculty of Science
Menoufia University, Egypt
Shelvin El Koum

Hardwood fibers of aspen in the form of chemithermomechanical pulp (CTMP) have been used as reinforcement in linear low density polyethylene (LLDPE). The effect of composite treatment (immersion in boiling water, heat exposure at 105°C for seven days or at a temperature of −40°C) on resulting mechanical properties were evaluated. The grafted aspen CTMP composites showed by far the best results with regard to secant modulus, tensile strength, energy, and strain when compared to those of wood flour, mica or glass–fiber filled LLDPE, as well as to virgin LLDPE. Finally, the dimensional stability of CTMP aspen-filled LLDPE composites immersed for four hours in boiling water was better than that of mica or glass–fiber filled LLDPE.

INTRODUCTION

Polymers belong to the most important class of materials. Their volume of production first caught up with metals in 1978, and surpassed it in 1983 by 29 percent (1). The growing demand for polymers may be explained by the fact that they produce items with tailor-made properties, with high tensile strength per weight unit, and at a relatively affordable price.

The main disadvantage of polymers lies in their somewhat low elastic modulus for certain applications. To increase polymer rigidity, more and more reinforcing agents are being used; the resulting polymer composites are stronger and/or less expensive. The use of reinforcing or filling agents (glass fibers, kaolin, mica, etc.) in the plastic industry in 1978 was 1,000,000 metric tons; the estimated volume for 1986 is 3,000,000 tons (2). According to estimates, in 1990 the production of thermoplastic polymers will reach 40,000,000 tons with 30 to 50 percent of that volume in the form of composites (1).

So far, the use of wood fibers for reinforcing thermoplastic polymers has been limited, mainly because of the following reasons: (1) a compatibility problem between hydrophylic wood fibers and hydrophobic thermoplastic; (2) thermal instability at temperatures above 150°C; (3) dimensional instability due to excessive water uptake; and (4) phase separation under stress, especially at subzero temperatures.

As we have recently suggested (3), the short wood fibers could present considerable advantages in the reinforcement of thermoplastics if the above-mentioned problems are overcome. Compared to inorganic fillers, they show the following benefits: (1) lower cost per unit volume; (2) flexibility during processing; (3) lower equipment abrasion; (4) no health problems; (5) low density; (6) high ability for surface modification; and (7) use of renewable, abundant resources especially in a form of hardwood fibers.

It is a well-known fact that there is an enormous amount of unused hardwood fibers in Canada. These hardwood fibers (e.g., aspen)

have a relatively high aspect ratio with a modulus several times higher than that of most thermoplastics (4).

The problem of the compatibility of wood fibers with thermoplastics can be overcome by attaching to their surface a polymeric segment with solubility parameters similar to those of the polymeric matrix. The mechanical properties of grafted aspen fiber-filled polyethylene composites were several times higher than those of pure LLDPE (3). In addition, their properties generally surpassed those of glass–fiber or mica–fiber filled LLDPE composites. At the same time, the estimated production cost of grafted aspen fibers ($250 to $400/ton) are more economical than silane-treated mica ($700/ton) or glass fibers ($2,900/ton).

Recently, Woodhams *et al.* (5) showed that softwood pulp composites equal or exceed the stiffness/weight efficiencies of most traditional construction materials including steel, aluminum, glass fiber composites, and talc-filled polyolefins, while retaining a major cost advantage.

Kokta *et al.* (6) prepared composites from aspen or birch chemithermomechanical pulps grafted with polystyrene. He found improvement in the composites mechanical properties in the 40 percent range compared to the original polystyrene when 40 percent of wood fibers were used.

In a recent study (7), it was shown that the fibers of aspen or birch can improve mechanical properties of polymethylmethacrylate such as elastic modulus: +95 percent; energy at break: +2000 percent; breaking strength: +400 percent; and elongation at break: +166 percent.

The same authors (3) have also reported that the aspen fibers in the form of chemithermomechanical pulp have improved mechanical properties of linear low-density polyethylene by a factor of: 2.6 for modulus, 2.3 for stress, 2.1 for energy (all properties measured at yield point) when used in a weight proportion of 40 percent.

The present study is directed to the effect of extreme conditions (such as exposure to boiling water and exposure to various temperatures: a high of +105°C and a low of −40°C) on grafted aspen fiber-filled LLDPE composites. Furthermore, the behavior of wood-filled polyethylene composites are compared to that of glass fiber– as well as mica–filled LLDPE composites.

EXPERIMENTAL

Materials

Linear low density polyethylene (LLDPE), Novapol LLGR-0534-A, was supplied by Novacor Chemicals Ltd. Reported properties of LLDPE as supplied by Novacor Chemicals are presented in *Table 1*.

The chemithermomechanical pulp of aspen used in this study was prepared in a Sund Defibrator under the conditions described in *Table 2*. Wood flour was made from wood chips and prepared mechanically on a laboratory grinder.

Table 1. Properties of Linear Low-Density Polyethylene—Novapoll LL GR-0534-A.

Resin Properties (a)(c)	ASTM	Units	Typical Value
Melt Index	D1238	g/10 min	5.0
Density	D1515	g/cm³	0.934
Bulk Density	D1895	g/cm³	0.42
Pourability	D1895	sec	17
Molded Properties (a)(b)			
Tensile Strength	D638	MPa	15.8
Ultimate Elongation	D638	%	620
Secant Modulus	D638	MPa	42.7
Flexural Modulus	D790	kg/cm²	62.01
Falling Dart Impact (−40°C)	Arm Method	J/cm	301

Notes: (a) Typical Properties.
(b) All Molded Values Obtained on Rotationally Molded Specimens.
(c) Stabilized Against Oxidation.

Mica 200-NP-Suzorite (200 mesh, coated) was supplied by Marietta Co., Montreal. The mica was in delaminated powder form in dimensions varying from 0.09 to 0.12 mm.

Glass Fibers 731 BA 1/32 (0.8 mm, coated) were supplied by Fiber Glass of Canada via Mia Chemical, Montreal. The length of fibers varied from 0.75 to 0.86 mm, and the diameter varied from 0.014 to 0.0144 mm (l/d = 52 to 61.4).

Treatment of Wood Pulp

The chemithermomechanical aspen pulp was oven-dried by circulating air at 55°C for 48 h, then grinded to a mesh size 60 mixture: 60.5 percent mesh 60, 20.2 percent mesh 80, 15.5 percent mesh 100, and 3.5 percent mesh 200.

Polymer loading of LLDPE on wood fibers was defined as follows: $[(A - B)/B] \times 100$ where A was the weight of the product after copolymerization and extraction, and B was the weight of fibers. In the present study, aspen CTMP fibers were grafted with polyethylene by radical initiation in the presence of maleic anhydride (8). The level of polymer (polyethylene) addition used was ten weight percents based on oven-dried fiber weight.

Preparation of Composites

Mixing of polymer with fillers was performed on a Roll Mill, C.V. Brabender Laboratory Prep. Mill, No. 065. Usually 15 to 20 grams of LLDPE were mixed with fibers at temperatures ranging from 150°C to 155°C. The resulting mixture was collected, re-mixed 10 to 15 times, then allowed to cool down to room temperature and ground to mesh size 20.

The above-prepared polymer-fiber mixture was compression molded into shoulder-type test specimens (24 at a time).

The weight of each specimen was 0.9 to 1.2 g after molding at a 155.5°C for 15 min under a pressure of 3.8 MPa. The initial molding temperature was 93.3°C with a 15 min cooling period. Samples were then heat treated (annealed) at 105°C in the oven for 1 to 2 h, and finally

Table 2. Conditions of the Preparation and Properties of Birch and Aspen Pulp.

Cooking Conditions	Birch	Aspen	Properties	Birch	Aspen
Temperature Max. (°C)	126	126	Drainage index (CSF), ml	117	119
Retention time (min)	5	5	Brightness, Elrepho (%)	55.7	60.9
Pressure (psig)	20	20	Opacity, (%)	94.1	91.4
Na_2SO_3 (%/Dry wood)	5	5	Breaking length, km	4.22	4.46
NaOH (%/Dry wood)	5	5	Elongation (%)	1.79	1.79
pH	12.9	12.9	Tear index, $mN.m^2/g$	6.08	7.20
Consistence During Refining, %	21.8	23.9	Burst, index, $kPa.m^2/g$	1.88	2.59
Refining energy, MJ/kg	5.26	5.15	Yield (%)	90.0	92.0
Refiner output, kg/h	46.8	45.6	Kappa index No	128.0	121.7
			Lignin %	18.8	17.9

	Average Fiber		
Mesh	Length (*) mm	Diameter (d) mm	Aspect (1/d)
20	1.107	0.024	46
40	0.46	0.027	17.7
60**	0.30	0.022	13.9
80	0.22	0.021	10.1
100	0.18	0.020	9.1
200	0.09	0.019	4.7

* Mesh 60 Mix is defined as the one containing the following fiber sizes: 60.5% of Mesh 60; 20.2% of Mesh 80; 15.5% of Mesh 100, and 3.5% of Mesh 200.
** Mesh 60 Mix the average aspect ratio is about 11.9.

allowed to stand at least 3 to 4 h in the testing room at 23°C and at 50 percent relative humidity.

Treatment of Composites

The composites of each filler type and each filler percentage, as well as molded samples of virgin LLDPE, were divided into the following groups:

Group 1 was evaluated at room temperature.

Group 2 samples were kept in 1 *l* conical flasks filled with 500 ml of boiling water (under reflux) for 4 h under atmospheric pressure. Subsequently, samples were dried between two paper sheet filters and then conditioned at room temperature at 50 percent level of relative humidity.

Group 3 samples were kept at 105°C in an air-circulating oven for 7 days before being cooled down and conditioned at room temperature.

Group 4 was kept at −40°C in the Thermostatic Instron Chamber (Model 311) and mechanical properties were evaluated at that temperature.

Water Uptake Measurement

Samples of each kind of composite, as well as virgin LLDPE, were submerged in water at room temperature for predetermined periods ranging from 48 h to 5 weeks. Subsequently, each sample was centrifuged at 2,500 rpm for 15 min, weighed, dried at 55°C for 24 h, and then reweighed.

The percentage of water uptake was calculated as follows:

$$\text{Water uptake} = 100(B - A)/A$$

where B is the weight of the centrifuged sample, and A is the sample weight after being dried at 55°C.

Mechanical Tests

The mechanical measurements were carried out using an Instron tester, Model 4200. The reported properties are those measured at yield point. The secant modulus was based on an original point defined by force 0.05 KN, and other points defined by load 0.08, 0.11, and 0.14 KN using the Instron A 479 to 521 Plastic Tensile Test Program. The secant modulus was used in order to compare our values with those provided by manufacturer. Full-scale load was 5 KN, gauge length was 17 mm, and crosshead speed was 10 mm/min. Cross section area for each sample as well as sample length were measured with the help of a micrometer. In general, samples were of the following size: 1.7 cm between grips, 3.175 mm in width, and 0.158 cm in thickness. All mechanical properties, measured at yield point that has corresponded to maximum stress and force values have been calculated by computer using the above mentioned program.

RESULTS AND DISCUSSION

Experimental results for composites, molded under optimal conditions (3) are summarized in *Figs. 1* to *21*. Mechanical properties are presented as a function of the weight fraction of fibers.

In *Figs. 1* to *5*, the effect of sample treatment on absorbed energy is compared with similarly treated polyethylene. It is obvious that the treated aspen pulp showed by far the best properties compared to either wood flour, mica, or glass fibers. The 40 percent grafted pulp fiber content indicated the best overall results in comparison to all other fillers used.

Figure 5 shows consistent improvement of energy (surface area under the stress/strain curve) for treated pulp no matter what condi-

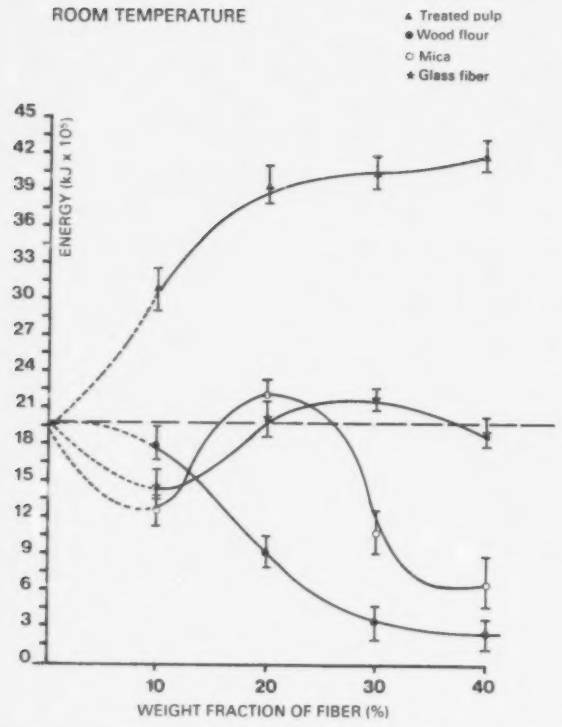

Fig. 1. Effect of weight fraction of fiber on energy (room temperature).

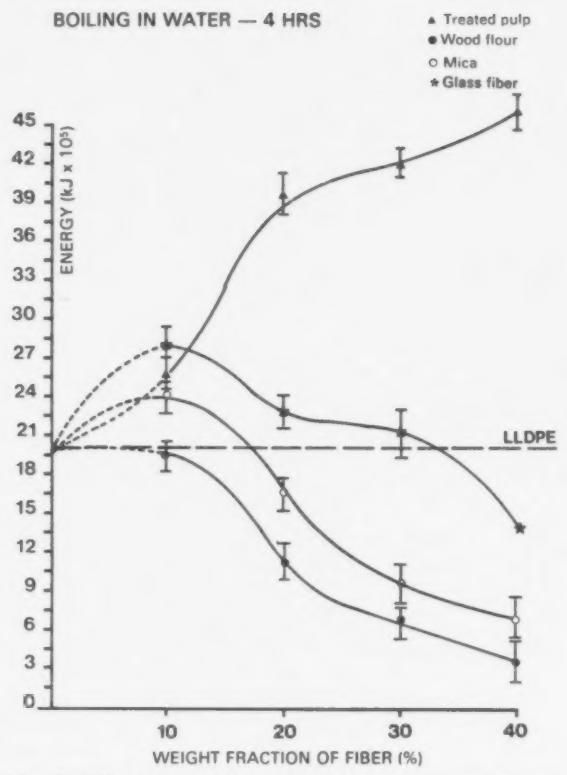

Fig. 2. Effect of weight fraction of fiber on energy (boiling water).

tions the composite samples were exposed to. The values for aspen-filled composites are usually double those of virgin PE. Composite energy even improved after heat or boiling water treatment as compared to energy measured for samples not exposed to these conditions. In the case of the other fillers, there was some improvement of energy due to the heat treatment (*Fig. 3*) compared to samples that have not been exposed to extreme conditions (*Fig. 1*).

Figures 6 to *10* compare secant modulus measured for all samples at load point 0.08 KN (the slope of the stress-strain line between the origin set at 0.05 KN and 0.08 KN approximate elastic modulus).

In *Fig. 10*, a linear increase of modulus with the fiber content is shown for all differently treated wood fiber composites. The highest increase in modulus, from 0.55 GPa to 1.15 GPa, was observed at −40°C for a 40 percent level of grafted aspen fibers (*Figs. 6* to *10*).

Figure 6 shows an increase from 0.11 (LLDPE) to 0.57 GPa (composites) in modulus value for ordinary samples. Due to the weakness of other samples containing mica or glass fibers (breakage prior to 0.08 KN), the modulus for the other composites was not recorded. The glass fiber and mica composites outperformed grafted aspen fiber composites only in the case of samples heat treated for 7 days (*Fig. 8*).

The surprisingly high modulus for wood flour filled composites (*Fig. 9*) at fiber loading level of 10 percent may be attributed to a higher local concentration of filler, which might have re-

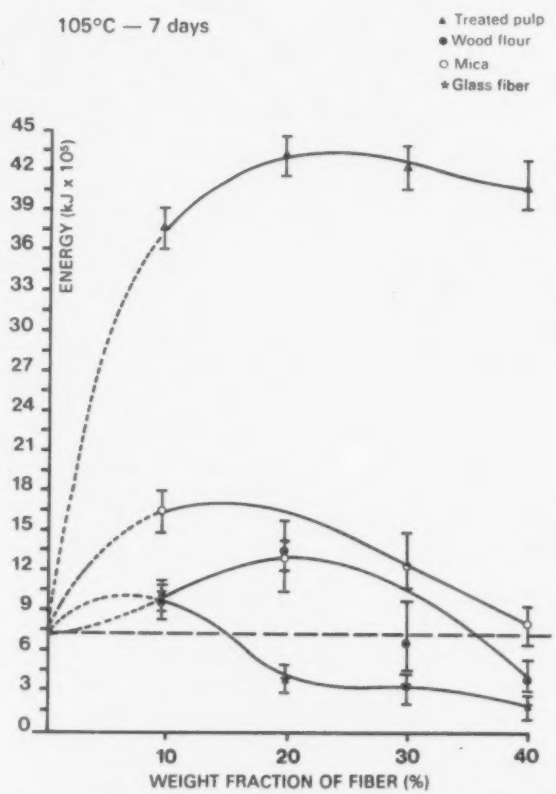

Fig. 3. Effect of weight fraction of fiber on energy (105°C).

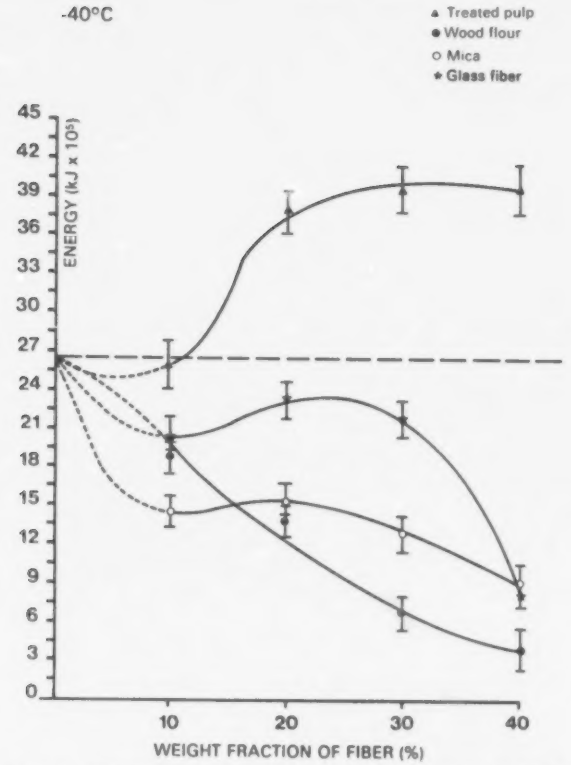

Fig. 4. Effect of weight fraction of fiber on energy (−40°C).

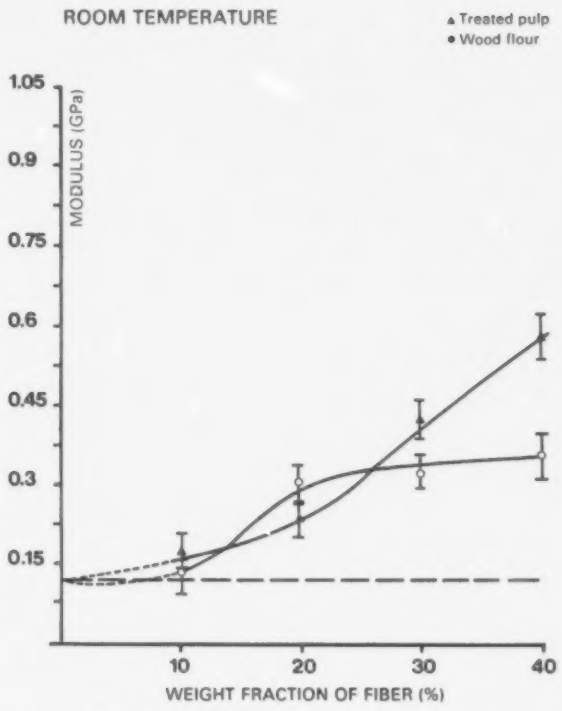

Fig. 6. Effect of weight fraction of fiber on modulus (room temperature).

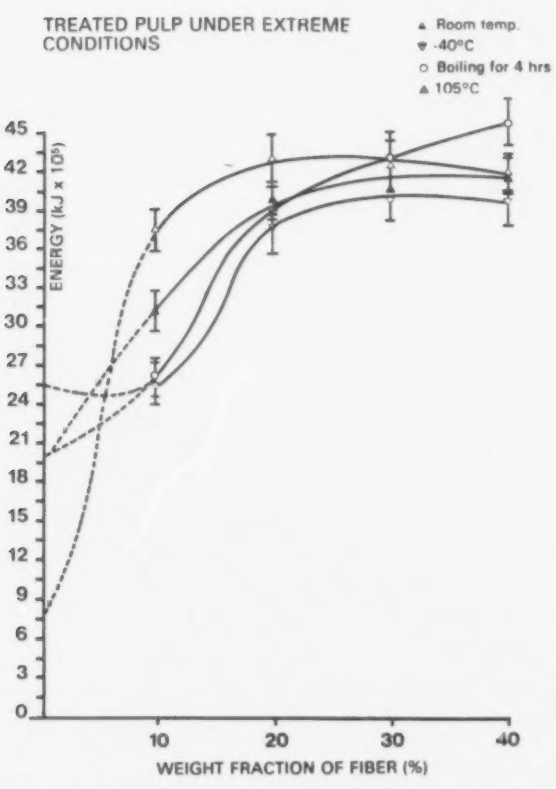

Fig. 5. Effect of weight fraction of fiber on energy (extreme conditions).

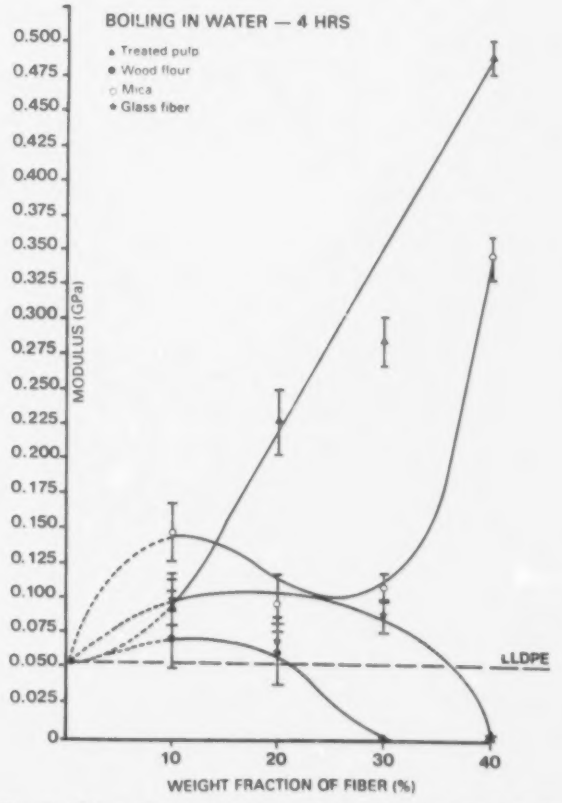

Fig. 7. Effect of weight fraction of fiber on modulus (boiling water).

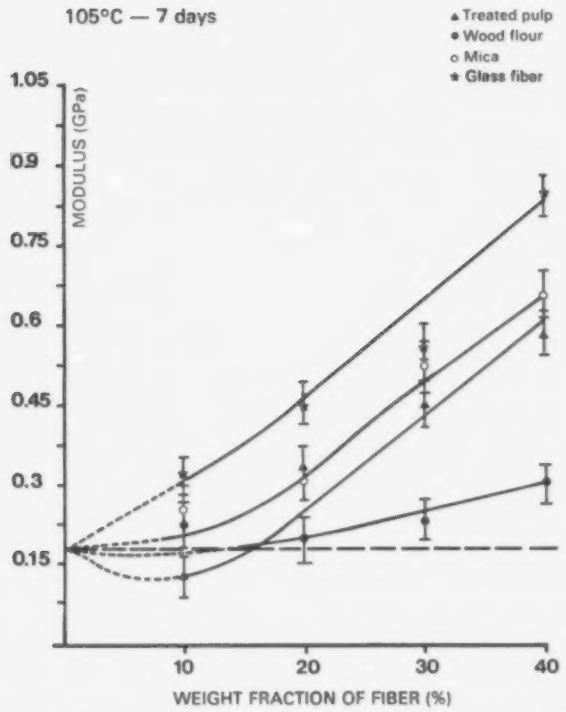

Fig. 8. Effect of weight fraction of fiber on modulus (105°C).

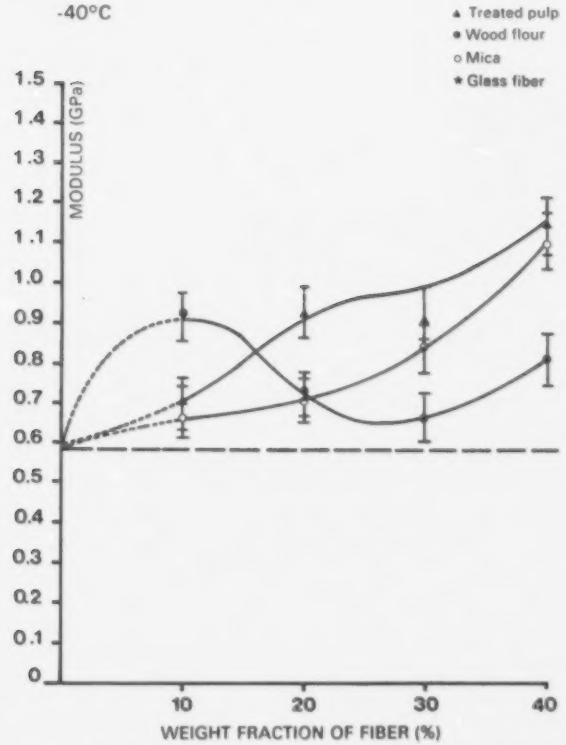

Fig. 9. Effect of weight fraction of fiber on modulus (−40°C).

sulted from difficulties in dispersing it uniformly in hydrophobic matrix.

Tensile strength values for virgin LLDPE, as

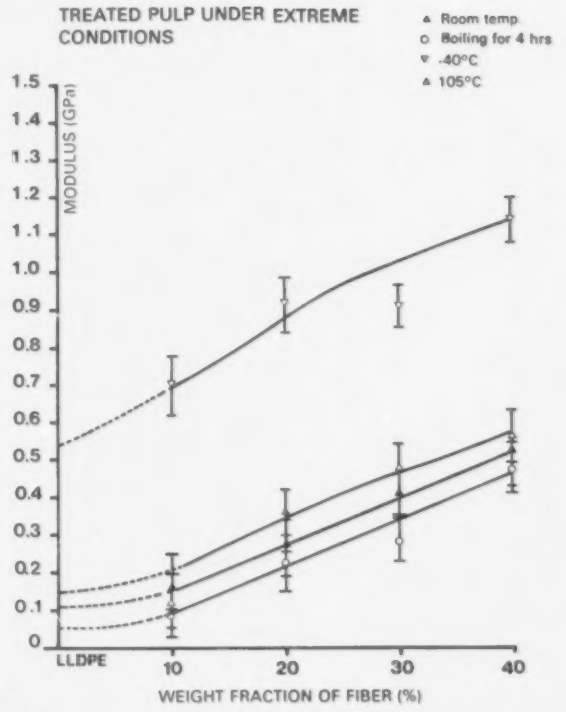

Fig. 10. Effect of weight fraction of fiber on modulus (extreme conditions).

well as for all the other composites, appear in *Figs. 11* to *15*. Grafted CTMP aspen filled composites scored the best strength values for all levels of weight fractions of fibers (considerably higher than those filled with wood flour, mica or glass fiber). These values showed an upward trend according to the percentage increase of fibers in composites. The strength values of composites not exposed to treatment under extreme conditions (*Fig. 11*) showed that at a 40 percent level of fiber loading, CTMP composites reached 32.5 MPa as compared to 20 MPa for mica, 12 MPa for glass fiber, and 9 MPa for wood flour-filled composites. Boiling water pretreatment (*Fig. 12*) did not affect treated CTMP composites (31.6 MPa at a 40 percent level of fiber loading), but there was a slight decrease in the strength of mica filled composites and a slight strength increase in the case of glass fiber or wood flour composites.

In general, heat treatment at 105°C slightly improved tensile strength (*Fig. 13*). Strength properties, measured at −40°C (*Fig. 14*), revealed an increase in the strength of virgin LLDPE to 31.2 PMa as well as the best values for treated CTMP of aspen-filled composites, which reached the 47 PMa value level.

Strength properties for treated CTMP composites are summarized in *Fig. 15*. It is obvious that the highest strength was obtained at the −40°C level. The similar results for pretreated composites measured at room temperature, indicates that there must have been a good interface contact unaffected by extreme conditions.

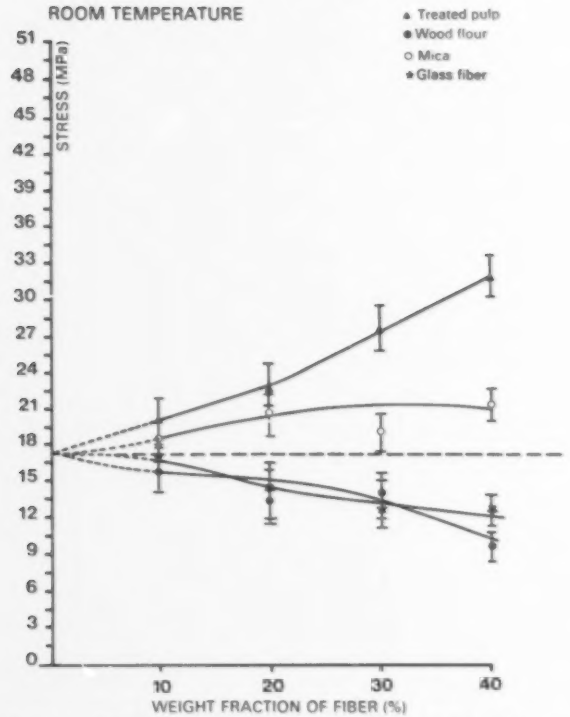

Fig. 11. Effect of weight fraction of fiber on stress (room temperature).

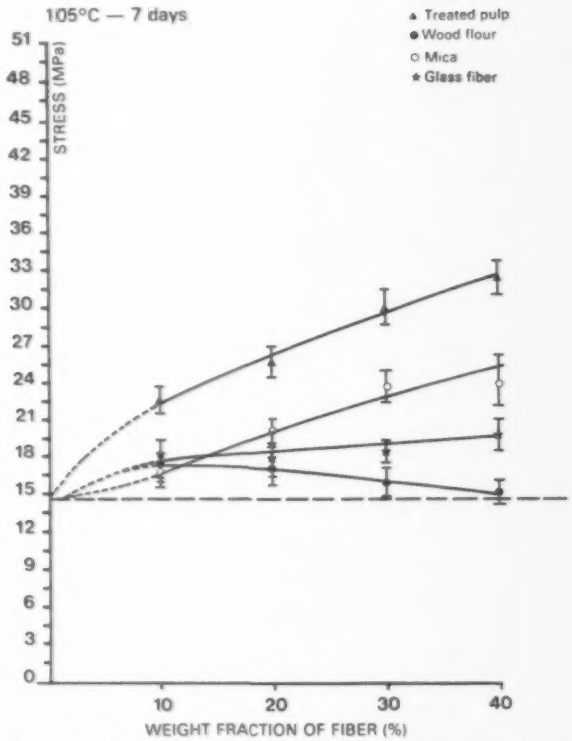

Fig. 13. Effect of weight fraction of fiber on stress (105°C).

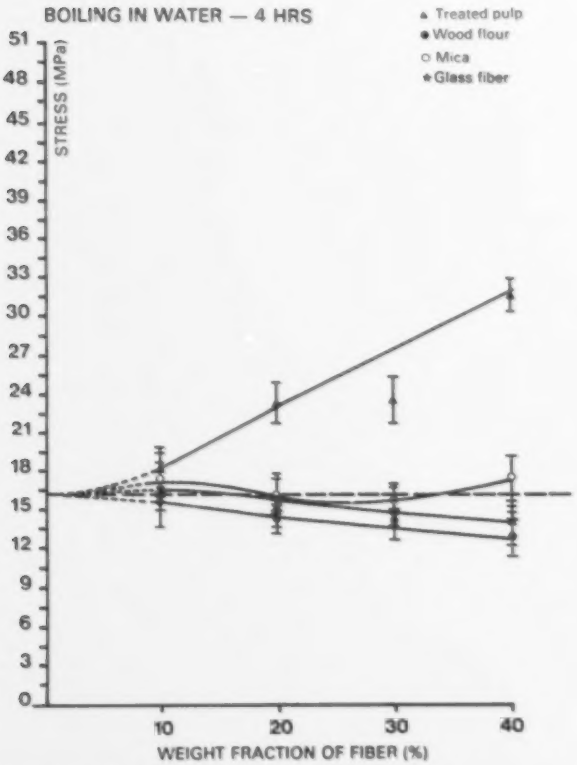

Fig. 12. Effect of weight fraction of fiber on stress (boiling water).

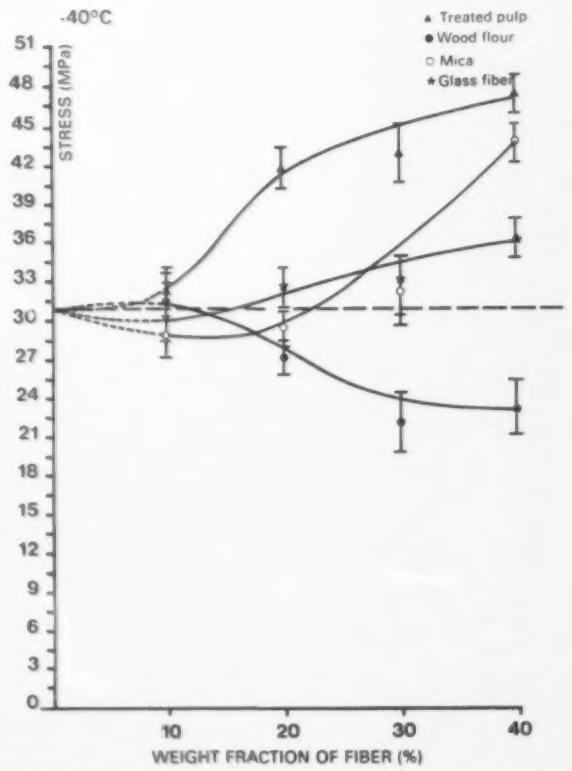

Fig. 14. Effect of weight fraction of fiber on stress (−40°C).

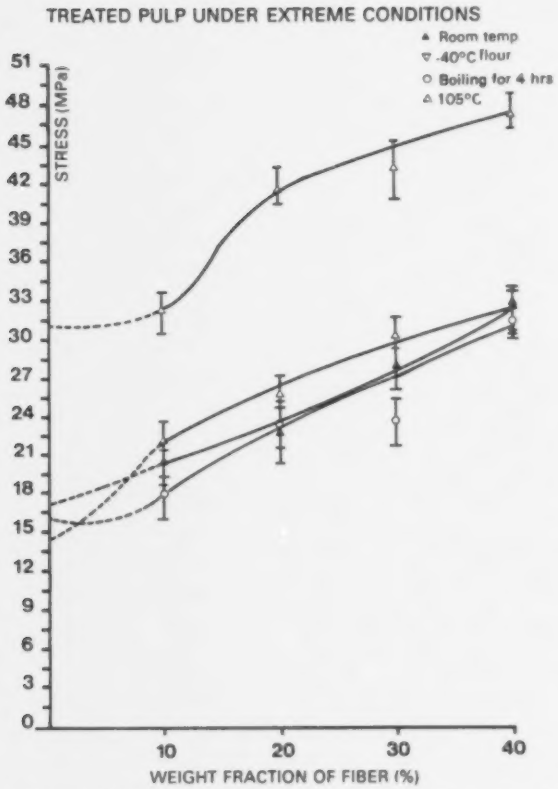

Fig. 15. Effect of weight fraction of fiber on stress (extreme conditions).

Results for strains at yield points are summarized in *Figs. 16* to *20*. Normally, the strain decreases with the filler content. Composites with the treated CTMP gave the highest strain values under all conditions comparable to that of virgin LLDPE, with lower values for wood flour, mica or glass fiber–filled composites. Strain values for grafted CTMP filled compos ites were similar when measured for ordinary or pretreated samples. Absolute values varied according to fiber loadings ranging from 15.7 to 22.5 percent (*Fig. 20*).

At −40°C, only the composites made of grafted CTMP kept the strain values at about the value level measured for virgin LLDPE. All other composites showed lower strains.

Sample Water Uptake

In *Table 3*, the results of water uptake in the case of treated CTMP composites are compared to those of virgin LLDPE. Water exposure, which varied from 2 days to 5 weeks at room temperature, lead to a water uptake of 0.61 to 3.97 percent (the highest water uptake corresponded to a 40 percent fiber content after 5 weeks of immersion in water).

The percentage of variation of cross sectional area caused by water uptake is presented in *Fig. 21*. From this figure, it is obvious that the highest cross section area variation, after a four-hour immersion period in boiling water,

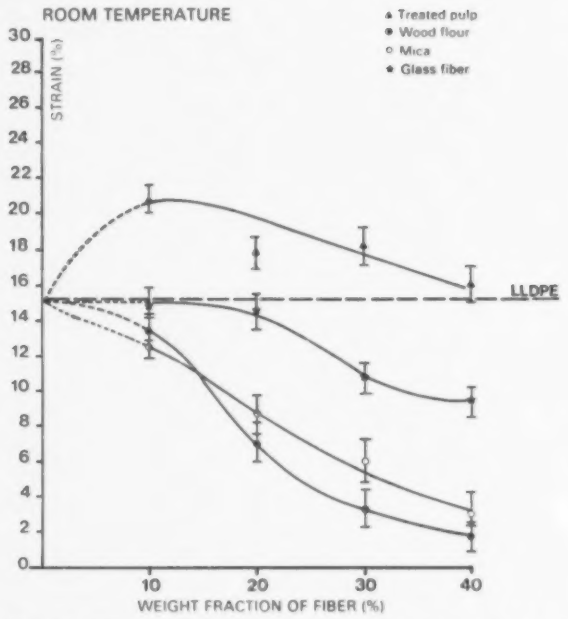

Fig. 16. Effect of weight fraction of fiber on strain (room temperature).

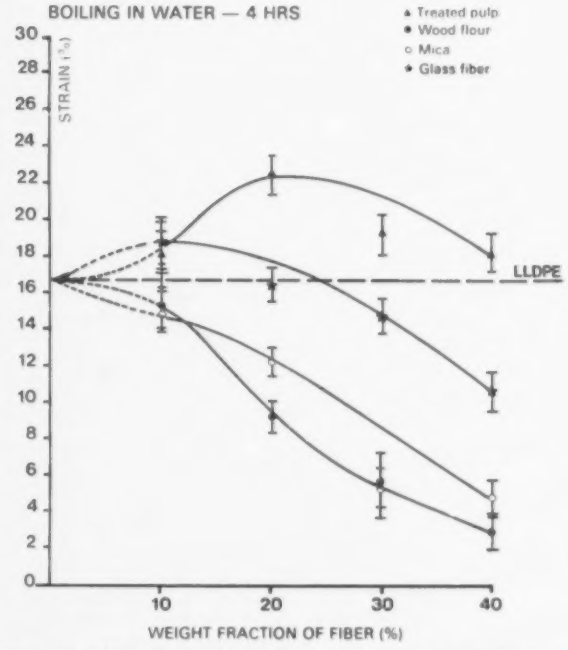

Fig. 17. Effect of weight fraction of fiber on strain (boiling water).

was for wood flour-filled composites (4 percent in the case of a 40 percent level of fiber content). Treated CTMP aspen filled composites showed better dimensional stability (1.9 percent) than those filled with mica or glass fibers (3 percent).

DISCUSSION

The above-mentioned results indicate excellent behavior of treated aspen wood fiber filled

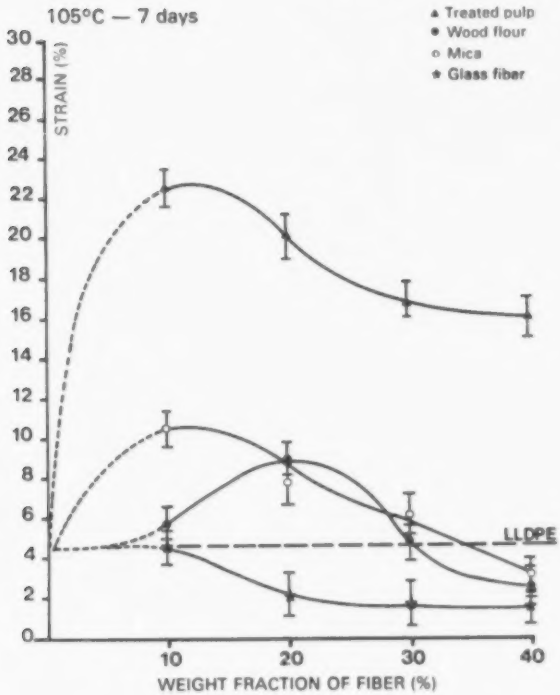

Fig. 18. Effect of weight fraction of fiber on strain (105°C).

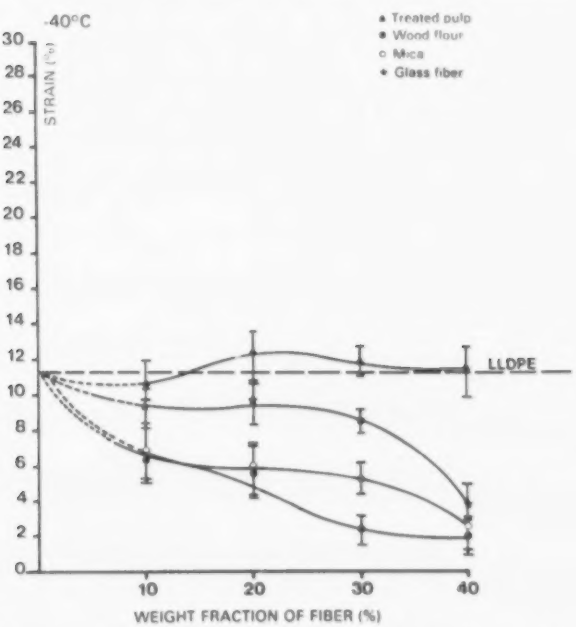

Fig. 19. Effect of weight fraction of fiber on strain (−40°C).

polyethylene (LLDPE) composites under all the conditions. More important, grafted wood fiber composites showed a clear superiority over mica or glass fiber composites. Overall, LLDPE filled with grafted wood fibers could become one of the lowest priced engineering composites with the considerable added advantage of surpassing (cost/properties) glass fiber filled resin.

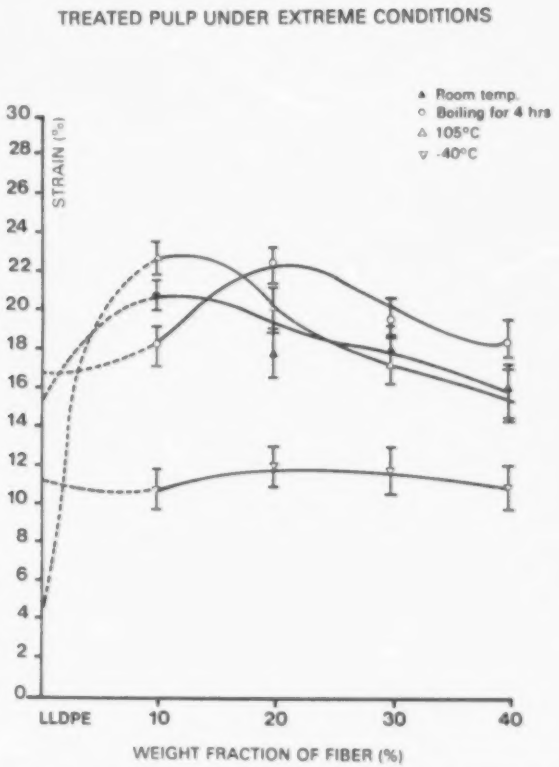

Fig. 20. Effect of weight fraction of fiber on strain (extreme conditions).

Table 3. * Water Uptake (%).

	2 Days	1 Week	2 Weeks	4 Weeks	5 Weeks
LLDPE	0	0.1	0.132	0.135	0.144
Wood Pulp (20%)**	0.61	1.47	1.57	1.9	3.03
Wood Pulp (30%)	0.71	2.25	3.00	3.05	3.23
Wood Pulp (40%)	0.85	2.87	3.77	3.87	3.97

* Room temperature.
** Wood pulp = LLDPE composites filled with grafted aspen CTMP.

Improvement in mechanical properties of treated CTMP aspen fiber filled composites after being exposed to heat treatment in boiling water or in an oven at 105°C can most probably be explained by an additional process of annealing the thermo-pressed composites. Some property improvement can be expected by increasing bonding between —OH groups on cellulosic fibers and some hydrophylic groups (formed during grafting) on polymer probably via hydrogen bonding.

This way also explains some improvement even in the case of wood flour filled composites. The lesser degree of improvement in that case might be explained by the lower hydrogen bonding capacity of wood flour that is ⟨⟨coated⟩⟩ with aromatic lignin.

A slight increase in mechanical properties in mica or glass fiber composites due to heat treatment may be explained by thermal annealing and, possibly, by reactivating coupling agents present in these composites.

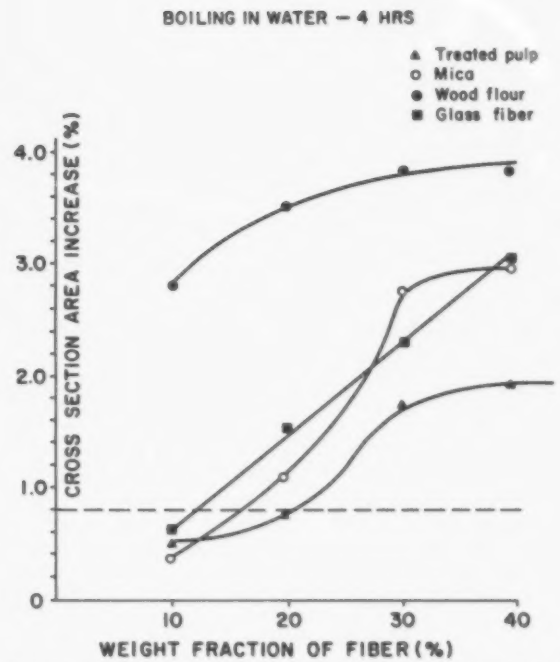

Fig. 21. Effect of weight fraction of fiber on dimensional stability.

The mechanical properties of treated CTMP composites at −40°C confirmed an excellent interface contact between filler and polymer. In addition, it must be noted that there was no phase separation under stress.

The relatively small water uptake and higher dimensional stability for treated CTMP aspen fiber filled composites, as opposed to mica or glass fiber ones, suggests a high level of compaction of wood fiber composites as well as strong bonding forces between the filler and the polymer.

The density of wood CTMP composites are lower than those for glass fiber composites when one compares the same property level. This represents an important asset for industrial applications of molded composites, e.g., the auto industry. Furthermore, since wood fibers are non-abrasive, they can easily be molded at a 40 percent weight level as compared to 20 percent to 30 percent for glass fibers.

In the case of injection molding, there could be further property improvement due to fiber orientation. Since the samples used in this study were compression molded, they had a random fiber orientation; this contributed to a coefficient of variation, as indicated in the graphs.

CONCLUSIONS

The objective of this study was to examine the effect of extreme conditions on grafted aspen fiber–filled LLDPE composites. It was demonstrated that:

1. Grafted pulp composites mechanical properties did not significantly change under extreme conditions, with the exception of modulus and stress (increased), and strain (decreased), when measured at −40°C.
2. In all instances, grafted pulp fibers improved polyethylene properties.
3. Grafted pulp fiber–filled composites showed better mechanical properties than composites filled either with glass fiber or mica.
4. Dimensional stability of grafted wood fiber composites (when immersed in boiling water) was better than that of glass fiber– or mica–filled composites.

ACKNOWLEDGMENT

The authors wish to thank the Natural Sciences and Engineering Research Council of Canada and the Fonds FCAC of the Province of Quebec for their financial support, as well as Novacor Chemical Ltd. Technical Center for its cooperation.

NOMENCLATURE

CTMP = chemithermomechanical pulp.
LLDPE = linear low density polyethylene.

REFERENCES

1. L. A. Utracki, *Composites '84 Symposium*, 8200-8-1-4, IMRI, Opening Address, NRCC, Boucherville (Nov. 1984).
2. R. B. Seymour, *Austr. Plast. Rubber*, **39**, 19 (1979).
3. A. D. Beshay, B. V. Kokta, and C. Daneault, Preprint of *NCR-IMRI Symposium COMPOSITES '84*, Boucherville, 8200-8-1.4, pp. 10.0–10.64 (Nov. 1984).
4. A. Y. Coran and R. Patel, U.S. Pat. 4,323,625 (1982).
5. R. T. Woodhams, G. Thomas, and D. K. Rodgers, *Polym. Eng. Sci.*, **24**, 1166 (1984).
6. B. V. Kokta, R. Chen, C. Daneault, and J. L. Valade, *Polym. Compos.*, **4**, 229 (1983).
7. B. V. Kokta, P. D. Kamdem, A. D. Beshay, and C. Daneault, *PMM Symposium Series*, Walter de Gruyler, Berlin, New York Scientific Publishers, accepted (1985).
8. N. G. Gaylord, U.S. Pat. 3,645,939 (1972).

DISCUSSION

L. A. Utracki: First, let me see if I have the facts straight. Your fillers are aspen fibers with about 10 weight percent of polyethylene grafted onto them. Is that correct? What is the method of grafting polyethylene onto wood fiber?

B. V. Kokta: This is an issue I do not want to talk much about because we are in the process of patenting. There are several ways one can attach polyethylene chains to the wood fiber surface. But we have not done it by polymerization of polyethylene. We do not have a reactor and we do not like to work with heptane.

L. A. Utracki: If you have only 10 percent polyethylene on the fiber, then this amount is insufficient to completely protect the wood fiber surface. You must have a certain amount of hydroxylic group exposed to the environment. Nonetheless, you are getting marvelous proper-

ties, as far as low temperature and boiling test are concerned. What mechanism is responsible for this?

B. V. Kokta: If you have a certain amount of polymer on the surface you may entangle the macromolecules of the matrix with it. Also there may be some enhancement of matrix crystallization near the fiber surface. Gaylord, in his patent (US Pat. 3,485,777, Dec. 23, 1969), declared that you do not have to have a large amount of grafting. Grafting primarily acts as a compatibilizer. In our previous work we have coated wood fibers with different amounts of polystyrene. At 20 weight percent of polymer loading the fibers were completely covered with polymer; we did not see any fiber surface.

L. A. Utracki: You compared the coated wood fibers with mica and glass fibers. Were these latter two fillers treated?

B. V. Kokta: Yes, according to our spectroscopic analysis they were silane treated. I do not know how much, but it must be above one percent.

L. A. Utracki: Your materials absorbed a lot of water, up to 4 weight percent for 40 percent loading in five weeks of immersion. Did you measure the low temperature properties of the samples after exposure to moisture?

B. V. Kokta: No.

L. A. Utracki: So, you tested only dry specimens at −40°C and wet specimens at ambient temperature. I think that the critical test of your material will come when you test the wet samples at low temperature.

B. V. Kokta: The people who work with polycondensation polymers advised us that putting polymer in boiling water is not a good test. Boiling water causes extraction, hydrolysis, thermal degradation, and so forth. Why should you be so severe on wood grafted fibers? Nevertheless, we will verify your point.

L. A. Utracki: The reason I suggested testing the wet samples at low temperature is a historical one. Wood and cellulosic fibers have been used as fillers. The initial properties of the composites were excellent, even when tested at −40°C. However, in the field, after a period of time, the product shattered on impact when the temperature fell below freezing. The classical example was the wood fiber-filled polypropylene cases for milk bottles. It has been found that during summer the filler slowly absorbed water, which upon crystallization in winter produced a dramatic, nearly explosive failure on impact. To overcome this, a test should be conducted at low temperature, not necessarily on samples after the boiling test, but after long term exposure to high humidity, simulating real conditions which may be encountered by the product.

B. V. Kokta: Yes, this is an excellent suggestion. We have an indication that the grafted fibers absorb less water so they should behave better, but we have to measure how much better.

J. L. White: Have you thought of taking the untreated cellulosic fiber and varying the polymeric matrix to see under which condition maximum enhancement of properties will occur? I would expect that the best characteristics could be achieved using cellulose acetate-butyrate, or acetate-propionate.

B. V. Kokta: I have already prepared a program nearly identical to what you suggested, and have given it to my graduate students. We have grafted cellulosic fibers with different types of polymers, then prepared paper-like sheets containing from 10 percent to 100 percent of graft polymer. The obtained composite sheet properties [Kokta B. V. and Daneault C., "Evaluation of Paper Properties of Ultra-High Field Hardwood Pulps Modified by Grafting," Tappi Pulping Conference, Houston, 429–442, Book 2 (Oct. 1983); Kokta B. V., Araneda L. and Daneault C., "Evaluation of Paper Properties of Thermomechanical Pulp Modified by Ozonation and Grafting with Thermoplastic Polymers," *Polym. Eng. Sci.*, **24**, 950 (1984)]. The problem is that paper is very inexpensive and any additional cost induced by grafting seems to be prohibitive to paper industry.

J. L. White: Can you use low molecular weight compounds with hydrophilic and hydrophobic groups, something like stearic acid, and see if they would upgrade the properties?

B. V. Kokta: Woodhams has done this and we have tried 50-odd combinations since this summer. Woodhams observed an enhancement of properties of the composite, wood flour/polyethylene, upon addition of 2 percent of stearic acid. We have tried to attach to cellulose different polyunsaturated acids either by radical initiation, by esterification or combination of both. The data have not yet been fully evaluated. I think that we achieved only a moderate success.

C. E. Chaffey: In your 20-odd figures, broadly speaking, the data could be approximated by straight lines, which would represent a sort of rule of mixtures. The curious thing which puzzled me was that with cellulosic fiber, the properties of the pure polyethylene as obtained by extrapolation to zero concentration of the filler were much different from the values known for pure polyethylene. It would appear that your fibers significantly modify the behavior of polyethylene. Why may that be? Suppose that you extrapolate the lines the other way. I would expect the values to be rather independent of treatment, indicating an inert character of these materials. Finally, the error bar representing the uncertainty of your data seems to be remarkably constant even when values themselves varied. I wonder how you obtained those error bars?

B. V. Kokta: We are using the Instron computer

program for the tensile test. After a series of tests, the program calculates the mean and the error. So far we have been interested in the relative properties. At the present time, in cooperation with Ecole Polytechnique, we have started fundamental research including the measurement of the absolute strength values of fiber as well as fiber bundles as a function of dispersion, orientation, etc. The direct evaluation of composite fracture surfaces by electron scanning microscopy is part of this effort.

C. L. Beatty: When you deformed your PMMA composite did you notice any whitening near the yield? Was there any crazing enhancement?

B. V. Kokta: I do not remember. However, the stress-strain did not show any yield.

C. L. Beatty: Did you measure if the bound water could be removed from your grafted fibers?

B. V. Kokta: I think that it is very difficult to remove bound water from cellulosic materials. Usually you dry out only the surface and loosely bound water at 45°C. The bound water would have to be removed at a high temperature usually above 105°C. However, compounding and pressing the compounds with polyethylene at 150°C did not show any bubbling or void formation. In short, if there was any water in the grafted samples, it stayed there.

C. L. Beatty: I thought that the mechanism for the increase of modulus of your composites on lowering the temperature may involve crystallization of the bound water, which would stiffen your filler.

B. V. Kokta: But we observed a large increase of modulus for pure polyethylene as well.

C. L. Beatty: These may be two independent mechanisms. I would think that it would be an interesting experiment to follow the change of modulus of the composites by varing the amount of bound water in the system.

Electrical Properties of Exfoliated-Graphite Filled Polyethylene Composites

Y. S. WANG, M. A. O'GURKIS, *and* J. T. LINDT*

Department of Material Science and Engineering
University of Pittsburgh
Pittsburgh, Pennsylvania 15261

An experimental study has been carried out to prepare and characterize high density polyethylene-based composites filled with exfoliated graphite particles of varied aspect ratios. It has been demonstrated that the dielectric constant of the composite correlates with the *in situ* volumetric fraction of the compressible exfoliated filler particles. The dielectric constant has been found to range from 2.23 to 125. The minimum electrical resistivity of the composites obtained was 0.1 Ω·cm at a graphite content of 40 percent by volume. The use of these composites is intended in electromagnetic radiation interference (EMI) shielding.

INTRODUCTION

It has been suggested previously that conductive fillers can increase the apparent dielectric constant when incorporated into a polymer matrix. As the concentration of the conductive filler increases, a continuous network of the filler particles tends to form throughout the matrix, and the composite tends to become conductive. Filler particles with large aspect ratios can induce apparent electric conductivity even at a relatively low concentration (1–3). On the other hand, it has been shown that as much as 38 percent per volume of conducting spherical particles was required to obtain an electrically conductive composite (4).

It is known that when certain graphite structures are penetrated (intercalated) with bromine or certain acids, they exfoliate upon heating (5). Depending upon the exfoliation temperature and the heating rate, the aspect ratio of the graphitic structure can increase by as much as two orders of magnitude during exfoliation. An exfoliated graphite sample is shown in *Fig. 1*. Compared to most other electrically conductive fibers, e.g., steel fibers, the exfoliated graphite has the added advantage of very low bulk density (cca. 3 kg/m^3), thus offering a substantial reduction in the composite density.

This paper is concerned with the electrical properties of polyethylene composites filled with exfoliated graphite flakes, which can be used in electromagnetic interference (EMI) shields. The advantages of using such polymer composites over metals are: light weight, low cost, and relative ease of processing. In this report, the electrical properties of such composites are examined involving both small- and large-aspect ratio filler particles.

EXPERIMENTAL

Arco Super Dylan, injection molding high density polyethylene grade, has been used as a base material. The particular grade of Super Dylan used in this work is claimed to have a narrow molecular weight distribution, a melt index 18, and the density of 957 kg/m^3. The polymer was used as a powder.

Exfoliated graphite particles (Union Carbide) of ash content of 5 percent by weight were used as a filler. The density of the flakes before exfoliation, after being intercalated with a mixture of sulphuric and nitric acid, was 2050 kg/m^3.

Before being mixed with the base resin, using two different procedures, the filler particles were exfoliated to 2:1 and 20:1 aspect ratios, respectively. The low aspect ratio (2:1) particles were obtained by slowly heating the acid treated flakes in an oven at 800°C for an hour.

The high-aspect ratio (20:1) exfoliated flakes were the commercial grade Grafoil particles commonly used in foundries under the name "hot topping." Based on the same intercalated material, the bulk density of this material was about 3 kg/m^3, the surface area being approximately 20000 m^2/kg.

When preparing the composite specimens, the exfoliated graphite was mixed with the polyethylene powder, both components being at

* To whom all correspondence should be sent.

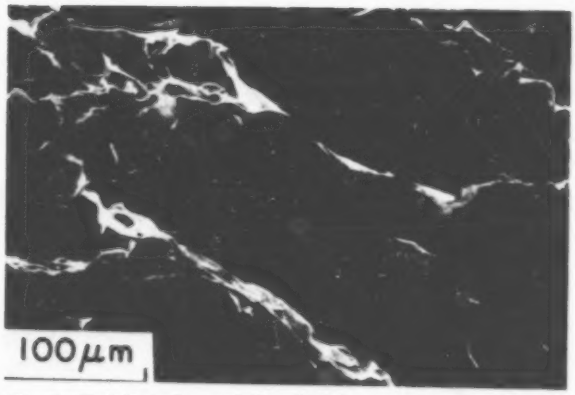

Fig. 1. Exfoliated graphite of high aspect ratio. (Reproduced with permission from D.D.L. Chung.)

room temperature, and placed in an open glass disc mold, 56 mm in diameter, pretreated with a mold release agent (Crown 6075).

The composite samples filled with the low aspect ratio particles were prepared by vacuum outgassing at 380 mmHg (50.66 kPa) for 100 min. The experiments were carried out at different polyethylene/graphite weight ratios, at temperatures ranging from 152 to 184°C. No compression was applied when processing these materials. Depending on the amount of material used, moldings ranging from 4 to 8 mm in thickness were obtained.

In order to accommodate the high-aspect ratio exfoliated "worms" in the composite, the method of sample preparation had to be modified to produce moldings of mechanical integrity comparable to that of the composites containing the shorter particles referred to above. Again, all experiments were carried out in vacuum at 380 mmHg (50.66 kPa); but this time, a static load was placed on the top of the melting sample to further enhance the melt penetration towards the graphite surface. The processing temperature ranged from 140 to 152°C, while the molding time was between 80 and 150 min. The variable mechanical load placed on the specimen surface during the outgassing procedure was between 0.35 and 7.5 kPa. By this technique as much as 45 percent per volume of graphite was incorporated into the polyethylene matrix.

The dielectric constants of the composite samples were measured at room temperature using a capacitance bridge (General Radio Company 1620-A), which is shown in *Fig. 2*.

The present measurements of the electrical resistivity were made on the four-probe apparatus shown in *Fig. 3*.

The density of the composite specimens was determined by weighing the samples in air and in hexane.

Finally, the morphology of the samples was examined using a Scanning Electron Microscope (SEM).

RESULTS AND DISCUSSION

Polyethylene Filled with Small-Aspect-Ratio Exfoliated Particles

The first group of our results concerns composites filled with exfoliated flakes of about 2:1 aspect of ratio. The experimental data, including the processing conditions, are collected in *Table 1*.

All samples showed good mechanical integrity. Both the graphite/polyethylene interface and the polymer phase were essentially free of

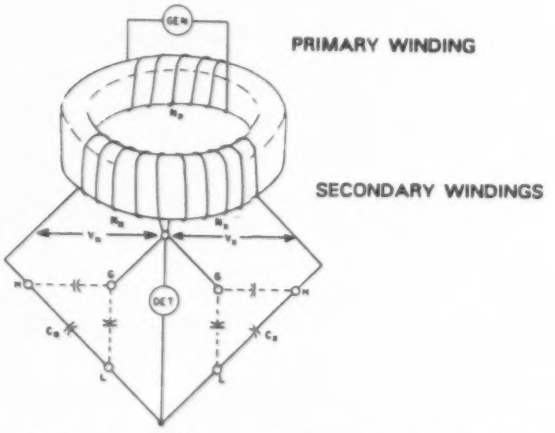

Fig. 2. A capacitance bridge with transformer arms.

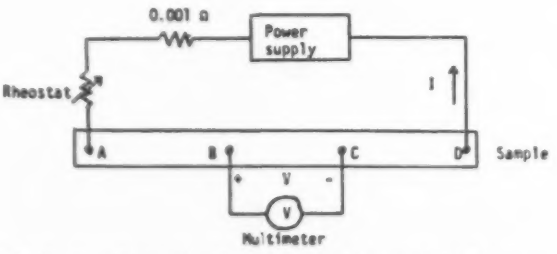

Fig. 3. A schematic of the four-probe method for measurements of electrical resistivity.

Table 1. Summary of Experimental Conditions for Samples Filled With Low-Aspect Ratio Exfoliated Graphite. (Gas Pressure 50.66 kPa; Molding Time 100 min).

Weight Fraction of Graphite	Density of the Composite [kg/m³]	Temperature [°C]	Dielectric Constant (Measured at 1 kHz)
0.0164	944	152	2.45
0.0244	937	152	4.03
0.0385	927	152	8.07
0.0802	885	152	23.4
0.0185	944	184	2.83
0.0244	937	184	3.75
0.0322	929	184	6.23
0.0384	923	184	4.62
0.0477	915	184	8.53
0.0551	908	184	6.68
0.0667	897	184	48.9
0.0768	888	184	17.6
0.0906	877	184	43.6

voids, thus indicating good adherence between the two phases (see *Fig. 4*). The graphite content of the sample shown here was 6.7 percent by weight.

It has been found that during the outgassing process, the exfoliated graphite tends to segregate due to flotation. To quantify this effect, the vertical density distribution established within the composite was measured. For this purpose, disc samples of about 25 mm in thickness were made. The samples were incrementally reduced in thickness on a lathe. The material was removed carefully to prevent melting or mechanical damage to the remaining sample. The machined surface was smooth and free of cracks. Each time the trimmed sample was weighed, the density of the removed layer was calculated. As seen in *Fig. 5*, in the sample prepared at 184°C, the density difference over the height of the sample was about 50 kg/m^3 while in the sample processed at 152°C, this difference had been reduced to less than a half. At the same time, the average density of the sample prepared at 184°C was 944 kg/m^3, while the average density of the sample made at 152°C was 925 kg/m^3.

Evidently, the effect of outgassing temperature on the sample morphology is significant. Data shown in *Fig. 5* imply the existence of two distinct temperature dependent flow effects during the formation of the composite. The rate of the particle migration responsible for the vertical stratification effects is dependent on the melt viscosity which, in turn, depends on temperature. By the same token, at higher temperatures the melt penetrates the interstices in the graphite structure more readily, thus yielding an overall denser composite.

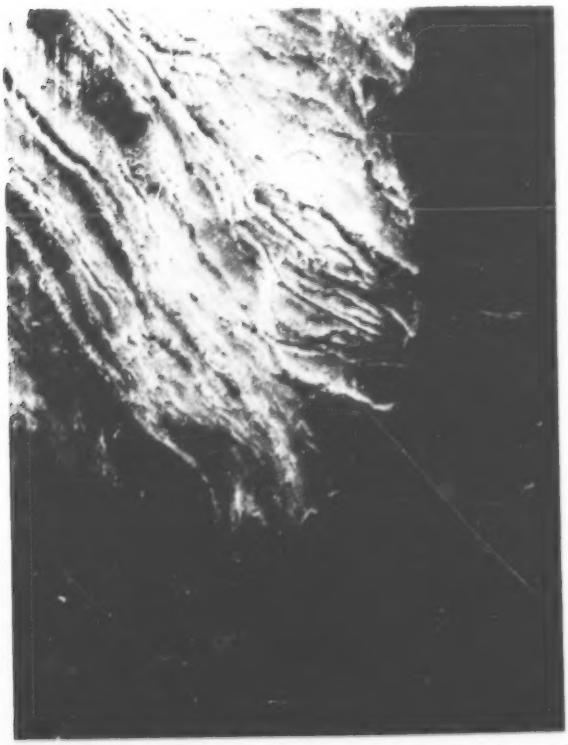

Fig. 4. SEM picture of the interface between graphite and polyethylene (× 400).

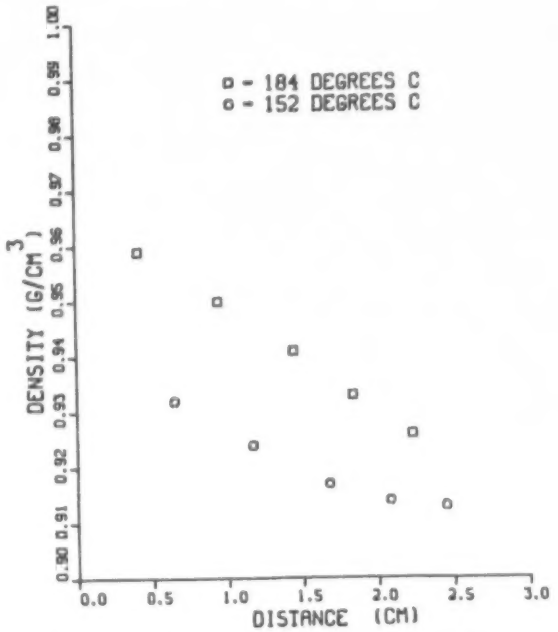

Fig. 5. Density distribution in the composite filled with low aspect ratio exfoliated graphite particles.

No analytical examination of thermal degradation due to the sample processing was done. Unfilled reference samples of the base resin, subjected to the same outgassing procedure as the filled specimens, did not show, however, any signs of visible signs of degradation, such as discoloration or release of low molecular weight species that might affect the electrical properties of the base resin.

As can be expected and seen in *Fig. 6*, the dielectric constant is a strong function of the graphite concentration. At low graphite concentrations, the dielectric constant of polyethylene is approached, viz., 2.23. It is also interesting to note that the differences in graphite distribution throughout the sample, as demonstrated in *Fig. 5*, do not play a significant role as far as the dielectric constant is concerned. For a given aspect ratio of the filler particles, the overall apparent dielectric constant seems to depend on the absolute amount of graphite rather than on its distribution. At graphite concentrations in excess of 7.5 percent by weight, the dielectric constant increases dramatically indicating that the filler starts forming an interconnecting network.

Polyethylene Filled with Large-Aspect-Ratio Exfoliated Particles

The aspect ratio of the exfoliated graphite flakes used in the experiments reported in this

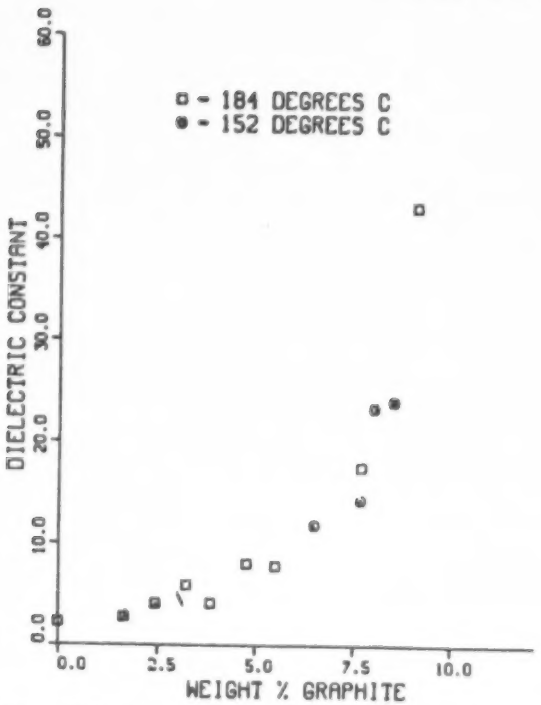

Fig. 6. Dielectric constant as a function of the graphite weight fraction (low aspect ratio filler).

section was about 20:1. It has been established that the amount of the highly exfoliated graphite allowed in the composite is a function of the processing time, temperature, and the mechanical load. A summary of experimental conditions pertaining to molding of the high-aspect ratio based composites along with the density data are given in *Table 2*. An example of the distribution of the high aspect ratio filler particles in the matrix is illustrated by an SEM micrograph shown in *Fig. 7*.

As expected, the apparent dielectric constant shows a more pronounced dependency on the weight fraction of graphite for the composite filled with the high-aspect ratio particles. A summary of our measurements of the dielectric constant on composites containing the high-aspect ratio at different frequencies is shown in *Fig. 8*. At this point, a qualitative observation can be made, that in order to achieve the same dielectric constant, about an order of magnitude higher concentration of the low-aspect ratio filler is required than that of the high-aspect ratio filler; it is interesting to note that this ratio of such concentrations (by weight) is similar in magnitude to the ratio of lengths of the respective filler particles. This observation is confirmed in *Fig. 9* showing all present measurements of the dielectric constant on the low- and high-aspect ratio based composites at 1000 Hz as function of the *in situ* volume fraction of the filler. The effective, *in situ*, volume fraction of the compressible exfoliated particles in the finished composite has been calculated from the

Table 2. Summary of Experimental Conditions for Samples Filled with High-Aspect Ratio Exfoliated Graphite. (Gas Pressure 50.66 kPa).

W/Fraction of Graphite	Comp. Density [kg/m³]	Temperature [°C]	Surface Load [kPa]	Time [min]
0.0130	816	146	0.3792	100
0.0200	764	152	0.4800	80
0.0180	760	146	1.9344	85
0.0200	735	146	1.9344	85
0.0230	716	146	1.9344	85
0.0250	732	146	1.9344	85
0.0300	695	140	3.1872	150
0.0300	705	140	4.2576	150
0.0425	622	140	4.2576	150
0.0300	700	140	5.4000	150
0.0450	602	140	7.4496	150

Fig. 7. SEM picture of composite filled with high-aspect exfoliated graphite particles.

given densities of the polymer and the composite and from the measured mass content of the resin and graphite in the sample. As seen, the dielectric constant correlates quite well with the volume fraction of the filler particles which, in turn, is proportional to the aspect ratio of the exfoliated particles. This finding is in line with Nielsen's theory predicting the thermal conductivity of systems filled with incompressible particles (6). Consequently, it may be suggested that barring significant thermal degradation of the matrix, deficiencies in outgassing, and, perhaps, particle orientation effects, the processing conditions—temperature, pressure, and time—affect the electrical properties of the composite through a single variable only—the

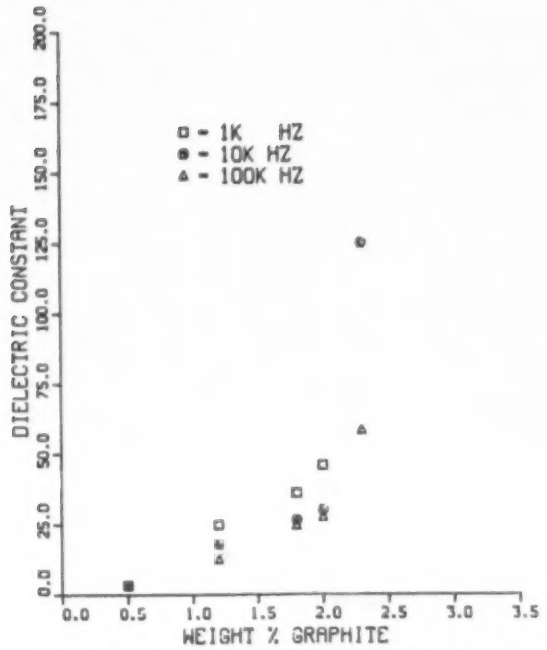

Fig. 8. Dielectric constant as a function of the graphite weight fraction (high aspect ratio filler).

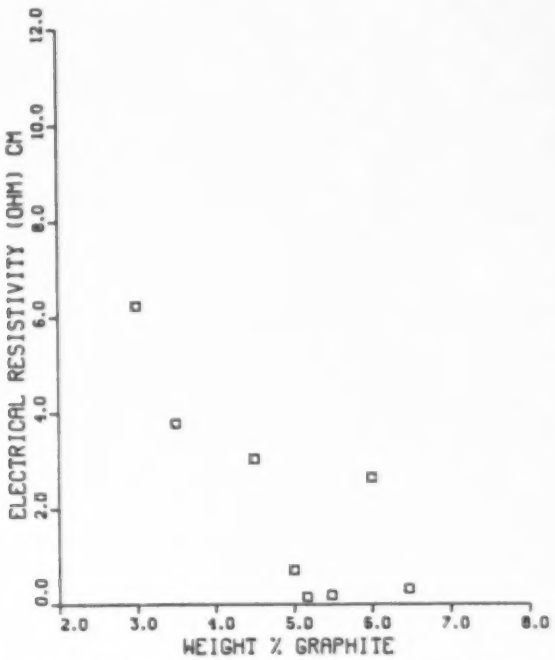

Fig. 10. Electrical resistivity of the composite.

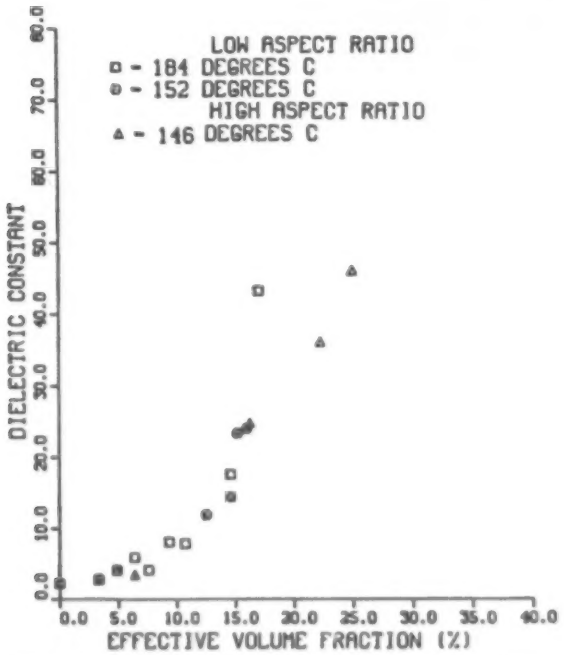

Fig. 9. Dielectric constant as a function of the effective (in situ) volume fraction of exfoliated graphite.

in situ mean volumetric fraction of the exfoliated graphite particles.

The measurements of the electrical resistivity, summarized in *Fig. 10*, indicate a steep dependence on the graphite content. These results lead to a conclusion that once the concentration of the exfoliated graphite in the composite exceeds about 5 percent by weight (approx. 40 percent by volume), the order of magnitude of the apparent electrical resistivity becomes equal to that of exfoliated graphite in the c-direction, namely, 0.1 Ω·cm, but still about two orders of magnitude higher than the electrical resistivity of exfoliated graphite in a and b directions (7).

Similar to some previous observations on polymer composites filled with steel fibers (2, 3), the formation of a network of the filler particles in the polymeric matrix seems to occur once a critical concentration of the filler particles is reached. Compared to the more conductive and more slender steel fibers, however, the leveling off of the electrical resistivity shown in *Fig. 10* occurs at relatively high volume concentrations, as expected, at volume concentrations approximately four time higher than those reported for steel fibers (2).

CONCLUSIONS

1. Vacuum outgassing has been successfully used to prepare light weight polyethylene based composites filled with exfoliated graphite. This method of preparation affords good adherence between the phases, good dispersion, and filler content up to 45 percent by volume.

2. The processing temperature can affect significantly the distribution of the graphite particles in the polymer matrix through viscous flow effects during the same preparation process. The average density of the composite is influenced by the processing temperature to a lesser degree.

3. The apparent dielectric constant correlates with the volume fraction of the filler par-

ticles over a range of aspect ratios between 2:1 and 20:1. Within the range of present experimental conditions, the spacial distribution of the filler particles is of minor importance. The range of dielectric constants measured at 1000 Hz on composites with the *in situ* volume fraction of the exfoliated graphite not exceeding 0.25 was between 2.2 (the value for pure polyethylene) and 125.

4. The electrical resistivity of the composite is a steep function of the graphite content. The minimum resistivity, measured in this work on a polyethylene filled with high aspect ratio exfoliated graphite particles was about 0.1 Ω·cm. This value was obtained at 45 percent by volume filler content.

ACKNOWLEDGMENTS

We gratefully acknowledge the financial and technical support received from the Carbon Division of Union Carbide. We wish to thank Professor Deborah Chung of the Carnegie Mellon University and Dr. Michael Dowell of Union Carbide for drawing our attention to the area of exfoliated graphite composites. We further acknowledge the use of Professor Chung's apparatus for our measurements of the electrical resistivity.

REFERENCES

1. D. M. Bigg, *Polym. Eng. Sci.*, **19**, 1188 (1979).
2. T. Katsura, M. R. Kamal, and L. A. Utracki, *Polym. Compos.*, **6**, 282 (1985).
3. T. Katsura, M. R. Kamal, and L. A. Utracki, *Adv. Polym. Technol.*, **6**, 193 (1986).
4. J. Gurland, *Trans. Mater. Soc. AIME*, **236**, 642 (1966).
5. J. E. Brocklehurst, *Nature*, **194**, 247 (1962).
6. L. E. Nielsen, *Ind. Eng. Chem. Fundam.*, **13**, 17 (1974).
7. D. D. L. Chung, unpublished results.

DISCUSSION

C. L. Beatty: Could you explain why you are using sintering instead of extrusion or injection molding?

J. T. Lindt: The exfoliated graphite particles in the composite can withstand relatively large normal stresses, but they break very easily in shear.

C. L. Beatty: It seems to me that the way you set up the experiment you are measuring the surface resistivity.

J. T. Lindt: The probe penetrated deeply into the samples.

L. A. Utracki: As I understand it, you have randomly oriented exfoliated graphite particles in polyethylene. The density of the composite varies. However, you said that the conductivity depends only on the effective volume fraction of graphite, not on the density. This means that you must have a random orientation, and that the percolation threshold value is independent of the aspect ratio or the degree of exfoliation. Furthermore, the path of conductivity seems to be independent of the void content.

J. T. Lindt: The voids are inside the exfoliated flakes, covered, you may say, by conductive sheets, so indeed they should not influence the conductivity.

L. A. Utracki: This makes sense. Now the supposition that the flakes are randomly oriented can be easily checked by measuring the conductivity in all three orthogonal directions.

J. T. Lindt: We have done that and the conductivities were the same.

Ultrasonic Evaluation of Filled Polymers: I. Techniques and Models for the Elastic Moduli of a Resin Filled With Iron Spherical Inclusions

L. PICHÉ *and* A. HAMEL

Industrial Materials Research Institute
National Research Council Canada
Boucherville, Québec, Canada J4B 6Y4

The ultrasonic technique for the nondestructive evaluation of elastic moduli is described. Its use in the application to polymers, whereby viscoelastic effects are eliminated, is discussed. Experimental results are given for composites containing high contrast (iron) spherical inclusions. The measurements are discussed in terms of available theoretical models. It is clearly demonstrated that models that account for the microscopic details of the material offer the best description of the bulk properties.

INTRODUCTION

New technologies require, and thus lead to, the development of new materials. Among these, composites are rapidly gaining ground over the more usual engineering materials for the good reason that many of their physical and mechanical properties can be custom tailored. Correspondingly, there is a growing need for methods and techniques for the evaluation and characterization of composites. Such methods would be useful for the optimization of design and would also become valuable aids for quality and process control. The present study is part of a continuing effort toward that goal.

The main factors that will determine the end properties of a composite are: the matrix properties, the inclusion properties, the phase geometry, and the nature of inclusion/matrix interfaces. Also, each of these factors includes a number of variables in its description. Polymer composites, where a polymeric matrix contains a second dispersed phase, constitute what probably is the most important class of composite materials. In these materials the viscoelastic nature of the matrix adds to the complexity of the problem.

The behavior of the elastic moduli stands out as a promising basis for the characterization of composites. The elastic modulus is a fundamental property which basically reflects the strength of the atomic links in the solid; it is also an important and significant engineering characteristic. The value of the elastic constants enter the description of a number of the physical properties such as stiffness, load bearing and fracture characteristics, hardness, residual and thermoelastic stress, thermal expansion, creep elongation, specific heat, and thermal conductivity. For this reason, the question of the elastic moduli of composites has been given a great deal of consideration, and a number of theoretical approaches have been proposed. There are, however, comparatively few published experimental results to evaluate these various models.

In this paper we shall describe and justify the use of an ultrasonic nondestructive method for measuring the moduli. We shall then present our experimental results on a model composite constituted of spherical iron particles dispersed in an epoxy matrix. The results will be compared to the different theoretical predictions. The ability of these models to link the microscopic details of the composites to their macroscopic end use properties will be discussed.

METHODS OF MEASURING THE ELASTIC MODULUS

The usual method for measuring the elastic moduli of most engineering materials is that of stress-strain (1) experiments. The sample is submitted to a force (extension, compression, or bending), which is measured together with accompanying changes in dimensions. Often the results will depend on strain and strain rate and these must be specified. For composites, the strain factor is important since yielding can occur unnoticed at weak matrix particle interfaces. For a polymer, the value of the modulus will depend on the strain rate because of the viscoelastic nature of the material. Both strain and strain-rate dependent effects are difficult to assess and their analysis can be complex (2).

In such cases where strain dependent effects are suspected, a most useful approach is provided by sound propagation techniques. The various sonic methods (3) can be classified into two main categories. In the first, the sample of known geometry is forced into oscillation as a whole (unbounded propagation). The vibration spectrum is analyzed in terms of its eigen-frequencies, and the modulus can be calculated from basic elasticity principles. Such methods, because they rely on the knowledge of the sample's geometry, are better suited for measurements of changes (e.g., with temperature) in the value of the moduli. However they have been used with success on composites (4). Sonic techniques of the second category involve measuring the velocity of both compressional, v_c, and shear, v_s, waves in the material. The values of velocity and of the density, ρ, allow calculation of the bulk modulus, B, and the shear modulus, G, which for an isotropic material are given by:

$$B = \rho(v_c^2 - 4v_s^2/3) \quad (1)$$

$$G = \rho v_s^2 \quad (2)$$

From these one may calculate the tensile (Young) modulus E, and the Poisson ratio:

$$E = 9BG/(3B + G) \quad (3)$$

$$\nu = \tfrac{1}{2} - E/6B \quad (4)$$

In these techniques, the strain is very small ($\Delta\epsilon/\epsilon \simeq 10^{-5}$), and the problem of strain dependence is virtually eliminated. On the other hand, the elastic properties of polymers depend on the rate of strain. The time dependence of the modulus is described in terms of a characteristic relaxation time, τ, (or rather a distribution of τ). The real part, M_1, of the storage modulus can be seen as the contribution of two components: the relaxed modulus, Mr, and the unrelaxed modulus, Mu. M_1 is written as:

$$M_1(\omega) = (Mr + \omega^2\tau^2 Mu)/(1 + \omega^2\tau^2) \quad (5)$$

where ω is the angular frequency ($\omega = 2\pi f$). For ultrasonics, the frequency is in the 10^6 Hz region. For most engineering polymers, the glass transition temperature, T_g, is usually very different from room temperature, T_0. If $T_g > T_0$, then $\omega\tau \gg 1$, thus *Eq 5* reduces to $M_1(\omega) = M_1 \simeq Mu$, and the ultrasonic modulus is equivalent to an infinite strain rate measurement at very low strain values. This defines a standardized reproducible measurement method where the influence of viscoelasticity is absent.

For most materials, the velocity of usual ultrasonic waves (low MHz) is to all intents independent (5) of the sound frequency. The problem of composites, however, deserves special attention. The inclusions act as scattering centers for the sound wave and this causes dispersion. The amplitude of the effect depends on the relative values of the acoustic wave number $k(k = 2\pi f/v)$ and the average size (D) of the inclusion. Dispersion is negligible when $kD \ll 1$, but will become significant (5) in the region of $kD \simeq 1$ where it can lead to results (6, 7) that require specific interpretation (8). In order to allow comparison of the acoustic moduli to the more usual (engineering) static quantities, the measurements must be performed in the low frequency regime where $kD \ll 1$.

EXPERIMENTAL PROCEDURE

Samples

The question of samples is a delicate one. In this first step of our approach to the evaluation of composites, we needed a model material that was well characterized. The main requisites were: the absence of porosity, good adhesion of the inclusion to the matrix, and uniform three-dimensional random distribution. Also, in order for our test of existing theoretical descriptions to be most sensitive and meaningful, we chose constituents such that the contrast between their respective elastic properties was high. The composites were made by compression molding techniques and obtained in the form of plaques with thicknesses of 2 mm to 4 mm. For the model composites, the matrix was a commercial thermoplastic resin powder, poly(methyl methacrylate) (PMMA) to which were added different amounts of iron powder.

The iron powder was spherulitic, *Fig. 1a*, with a rather narrow distribution of diameters ($D = 60\ \mu m \pm 20$). A bulk sample made by Hot Isostatic Pressing techniques allowed us to characterize the inclusion material. The results, which are given in *Table 1*, are in close agreement with average values found in the literature for steels and iron.

We prepared a number of samples with inclusion contents up to 40 volume percent. This was the nearest we could reasonably come to the maximum theoretical (9) value (≃60 percent) while avoiding contiguity. *Figure 1* shows micrographs taken with a scanning electron microscope of polished samples containing respectively 8 percent (b) and 40 percent (c) per volume of iron. As can be seen, the distribution appears homogeneous. It also appears that even at high concentrations (40 percent), the particles are separated. A rapid theoretical estimate shows that the average distance between particles should be $1.5 \times D$, which corresponds roughly to what is observed in *Fig. 1c*. Examination of the sample at an angle (*Fig. 1d*) shows that the spheres are left protruding while the matrix material has been removed during the polishing operation. This clearly indicates that the particles are well bonded to the matrix.

The volume contents were determined through careful weighing of components before mixing. The densities of the finished composites were obtained both through picometric techniques and by mass and volume measurements.

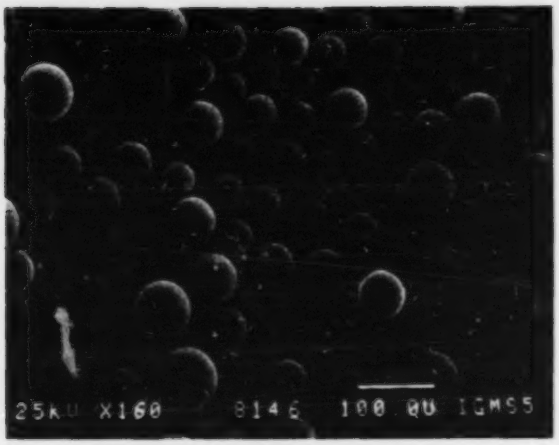

(a)

(b)

(c)

(d)

Fig. 1. Scanning Electron Micrographs showing (a) the size distribution of the iron spherulitic inclusions; (b) the volume distribution of inclusions in a sample with 8 percent volume concentration of inclusions; (c) a sample with 40 percent volume concentration; (d) a side view of an inclusion still adhering to the bulk while the softer matrix material was removed by polishing.

Table 1. Properties of Basic Constituents.

Property	Matrix Resin (1)	Inclusion Iron (2)
Density ρ(g/cm^3)	1.175	7.84
Compressional Velocity v_c (km/s)	2.669	5.941
Shear Velocity v_s (ks/s)	1.306	3.251
Bulk Modulus B(GPa)	5.697	166.20
Shear Modulus G(GPa)	2.004	82.90

The Ultrasonic Techniques

Even though it is not common practice to use ultrasonic techniques for the study of polymers, the methods are well-established (10, 11). We shall thus give only a brief description of our apparatus. In the present study, we have chosen to use a water immersion technique because of the ease with which the measurements can be made and repeated. The setup is depicted in *Fig. 2*. A fast pulser excites a highly damped transducer, which produces a short (1 or 2 periods) burst of high frequency (f = 1.0 MHz) sound. In the absence of a sample, the sound pulse travels in the water as a pure compressional wave with a velocity, V, and arrives at the receiving transducer (identical to the first) at time, t_0. The signal is first amplified, then is sent to an oscilloscope equipped with a dual-time base that allows precise (±2 *ns*) time delay measurements. In order to measure the compressional wave velocity, v_c, the sample (in the form of a plate of thickness (l) is introduced with its parallel faces perpendicular to the beam. Part of the sonic energy which arrives on the sample (face 1) is transmitted forward in the material. There it travels at time, t_s, before it meets the other face (2). At that point, part of the energy is transmitted to the liquid and picked up by the receiver at time, t_c:

$$\Delta t = (t_c - t_0) = l/v_c - l/V \qquad (6)$$

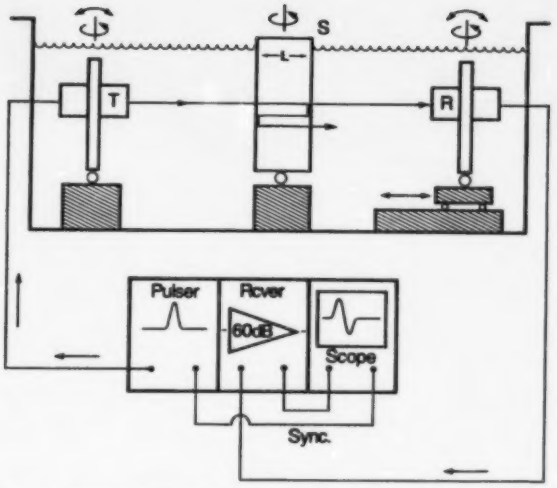

Fig. 2. Schematic of the ultrasonic immersion system, illustrating the different paths followed by the sound pulse.

There (face 2) a reflection also occurs, which sends part of the signal back to face 1 . . . and so on. This gives rise to the formation of echoes that are observed at equal time intervals, t_e:

$$t_e = l/v_c \tag{7}$$

The velocity is obtained from *Eqs 6* and *7*:

$$v_c = V(1 - \Delta t/t_e) \tag{8}$$

The value of V can be found with great accuracy by changing the distance between transducers. The velocity, v_c, is thus obtained solely from the measurement of time delays, which gives the technique a high degree of accuracy: $\Delta v_c/v_c \simeq 0.1$ percent.

The procedure to obtain the shear velocity, v_s, is somewhat more involved. The sample is inclined so that the normal to its faces makes an angle, δ, with the direction of propagation in the water. Then, according to the acoustical analogue of Snell's law:

$$(\sin \delta)/V = (\sin \alpha)/v_c = (\sin \beta)/v_s \tag{9}$$

The incident compressional wave from the water will be refracted in the sample with both a compressional component at an angle, α, and a shear component at an angle, β. In practice, if $v_c > V$, (which will be seen to be so in our case), δ is chosen such that only the shear wave can propagate. The arrival time of the signal, t_s, is measured. From the difference in travel times $\Delta t_s = (t_s - t_0)$ and *Eq 8*, and with some geometrical considerations to account for the actual sound path in the sample, v_s is given by:

$$v_s = V[(\cos \delta + V\Delta t_s/l)^2 + \sin^2\delta]^{-1/2} \tag{10}$$

The angle δ and the corresponding time delay, Δt_s, are measured, l is deduced from *Eqs 7* and *8* and v_s is computed. The accuracy in this case is $\Delta v_s/v_s \simeq 0.5$ percent.

EXPERIMENTAL RESULTS AND DISCUSSION

The properties of the matrix material and those of the inclusion material were measured. The results shown in *Table 1* illustrate the strong contrast that exists between the properties of each component. In all that follows, the properties (density, compressional and shear velocities, bulk, shear moduli) of the matrix will be written as ρ_1, v_{c1}, v_{s1}, B_1, G_1, those of the inclusion as ρ_2, v_{c2}, v_{s2}, B_2, G_2, and those of the composite as ρ, v_s, v_c, B, G; c indicates the fractional volume content.

The density ρ of the composites was measured and the results, *Fig. 3*, show that ρ increases linearly with the volume content, c, of particles. The measured values can be described to better than 1 percent by a rule of mixtures:

$$\rho = (1 - c)\rho_1 + c\rho_2 \tag{11}$$

The fact that the measured densities are so close to the theoretical values confirms the micrographic observations and suggests that the samples are tightly packed with very little porosity.

Velocity measurements were carried out at frequencies ranging from 0.5 to 5 MHz, and the signals were analyzed in terms of their frequency spectrum. It was clearly established that the dispersive effect of sound scattering was negligible at frequencies below 1.5 MHz. This corresponds to a value of $kD \simeq 0.2$, which

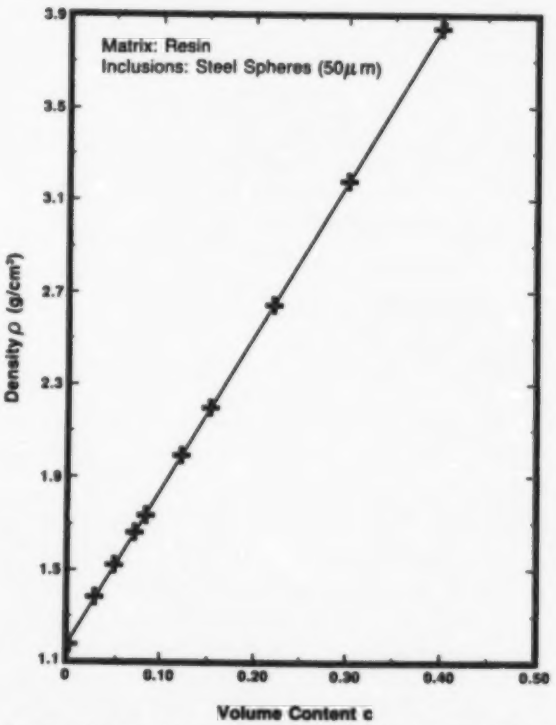

Fig. 3. Measured density of the samples versus volume content. The solid line corresponds to the prediction of a law of mixtures.

satisfies the condition $kD \ll 1$. As an added precaution, we chose 1.0 MHz as our measuring frequency ($kD \simeq 0.1$). This ensures that the measurements were made in the long wavelength regime, and that the results can be compared to the usual engineering static quantities. The values obtained for both the compressional (v_c) and shear (v_s) velocities are shown in *Fig. 4*. Measurements were performed at different locations on the samples and were within the expected accuracies. From this it can be said that the samples were homogeneous within a section corresponding to the diameter of the sound beam (1.5 cm). Measurements were also taken at different orientations without any observable variation of velocity, indicating that the composites were isotropic. As can be observed in *Fig. 4*, the velocity is very sensitive to the presence of inclusions and shows a behavior that cannot be easily described without the help of a model.

A great deal of attention has been devoted to the theoretical calculation of effective static moduli of multiphase materials. We shall very briefly present some of the models (12) which either are most often used or appear to be the most pertinent. In all cases, the composite material is considered as an homogeneous isotropic, infinite elastic medium (matrix) in which are embedded a number of independent inhomogeneities that are supposed to be distributed at random and bonded to the matrix. Here we shall distinguish those models that are based on global energy considerations from those that account for the local perturbation of the strain field at the level of the individual particle. Models of the first category are the better known and have been reviewed (12, 13). The first is the Voigt average, which is based on the assumption that the strain is uniformly distributed. Averaging yields the so-called rule of mixtures also referred to as the series model:

$$B = (1 - c)B_1 + cB_2 \tag{12}$$

$$G = (1 - c)G_1 + cG_2 \tag{13}$$

Proceeding in a similar way but this time assuming that the stress is uniform, Reuss proposed the parallel model:

$$1/B = (1 - c)/B_1 + c/B_2 \tag{14}$$

$$1/G = (1 - c)/G_1 + c/G_2 \tag{15}$$

Both approaches will yield extreme values of B and G. It has been suggested by several authors that both models could be combined into a series-parallel model (Takayanagi). However this implies the introduction of an additional unknown (12) and arbitrary parameter to describe the relative contribution of each phase.

Using variational methods Hashin and Shtrickman (14), and Hashin (15) were able to establish bounds for the upper (U) and lower (L) values of the moduli. The bounds which are exact are given by the following expressions:

$$B_U = B_1 + c(B_2 - B_1)(3B_1 + 4G_2)/[3B_2 + 4G_2 - 3c(B_2 - B_1)] \tag{16}$$

$$B_L = B_1 + c(B_2 - B_1)(3B_1 + 4G_1)/[3B_2 + 4G_1 - 3c(B_2 - B_1)] \tag{17}$$

$$G_U = G_1 + c(G_2 - G_1)(G_1 + F_2)/[G_2 + F_2 - c(G_2 - G_1)] \tag{18}$$

$$G_L = G_1 + c(G_2 - G_1)(G_1 + F_1)/[G_2 + F_1 - c(G_2 - G_1)] \tag{19}$$

where

$$Fi = (G_1/6)(9Bi + 8Gi)/(Bi + 2Gi) \tag{20}$$

We applied these various models. The results for B are illustrated in *Fig. 5*, where label 1 refers to the series model; label 2 to the parallel model; label 3 to the series-parallel model with 0.5 given as a value of the arbitrary parameter; label 4 to the upper bound of the variational model; and label 5 to the lower bound. *Figure 5* also shows our experimental values obtained from the densities and velocities using *Eqs 1* and *2*. As can be seen, the rule of mixtures (curve 1) can by no means describe our results. On the other hand, the parallel model (curve 2) appears as a better description, and it would probably be possible to find a fitting parameter that would bring the series-parallel model (curve 3) to a better agreement but without any clear meaning. Also it can be observed that the variational bounds (curves 4 and 5), even though far apart, constitute closer bounds for

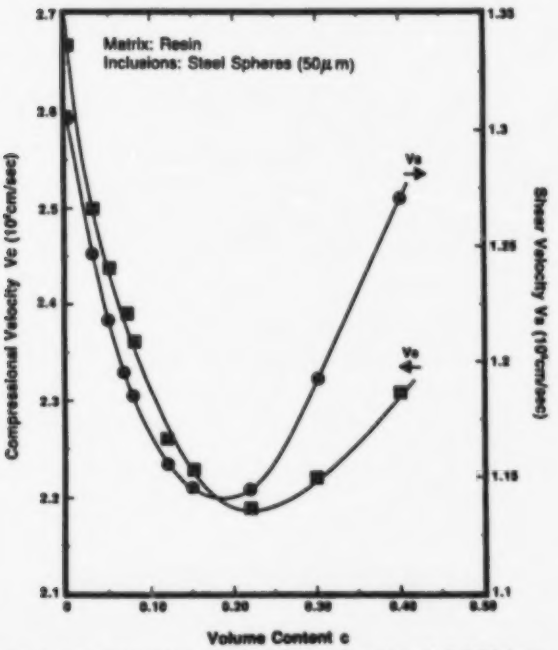

Fig. 4. Compressional and shear velocities (1.0 MHz) versus volume content. The solid lines are included as guides for the eye.

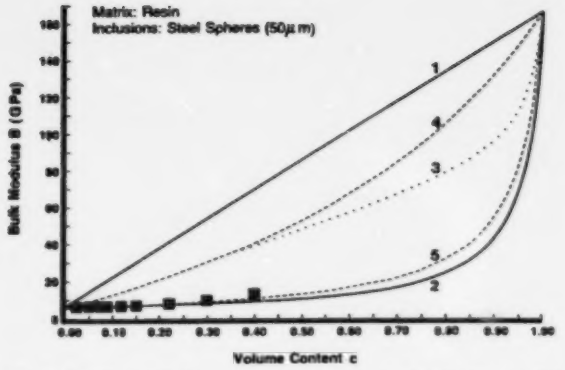

Fig. 5. Bulk modulus versus volume content. The solid symbols indicate the experimental data, which is compared to predictions of 1) Voigt; 2) Reuss; 3) Voigt + Reuss; 4) Hashin-Shtrickman upper bound; 5) lower bound.

the data. In fact, the data is best described by the lower bound; the reason for this will become apparent later on.

Finally, it is important to note that the high level of discrimination between the curves in *Fig. 5* has its origin in the strong contrast that exists between the properties of the constituents that we have chosen for the composite. For a low contrast of elastic properties, the curves would tend to merge to the limiting case of the Voigt model (series-model). This explains why the rule of mixtures appears satisfactory in a number of cases.

In contrast to models of the first category, those of the second category are sensitive to the microscopic details of the composite. They are based on the calculation of the elastic field that surrounds the individual inclusion. The reference work is that of Eshelby (16) who, by using topological arguments, produced an elegant solution to this complicated problem. Other authors using different techniques such as Green's functions (17) arrived at the same results. The formulation, which is quite involved for the case of the ellipsoïdal shaped particle, is greatly simplified for a spherical particle:

$$(B - B_1)/(B_2 - B_1) = c/[1 + 3(B_2 - B_1)/(3B_1 + 4G_1)] \quad (21)$$

$$(G - G_1)/(G_2 - G_1) = c/[1 + (G_2 - G_1)/(G_1 + F_1)] \quad (22)$$

where

$$F_1 = (G_1/6)(9B_1 + 8G_1)/(B_1 + 2G_1) \quad (23)$$

Here, it might be of interest to note that by setting $G_1 \ll B_1$ (for a liquid) and $G_2 \gg G_1$ (for rigid solid), one recovers Einstein's relation $G = (1 + 2.5c)G_1$.

The approach is, however, limited to low concentrations. A number of schemes have been proposed to extend the solution to the case of finite concentrations. Kuster and Toksöz (18) formulated the problem in terms of scattering, and using integral equations obtained the following (KT) expressions:

$$(B - B_1)/(3B + 4G_1) = c(B_2 - B_1)/(3B_2 + 4G_1) \quad (24)$$

$$(G - G_1)/(G + F_1) = c(G_2 - G_1)/(G_2 + F_1) \quad (25)$$

where F_1 is the same as above, *Eq 23*. It can be noted that *Eqs 24* and *25* reduce to those of Eshelby in the limit of $c \simeq 0$. Also it is interesting to see the similarity between the KT model and the lower bound of the variational model, *Eqs 17* and *19*. Another approach is that of making the problem self-consistent, SCS (19, 20). In this (SCS) approach (which has been highly criticized, but is widely used in the field of solid state physics), any particle that is added to the composite is assumed to be embedded in a medium that actually possesses the properties of the final composite. The equations that must be solved by iteration are:

$$1/(3B + 4G) = (1 - c)/(3B_1 + 4G) + c/(3B_2 + 4G) \quad (26)$$

$$1/(G + F) = (1 - c)/(G_1 + F) + c/(G_2 + F) \quad (27)$$

where

$$F = (G/6)(9B + 8G)/(B + 2G) \quad (28)$$

In a last approach, a differential scheme (DS) is proposed (21), whereby a new inclusion is added to the existing effective media. Starting from the exact solution at small concentrations, *Eqs 21* to *23*, the composite is built up by adding particles. This is expressed by a system of nonlinear differential equations that must be solved numerically:

$$\frac{db}{dc} = \frac{1}{(1 - c)} \frac{(1 - b)(3b + 4\,Mg)}{(3 + 4\,Mg)} \quad (29)$$

$$\frac{dg}{dc} = \frac{1}{(1 - c)} \frac{5g(1 - g)(3b + 4\,Mg)}{3b(2 + 3g) + 4\,Mg(3 + 2g)} \quad (30)$$

where

$$b = B/B_2$$

$$g = G/G_2$$

$$M = G_2/B_2$$

We applied these microscopic models to our system. The results for the bulk modulus B are illustrated in *Fig. 6a*, those for the shear modulus G in *Fig. 6b*. Here, label 1 refers to Eshelby's calculation, label 2 to the model of Kuster and Toksöz (KT), label 3 to the self consistent scheme (SCS), and label 4 to the differential scheme (DS). As can be observed, Eshelby's calculation is indeed valid only at low volume contents. The KT model (curve 2) appears as a better approximation, but at concentrations

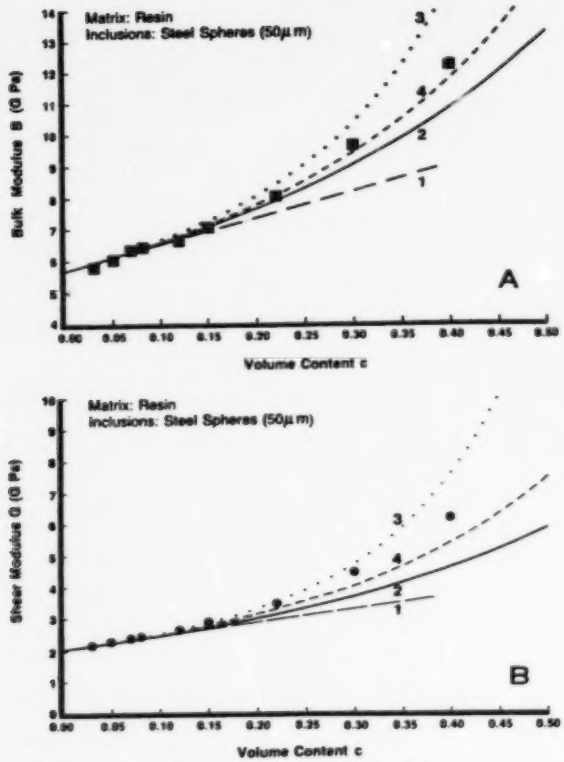

Fig. 6. (a) Bulk elastic modulus and (b) Shear modulus versus volume content. The solid symbols are the experimental data, which are compared to predictions of 1) Eshelby; 2) Kuster-Toksoz; 3) Self Consistent Scheme; 4) Differential Scheme.

higher than 15 percent, it yields values for the moduli which are too small. In contrast, the SCS (curve 3) gives values that are too high. On the whole the DS (curve 4) appears as the most satisfactory description of the data.

Some caution, however, must be exerted when considering the problem at high concentration values. The micrographic observations seemed to indicate that the inclusions were not in mutual contact. However, the presence of at least some contiguity cannot be ruled out. The different models presented here are actually schemes that allow extrapolation of the solution obtained for the perfectly dilute problem to the region of higher volume contents. The schemes can be looked upon as equivalent to mean-fields approximations. They retain the basic hypothesis of dilution and they do not contain the necessary ingredients (correlation function) to account for particle-particle interactions, the penetrable sphere (22) problem.

CONCLUSION

In the course of this study, an ultrasonic approach to the measurement of elastic constants was presented, and it was established that the ultrasonic moduli were equivalent to the usual engineering quantities. Some of the advantages of this technique over the more common methods in the case of polymer composites were put forth. One of the main advantages was the fact that viscoelastic effects are de facto eliminated, which greatly simplifies interpretation. Also the technique is nondestructive and simple; the accuracy is high (1 percent), and the measurements can be repeated and reproduced. The samples prepared from high contrast materials were composed of a resin matrix in which iron particles with volume concentrations up to 40 percent were embedded. Care was taken so that the microscopic morphological characteristics of the test samples were well defined.

The results for the measurement of the elastic moduli were presented and discussed in terms of existing theoretical models. The experiments, having been made on composites of high contrast materials, allowed determination of a clear distinction between models. It was established that models that account for the microscopic details of the composite provided the better description of the moduli.

Thus it can be concluded that the bulk properties of the material are governed by the actual details of its microstructure, as opposed to being governed by the mixed averaged properties of the individual constituents. The behavior of the sound velocity is thus correlated to the morphological characteristics of the composite through careful modeling of the elastic moduli. As such, there is hope that the ultrasonic measuring technique will prove to be a powerful tool for the evaluation of filled polymer composites. The effects of the different factors that are known to affect the bulk properties, such as the shape of inclusions, their distribution in size and orientation, and the quality of their interface with the matrix, still need to be assessed and will be the subject of forthcoming reports.

REFERENCES

1. J. V. Schmitz, ed. "Testing of Polymers," Interscience Publishers, John Wiley & Sons, New York (1965).
2. I. M. Ward, "Mechanical Properties of Solid Polymers," John Wiley & Sons, New York (1983).
3. E. Schreiber, O. L. Anderson, and N. Soga, "Elastic Constants and their Measurements," McGraw Hill, New York (1973).
4. H. M. Ledbetter, Ming Lei, and M. W. Austin, *J. Appl. Phys.*, to be published.
5. F. E. Stanke and G. S. Kino, *J. Acoust. Soc. Am.*, **75**, 665 (1984).
6. V. K. Kinra and A. Anand, *Int. J. Solids Structures*, **18**, 367 (1982).
7. V. K. Kinra, E. Kerr, and S. K. Datta, *Mech. Res. Comm.*, **9**, 109 (1982).
8. C. M. Sayers and R. L. Smith, *J. Phys. D: Appl., Phys.* **16**, 1189 (1983).
9. D. M. Smith and D. G. Huizenga, *J. Phys. Chem.*, **89**, 2394 (1985).
10. B. Hartmann, "Methods of Experimental Physics," Ch. 12, Vol. 16, part C, Academic Press, New York (1980).
11. B. Hartmann and J. Jarzynski, *J. Acoust. Soc. Am.*, **56**, 1469 (1974).
12. T. S. Chow, "Review: The effect of particle shape on the mechanical properties of filled polymers," *J. Mater. Sci.*, **15**, 1873 (1980).
13. O. L. Anderson "Determination and some uses of isotropic elastic constants of polycrystalline aggregates

using single-crystal data," in Physical Acoustics Vol 3-A, W. P. Mason, ed., Academic Press, New York (1965).
14. Z. Hashin and S. Shtrickman, *J. Franklin Inst.*, **271**, 336 (1961).
15. Z. Hashin, *J. Appl. Mech.*, **29**, 143 (1962).
16. J. D. Eshelby, *Proc. R. Soc.*, **A241**, 376 (1957).
17. A. K. Mal and L. Knopoff, *J. Inst. Maths. Applics.*, **3**, 376 (1967).
18. G. Kuster and M. N. Toksöz, *Geophysics*, **39**, 587, and 607 (1974).
19. B. Budianski, *J. Mech. Phys. Solids*, **13**, 223 (1965).
20. J. G. Berryman, *J. Acous. Soc. Am.*, **68**, 1809 (1980).
21. S. Boucher, *Revue M.* **21**, 243 (1975) and *Revue M*, **22**, 31 (1976).
22. J. G. Berryman, *J. Phys. D: Appl. Phys.*, **18**, 585 (1985).

Buckling of Composite Cylinders Under External Pressure*

P. OUELLETTE, S. V. HOA, *and* T. S. SANKAR

Composite Materials Research Group
Department of Mechanical Engineering
Concordia University
Montreal, Quebec, Canada H3G 1M8

Experimental results from buckling tests on thin shell structures made of filament-wound glass fiber reinforced plastic are compared to values calculated with three different procedures. These procedures are: 1) a linear stability analysis for anisotropic, heterogeneous, thin, cylindrical shells, 2) a proposed design code, and 3) a national standard. Imperfection surveys in the circumferential direction were conducted and were found to be much larger than imperfections typical for metallic thin shells. All three procedures yield design pressures lower than observed buckling pressures. The analytical method and the standard are less conservative than the proposed design code and may possibly permit the fabrication of safe and more economical structures.

INTRODUCTION

The stability analysis of thin shells has presented problems ever since the subject was addressed at the turn of the century. In the late 1920s and early 1930s, shell structures became still thinner for applications in aircraft (1). As a result, workers in this field witnessed the gap between predicted critical buckling load and actual buckling load widen. Over the last half century a tremendous amount of work has been done in the area of stability analysis of thin shells in an attempt to narrow this gap.

It is only since the mid 1950s that some attention has been directed to thin shells made of composite materials. Because these early structures were intended for use as rocket motor casings, the loading case given the most attention was axial compression. Again workers found large differences between predictions and experiments. Since those days, the use of powerful computers has permitted more accurate modelling of the actual nonlinear behavior of thin shells, whether they be isotropic metals or generally anisotropic laminated composites. Nevertheless, these improvements have not yet advanced to the point where the problem can be considered solved. Recent review articles emphasize the need for more work on buckling of composite shells (2, 3).

The purpose of the work described here was to conduct experiments on thin composite shell structures subjected to hydrostatic pressure and to compare the results to a linear buckling analysis, to a proposed design code, and to an existing design standard.

In the following sections, the experimental program and results are presented first, then the three selected procedures are outlined. Finally, the experimental buckling pressures and the design pressures calculated using the three procedures are compared and discussed with the aim of contributing to the efforts presently underway to establish more reliable design methods and possibly permit more economical thin-shell structures made of composite materials.

EXPERIMENTAL PROGRAM

The program consisted of four phases: 1) the fabrication of the tubes using material and practices common to suppliers of good quality pressure vessels; 2) the inspection of the tubes and the recording of initial imperfections; 3) the testing of the tubes to destruction; 4) cutting samples from the failed tubes to determine glass content and to verify the wall construction and the thickness. These four phases are addressed individually below.

Fabrication of the Tubes

Four polymer composite tubes were made for the experimental program by CPF Dualam Ltd. They were made with materials typically used in many pressure vessel applications. The polymer matrix is a vinyl ester marketed by Dow Chemical Canada Ltd. under the name Derak-

* Based on P. Ouellette, "Buckling of Glass-Reinforced Plastic Filament-Wound Pressure Vessels Under Hydrostatic External Pressure," M. Eng. Thesis, September 1985.

ane 411. The resin is activated and cured with 1 percent MEK peroxide (max.) and 0.2 to 0.3 percent cobalt naphthenate. The reinforcement consisted of glass roving supplied by Fiberglas Canada under the designation E-Cr roving. Two of the tubes had a poly(vinyl chloride) (PVC) liner, which is used to protect the structural layers of a vessel against corrosive contents. The PVC was supplied in the form of extruded pipe by Harvel Plastics. Applicable mechanical and physical properties are given in *Table 1*. Note that all three constituents above are considered isotropic.

The tubes were made using the process of 'wet' filament-winding. This consists of winding continuous lengths of glass roving in the form of a band about 100 mm wide unto a rotating mandrel. When the winding process is finished, the tube is cured on its mandrel (at ambient conditions in this case). All four tubes were prepared on PVC pipes, which served as the mandrels. For tubes 3 and 4, a release film was put on the pipe before winding so that the tube could be taken off the PVC pipe. For the other two, no release film was used; on curing, the PVC pipe became consolidated into the structure as the corrosion liner. After curing, the tubes were cut to length, and the flanges were built up at the ends. The flanges were of glass mat and woven roving construction, while the covers were of glass mat; both were impregnated with the same resin used in the winding process.

Inspection of the Tubes

This second phase of the experimental program can be divided into two parts: 1) the tubes were visually inspected for gross damage, delaminations, and surface flaws, and measures of winding angles and wall thickness were made; 2) the initial outer surface imperfections were recorded.

Part 1: No gross damage or delaminations were observed. Wall thickness measurements were made using a magnetic reluctance thickness sensor. The sensor thickness values are corrected for the curvature of the tubes. *Table 2* lists the information gathered on the four tubes.

Part 2: As mentioned in the first section, initial shape imperfections of fabricated shell structures have been identified as one of the principal reasons for the discrepancy between experimental and predicted critical loads. While this effect is most serious for axial compression, it was decided that some data on the imperfection patterns produced by a filament-winding technique might prove useful. This is especially so, since no such information seems to have been published yet.

Accordingly, a setup was prepared using a lathe to mount the tubes. *Figure 1* shows a top view of the rig with the instrumentation shown in block form.

Eight circumferential scans and eight axial scans were recorded for each tube. *Figure 2* shows the developed surface of a tube without the flanges and the traces of the scans.

After the instruments were suitably calibrated, the scans were recorded, and they are shown in *Figs. 3* to *6*. The circumferential scans of tube 3 and tube 4 show a clear pattern. This was less evident for tube 1, and not at all evident for tube 2. Therefore, a spectral analysis was made to see if patterns could be extracted from the circumferential scans of tubes 1 and 2.

The setup of *Fig. 1* was used, except that the output from the radial pot was directed to an FFT analyzer while the tubes were rotated at a nominal 30 rpm on the lathe. A complete set of circumferential scans were recorded on tubes 1 and 2. The results are displayed in *Figs. 7* and *8*. Since the pattern with the largest amplitude is by far the most important, we may concentrate on the highest peaks.

The first peak at 31.5 cycles per minute (CPM) can be due to the fact that the tubes are not

Table 2. Geometric Data for Four Tubes.

	Tube 1	Tube 2	Tube 3	Tube 4
Uncorrected total thickness (mm) (1)	6.5	6.4	3.5	3.4
Corrected total thickness, t (mm) (2)	5.8	5.7	2.8	2.7
PVC liner thickness, t_1 (mm)	4.76	4.76	N.A.	N.A.
Filament winding thickness, $(t - t_1)$ (mm)	1.04	0.94	2.8	2.7
Number of filament wound layers (3)	2	2	6	6
Winding angle (degree)	54	63	54	63
Mean inside radius, R_1 (mm) (4)	133	133	137	136
Radius to mid-surface, $(R = R_1 + (t/2)$ (mm)	136	136	138	137
Tube length (mm) (5)	864	864	876	868

Notes: 1. Measured at mid-length; 4 readings: C.O.V. = 3.3%, 2.7%, 6.4%, 4.4%, for tubes 1, 2, 3, 4 respectively.
2. Subtract 0.7 mm from sensor readings to compensate for tube curvature.
3. One filament wound layer is about 0.5-mm thick.
4. Measured at the end of the tube.
5. Excluding flanges which were about 20-mm thick.

Table 1. Some Mechanical and Physical Properties of the Constituents.

	Tensile Modulus, E (GPa)	Shear Modulus, G (GPa)	Poisson's Ratio, ν	Specific Gravity
Dow Derakane 411	3.45	1.28	0.35	1.13
Fiberglas Can. E-Cr roving	77.2	30.9	0.25	2.72
Harvel Co. PVC pipe	2.76	1.00	0.38	1.4

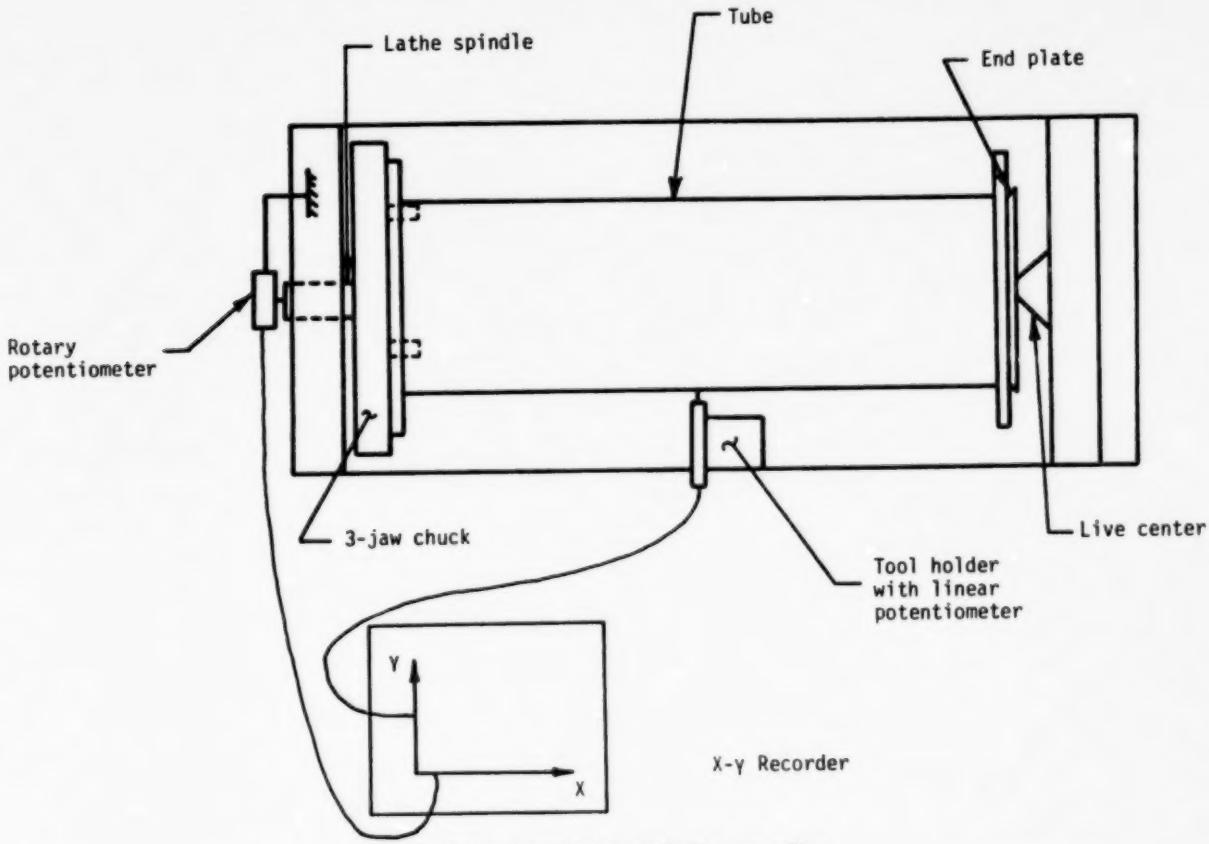

Fig. 1. Setup for initial imperfection recording.

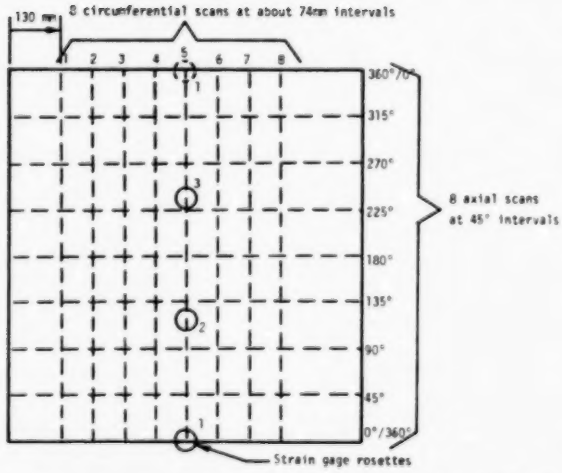

Fig. 2. Developed surface of typical tube showing scan lines and strain gage positions.

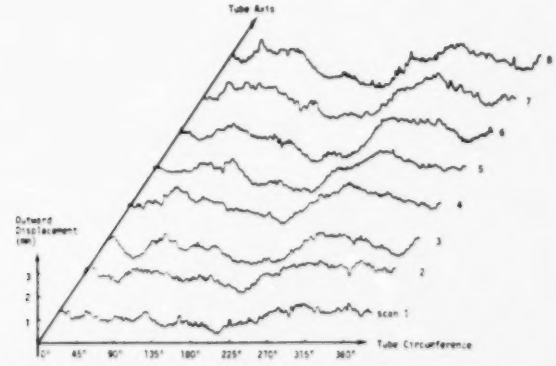

Fig. 3. Circumferential scans of tube 1. Two wavelengths can be discerned.

perfectly axial with respect to the lathe spindle. The second peak at 64.5 CPM represents two waves per revolution of the tubes, and this corresponds to an elliptical shape. These are seen to be the major patterns in tube 1, and indeed we can make out the two waves in *Fig. 3*, in retrospect. Tube 2 shows no clearly predominant pattern from *Fig. 4*, and the spectrum of *Fig. 8* shows that, apart from the peak at 31.5 CPM, there are only relatively low peaks at 64.5 CPM, 129 CPM, and 258 CPM representing an elliptical shape, a four-lobe pattern, and an eight-lobe pattern respectively.

Figures 3 to *6* can be used to determine the size of the imperfections, as well as the general shape patterns, and these data are brought together in *Table 3*.

Buckling Test on the Tubes

Each tube was instrumented with three strain gage rosettes at its mid-length about 120°

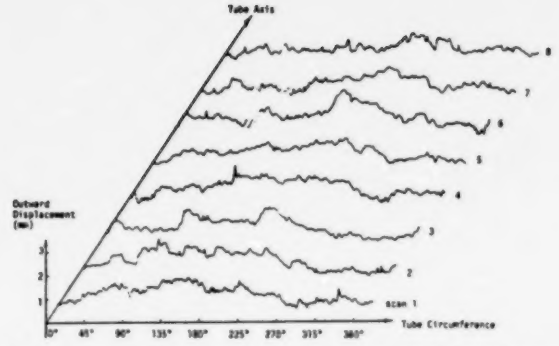

Fig. 4. Circumferential scans of tube 2. No clear pattern can be seen.

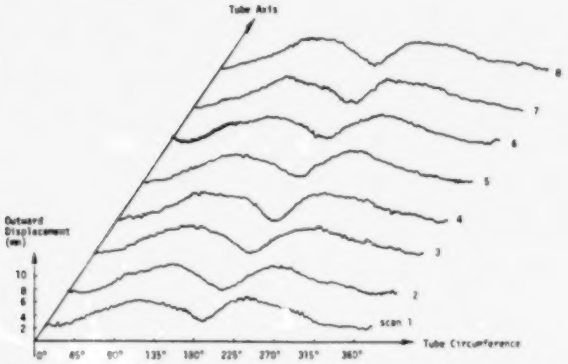

Fig. 5. Circumferential scans of tube 3. Two wavelengths are evident.

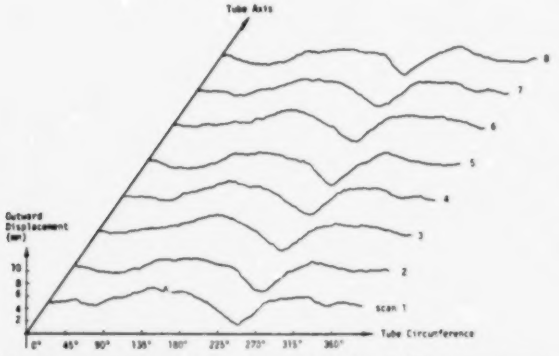

Fig. 6. Circumferential scans of tube 4. The two wavelength pattern is the same as for tube 3, and amplitudes are similar.

apart (see *Fig. 2*). Each rosette had three gages positioned as shown in *Fig. 9*, which also gives the gage numbering scheme used for all the tubes. The gages were MM type CEA-6-25OUR-120, bonded with M-Bond 200 adhesive to the outside surface.

The first tube tested was unlined tube 3. It was decided to test this tube first by pulling vacuum only. The tube was stood on end and the setup was made as shown in *Fig. 10*. The nine strain gages and the pressure transducer were also monitored with a data logger. Vacuum was pulled to about 95 kPa and no evidence of

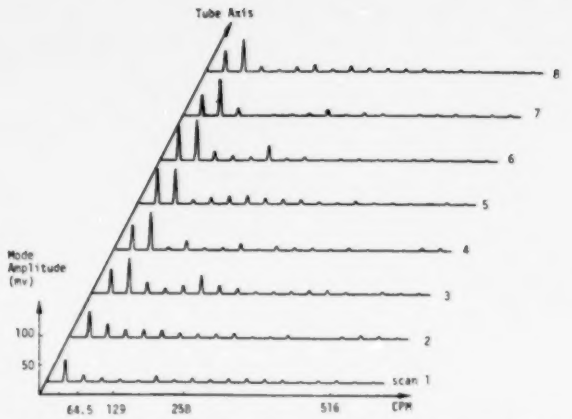

Fig. 7. FFT analysis of circumferential scans on tube 1, showing a predominance of 2, and the presence of 6-wave modes.

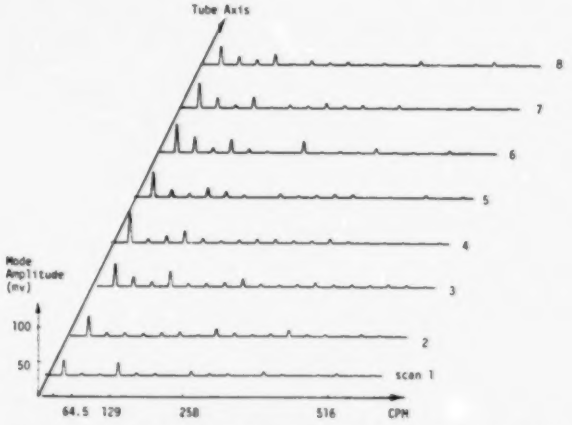

Fig. 8. FFT analysis of circumferential scans on tube 2, showing the presence of 2, 4, and 8-wave modes at various scan positions.

Table 3. Initial Imperfections of the Tubes.

	Tube 1	Tube 2	Tube 3	Tube 4
Imperfection Pattern (circum. wave-length)	major: 2 minor: 6	major: — minor: 2, 4, 8	major: 2 minor: _	major: 2 minor: _
Max. circum. Imperfection Envelope, Δ_w (mm)	2.1	1.9	5.5	6.1
Max. relative Circum. Imp. Envelope, $(\Delta_w/t)^*$	0.36	0.33	1.96	2.26
Max. Axial Imperfection Envelope, Δ_a (mm)	1.1	1.5	2.4	2.4
Max. Relative Axial Imp. Envelope, (Δ_a/t)	0.19	0.26	0.86	0.89

* t is tube thickness (mm).

instability was observed. To increase the external hydrostatic pressure it was necessary to place the tube into a steel pressure chamber.

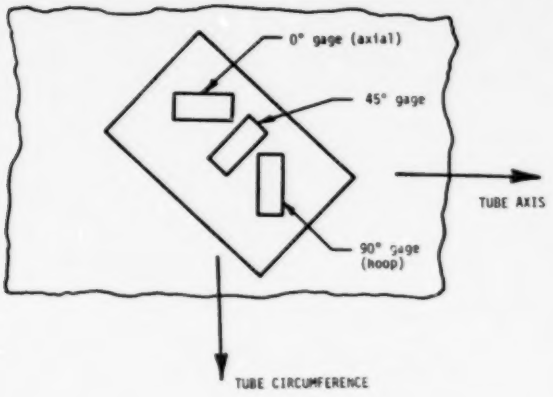

Rosette position*	Axial gage #	45° gage #	Hoop gage #
1	1	2**	3
2	4	5**	6
3	7	8**	9

* See Figure 2 for position on developed cylinder.
** These gages were disconnected for tests in the pressure chamber.

Fig. 9. Position and numbering scheme of strain gage rosettes.

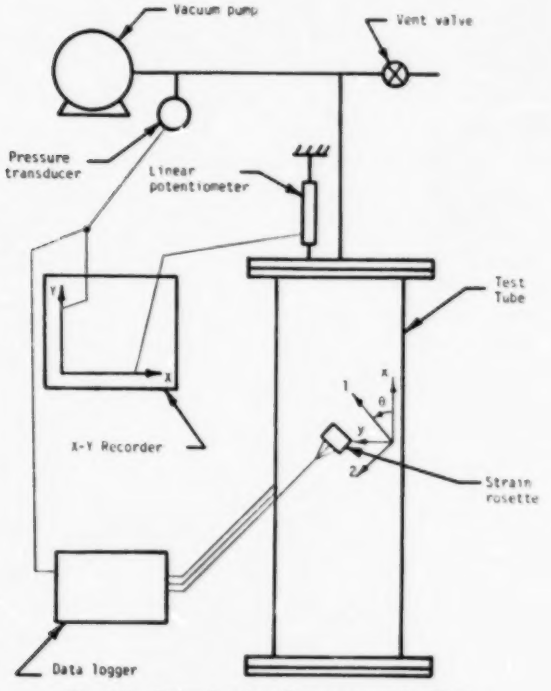

Fig. 10. Tube 3 setup for vacuum testing.

This required that some changes be made in the instrumentation of the tubes. First, the end deflection could no longer be measured. Second, only six strain gages could be monitored. All the 45° gages were disconnected, but the same gage numbering scheme was retained. Unfortunately, visual observation was no longer possible.

Tube 3 was put into the pressure chamber with its contained air at atmospheric pressure. Air from a utility line at 8.8 atmospheres was slowly let into the chamber. Strains and pressure were recorded with the data logger. At a net external pressure of 250 kPa, the test was stopped, the pressure was released, and the tube was examined for damage. The results of this second run on tube 3 are shown in *Fig. 11*. The residual strains were small, and there was no visible damage. Once more the same tube was pressurized, this time to destruction. Failure was sudden and catastrophic, producing a loud explosive noise. Failure was accompanied by a sudden pressure drop and by the destruction of strain gages. The plotted data from the final run on tube 3 is shown in *Fig. 12*.

Unlined tube 4 was tested to destruction in a single run, and the results are displayed in *Fig. 13*.

Tubes 1 and 2 had liners, and the necessary buckling pressure was expected to be higher than for tubes 3 and 4. To prevent possible leaks to the inside of the tubes, tacky-tape was used to seal the end closures. All other conditions were unchanged. Each tube was tested to destruction in a single run. The data are plotted in *Figs. 14* and *15*.

Tubes 1 and 2 with liners showed extensive cracking and delamination around the whole tube. Much of the PVC liner shattered and disbonded from the filament-wound layers. Tubes 3 and 4 without liners showed more localized cracking and delamination centered about the generators where the curvature was greatest. Recall that these latter two tubes showed the most clearly elliptical cross sections as fabricated.

All the above testing was done at about 21°C and 30 percent relative humidity.

Testing of Tube Samples

After the four tubes were tested, one rectangular sample was cut from each tube wall where the damage was not visible. Each tube sample was cut into smaller pieces, the aim being to determine the amount of reinforcement present, and the lay-up sequence in the laminated wall. Both factors have an important effect on stiffness and deformation behavior of the shell wall, and both can be found by using a "burn off" test. Knowing the densities of the resin and the reinforcement (*Table 1*), the volume fraction of glass can be calculated. Three samples from each tube were tested, and the average fractions are shown in *Table 4*.

DESIGN PROCEDURES

The first procedure is the most complex and complete of the methods. It will be considered before the others because this will present an opportunity to sketch the analysis of generally anisotropic laminated cylindrical thin shells subjected to buckling loads. Also, some of the

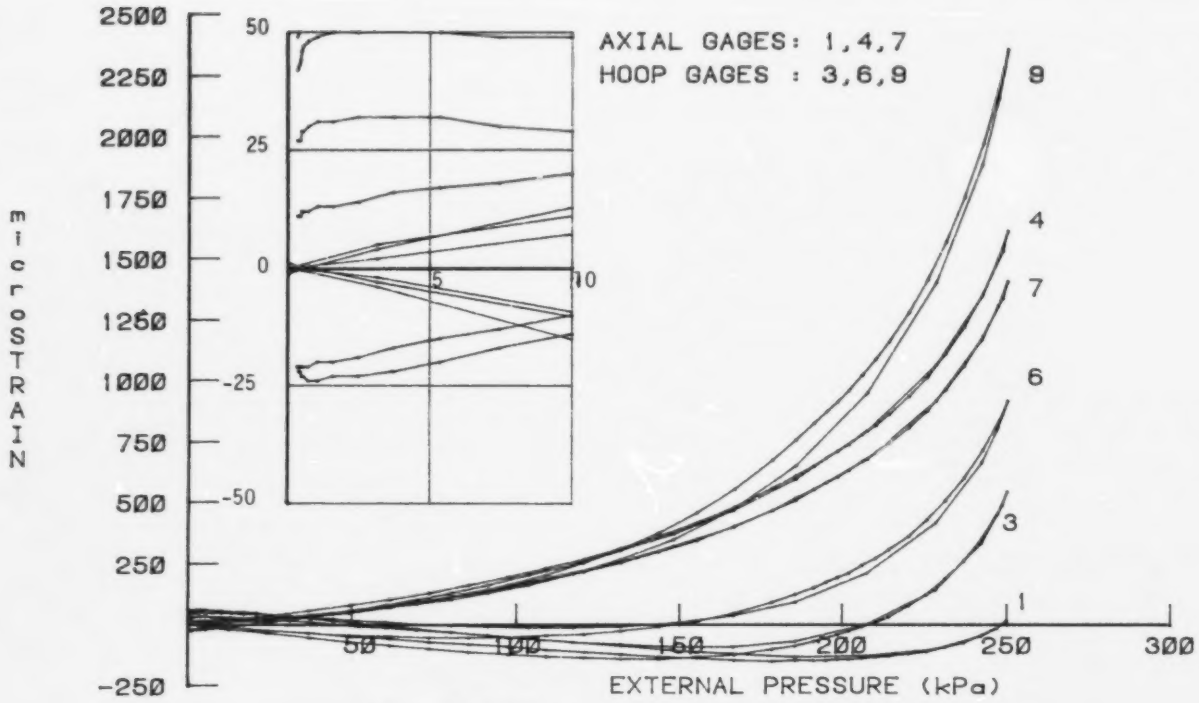

Fig. 11. Test of tube 3, loading and unloading (2nd run).

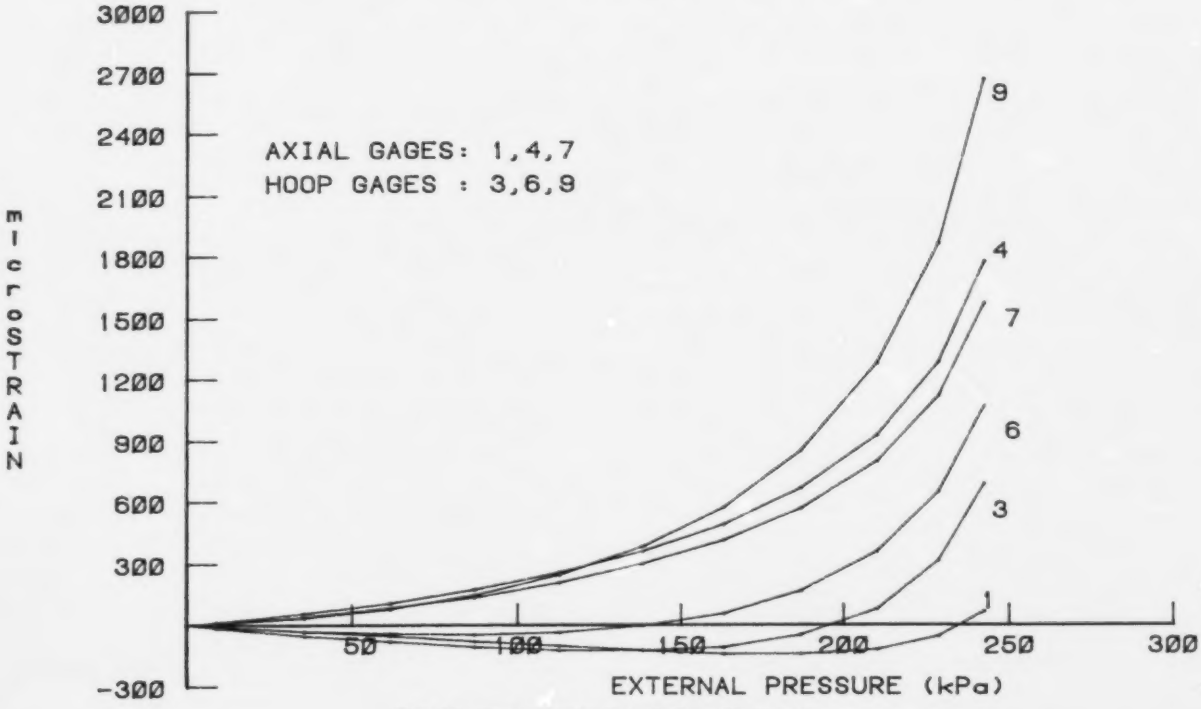

Fig. 12. Test of tube 3, to failure (3rd run).

details in the analysis will be required in using the other methods.

Present Design Procedure

Thus, we now consider the analysis presented in 1963 by Cheng and Ho (4). These workers considered cylindrical shells made of laminated anisotropic materials, subject to axial compression, lateral pressure, and torsional loads, or combinations thereof. Their analysis is based on shell theory assumptions, viz., 1) the shell wall is thin compared to the shell mid-surface

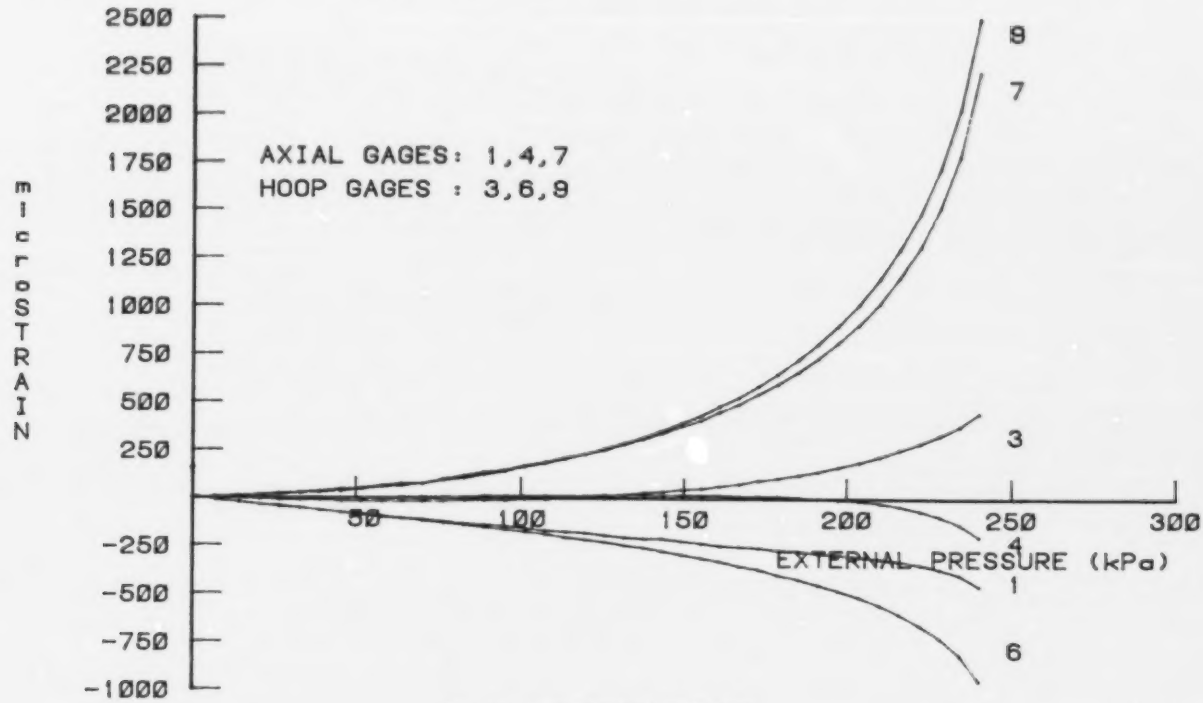

Fig. 13. Test of tube 4 to failure.

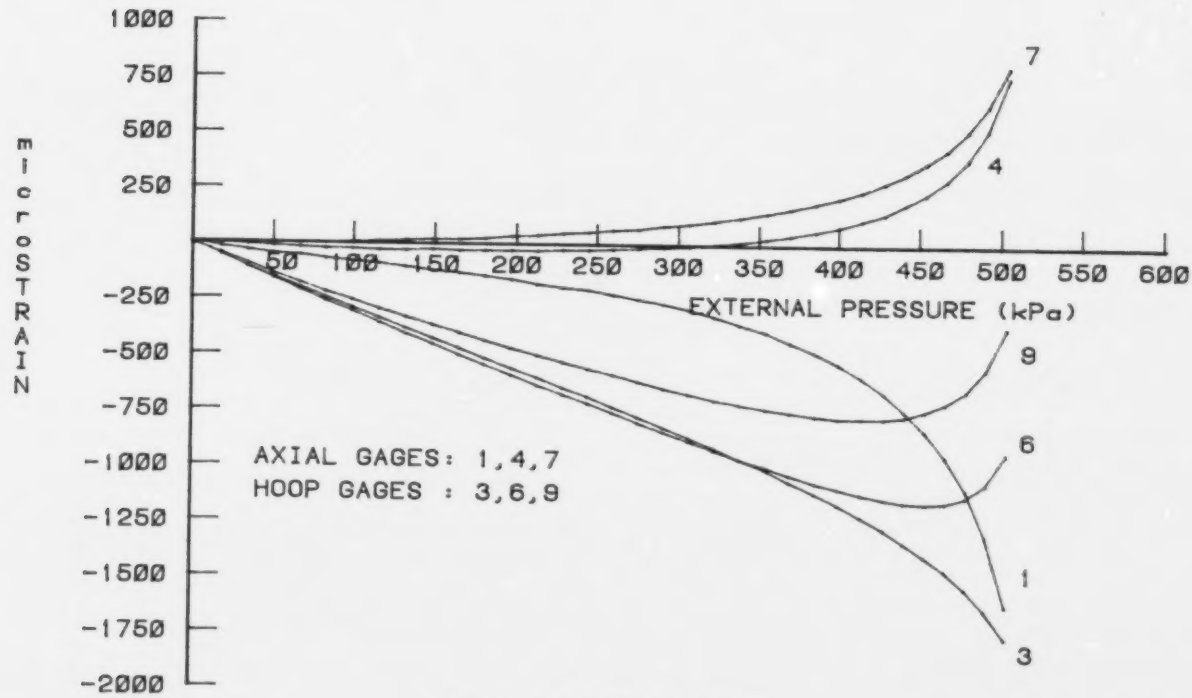

Fig. 14. Test of tube 1 to failure.

radius, 2) displacements are small compared to the shell thickness, 3) transverse or thickness shear strains and thickness normal strains are negligibly small compared to in-plane strains.

The procedure is identical to that required for isotropic shell analysis except that the stress-strain relations are in a more general form. Since Cheng and Ho concisely give the requisite equations, only some points will be detailed here.

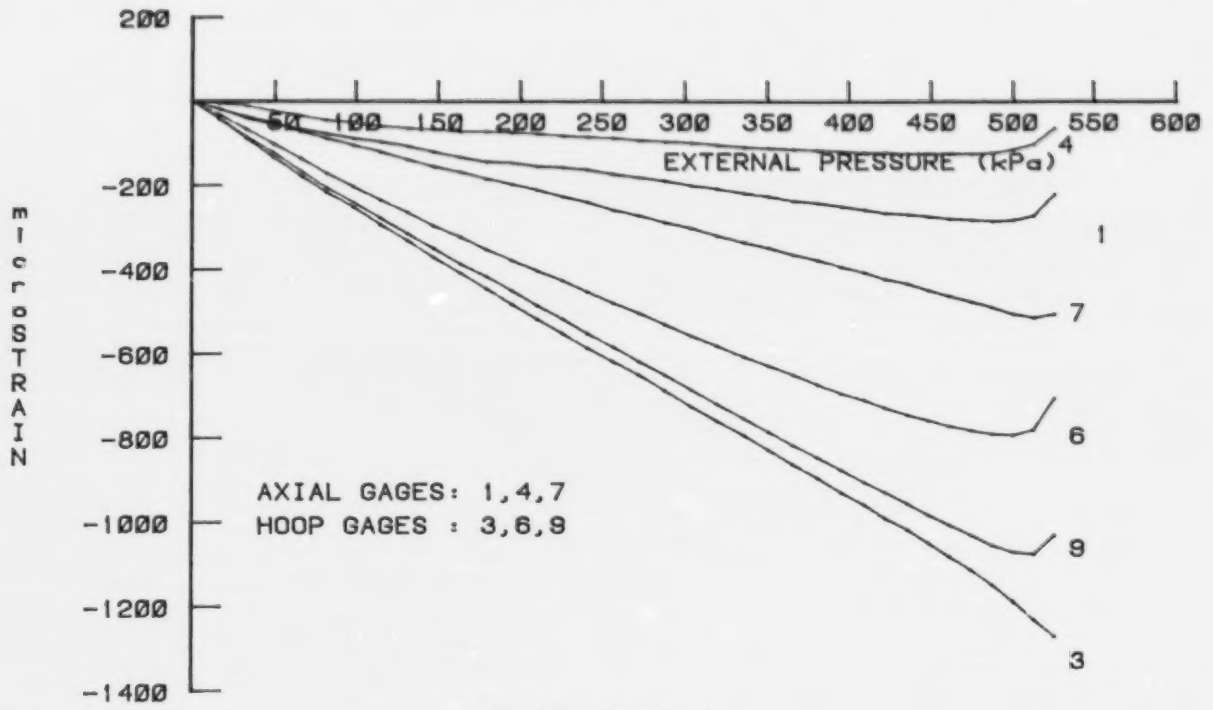

Fig. 15. Test of tube 2 to failure.

Table 4. Amount of Reinforcement in Tubes.

	Tube 1	Tube 2	Tube 3	Tube 4
	8.1678	6.1432	3.3138	3.5883
	5.1298	5.3059	4.6765	3.2674
Wt. of laminate (g)	4.9379	4.6039	4.3142	3.5837
	6.1774	4.4925	N.A.	N.A.
	4.0005	4.0808	N.A.	N.A.
Wt. of PVC (g)	3.7665	3.5372	N.A.	N.A.
	1.2400	1.1465	2.1337	2.5389
	0.7298	0.8577	2.9945	2.3205
Wt. of glass (g)	0.7068	0.7635	2.7627	2.5678
	2	2	6	6
	2	2	6	6
No. of glass layers	2	2	6	6
	0.62	0.69	0.64	0.71
	0.65	0.70	0.64	0.71
Wt.-fraction	0.60	0.72	0.65	0.72
	0.40	0.48	0.42	0.50
	0.44	0.49	0.42	0.50
Vol.-fraction	0.38	0.52	0.44	0.52
Average vol.-frac.	0.41	0.50	0.43	0.51

Note: The weight of PVC was determined by measuring the volume of the PVC layer, and using a specific gravity value of 1.4.

The most general form of the stress-strain relations is given by generalized Hooke's Law (assuming linear elastic behavior):

$$s_i = C_{ij} e_j, \qquad i, j = 1 \text{ to } 6 \tag{1}$$

where C_{ij} is the elastic stiffness matrix, s_i are engineering stresses, and e_j are engineering strains.

Considerations of the strain energy in a conservative material system has shown that the elastic stiffness matrix must be symmetric, i.e., $C_{ij} = C_{ji}$. Thus, the 36 constants in *Eq 1* are reduced to 21. Material layers of technological importance do not have the general anisotropy described by *Eq 1*. Some are orthotropic, some are isotropic in their plane of lamination, while others are conventional isotropic materials. In our case, all the materials have properties that can be given by a subset of the constants in *Eq 1*:

$$\begin{bmatrix} s_1 \\ s_2 \\ s_3 \\ s_4 \\ s_5 \\ s_6 \end{bmatrix} = \begin{bmatrix} C_{11} & C_{12} & C_{13} & 0 & 0 & 0 \\ C_{12} & C_{22} & C_{23} & 0 & 0 & 0 \\ C_{13} & C_{23} & C_{33} & 0 & 0 & 0 \\ 0 & 0 & 0 & C_{44} & 0 & 0 \\ 0 & 0 & 0 & 0 & C_{55} & 0 \\ 0 & 0 & 0 & 0 & 0 & C_{66} \end{bmatrix} \begin{bmatrix} e_1 \\ e_2 \\ e_3 \\ e_4 \\ e_5 \\ e_6 \end{bmatrix} \tag{2}$$

where we have applied $C_{ij} = C_{ji}$ in the notation.

Using the first assumption (i.e., $s_3 = 0$) and the third assumption (i.e., $e_4 = e_5 = 0$), the system is reduced to the two-dimensional form used for the thin shell analysis:

$$\begin{bmatrix} s_1 \\ s_2 \\ s_6 \end{bmatrix} = \begin{bmatrix} Q_{11} & Q_{12} & 0 \\ Q_{12} & Q_{22} & 0 \\ 0 & 0 & Q_{66} \end{bmatrix} \begin{bmatrix} e_1 \\ e_2 \\ e_6 \end{bmatrix} \tag{3}$$

where the Q matrix is the modulus matrix or reduced stiffness matrix for our specially orthotropic layers. The fibers make an angle θ with the shell axis. Because the equilibrium equations will be expressed in the natural coordinate system of the shell (where x is the axial direc-

tion, y is the circumferential direction, and z is the direction normal to the mid-surface and positive outward), *Eq 3* must be transformed from the material directions '1-2' to the shell 'x-y' system (*Fig. 10*). Transformation gives

$$\begin{bmatrix} s_x \\ s_y \\ s_{xy} \end{bmatrix} = \begin{bmatrix} \bar{Q}_{11} & \bar{Q}_{12} & \bar{Q}_{16} \\ \bar{Q}_{12} & \bar{Q}_{22} & \bar{Q}_{26} \\ \bar{Q}_{16} & \bar{Q}_{26} & \bar{Q}_{66} \end{bmatrix} \begin{bmatrix} e_x \\ e_y \\ e_{xy} \end{bmatrix} \quad (4)$$

where the $\bar{Q}$ matrix is the transformed modulus matrix.

Note that strains can be given in terms of stress as

$$\begin{bmatrix} e_x \\ e_y \\ e_{xy} \end{bmatrix} = \begin{bmatrix} \bar{S}_{11} & \bar{S}_{12} & \bar{S}_{16} \\ \bar{S}_{12} & \bar{S}_{22} & \bar{S}_{26} \\ \bar{S}_{16} & \bar{S}_{26} & \bar{S}_{66} \end{bmatrix} \begin{bmatrix} s_x \\ s_y \\ s_{xy} \end{bmatrix} \quad (5)$$

where $[\bar{S}] = [\bar{Q}]^{-1}$.

We can see that *Eq 5* may be used to relate these transformed reduced compliance coefficients $\bar{S}_{ij}$ to the familiar engineering constants, viz.,

$$e_x = \bar{S}_{11}s_x + \bar{S}_{12}s_y + \bar{S}_{16}s_{xy}. \quad (6)$$

In the uniaxial tensile test in the x-direction,

$$s_y = s_{xy} = 0 \quad (7)$$

thus,

$$e_x = \bar{S}_{11}s_x \quad (8)$$

but,

$$e_x = s_x/E_x \quad (9)$$

therefore,

$$E_x = \bar{S}_{11}^{-1}. \quad (10)$$

Other such relations can be found for different engineering constants.

By definition, the stress resultants for the shell theory being used are:

$$\begin{aligned} N_x &= \int_{-h/2}^{h/2} s_x[1 + (z/a)]dz, \\ M_x &= \int_{-h/2}^{h/2} s_x[1 + (z/a)]zdz \\ N_y &= \int_{-h/2}^{h/2} s_y dz, \\ M_y &= \int_{-h/2}^{h/2} s_y zdz \\ N_{xy} &= \int_{-h/2}^{h/2} s_{xy}[1 + (z/a)]dz, \\ M_{xy} &= \int_{-h/2}^{h/2} s_{xy}[1 + (z/a)]zdz \\ N_{yx} &= \int_{-h/2}^{h/2} s_{yx} dz, \\ M_{yx} &= \int_{-h/2}^{h/2} s_{yx} zdz \end{aligned} \quad (11)$$

where a is the radius to the mid-surface, and h is the shell thickness.

As given in *Eq 11*, these quantities result from integration over the full thickness of the shell wall. For homogeneous shells, this presents no problem since when *Eq 4* is substituted into *Eq 11*, the $\bar{Q}$ matrix is not a function of the z-coordinate. In the case of a heterogeneous laminated structure with either varying winding angles, or varying materials, or both, the procedure is modified. First, the integration is carried out over the thickness of each layer separately, then the results are summed over the whole thickness. i.e.,

$$N_x = \sum_{k=1}^{n} \int s_x[1 + (z/a)]dz, \quad \text{and so on.} \quad (12)$$

where k refers to a particular layer, n refers to the total number of layers, and the limits of integration are from the bottom to the top of layer k.

The strain-displacement relations are those developed by Flügge (5) in terms of mid-surface displacements. The stress resultants may then be expressed in terms of the material properties, the lamination structure (i.e., position, thickness, and orientation of the various layers), mid-surface displacements, and shell geometry. The equilibrium of a differential element may be expressed in terms of the stress resultants, and the external loads. Finally then, the equilibrium equations are given in terms of material properties, lamination structure, mid-surface displacements u, v, w, shell geometry, and external loads.

Since the displacements are in terms of differentials of the space coordinates, we have a system of three differential equations of fourth order. Cheng and Ho's displacement field is:

$$\begin{aligned} u &= U \sin[(\lambda x/a) + ny] \\ v &= V \sin[(\lambda x/a) + ny] \\ w &= W \cos[(\lambda x/a) + ny] \end{aligned} \quad (13)$$

where y is the circumferential coordinate (denoted by θ in Cheng and Ho), $\lambda = m\pi a/L$, L is the shell length, m is an integral number of axial half-waves, n is an integral number of hoop waves, and U, V, W are unknown constants. Upon substituting the displacements into the equilibrium equations, there remains a set of three homogeneous algebraic equations in U, V, W. These equations are:

$$\begin{bmatrix} (F_{11} - \lambda^2 q_2 - 2n\lambda q_3 - n^2 q_1) & (F_{12}) & (F_{13} + \lambda q_1) \\ (F_{12}) & (F_{22} - \lambda^2 q_2 - 2n\lambda q_3 - n^2 q_1) & (F_{23} - 2\lambda q_3 - n q_1) \\ (F_{13} + \lambda q_1) & (F_{23} - 2\lambda q_3 - n q_1) & (F_{33} - \lambda^2 q_2 - 2n\lambda q_3 - n^2 q_1) \end{bmatrix} \begin{bmatrix} U \\ V \\ W \end{bmatrix} = 0 \quad (14)$$

where F is a function of material properties, lamination structure, shell geometry, λ, and n; q_1 is the external radial pressure loading factor; q_2 is the axial loading factor; and q_3 is the torsional loading factor. Non-trivial solutions exist if and only if the determinant of the coefficient matrix equals zero.

Thus far we have followed the analysis of Cheng and Ho. Now we particularize it to our specific problem. Of the three external loadings considered by these authors, we drop the torsion factor q_3 in (14). Since we are concerned with hydrostatic external pressure, the loading factors q_1 and q_2 are uniquely related. Viz., by definition

$$q_1 = pa/A_{22}. \tag{15}$$

and

$$q_2 = P/A_{22}. \tag{16}$$

Also,

$$s_y = pa/h, \tag{17}$$

$$s_x = (2\pi aP)/(2\pi ah) = P/h. \tag{18}$$

But

$$s_y = 2s_x. \tag{19}$$

Therefore,

$$P = pa/2 \tag{20}$$

Substituting *Eq 20* in *Eq 16*,

$$q_2 = pa/2A_{22} \tag{21}$$

Thus, comparing *Eq 15* and *Eq 21*,

$$q_1 = 2q_2. \tag{22}$$

In the above, p is the external lateral pressure, P is the axial load, and

$$A_{22} = \sum_{k=1}^{n} \int \bar{Q}_{22} dz,$$

where the integration is done from the lower to the upper surface of the kth layer.

If we now expand the determinant, the characteristic equation is in terms of F, n, λ, and q_1. The object then is to determine the root q_1 which is the least positive real root that satisfies the characteristic equation. The least value of q_1 is chosen as the critical loading factor, and the critical pressure is calculated as

$$p_{cr} = q_{1(\min.)}A_{22}/a \tag{23}$$

Since manual computations are not practical, a program was coded in subset FORTRAN 77 for use on personal computers. The calculated critical external pressures for tubes 1 to 4, are respectively, 317, 305, 134, and 173 kPa.

Some remarks on the analysis and our specific implementation are in order. The simplifications due to the effective assumption of the Love-Kirchoff hypotheses and small deformations have already been mentioned. Furthermore, the assumed displacement field will not completely satisfy any of the traditional shell boundary conditions (B.C.). Thus, the solution having been determined from the characteristic equation without imposing boundary conditions can only be approximate unless the shell is infinitely long.

As mentioned, no boundary conditions were imposed when solving for critical pressure. In order to get an idea of the effect of this neglect, results from the computer solution were compared with curves by Ho and Cheng (6). The latter paper shows that the effect depends on lamination structure, boundary conditions and length-to-radius ratio. The effect is most serious for generally anisotropic layups, for hinged boundary conditions, and small (L/a) ratios. For these cases, they report the ratio of critical pressure without B.C. to that with B.C. is about 1.7 at (L/a) = 1, about 1.3 at (L/a) = 10, and 1 at (L/a) = 100. Results from the present computer program were compared to results for B.C. SS1 plotted in Ref 6. This comparison gives ratios of our computed results without B.C. to plotted values with B.C. of about 1.7 at (L/a) = 1, to about 1.2 at (L/a) = 30. Thus, the present program implementation gives solutions comparable to those in ref. 6. For isotropic and orthotropic cases, the agreement is within about 5 percent. Similar results were obtained in comparisons made with (7) for orthotropic shells, and with (8) for isotropic shells.

RTP Draft Proposal No. 5

This document (9) is *not* a standard but has been submitted for consideration to a Subcommittee of the ASME on fiber-reinforced plastic vessels. We consider design by rules as given in subpart 3A, article −310.

The procedure is relatively simple and does not require long calculations. The equation for critical pressure, in its original context, refers to isotropic shells. The draft proposal merely chooses the lesser of the axial and hoop moduli in place of the isotropic modulus, and maintains the assumption of a Poisson's ratio of 0.3. For our structures the axial modulus is the lower. The critical pressures calculated for tubes 1 to 4, respectively, are 196, 201, 68.6, and 78.2 kPa.

French Standard (10)

This standard was published in December 1976 by the Commission Chaudronnerie Génie Chimique du Syndicat Général de l'Industrie du Plastique Armé. It deals with thermoset resins reinforced with glass, including containers made by filament winding. The problem of cylinders buckling under external pressure or vacuum is addressed in article 3.11.

We have no experimental data for the flexural modulus of the tube walls required in this standard. However, previous testing of similar materials (11) indicates that a value of 80 per-

cent of the tensile modulus is not unreasonable. We used this value in the calculations. (We point out that, unlike the American proposal, a safety factor of 3 is recommended for buckling in article 3.1.2. c.) The critical pressures for tubes 1 to 4, respectively, are 183, 206, 71.2 and 90.0 kPa.

DISCUSSION

Data Interpretation

When strain gages are used in buckling tests it is usual to take the load value where strain reversal occurs as the critical load. This is done because buckling causes a large change in the shape of the shell, which can cause more-or-less sudden reversal in the strain. There are at least six strain gages bonded to each tube (9 in the case of the first test run on tube 3). Since the shell may become unstable at one location before others, we must take the lowest pressure, where evidence of instability appears to be the buckling pressure. Since we do not have full-field monitoring of the tubes, there is a possibility that instability may occur at an uninstrumented location at a pressure lower than that identified as the buckling pressure. The data shows the buckling pressures for tubes 1 to 4, respectively to be 148, 460, 86 and 58 kPa.

A perfectly cylindrical tube would be expected to give compressive strains in both axial and circumferential directions during pressurization. Looking at the results from tube 2 in *Fig. 15*, we see this is the case for the tube showing the least imperfection amplitudes combined with the most cylindrical form. In the case of the other three tubes, which had a clearly elliptical form, the signs of the strains could not consistently be explained a posteriori.

As mentioned previously, three runs were made on tube 3 before it collapsed on the third run. We should point out that despite the nonlinear strain-pressure behavior, the strains on the second run returned almost to zero (see inset in *Fig. 11*), and after a longer time at zero pressure, the values would no doubt have been even closer to zero. Thus, the elastic regime seems not to have been exceeded. Furthermore, the final collapse pressure is 2.8 times higher than the buckling pressure established above, giving a margin of safety to this tube. It should be cautioned, however, that the final collapse pressure is slightly lower than the maximum pressure attained in the second run, and damage, invisible to the unaided eye, may have been incurred during the penultimate pressurization.

Comparison of Results

The comparison of the predicted an.' experimental buckling pressures are tabulated in *Table 5*.

The experimentally determined buckling pressure for tube 2 is 1.51 to 2.29 times greater than the prediction. Recall that this tube did not have an elliptical shape. Furthermore, it has relatively small imperfections compared to tubes 3 and 4 (see *Table 3*). Since the critical pressure also corresponds to an elliptical shape according to the analysis, tube 2 may be said to be the least imperfect of the structures tested. Thus, that the ratio of experimental to calculated pressure is highest might have been expected. However, that the ratio is greater than 1.0 is unexpected. Re-examining the data shows no great difference between tubes 1 and 2, except in the shape and winding angle. The large ratios of pressures must therefore be attributed to the small number of locations gaged. In other words, it is thought that, had many more gages been used, a much lower instability pressure might have been detected. Note that the present method of calculation gives the closest prediction. Pressure ratios larger than 1.0 for tube 3 also are given by the Proposal and the Standard, but not by the present method.

Tubes 3 and 4, with winding angles of 54° and 63° respectively, have unexpected buckling pressures with respect to each other; i.e., tube 4 should exhibit a higher buckling pressure than tube 3, but the reverse is observed. The major contributing factor is considered to be the larger relative circumferential imperfections of tube 4 as shown in *Table 3*.

From *Table 5* we see that the RTP Draft Proposal No. 5 and the French Standard are more conservative than the present method, and the former two give similar results for the structures tested. If we incorporate the recommended safety factors of 5 for the Proposal and 3 for the Standard, and a reduction factor of 5 for the present method (based on a factor of 1.7 due to neglect of boundary conditions, and a factor of 3 based on the lowest ratio of 0.34 shown in *Table 5*), *Table 6* results. The RTP Draft Proposal No. 5 gives the most conservative design pressures. The French Standard and the present method give very similar results, and both provide some safety margin.

Table 5. Experimental Versus Calculated Pressures (kPa).

	Experimental Result	Present Method	RTP Draft Proposal	French Standard
Tube 1	148	317 (0.47)*	196 (0.76)	183 (0.81)
Tube 2	460	305 (1.51)	201 (2.29)	206 (2.23)
Tube 3	86	134 (0.64)	68.6 (1.25)	71.2 (1.21)
Tube 4	58	173 (0.34)	78.2 (0.74)	90.0 (0.64)

* Numbers in parentheses are the ratios (Experiment/Calculation).

Table 6. Experimental Versus Design Pressures (kPa).

	Experimental Results	Present Method	RTP Draft Proposal	French Standard
Tube 1	148	63 (2.3)*	39 (3.8)	61 (2.4)
Tube 2	460	61 (7.5)	40 (11.5)	69 (6.7)
Tube 3	86	27 (3.2)	14 (6.1)	24 (3.6)
Tube 4	58	35 (1.7)	16 (3.6)	30 (1.9)

* Numbers in parentheses are the ratios (Experiment/Design).

CONCLUSION

The principal objective of the work described here was to compare experimental buckling pressures and design pressures as calculated using three selected procedures. A secondary objective was to determine the initial shape imperfections of tubes produced with commercial filament winding techniques using typical glass fiber and resin materials.

All three procedures give design pressures that are lower than the experimental buckling pressures. The ASME RTP Draft Proposal No. 5 gives the most conservative design pressure with values ranging from 3.6 to 11.5 times less than the observed buckling pressures. The present method, which is an implementation of the analysis by Cheng and Ho (4), and the French Standard give similar results, the comparable factors ranging from 1.7 to 7.5. (The reader is cautioned that the factor of 5 used to calculate the design pressure from the critical pressure using the present method does *not* mean that a structure can withstand a buckling pressure of 5 times greater than the design pressure, as the present data slows!)

The principal areas of damage occur at the lines of maximum curvature of the elliptically shaped tubes 3 and 4. Tubes 1 and 2, which did not have such pronounced imperfections, show more widespread damage. Though imperfections are larger than those reported for steel shells, it is encouraging to note that acceptable design pressures can still be arrived at, and that the ultimate collapse pressure is higher than the buckling pressure in each case.

It must be remembered that only four tubes were tested in this study, and each tube was different in some respect from the others. Clearly, the results must be used with prudence in the absence of a larger data base. More extensive testing might uncover typical shapes and imperfection amplitudes for the filament winding process. This statistical information could then be used to impose more appropriate knock-down factors in designing.

REFERENCES

1. N. J. Hoff, *Israel J. Technol.*, **4**, 1 (1966).
2. D. Bushnell, *AIAA J.*, **19**, 1183 (1981).
3. J. Singer, *Solid Mech. Arch.*, **7**, 213 (1982).
4. S. Cheng and B. P. C. Ho, *AIAA J.*, **1**, 892 (1963).
5. W. Flügge, "Stresses in Shells," Springer-Verlag, Berlin (1960).
6. B. P. C. Ho and S. Cheng, *AIAA J.*, **1**, 1603 (1963).
7. M. M. Lei and S. Cheng, *J. Appl. Mech., ASME Trans.*, **91**, 791 (1969).
8. N. Yamaki and K. Otomo, *Exp. Mech. (SESA)*, **13**, 299 (1973).
9. "RTP Draft Proposal No. 5," submitted to Subcommittee X of ASME, (1984).
10. "Code de construction des appareils chaudronnes en plastique armé," AFNOR, Paris (1976).
11. S. V. Hoa, T. S. Sankar, and P. Ouellette, PRAI Report No. 1 (1983).

DISCUSSION

C. L. Beatty: What is the origin of the variation of diameter for your pipes? The waviness?

S. V. Hoa: There are two parameters involved: (1) the very thin wall, only two filament layers and, (2) not well refined manufacturing process.

C. L. Beatty: Do you cure the tubes on the mandrel?

S. V. Hoa: Yes.

Impact Fracture of Glass-Flake Reinforced Polypropylene

T. VU-KHANH *and* B. FISA

Industrial Material Research Institute
National Research Council of Canada
Boucherville, Quebec, Canada J4B 6Y4

The impact resistance of glass-flake reinforced polypropylene was analyzed over a wide range of loading rates and glass-flake concentrations. It was found that the dynamic fracture toughness, K_d, of the composite is strongly rate-dependent. When impact velocity is increased, K_d first decreases, attains a minimum value, and then increases with impact speed. The increase in K_d with loading rate is attributed to the blunting effect at the crack tip, induced by adiabatic heating. The addition of glass flakes substantially increases the dynamic fracture toughness of polypropylene. The increase in K_d with glass-flake content is also more pronounced when the loading rate is increased. The blunting effect was found to increase with glass-flake concentration up to 30 percent by weight, leading to a stronger increase in K_d with glass-flake content from 0 to 30 percent. Above 30 percent, the blunting effect diminishes with concentration.

INTRODUCTION

The mechanism of reinforcement of plastics by fillers still remains unclear. Many factors affect the strength of composite materials. The addition of a filler can increase or decrease the mechanical resistance of a plastic depending on the nature of the polymer and the filler. What is often assumed is that if polymers become more rigid through the addition of fillers, they also become more brittle. According to the type of reinforcement provided, fillers are often divided into three classes: one dimensional (fibers), two dimensional (flakes or platelets), or three dimensional (spheres or beads).

Much work has been carried out to study the factors that affect the toughness of a fiber-reinforced composite. Several different interactions have been identified as contributors to fracture (1 to 7) such as: ductilities of the fiber and the matrix, friction between fibers and matrix after the debonding process has occurred, interfacial fracture energy, fiber retraction into the matrix after brittle fracture at the crack plane, etc. When three-dimensional fillers are incorporated, the fracture properties of composites vary quite unpredictably. Particulate fillers can reduce (8) or enhance (9) the toughness of plastics. Due to a concentration of stress at the matrix/filler interface, interfacial adhesion is an important factor which strongly affects the fracture toughness (10, 11). Good adhesion does not necessarily lead to an increase in fracture energy (12, 13). However, it can affect the mechanism of plastic deformation of the matrix. Consequently, the nature of the polymer itself also plays an important role in determining the effect of a given filler on mechanical properties.

Among the three classes of fillers, fibers and platelets are often considered to be more attractive than spheres since they result in greater stiffness and strength (14, 15). Although fibers have advantages over platelets in terms of efficiency of stress transfer, the latter are often chosen for reinforcement of planar structures because they can reinforce in two dimensions. However, at this time, there is very little in the literature that enables prediction of the effects of two-dimensional fillers on the impact resistance of plastics.

In the case of mica-reinforced polypropylene, a previous investigation (16) indicated that under hydrostatic stress near a crack tip, polypropylene breaks in a brittle manner. The addition of mica promotes a micromechanism of plastic deformation by shear yielding, resulting in a substantial increase in the crack growth resistance.

The purpose of this work was to investigate the effect of another two-dimensional filler, glass flakes, on the impact resistance of polypropylene. The impact fracture of glass-flake reinforced polypropylene was analyzed by a fracture mechanics approach. Since it has been shown that the loading rate strongly affects the

impact fracture toughness of polymers (17 to 19), impact tests were carried out over a wide range of impact velocities.

EXPERIMENTAL

Materials

A commercial grade of glass flakes (Hammer-milled Flakeglas 1/64"), supplied by Owens-Corning Fiberglas, was chosen for this study. The approximate flake size distribution curve, determined by sieving, is shown in *Fig. 1*. The average thickness of this grade as determined by microscopy, was found to be about 10 μm.

The polypropylene used in this study was an injection grade, Profax 6301, from Hercules. The resin was in powder form and had a melt index of 12 g/min (ASTM D 1238).

Sample Preparation

Polypropylene powder and glass flakes were dry blended in a Welex high intensity mixer, Model ESK-8C. Glass-flake concentration was varied over the range of 0 to 65 percent by weight. Sample plates of 3 by 30 by 90 mm were prepared by injection molding using an Engel reciprocating injection molding machine (Model Es 150-70).

Three-point-bend specimens having a sharp notch were used for the impact fracture tests. The specimens, measuring 3 by 13 by 90 mm, were cut out from the injection molded plates.

The ratio of initial crack length (a_o) to specimen width (D) was kept at a constant value, 0.4. A prenotch was first made by a saw cut and the exact final crack length was created by forcing a razor blade into the specimen using a special jig on a laboratory press. The ratio of distance between supports to specimen width was 4.

Test Methods

Instrumented impact tests were carried out on a Dynatup drop-weight device, Model 600. The striking tup of the impact machine was instrumented with strain gages and the load-time curve during impact was recorded by a rapid data acquisition system. The machine was also equipped with an optical cell, enabling measurement of the velocity of the striker just before impact. The load-deflection trace was then computed from the average impact velocity.

Impact tests were carried out over a wide range of velocities. Variation of the drop height permitted the variation of the impact velocity over the range of 0.5 to 5 m/s. Low impact speeds (below 0.5 m/s) were performed by affixing a hydraulic damping system to the tower, which enabled reduction of the velocity of the striker down to 0.01 m/s.

All specimens were conditioned and tested at 23°C and 50 percent relative humidity.

RESULTS AND DISCUSSIONS

Figure 2 shows the impact fracture toughness as a function of glass-flake content at different impact speeds: 2, 3.4, and 5.3 m/s. The dynamic fracture toughness, K_d, was calculated, using the impact load-deflection curve (20), as in the static case,

$$K_d = \frac{P_c S}{BD^{3/2}} Y \qquad (1)$$

where P_c is the load at fracture, B is the specimen thickness, D is the specimen width, and Y is a geometrical factor obtained from Ref. 21 for three-point-bending samples.

For all impact velocities, K_d increases with

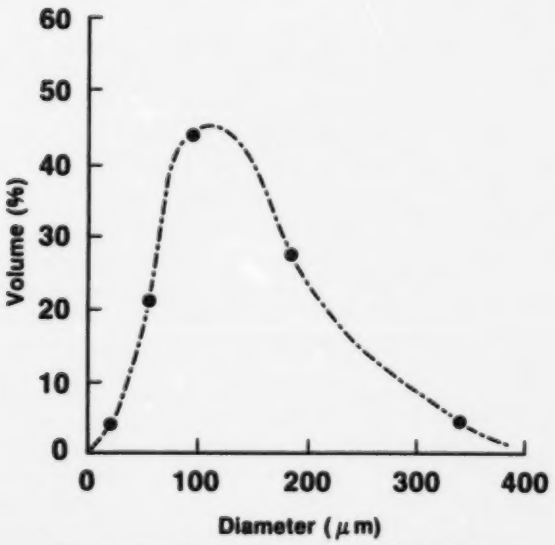

Fig. 1. Size distribution curve of glass flakes.

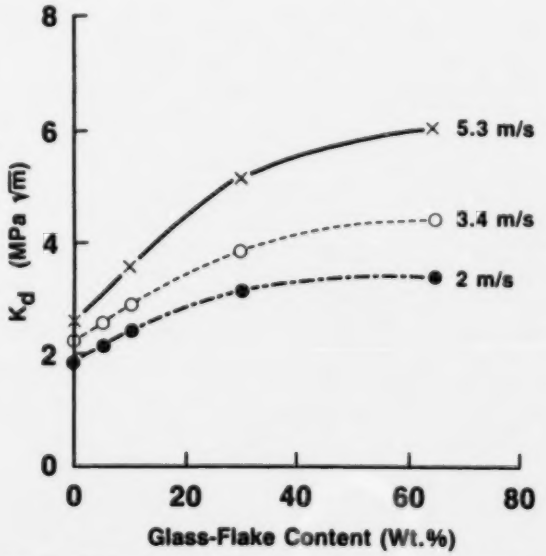

Fig. 2. Dynamic fracture toughness as a function of glass-flake concentration at different impact velocities.

increasing glass-flake concentration. It is also obvious that the effect of glass flakes on the dynamic fracture resistance of polypropylene depends on the impact velocity. This effect is more significant with higher impact speed. At 2 m/s, addition of glass flakes increases the dynamic fracture toughness only slightly. However, at 5.3 m/s, the impact resistance of the composite augments significantly with concentration. The effect of glass flakes was also found to be more pronounced in the range of 0 to 30 percent by weight. This is consistent with previous results on mica-reinforced polypropylene (16). It was found that the crack growth resistance at low loading rates also increased strongly with mica content up to 30 percent by weight. This is due to the fact that under hydrostatic stress around a crack tip, crazes are formed in pure polypropylene. Coalescence of voids in the crazed region leads to a very brittle fracture. When mica was added, plastic deformation by shear yielding occurred due to the debonding between mica flakes and polypropylene. The stretching effect of the matrix restricts void formation and void coalescence. Fracture becomes more ductile, resulting in an increase in the crack growth resistance. In the case of impact fracture, the microscopic drawing of the matrix is not apparent on the fracture surface of glass-flake reinforced polypropylene. However, the debonding between glass flakes and polypropylene was significant.

The observed increase in impact resistance with the incorporation of glass flakes is most probably not due to a single mechanism, as in the case of low loading rate. The fracture process may involve different glass flake/polypropylene interactions. The interactions are likely very complex and are not clear at the moment. However, whatever the mechanisms involved, the addition of two-dimensional fillers into polypropylene results in an interesting synergistic effect leading to an increase in both toughness and stiffness.

Figure 3 shows the variation of the effective modulus, E_{eff}, with glass-flake concentration. E_{eff} was determined by the initial compliance of the specimen, measured on the load-deflection curve at 2 m/s. The measured compliance probably includes errors due to friction, stress concentrations, etc., so that the effective modulus does not necessarily correspond to the true elastic modulus of the composite. It is, however, an indication of the effect of glass-flake concentration on the stiffness of the material.

In order to examine in more detail the dynamic fracture behavior of glass-flake reinforced polypropylene, impact tests were carried out over a wide range of loading rates. By ignoring the effect of the crack, the nominal macroscopic strain rate, $\dot{\epsilon}$, in the three-point-bend specimen is given by:

$$\dot{\epsilon} = 6\,\frac{VD}{S^2} \qquad (2)$$

where V is the impact speed and S is the distance between supports. *Figure 4* shows the dynamic fracture toughness, K_d, as a function of loading rate for different glass-flake contents. At very low impact speeds, the load-deflection diagrams feature a curvature before the point of fracture as shown in *Fig. 5*, suggesting that significant plastic deformation occurs at the crack tip. The fracture was also brittle at all glass-flake contents with an instantaneous drop in the load. In this case, the dynamic fracture toughness was calculated by using the load

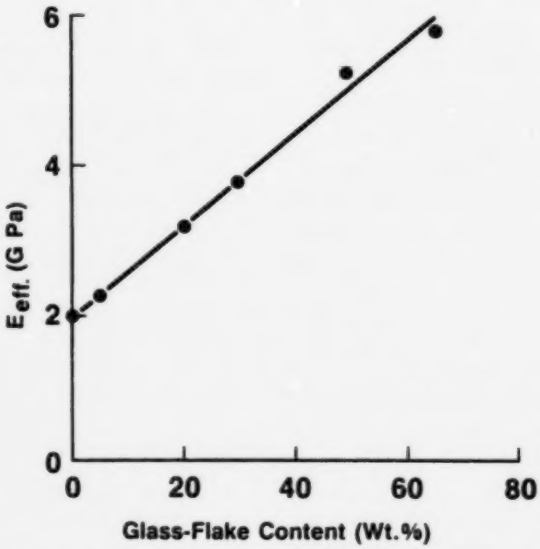

Fig. 3. Effective modulus as a function of glass-flake concentration (impact speed 2 m/s).

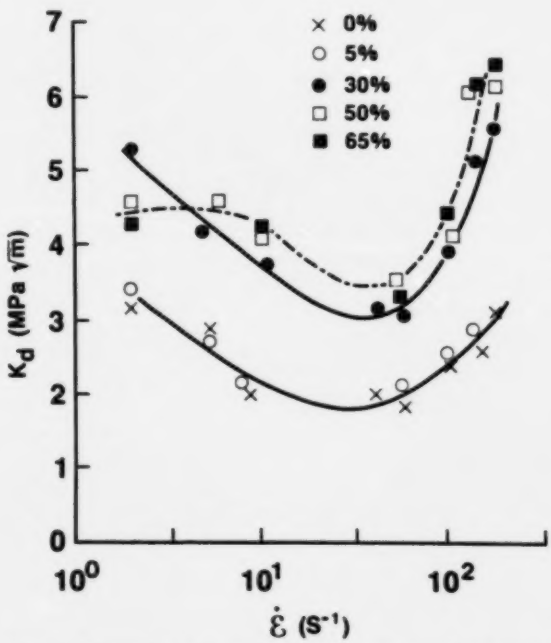

Fig. 4. Dynamic fracture toughness as a function of loading rate for different glass-flake concentrations.

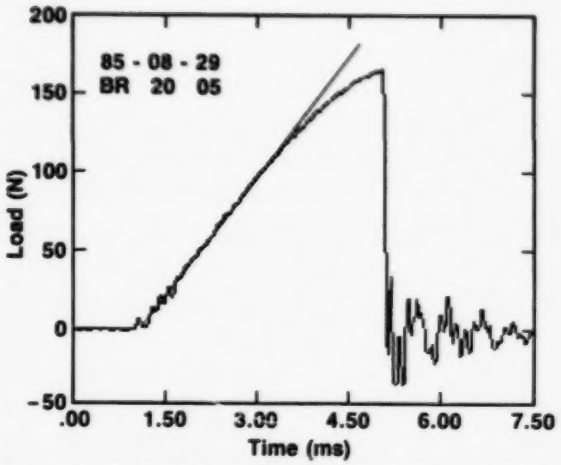

Fig. 5. Curvature of load-time trace at low impact speed.

at fracture and the corresponding effective crack length, the effective crack length being the physical crack size corrected for plastic deformation at the crack tip. This was determined by the secant method described previously (16). *Figure 4* shows that the impact resistance increases with glass-flake concentration for all loading rates. The latter also has a strong effect on the dynamic fracture toughness. When the strain rate is increased, the impact resistance first decreases, attains a minimum value at $\dot{\epsilon}$ about 20 s^{-1} and then increases.

In the range of strain rates studied here, the effect of adiabatic heating at the crack tip, arising from the plastic work, should be significant. Since the thermal conductivity of polymers is relatively low, the heat generated at the crack tip cannot be dissipated during the time to fracture, t_f, defined as the time spent from the first striker/specimen contact to the point at fracture. Consequently, the accumulation of heat leads to an increase in temperature at the crack tip. *Figure 6* shows the variation of the dynamic fracture toughness with the time to fracture, t_f. The temperature rise in a parallel strip embedded in an infinite medium, has been calculated by Carslaw and Jaeger (22) for a fixed rate of energy input. By assuming that the thickness of the plastic zone at the crack tip is very small, Williams and Hodgkinson (18) have calculated the temperature rise at the crack tip at time, t:

$$\Delta T = \frac{G_c}{\sqrt{\pi \rho c k}} \frac{1}{\sqrt{t}} \qquad (3)$$

where ρ is the density, c is the specific heat, and k is the thermal conductivity of the material. G_c is the fracture energy that is related to K_d by:

$$G_c = \frac{K_d^2}{E}(1 - \nu^2) \qquad (4)$$

where E is Young's modulus and ν is the Poisson ratio.

Figure 7 shows the estimate of temperature rise at the crack tip, ΔT, as a function of $1/t_f$ for 0 and 30 percent glass-flake content. ΔT is probably overestimated since a perfectly sharp crack does not exist, hence, the energy must be dissipated in a more diffuse zone around the crack tip. It can be seen that the temperature variation at the crack tip can be quite large for

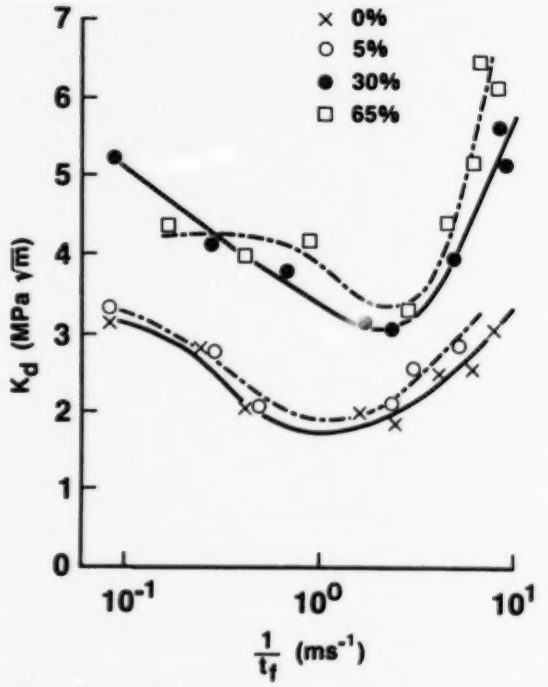

Fig. 6. Dynamic fracture toughness as a function of $1/t_f$ for different glass-flake concentrations.

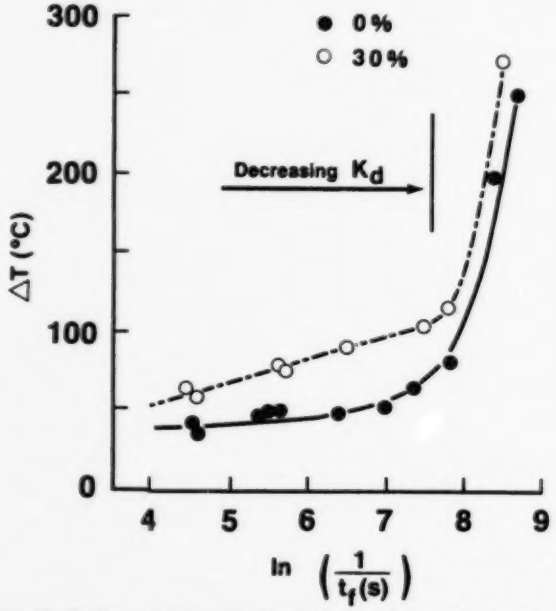

Fig. 7. Estimate of temperature rise at the crack tip at 0 and 30 percent glass-flake content.

the studied range of loading rates. It has also been suggested (18) that high temperature can lead to a blunting mechanism of the crack tip. This explains the region of high positive variation of the dynamic fracture toughness with $1/t_f$ as shown in *Fig. 6* and will be discussed later in more detail.

In the region of decreasing K_d with $1/t_f$, it appears that the time-temperature dependence may be associated with the viscoelastic nature of the polymer. Since the time-temperature superposition for the relaxation processes may be described by the Arrhenius equation, the time to fracture can be related to the temperature at the crack tip by:

$$\frac{1}{t_f} = \frac{1}{t_o} \exp\left(\frac{-H}{RT}\right) \tag{5}$$

where H is the activation energy, R is the gas constant, t_f is the time to fracture, T is the temperature at the crack tip, and t_o is a constant. *Figures 8* and *9* show the plots of $1/T$ versus $\ln(1/t_f)$ for 0 and 30 percent glass flake respectively. These curves exhibit a linear relationship between $1/T$ and $\ln(1/t_f)$ according to *Eq 5*. The slopes of these plots yield the values of activation energy of 113 and 80 kJ/mole for 0 and 30 percent glass-flake content respectively. These values are of the same order of magnitude as the activation energy of 117 kJ/mole measured for the glass transition in polypropylene (23). Taking the glass-to-rubber transition of polypropylene as 0°C at a frequency of 1 Hz (24) and using the measured activation energy of 113 kJ/mole, the relaxation time of around 2 m/s at 25°C can be calculated. This is within the studied range of time to fracture and suggests that the glass relaxation may govern the adiabatic heating effect.

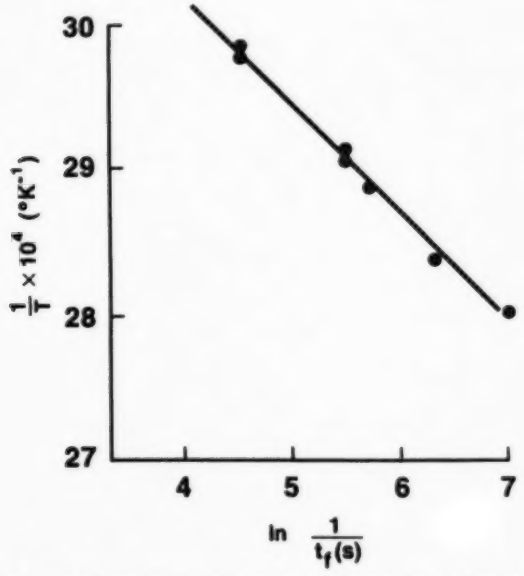

Fig. 8. (1/T) as a function of $\ln(1/t_f)$ for pure polypropylene.

It is also worth noting that for $\dot{\varepsilon} < 20\ s^{-1}$, the curvature on the load-deflection diagram becomes more pronounced as the loading rate is reduced. At this time, it is not clear whether some stable crack growth had occurred before the unstable fracture. The conditions for stable and unstable crack propagations have been discussed thoroughly in a previous paper (16). If there is no stable crack growth before instability, then the curvature on the load-deflection trace should be related to the plastic deformation at the crack tip. The plastic zone can be qualitatively represented by the difference between the effective crack length calculated at the instability point and the physical crack size $(a_{eff} - a_o)$. *Figure 10* shows $(a_{eff} - a_o)$ as

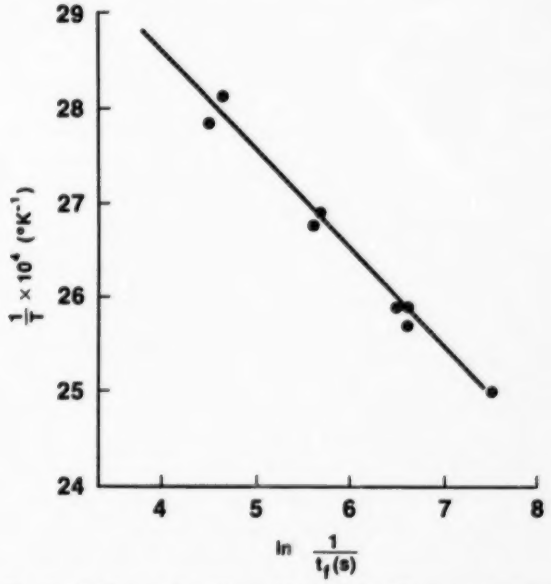

Fig. 9. (1/T) as a function of $\ln(1/t_f)$ for 30 percent glass-flake content.

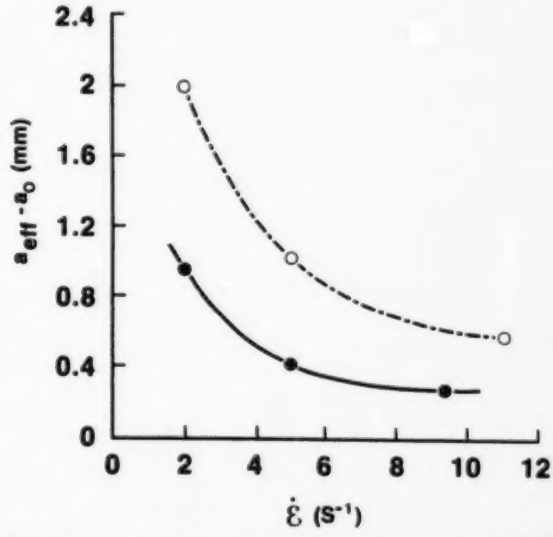

Fig. 10. $(a_{eff} - a_o)$ as a function of strain rate (○: 30%, ●: 0%).

a function of loading rate. When $\dot{\epsilon}$ increases, $(a_{eff} - a_o)$ decreases substantially, suggesting that the yield stress must increase with loading rate. This is true for an isothermal condition, but inconsistent with the calculated rise in temperature due to adiabatic heating as discussed above. This point requires further study. *Figure 6* shows that the lowest value of the impact fracture toughness of polypropylene, $K_{d,min}$, increases with the incorporation of glass flakes. The variation of $K_{d,min}$ with glass-flake content is shown in *Fig. 11*. $K_{d,min}$ is significantly improved up to 30 percent by weight. Above 30 percent, it remains relatively constant.

For very short times to fracture, Williams and Hodgkinson (18) suggested that high temperature at the crack tip causes the yield stress to decrease which, in turn, results in crack tip blunting. The fracture was postulated to occur when a critical stress, σ_c, is reached at a certain distance, r_c, ahead of the crack tip. The apparent fracture toughness of the blunted crack, G_b, was then evaluated as:

$$\frac{G_b}{G_c} \simeq \frac{1}{2} + \frac{R}{8r_c} \tag{6}$$

where G_c is the fracture toughness of a sharp crack and, R is the radius of the crack tip. By assuming a linear relationship between yield stress and temperature, a model relating the dynamic fracture toughness to the fracture time was proposed (18):

$$\frac{G_b}{G_c} = \frac{1}{2} + \left(\frac{N}{1 - \sqrt{t_1/t_f}}\right)^2 \tag{7}$$

where t_1 is the fracture time in which the temperature at the crack tip attains the softening temperature of the material. N is a measure of ductility of the material and was defined as:

$$N = \frac{\sigma_c}{\sigma_y}\sqrt{\epsilon_y/2} \tag{8}$$

where σ_y is the yield stress and ϵ_y is the yield strain.

The plots of $((G_b/G_c) - 1/2)^{-1/2}$ against $t_f^{-1/2}$ are shown in *Figs. 12* to *14* for 0, 30, and 65 percent glass-flake content respectively. The

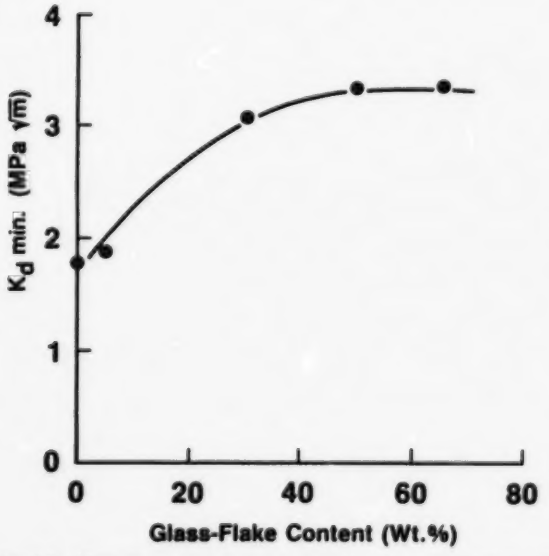

Fig. 11. Minimum impact resistance as a function of glass-flake concentration.

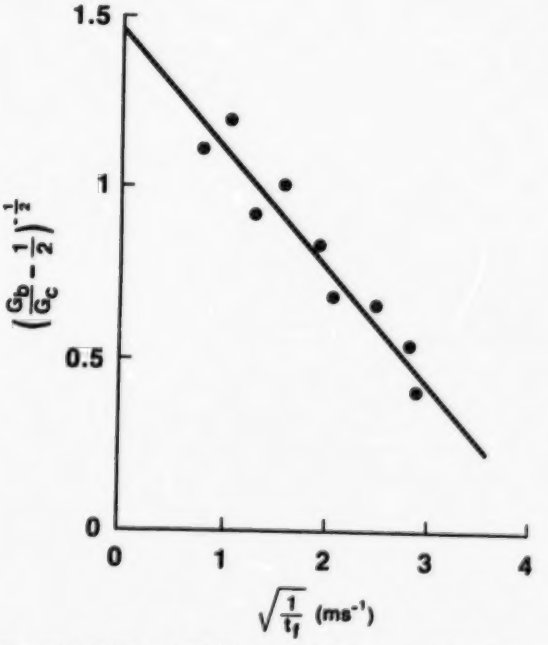

Fig. 12. $[G_b/G_c - 1/2]^{-1/2}$ as a function of $1/\sqrt{t_f}$ for pure polypropylene.

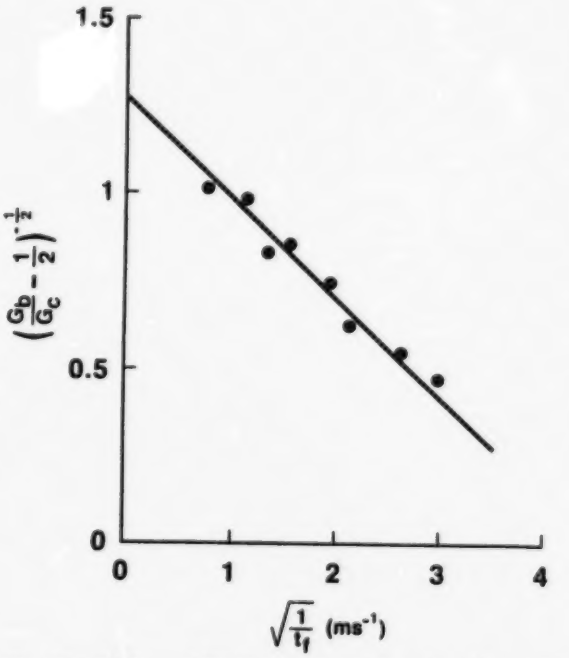

Fig. 13. $[G_b/G_c - 1/2]^{-1/2}$ as a function of $1/\sqrt{t_f}$ for 30 percent glass-flake content.

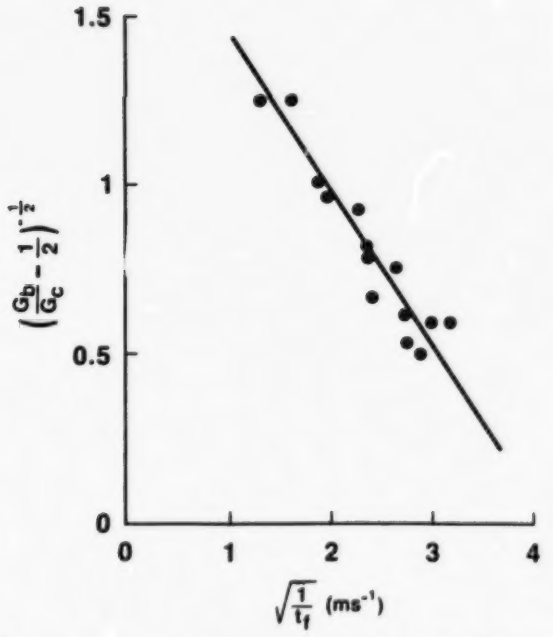

Fig. 14. $[G_b/G_c - 1/2]^{-1/2}$ as a function of $1/\sqrt{t_f}$ for 65 percent glass-flake content.

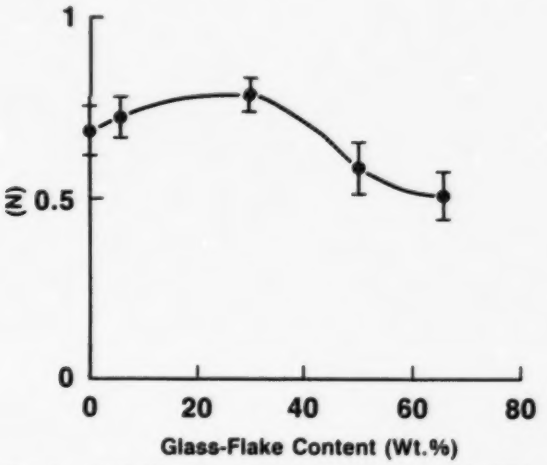

Fig. 15. Variation of N with glass-flake concentration.

model by Williams and Hodgkinson (18) appears to be a good description of the variation of the dynamic fracture toughness with loading rate. From these curves, the values of N can be deduced. *Figure 15* shows the variation of N versus glass-flake concentration. The bars represent the 90 percent confidence limits of N. N increases from 0 to 30 percent whereas above 30 percent it declines. This suggests that the blunting effect under adiabatic heating in polypropylene increases with the incorporation of glass flakes up to 30 percent by weight. Since N represents the ductility of the material in dynamic fracture, the fracture behavior of polypropylene becomes more ductile with the addition of up to 30 percent glass flakes. This explains the significant increase in K_d with glass-flake content as shown in *Fig. 2*. The earlier investigation of mica-reinforced polypropylene (16) showed that the debonding at the interface between mica flakes and polypropylene leads to a micro-mechanism of plastic deformation by shear yielding, resulting in an increase in the microscopic ductility of the matrix. The maximum crack growth resistance was also found to significantly increase up to 30 percent mica by weight. Above 30 percent, the effect of matrix stretching still occurs, but due to the reduction of matrix material, the ability of the composite to resist crack propagation is reduced. The variation of N with glass-flake concentration in this study is thus probably due to the same mechanism, although the microscopic stretching of the matrix is not apparent on the impact fracture surface of the composite in this study. From 0 to 30 percent glass-flake content, the increase of N suggests that the ductility of the composite increases on a microscopic scale. Above 30 percent, the microscopic ductility of the composite decreases, resulting in a decline in N. This is probably due to a significant reduction of matrix material.

SUMMARY AND CONCLUSION

Over the range of impact speeds studied, the dynamic fracture toughness of polypropylene is substantially increased with the addition of glass flakes. The impact resistance increases significantly with glass-flake content up to 30 percent by weight. Above 30 percent, it remains relatively constant. The effect of glass flakes also depends strongly on the impact velocity. The positive variation of the dynamic fracture toughness with glass-flake concentration was found to be larger for higher impact speeds.

Regardless of glass-flake concentration, when the loading rate is varied, the impact resistance also varies strongly. First, it decreases with impact speed, attains a minimum value, and then it increases with increasing loading rate. The rate-dependence of the dynamic fracture toughness was found to be governed by the glass-to-rubber relaxation of polypropylene. Due to the viscoelastic nature of the yielding process and low thermal conductivity of the material, the temperature can rise significantly at the crack tip, leading to a strong variation of the fracture toughness with impact velocity.

At high impact speeds, the increase in the fracture toughness with loading rate seems to be due to a blunting effect of the crack tip, which is induced by a local temperature increase. The model proposed by Williams and Hodgkinson satisfactorily describes crack blunting in impact fracture of glass-flake reinforced polypropylene. The blunting effect was found to be increased with glass-flake concentration up to 30 percent by weight. Above 30 percent, it is reduced. This is probably due to the debonding at the interface between glass

flakes and polypropylene. The debonding would lead to an increase in the microscopic ductility of the material at the crack tip by promoting plastic deformation by shear yielding. Above 30 percent, due to the substantial reduction of the matrix material, the ductility of the composite is reduced. The variation of the microductility of polypropylene in the presence of different glass-flake concentrations may be an explanation of the increase of the dynamic fracture toughness of the composite with the addition of glass flakes.

ACKNOWLEDGMENT

The authors would like to express their appreciation to Mr. Dufour for his great care in performing the experimental work.

NOMENCLATURE

a_o = Initial crack length.
a_{eff} = Effective crack length.
B = Specimen thickness.
C = Specimen compliance.
c = Specific heat.
D = Specimen width.
E = Elastic modulus.
E_{eff} = Effective modulus.
G_c = Fracture energy of a sharp crack.
G_b = Fracture energy of a blunted crack.
H = Activation energy.
K_d = Dynamic fracture toughness.
$K_{d.min}$ = Minimum dynamic fracture toughness.
k = Thermal conductivity.
N = Ductility of the material.
P_c = Load at fracture.
R = Gas constant.
r_c = Critical distance ahead of the crack tip.
S = Specimen span in impact.
t = Time.
t_f = Time to fracture.
t_1 = Critical time to fracture.
T = Temperature.
V = Impact velocity.
Y = Geometric correction factor.
$\dot{\epsilon}$ = Nominal macroscopic strain rate.
ϵ_y = Yield strain.
σ_c = Critical stress ahead of the crack tip.
σ_y = Yield stress.
ν = Poisson ratio.

REFERENCES

1. J. L. Helfet and B. Harris, *J. Mater. Sci.*, **7**, 494 (1972).
2. G. A. Cooper, *J. Mater. Sci.*, **5**, 645 (1970).
3. P. W. Beaumont and B. Harris, *J. Mater. Sci.*, **7**, 1265 (1972).
4. M. R. Pigott, *J. Mater. Sci.*, **9**, 494 (1974).
5. T. U. Marston, A. G. Atkins, and D. K. Felbeck, *J. Mater. Sci.*, **9**, 447 (1974).
6. B. Harris, J. Morley, and D. C. Philips, *J. Mater. Sci.*, **10**, 2050 (1975).
7. M. Miwa, T. Ohsawa, and N. Tsuji, *J. Appl. Polym. Sci.*, **23**, 1679 (1979).
8. K. Friedrich and U. A. Karsch, *J. Mater. Sci.*, **16**, 2167 (1981).
9. M. Bramuzzo, A. Savadori, and D. Bacci, *Polym. Compos.*, **6**, 1 (1985).
10. J. Leidner and R. T. Woodhams, *J. Appl. Polym. Sci.*, **18**, 1639 (1974).
11. J. A. Radosta, *SPE Tech. Papers*, **22**, 465 (1976).
12. T. Vu-Khanh and B. Fisa, *Polym. Compos.*, in press.
13. G. F. Abate and D. Heikens, *Polym. Commun.*, **24**, 342 (1983).
14. G. C. Richardson and J. A. Somer, *Polym. Eng. Sci.*, **16**, 252 (1976).
15. C. Busigin, G. M. Martinez, R. T. Woodhams, and R. Lahtinen, *Polym. Eng. Sci.*, **23**, 766 (1983).
16. T. Vu-Khanh, B. Sanschagrin, and B. Fisa, *Polym. Compos.*, **6**, 249 (1985).
17. M. W. Birch and J. G. Williams, *Int. J. Fract.*, **14**, 69 (1978).
18. J. G. Williams and J. M. Hodgkinson, *Proc. R. Soc. Lond.*, **A375**, 231 (1981).
19. J. M. Hodgkinson, N. S. Vlachos, J. H. Whitelaw, and J. G. Williams, *Proc. R. Soc. Lond.*, **A379**, 133 (1982).
20. T. Vu-Khanh and J. M. Charrier, "Proc. Symp. Quantitative Characterization of Plastics and Rubber," J. Vlachopoulos, ed, p. 114, McMaster Univ., Ontario, Canada (1984).
21. E-399 Standard Test Method for Plane Strain Fracture Toughness of Metallic Material, Annual Book of ASTM Standards (1983).
22. H. S. Carslaw and J. G. Jaeger, "Conduction of Heat in Solids," 2nd ed., Oxford University Press, Oxford (1959).
23. H. Kramer and K. E. Helf, *Kolloid Z.*, **180**, 114 (1962).
24. M. M. Dumoulin and L. A. Utracki, "Proc. Symp. Quantitative Characterization of Plastics and Rubber," J. Vlachopoulos, ed, p. 68, McMaster Univ., Ontario, Canada (1984).

DISCUSSION

J. T. Lindt: You calculated the temperatures at crack tip well above the melting point of polypropylene.

T. Vu-Khanh: Those temperatures are overestimated.

J. T. Lindt: But if you suspect the temperatures to be so high, it would be simple to incorporate the latent heat of fusion in your energy balance. Furthermore, if you have melting and crystallization at the crack, the morphology of polypropylene should be very much different at the broken surface than anywhere else. Did you check the morphology?

T. Vu-Khanh: We are doing this right now.

Anonym: The impact test; was it done only at room temperature? Did you test your samples at low temperatures like −40°C?

T. Vu-Khanh: We will do it in the near future.

Anonym: Did you at any point compare the system with glass fiber-copolymer composite?

T. Vu-Khanh: Not yet.

Mechanical Performance of Various Nylon 6 Composites Formed by *In-Situ* Polymerization of Caprolactam*

LLOYD A. GOETTLER *and* WILLARD J. NEFF

Monsanto Company
Akron, Ohio 44313
and
St. Louis, Missouri 63167

This paper describes the fabrication and mechanical characterization of composites made by incorporating various types of glass as bead or fiber into an activated caprolactam melt, which is then caused to anionically polymerize to a nylon 6 resin. Three types of composites are discussed and compared under separate headings: glass bead filled, sheet reinforced with a random fiberglass mat, and sheet reinforced with a unidirectional fiberglass mat that is studied under transverse loading to emphasize the role of the nylon 6 matrix resin. High molecular weight, better wet-out and adhesion to the reinforcement, and cold drawing of the polycaprolactam resin lead to homogeneous cavitation that increases composite toughness in comparison to epoxy or other nylon matrices of equivalent stiffness.

INTRODUCTION

The particular advantages of each of the nylon composite forms mentioned above will be developed and summarized. Although these studies relate to the growing interest in reinforced reaction injection molding, the laboratory process utilized in sample preparation is more akin to casting. Nevertheless, the properties of the resulting composites should be representative of materials made by either fabrication technique.

The single component monomer utilized in this work produces a non-elastomeric nylon resin in contrast to the block copolymers receiving recent attention for flexible automotive body parts (1). The chemistry of the lactam ring-opening polymerization and the mechanical properties of the resulting nylon 6 resin have been reviewed by Fahnler (2) and more recently by Hedrick *et al.* (3). The chemical kinetics and rheology are described by Sibal, Camargo, and Macosko (4). This work will concentrate on the mechanical properties of the composites made therefrom with attention given to the peculiarities of the polycaprolactam resin and its beneficial effect on composite strength and toughness, especially in comparison to an epoxy matrix of equivalent modulus.

* Prepared in part for presentation at April 1985 meeting of the American Chemical Society (Division of Polymer Chemistry), Miami, Florida.

EXPERIMENTAL

Beads

Composites of glass beads (Cataphote, Class IV, Type 4000 A, 0 to 40 μm) were incorporated into an anionic nylon 6 matrix by suspending them in the caprolactam monomer, activating the polymerization, and casting the composite into a mold during the induction period before viscosity increase began. Production of a typical 24 volume percent composite involved the following steps:

1. Melt 270 grams of ε-caprolactam (m.p. 69°C) in a 1 *l* round-bottomed, three-neck flask that is purged with dry nitrogen.
2. While stirring, add 155 grams of glass beads. Beads heat treated at 500°C for several hours were cleaner (fewer fragments adhering to the surface) than as-received beads, but equivalent tensile properties were obtained in the composite.
3. Add 1.8 ml γ-aminopropyl silane with a syringe. The coupling agent is hydrolyzed by water that was absorbed in the caprolactam.
4. Vacuum distill off 50 ml of caprolactam high in water and uncoupled silane. This comes over at about 190°C under 70 mm Hg pressure.
5. Cool to 130°C.

6. Add catalyst, such as sodium caprolactam.
7. Degas at 130°C under full vacuum to ensure anhydrous condition.
8. Add initiator, such as acetyl caprolactam.
9. Pour into a 3 mm by 300 mm by 450 mm vertical plate mold heated to 180°C. The melt should set in about 2 min and fully polymerize by 10 min.
10. Remove sheet, allow to cool, and store in desiccator for later testing.

Random Mat

The anionic polymerization of caprolactam was also carried out in the presence of long glass fibers arranged in the form of a random mat. In contrast to the procedure previously described utilizing a filler suspended in the molten monomer, the latter in this case does not contact the fiberglass until after the polymerization is initiated. The melt was poured onto a mat lying in a mold at 190°C, the mold was closed, and 3.5 MPa pressure was applied in a heated compression press to aid in void elimination. This procedure is similar to that utilized by Bessell *et al.* (5).

Some of the mats were custom made from 13 mm chopped roving that was dispersed in water and then matted in a paper-making device. An excellent individual fiber dispersion, which is superior to that found in commercial mats, can be obtained in this way. The mat was then heat cleaned at 400°C to remove unwanted sizing and to dry the glass surfaces. A commercially available random mat was employed as a control.

Although it is more proper to precoat the fiberglass mats with the silane coupling agent used, equally good results were obtained by adding it to the monomer (at 1 percent by weight) as an integral blend. As long as the silane does not completely condense after it is hydrolyzed by water in the caprolactam and before contacting the fiber, adequate bonding could be expected.

Transverse Fiber Mats

Unidirectional continuous glass fiber composites were made from a warp sheet designated Liasil 1300 and manufactured by Fiber Glass Industries, Inc. of Amsterdam, NY. In this sheet, continuous rovings are intermittently stitched together at 76 mm intervals to yield a "cloth" in which >99 percent of the fibers lie in the warp direction. The minimal cross stitching would have a negligible influence on the transverse properties of composites made from this material.

In the fabrication procedure, 8 plies, all lying in the same direction, were stacked, heat treated at 400°C for 5 hours to remove the starch-oil sizing initially coating the fibers, precoupled using a 1 percent solution of silane in a 90 percent aqueous alcohol solution, washed, dried at 130°C for 1 hour to set the silane, laid into a 180 mm by 180 mm compression mold, impregnated with activated monomer at 130°C, and compressed in a 190°C press under a low melt pressure of 1.4 MPa to enhance resin infiltration and to remove voids.

Upon contact, the activated caprolactam monomer had a viscosity of only several centipoise. Consequently fiber wet-out was good. After 90 sec, the viscosity rose sufficiently so that the low platen pressure could be applied. The polymerization was allowed to proceed at 190°C for 10 min; the mold was then cooled, and the 3-mm thick sample was removed and immediately placed in a desiccator to prevent water absorption. In all cases the silane was precoated onto the mat fibers since, in this more severe test, a higher interfacial strength was obtained than by adding it directly to the monomer as an integral blend.

For tensile testing of all composite samples, 19-mm wide strips were cut from the cast plates using a dry band saw. These were then routed into a standard ASTM tensile bar shape (type I). Although in some cases specimens were remolded in the cavity of an ASTM tensile bar compression mold to heal the cut edges before testing, this was unnecessary. Identical results were obtained on the average from samples with cut edges. Testing was generally done at room temperature and at a speed of 3.5 percent/min.

Impact tests were run on 3 mm thick plaques using either a falling ball or hemispheric pendulum impact tester. The reported impact strength refers to the energy at which 50 percent of the samples tested show visible cracking.

RESULTS

Beads

Bead castings were found to exhibit high property levels not usually seen in particulate composites: tensile strength slightly above that of pure resin, doubling of tensile modulus, tensile elongation as high as 15 percent, and high (25 to 40 J) multi-axial impact strength for a 3-mm thick plaque. Mechanical properties are compared with those of similar materials in *Table 1*. The tensile stress-strain curve for a 24 volume percent composite casting using glass beads is compared with a mineral reinforcement, having an aspect ratio below 20, in *Fig. 1*. The higher elongation of the bead composite is evident. Neither show an abrupt pre-yield modulus decrease or post-yield stress drop that is symptomatic of filler dewetting, although a degree of stress whitening still occurs.

Elongation is at least doubled over that of the unfilled polymer at strains rates above the threshold for necking to occur in the unfilled

Table 1. Properties of Particulate and Short Glass Fiber Composites With Anionic Nylon 6.

Filler	Filler Content, volume/ percent	Resin	Water Equilibration, % RH	Tensile Strength, MPa	Tensile Modulus, GPa	Tensile Elong., %	Multiaxial Impact Strength, J
Unfilled	0	anionic nylon 6	0	77.9	3.4	3.5 yld.	20 to 27
Glass beads	24	anionic nylon 6	0	84.8 yld. 83.4 ult.	5.6	3.9 yld 10–15 ult.	20 to 27*
Glass beads	50	anionic nylon 6	0	89.0 yld. 88.3 ult.	9.8	3.0 yld. 3.8 ult.	27 to 34
Glass beads	24	anionic nylon 6	50	47.6 yld.	2.8	>8 ult.	>50
Glass beads	24	nylon 66	0	84.4 yld. 83.4 ult.	6.5	3.6 yld. 6.1 ult.	—
Glass beads	24	amorphous nylon	0	84.8	4.3	3.6	—
Mineral (<20:1 l/d)	24	anionic nylon 6	0	104.8 yld. 104.8 ult.	7.7	3.1 yld. 4.3 ult.	20
0.8 mm Milled Glass	24	anionic nylon 6	0	103.4	7.2	3.3	2.7

* Reduced to 7 to 13 J when beads are heat cleaned.

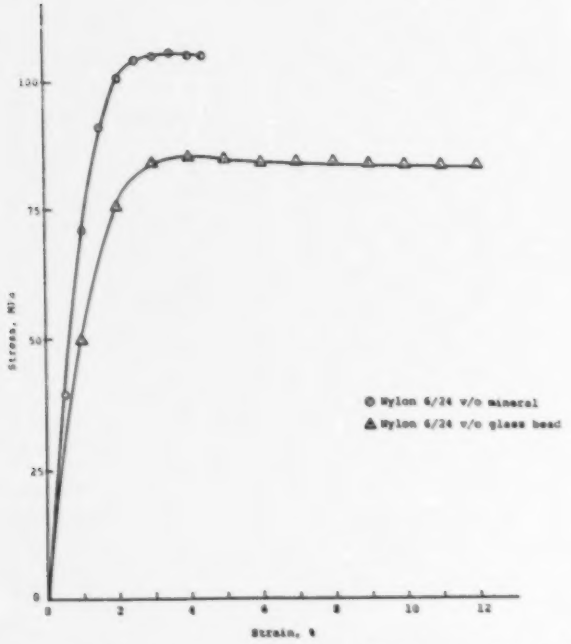

Fig. 1. Tensile stress-strain curves for glass beads and mineral filler at 24 volume percent in in-situ polymerized in nylon 6 castings.

polymer. Although it dropped off at high deformation rates, ultimate elongation exceeded 8 percent even at a high testing speed of 300 percent/min.

Izod impact strength is doubled from .25 to .50 J/cm by the addition of beads to nylon 6, but the multi-axial impact only increases slightly with increasing bead concentration up to 50 volume percent. However, if the bead composite is prestressed, for example by impacting a plaque at low energy (7 J) to induce cavitation, a much higher energy can be later sustained without visible cracking. At 24 volume percent beads, the impact strength can be increased from 20 to 27 J to 61 J by this procedure.

The bead composite Young's modulus is readily predicted to within 5 percent error by the Halpin-Tsai Equation, a generalized form of the Kerner Equation (6), using the Einstein coefficient value of 2.5 for spheres and not correcting for packing effects, as the broad size distribution of the spheres would permit very tight packing.

The dependence of impact strength on level of bond strength to a reinforcing filler is not shown in the table. But, with 24 volume percent of a wollastonite mineral, the multi-axial impact strength rose from 1.4 to 8.0 J as the silane concentration was increased from 0 to the 1 percent by weight level used in the glass bead composites. Equilibration to 50 percent relative humidity trebled the impact values, as also is the case for bead composites. Unfortunately, tensile strength drops precipitously.

It can be seen from *Table 1* how increasing the reinforcement aspect ratio reduces tensile elongation and impact strength. Thus, the latter decreases to 2.7 J in a .8 mm milled glass composite ($l/d \leqq 30$), and about 1.9 J for an injection molding of 40 volume percent fiberglass in a commercial nylon 6 thermoplastic molding compound.

Further experimentation undertaken to characterize this high ductility for a composite and to determine its cause in the failure mechanism is described in the *Discussion*. Mechanical property data for similar particulate composites made by melt blending into prepolymerized nylon 66 and Trogamid T (Dynamit Nobel Chemicals Co.), an amorphous nylon, are also included in *Table 1*. The elongation is especially lower in the non-crystalline resin, which also shows a considerably higher degree of stress whitening attributed to crazing.

Random Mat

The dry random mat nylon 6 composites can have tensile strengths nearly double those ob-

tained with commercial reinforced polypropylene and SAN sheet. The strength data summarized as a function of fiber content in *Fig. 2* also show that the better dispersed custom mats are definitely superior to commercial ones, and that the method of silane application is inconsequential. Indeed the adhesion of resin to the fibers shown in the scanning electron micrographs of tensile fracture surfaces in *Fig. 3* is equally good for these two different methods.

These fractures were made in dry samples (<.06 percent water by weight). The corresponding micrograph of the fracture surface of a duplicate sample that was equilibrated to a 50 percent relative humidity (RH) atmosphere appears in *Fig. 4*. Notice that the plasticization of the nylon results in an increase in its ductility as evidenced by the long fibrils that are drawn off from resin clinging to the fiber surfaces.

In addition to good adhesion, there appears to be a good wet-out of the fibers due to the low initial viscosity of the activated melt and an absence of voids.

According to *Fig. 2*, tensile strengths exceeding 210 MPa are possible for these two-dimensionally isotopic composites (when dry) at a fiber content below 30 volume percent. However, as with all nylon composites, the absorption of water is deleterious. A reduction in tensile strength to the performance levels of the SAN and polypropylene sheet occurs when the sample is equilibrated to 50 percent RH.

For all the dry data reported above, the elongation to failure is in the range of 1.9 to 2.5 percent. The equilibration to 50 percent RH causes a slight decrease to 1.7 to 1.9 percent. Although the tensile behavior of random mat composites is generally thought to be controlled by the fiber properties, causing failure to occur at about 2 percent, the higher curvature in the stress-strain curve shown in *Fig. 5* for the nylon composite indicates some resin contribution.

The elastic modulus of dry samples displays a linear increase with fiber content for all com-

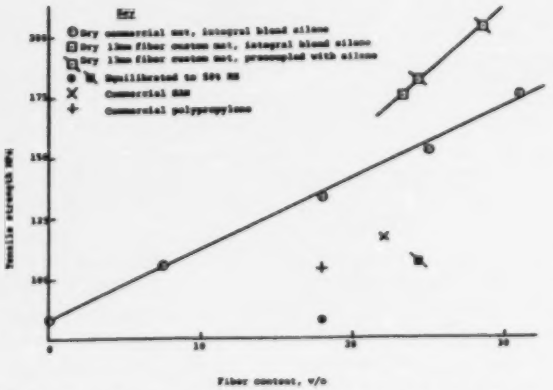

Fig. 2. Tensile strength of in-situ polymerized nylon 6/random fiberglass composites (2D random reinforced nylon sheet).

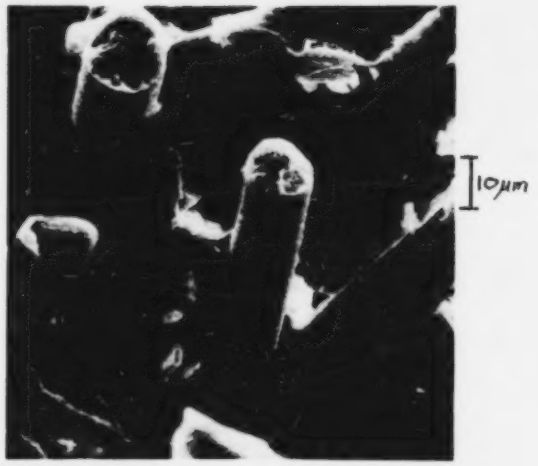

(a)

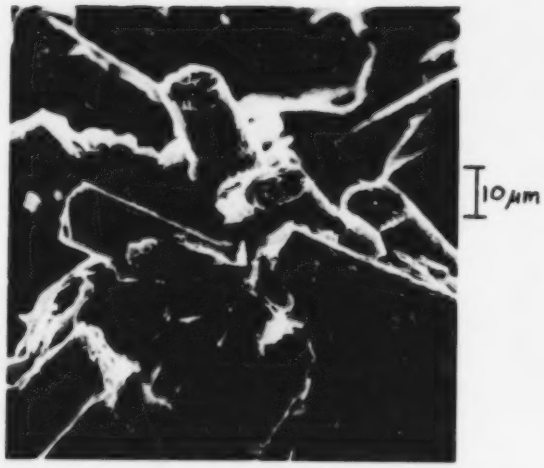

(b)

Fig. 3. SEMs of tensile fracture surfaces on in-situ polymerized dry composites of nylon 6 and random fiberglass mat; (a) is integral blend of silane; (b) is precoupled fibers.

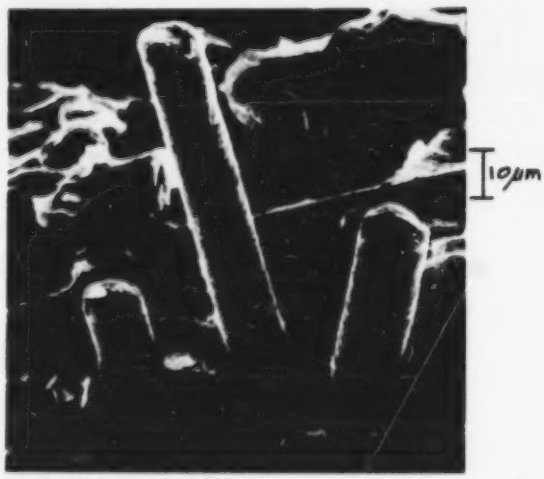

Fig. 4. SEM of a surface similar to Fig. 3, but in which the composite was equilibrated to 50 percent RH.

posites made with glass fibers (*Fig. 6*). At a 50 volume percent loading, it reaches a value of 18 GPa and is predictable within 2 percent from the Voigt average taken over a 2-dimensional fiber array when aligned properties are calculated according to the Halpin-Tsai equation (7, 8). Mats produced from the stiffer graphite fiber provide an even higher stiffness level. For example, a tensile modulus of 18 GPa occurs at only 16.5 volume percent. Equilibration to 50 percent RH water causes a 33 percent decrease in stiffness.

The incorporation of a fibrous reinforcement into the polycaprolactam results in low impact strength that is common to other fiberglass composites. In a falling ball multidirectional impact test, initial cracking occurs at about 1.5 J for both dry and water equilibrated samples containing 18 volume percent fiber. Decrease of the fiber level to 7.5 volume percent raises the impact strength into the 3 to 4 J range. Commercial SAN sheet showed initial cracking at lower levels (0.3 J), but more severe cracking was resisted up to energy levels of 27 J. With the polypropylene, initial cracking occurred at 3 J. In impact, both commercial products outperformed the nylon 6, which showed severe damage at 14 J. The fiber bundling (low fiber dispersion) in these commercial samples could be the reason for their higher impact levels, but might also contribute to their lower tensile strength.

Transverse Fiber Mats

The tensile data are presented in *Table 2*. The tensile modulus is predictable within 5 percent by the Halpin-Tsai equation for transverse fiber orientation (7, 8).

A tensile strength of 81 MPa, about equal to that of the matrix, and an elongation of 1 to 4 percent are interpolated for a 40 volume percent fiber content. Values this high have been previously unattainable with a resin whose T_g lies appreciably above room temperature. In contrast, a typical brittle epoxy reinforced with 40 volume percent transverse fibers, such as Epon 828/curing agent Z (Shell Chemical Co.), breaks at only 0.6 percent strain and about 50 MPa tensile stress (see *Table 3*). While tensile strength typically drops in half in the epoxy composite as the transverse fiber loading increases to 40 volume percent, it actually rises slightly in the nylon 6 composite. Modulus val-

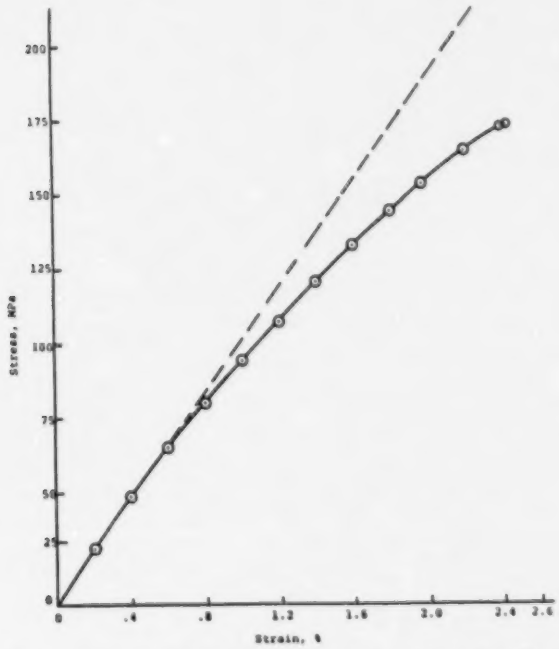

Fig. 5. Tensile stress-strain curves for random fiberglass mat in-situ polymerized in nylon 6; 13 mm E-glass, 23.4 volume percent.

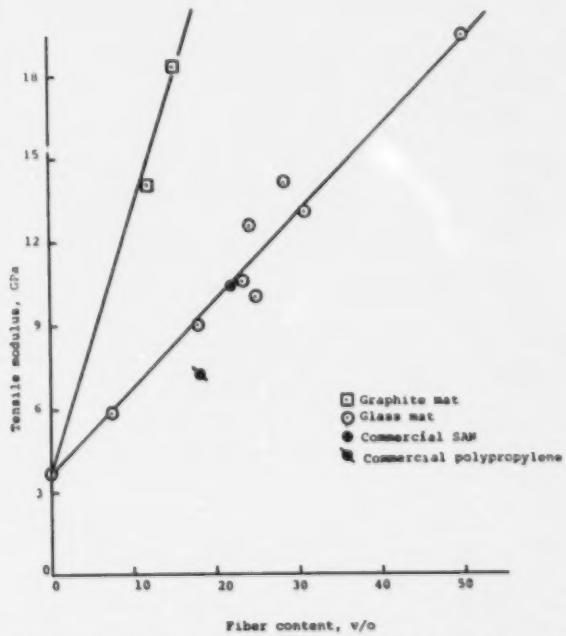

Fig. 6. Tensile modulus of same material as shown in Fig. 2.

Table 2. Tensile Data for Uniaxial Continuous Glass Fiber/Nylon 6 Composites Prepared by Anionic *In-Situ* Polymerization and Tested Transverse to the Fiber Direction.

Fiber Content, volume/percent	% RH Equilibration	Tensile Strength, MPa	Tensile Modulus, GPa	Tensile Elongation, %
47.6	0	78.0	11.2	1.19
47.6	50	40.7	7.0	1.36
33	0	84.1	7.3	1.41–2.00

Table 3. Comparative Epoxy Properties.

Material	Young's Modulus, GPa	Strength, MPa		Elongation, %	
		Yield	Ultimate	Yield	Ultimate
Unfilled resin	3.4	93.1	90.2	5.0	6.1
40 volume/percent Glass bead composite	8.7		81.8		1.2
40 volume/percent Transverse glass fiber composite	9.2		50.1		0.6

ues are similar for the two systems. A stress-strain curve for 38 volume percent transverse fibers in nylon 6 is presented in *Fig. 7*.

DISCUSSION

Beads

The bead samples stress-whiten when stretched above the yield point. Shear bands are not evident, but the high ultimate elongation of the bead samples is attributed to microcavitations that form in the matrix around the beads under stress. When the temperature is sufficiently low or the strain rate sufficiently high so that a homogeneous ductile plastic yield is not possible, this inhomogeneous deformation occurs at a lower energy threshold than immediate brittle fracture. It is accompanied by local microscopic cold drawing of the polymer.

A collection of papers dealing with microcavitation phenomena is found in ref. 9. Two stages of microcavitation observed in nylon 6 composites are described below.

The first, crazing, occurs primarily in brittle fractures of amorphous materials, and is enhanced by the presence of bead fillers (10). It is a localized micro-yielding phenomenon that is observed only infrequently in these nylon composites. The microcracks pictures in the scanning electron micrographs (SEM) of *Fig. 8* are similar to craze-like structures, which are also uncharacteristic of the unfilled nylon 6 resin. More likely, the localized drawing that is starting to form in the nylon 6 matrix here is facilitated by the release of triaxial stresses through microcavitation induced by the presence of the spheres. Thus, these microcracks may not be true crazes, as evidenced by the rather large diameter of the fibrils.

These samples were produced by pulling a tensile specimen to 4 percent elongation, releasing the stress, freezing the sample, and snapping in flexure perpendicular to the original tensile stress direction. Consequently, the original tensile stress was in the plane of the figures in the direction indicated.

Figure 9 shows how latticework can form around a growing hole in a drawn region of the fiber. The voids are somewhat larger in this case. These SEMs are from the tensile fracture surface of a 24 volume percent *in-situ* composite of short milled glass fibers, which induce a grosser structure with more localized drawing than the glass beads, probably as a result of greater stress concentration.

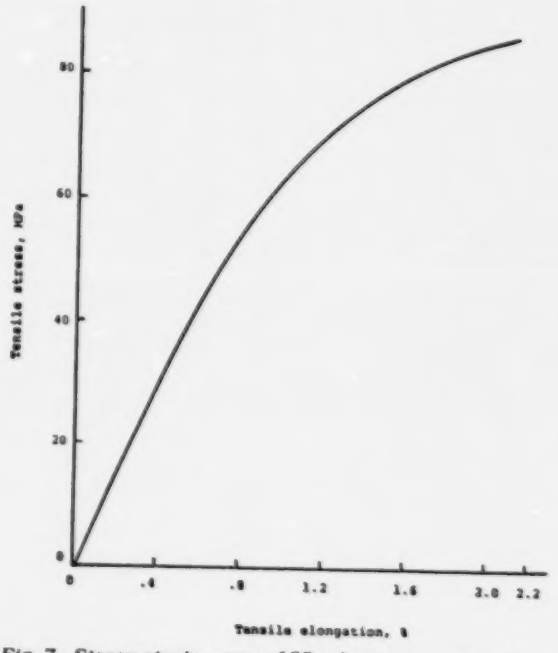

Fig. 7. Stress-strain curve of 38 volume percent unidirectional transverse glass fiber composites with anionic nylon 6 matrix.

A second, more homogeneous occurrence of microvoids ranging up to 1,000 Å in diameter has been termed blushing because the stress whitening is less severe than with crazing. It occurs predominantly in ductile polymers, and may relate to the initial breakdown in the crystalline structure (9). The rough surface filled with such microvoids, as shown in *Fig. 10*, is typical of the fracture surfaces observed in the bead composites in nylon 6, especially near the filler interface. It is perhaps a precursor to the more extensive drawing seen in the fiberglass composites that does not fully develop under the smaller stress concentrations induced by the beads. The cavitation behavior observed here is thus an intermediate region between true crazing and shear banding in which cavitation relieves the triaxial stress and allows islands of ductility to form.

Tensile stresses in the resin are high near the poles of high modulus spherical inclusions. More cavitation could occur there not only because of stress concentration, but because the resin is more constrained by the excellent adhesion obtained to the glass surface. The thickness of such a bound layer, comprised perhaps

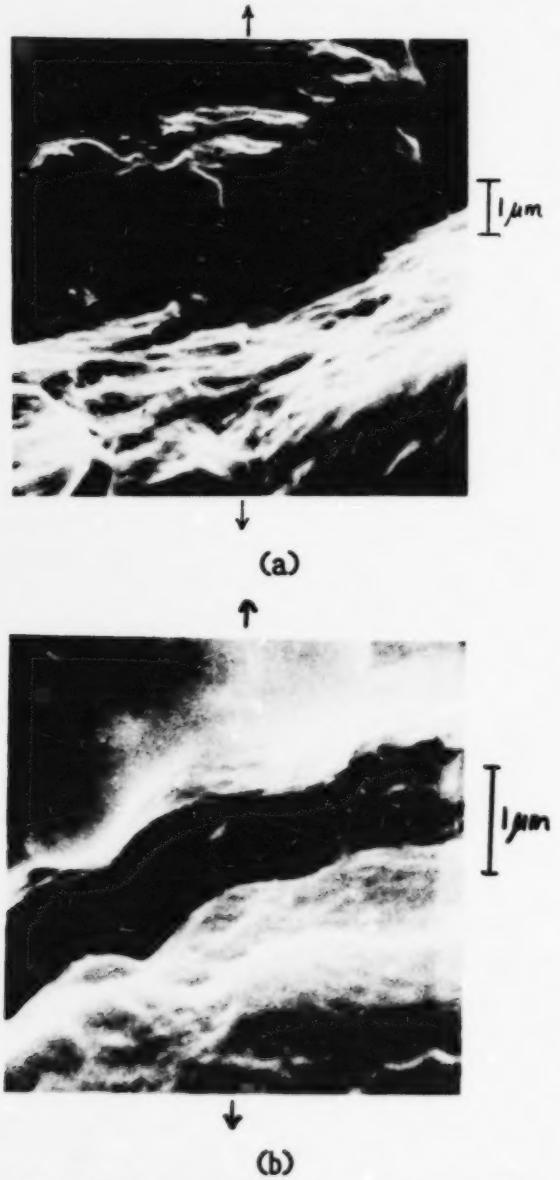

Fig. 8. SEMs of crazes in a 24 volume percent bead filled nylon 6; stress direction is indicated by the arrow in the plane.

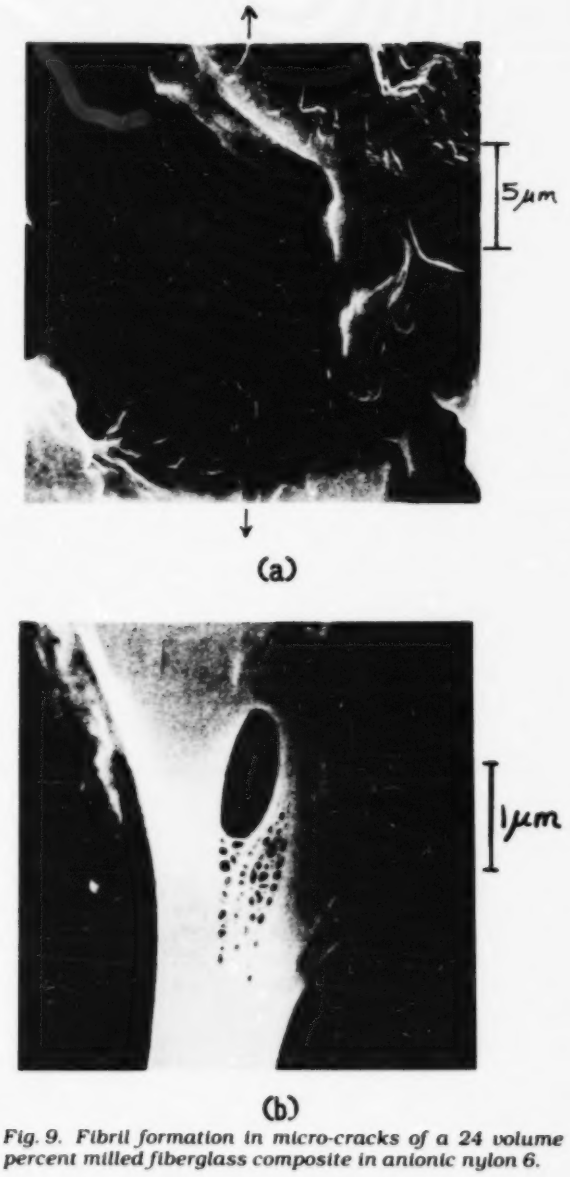

Fig. 9. Fibril formation in micro-cracks of a 24 volume percent milled fiberglass composite in anionic nylon 6.

by a transcrystalline form of the polymer (5), is shown on the fractured bead in *Figure 11 (a)*. Without good adhesion, dewetting instead would ensue, which would produce a more severe stress-whitening.

There is some evidence that the balance between the two predominant forms of microcavitation, crazing and blushing, is determined by the degree of adhesion to the filler surfaces. When the adhesion is poorer, the resin is not as uniformly strained, and crazes, which are more localized, may initiate at the free surface following dewetting, and propagate under plane strain into the matrix. This occurs with a melt-blended polyamide sphere composite when no silane coupling agent is used. In support of this argument, it has been reported for rubber-modified polystyrenes that the better adhesion resulting from grafted rubber inclusions results in a higher density of microvoids, fewer rupture cracks, and better energy absorption (11). In glass bead composites, an improved yield stress (though still below matrix strength) but decreased elongation and toughness have been reported (9) with improved adhesion to thermoplastic matrices that craze.

In this work, both tensile strength and ultimate elongation decrease when void consolidation into craze-like structures replaces blushing. With the more homogeneous cavitation that occurs in blushing, the material under plane stress is not locally weakened, and the greater number density of smaller-sized voids (10^{12}/

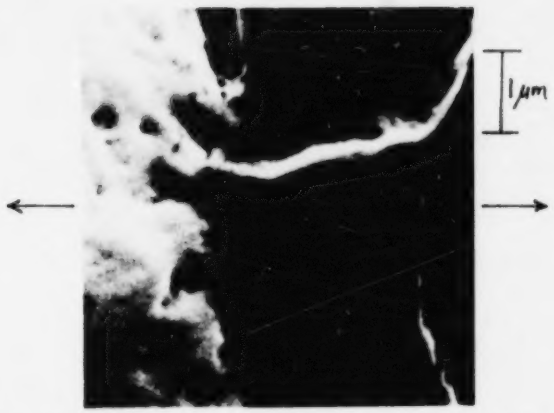

Fig. 10. SEM of microvoids in a 24 volume percent bead composite in anionic nylon 6; arrows indicate tensile stress direction.

cm^3) can better prevent the formation of critical flaws. Donald and Kramer (12) describe the role of small rubber particles in ABS in relieving stress through cavitation, allowing the matrix to shear yield under a plane stress condition.

Figure 11 shows indications of the cold drawing into fine filaments that can occur primarily in the vicinity of the filler. In the case of well-bonded spheres, the filaments are finer and more uniformly distributed over the coated surface of the sphere. The cold drawing and tendency to cavitate are induced in the resins by the presence of filler, since neither fibrils nor microvoids are observed in the fracture surfaces of unfilled nylon 6 samples prepared by the same technique. This has also been observed in rubber-modified glassy polymers (13) and in polyphenylene oxide (PPO) filled with glass spheres (9).

According to theories reviewed in ref 13, the local cold drawing may relate to an increase in free volume in the polymer matrix. With glass spheres, toughening by classical crazing, identified with a knee (modulus decrease) in the stress strain curve, occurs in glassy composites and even with a ductile PPO matrix (9).

Thermal stress induced in the resin by contraction around the filler particle could be a contributing cause. Although thermal stresses are calculated at 21 MPa in the matrix by the interface, some tests with samples in which these were annealed out at 65°C for one week also produced a high elongation (13.4 percent compared with 18.8 percent for the control). Ultimate strength in the annealed samples increased from 87 to 94 MPa. Thus, it appears that thermal stresses may have some minor significance.

The resin fibrillation is illustrated for short fiber composites in *Fig. 11* (*c*). *Table 1* shows the composite ductility to be lower, but localized cavitation and drawing are evident. Such phenomena are unusual in fiber reinforced composites of less ductile resins.

Fig. 11. The interface and cold drawing in nylon 6 composites; (a) and (b) are bead filled; (c) is milled fiberglas.

The microcavitation phenomenon occurs in dry samples and is not the result of water on the filler surface or in the resin. The beads were thoroughly dried before being suspended in the monomer, and absorbed water in the caprolactam melt was removed by distillation, as described in the procedure, to yield less than .06 percent by weight water in the test samples.

If the load on a cavitated sample is cycled, the modulus decreases by about 50 percent, but there is little reduction in the ultimate elongation based on the initial sample dimensions. Annealing at a temperature above T_g (about 100°C) completely restores the initial modulus. This is not unusual for cavitated polymers.

When beads are melt blended instead into a prepolymerized nylon resin, a similar microcavitation occurs, but to a lesser degree. With nylon 66 the bead wet-out is not as good as in polycaprolactam (*Fig. 12 (a)*), but some cold drawing still occurs, although to a lesser extent (*Fig. 12 (b)*), and the stress-strain curve shows a lesser, but still considerable, elongation (*Fig. 13*).

It is likely that differences in resin morphology cause this difference in composite tensile behavior. The anionic nylon 6 has a molecular weight of 90,000, compared with 35,000 for the nylon 66. In addition, it has a high degree of crystallinity (14) as well as an equilibrium monomer content of 1.0 percent by weight. These factors might all contribute to higher ductility.

Some comparable tensile properties of an Epon 828 epoxy composite crosslinked with curing agent Z and cast between glass plates are given in *Table 3*. This epoxy matrix is of the same modulus as the nylon 6 polycaprolactam under study. However, both its strength and elongation are slightly higher. With 40 volume percent glass beads, on the other hand, the tensile strength is reduced by 12 percent; whereas in the nylon 6 composite, the strength *increases* by the same amount, to surpass the strength of the epoxy composite. The tensile elongation shows an equally dramatic effect. It decreases to only 1.2 percent for the epoxy composite, but remains high (above 3 percent) in the nylon 6.

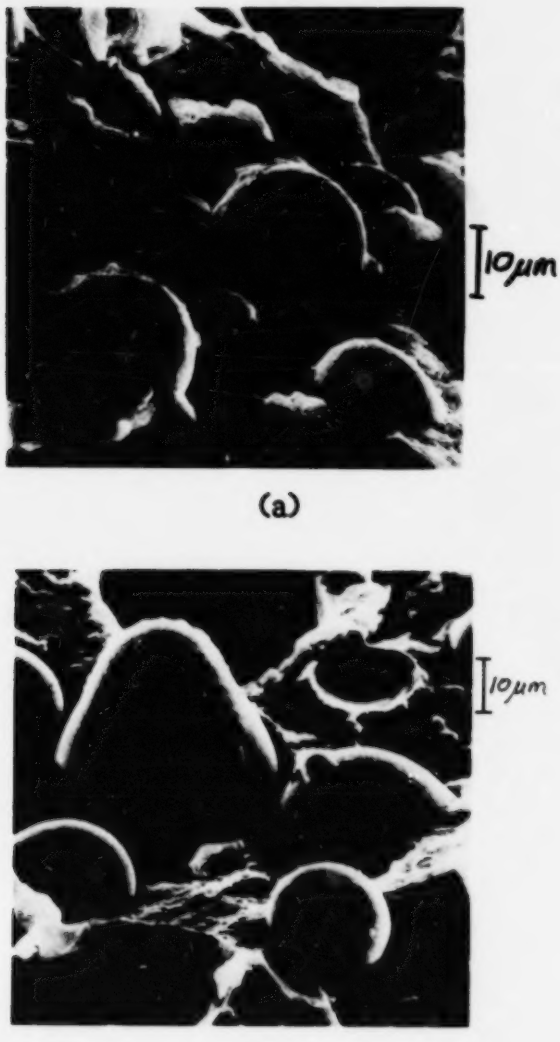

Fig. 12. Fracture surface of injection molded composite of glass beads melt blended into nylon 66.

Transverse Fiber Mats

A comparison of tensile properties of the dry nylon composite given in *Table 2* to a bench-

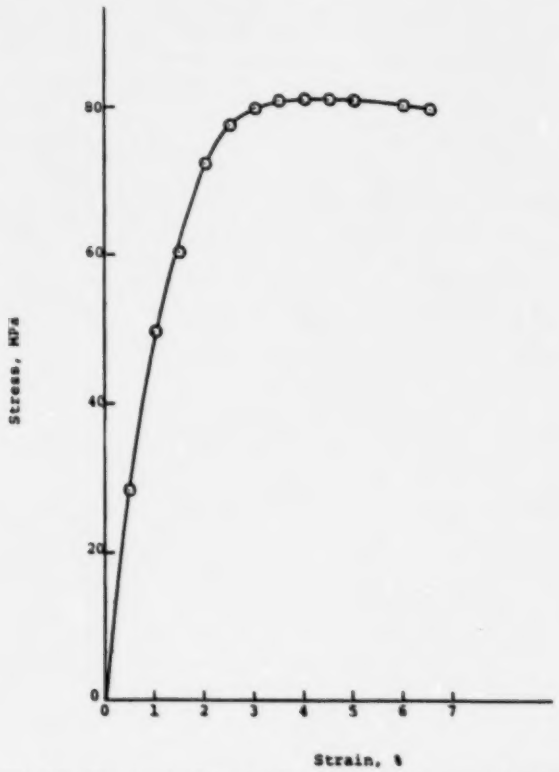

Fig. 13. Stress-strain curve for a 24 volume percent composite of precoupled glass beads in nylon 66.

mark epoxy composite (last line of *Table 3*) shows equivalent modulus but considerably higher tensile strength (62 percent) and ultimate elongation (140 percent) in the nylon system. The data of *Table 2* lines 1 and 3 are averaged to yield the same 40 volume percent fiber concentration base in making this comparison.

The causes underlying the superior transverse tensile properties of transversely aligned fiber composites may involve one or more of the following factors:

1. High ductility of the nylon, including the ability to cold draw.
2. Tendency of the nylon to microcavitate (blush), in order to relieve the stresses that would otherwise lead to a premature brittle failure.
3. Excellent adhesion of nylon to glass surfaces.
4. Excellent wetting of the fibers produced by the *in-situ* polymerization.
5. Formation of an unusual (crystalline) morphology at the interface.

These are the same factors that also affect composite performance in other matrix-dominated situations, such as in particulate composites. Unfortunately, moisture has a deleterious effect on the tensile strength, reducing it below that of the epoxy composite.

Some SEMs of these transverse composites are shown in *Fig. 14*. Fiber content is 47.6 volume percent. Note in *Fig. 14 (a)* the excellent wetting and adhesion. Of particular importance is the tendency of the resin to flow, seen by the flow lines beneath the lowest fiber and, at the left end of that fiber, a drawn film. The fiber surface pictured in *Fig. 14 (b)* at higher magnification also shows evidence of local drawing.

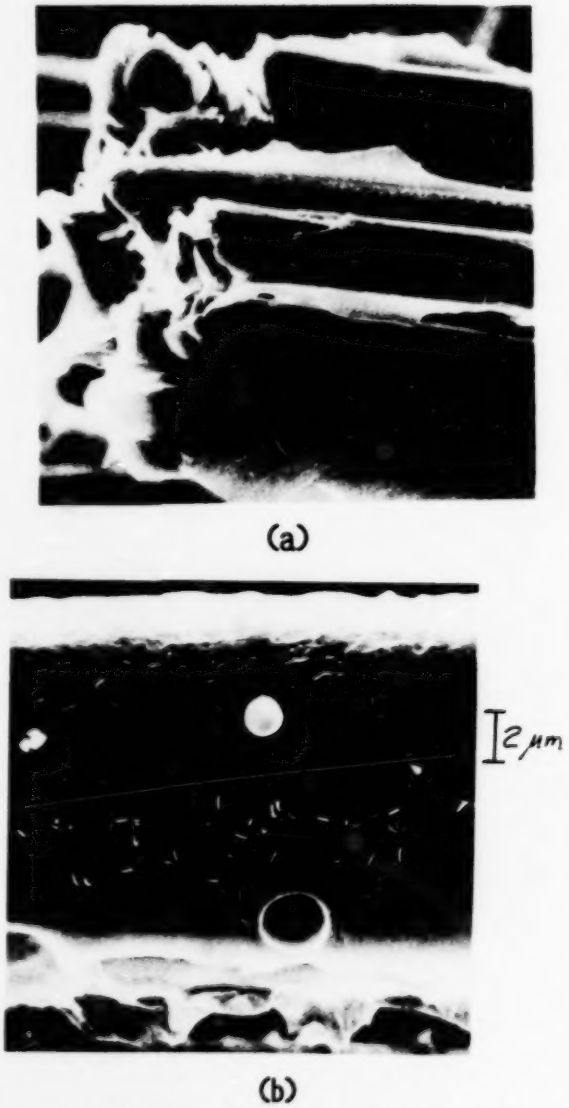

Fig. 14. SEMs of a 47.6 volume percent unidirectional transverse glass fiber/anionic nylon 6 composite fracture surface.

SUMMARY

Bead Composites

The inclusion of glass bead fillers in ϵ-caprolactam, which is then anionically polymerized to nylon 6 resin, produces high elongation (15 percent) and toughness that surpass the performance of mineral and fiber composites in these respects. Along with increased stiffness, tensile strength is augmented slightly over that of the unfilled resin. This has not been previously reported for particulate composites. A strong interface with the beads results from good wet-out and possible polymer modification in the interfacial region. The high elongation without a strength loss that is unusual in bead composites is attributed to a strong interface and microcavitation, similar to blushing, that is induced in the resin by the bead reinforcement. The ability of the nylon to cold draw rather than craze during fracture is also important to the mechanism. Dewetting of the reinforcement does not occur.

Several resin characteristics are believed to contribute to the extensive microcavitation. Generally, they are the ones that lead to high draw ratios in unfilled polymers, such as high molecular weight and crystallinity. The cavitation mechanism also seems to operate, but to a lesser extent, with mineral reinforcements. Higher strength, but lower elongations result.

Poorer adhesion causes craze-like structures with extensive resin drawing rather than blushing to occur on stretching, because after dewetting the resin is less uniformly constrained. Since crazes are less homogeneous, failure results at a lower strength and elongation. These also occur in fiber composites, where the fibers that bear a large part of the stress and localized regions of the resin at the fiber tips are subject to high elongation.

Mats

At the same fiber loading, random-in-a-plane nylon 6 composites have a higher tensile strength and ultimate elongation than commercial products using SAN or polypropylene resin. This results from better bonding to the fibers and retarded crack propagation due to the high matrix ductility in combination with excellent fiber dispersion in the experimental mats. Moisture is unfortunately very deleterious in the nylon composites.

Transverse Fiber

Transverse tensile elongations in 33 volume percent composites can be as high as 2.0 percent, but average 1.7 percent. At 40 volume percent, 1.4 percent is obtained, compared to 0.6 percent for Epon 828/Z composites. Thus, the nylon would give superior performance in a 0 to 90° laminate where the design ultimate is frequently limited by cracking in the transverse laminae. Tensile strength is high at 78 MPa, equal to the unfilled resin even when the fiber content is high (48 volume percent).

CONCLUSIONS

The evidence of this study indicates that the anionic nylon 6 becomes a superior matrix resin when produced by *in-situ* polymerization of ε-caprolactam in cast composites. High molecular weight, better wet-out of the reinforcement, better adhesion, and more cold drawing lead to the ability to cavitate in a more homogeneous manner than the strict crazing following dewetting observed with other thermoplastic polymer systems. In contrast to epoxy and other matrices, both extension to break and ultimate strength are increased, leading to higher toughness in bead and transverse fiber composites whose mechanical performance is matrix dominated. In random mat composites where fiber interactions predominate, the primary advantage lies in dry strength improvement over commercial reinforced sheets.

NOMENCLATURE

SEM = Scanning electron micrograph.
T_g = Glass transition temperature, °C.
l = Fiber length, mm.
d = Fiber diameter, mm.

ACKNOWLEDGMENT

This research was supported by the Advanced Research Projects Agency of the Department of Defense and was monitored by the Office of Naval Research under Contract No. N00014-67-C-0218.

DISCLAIMER OF WARRANTY AND LIABILITY

While this information is presented in good faith and believed to be accurate, Monsanto Company does not guarantee satisfactory results from reliance upon such information and disclaims all liability for any loss or damage arising out of its use and makes no express or implied representation or warranty as to the fitness, merchantability or any other matter with respect to the product or processes referred to herein.

REFERENCES

1. A. S. Wood, *Mod. Plast.*, **58**, 44 (1981).
2. F. Fahnler, *Plastics Rubber Intern.*, **5**, 251 (1980).
3. R. M. Hedrick, J. D. Gabbert, and M. H. Wohl, ACS Monograph, to be published.
4. P. W. Sibal, R. E. Camargo, and C. W. Macosko, "Designing Nylon 6 Polymerization Systems for RIM," proceedings of 2nd Int'l. Conference on Reactive Polymer Processing, Society of Plastics Engineers, Pittsburgh (Nov. 1982).
5. T. Bessell, D. Hull, and J. B. Shortall, *Nature Physical Sci.*, **232**, 127 (1971).
6. L. E. Nielsen, "Mechanical Properties of Polymers and Composites," Marcel Dekker, New York (1974).
7. J. C. Halpin, *J. Compos. Mater.*, **3**, 732 (1969).
8. J. E. Ashton, J. C. Halpin, and P. H. Petit, "Primer on Composite Materials: Analysis," p. 77, Technomic, Stamford, CT (1969).
9. H. H. Kausch, ed., "Crazing in Polymers," Springer-Verlag, Berlin (1983), especially K. Friedrich, "Crazes and Shear Bands in Semi-Crystalline Thermoplastics," p. 225.
10. R. E. Lavengood, L. Nicolais, and M. Narkis, *J. Appl. Polym. Sci.*, **17**, 1173 (1973).
11. S. G. Turley, *Appl. Polym. Symp.*, **7**, 237 (1968).
12. A. M. Donald and E. J. Kramer, *J. Mater. Sci.*, **17**, 1765 (1982).
13. S. Strella, *Appl. Polym. Symp.*, **7**, 165 (1968).
14. R. S. Kubiak, *Plast. Eng.*, **36**, 55 (1980).

DISCUSSION

M. Lambla: You showed large increase in tensile strength of your product filled with glass beads. It is well known that caprolactam polymerization is rapid. Would you say that in the presence of filler you may have some changes in the heterogeneity of the product? The heterogeneity may be larger in the bulk polymerization than in the presence of glass beads.

L. A. Goettler: By heterogeneity you mean differences in molecular weight?

M. Lambla: Molecular weight, crystallinity and so on.

L. A. Goettler: I think that this is possible. As I indicated, the polymerization takes place at low temperature so there may be less thermal stress. I also believe that 140 to 150°C is the optimum range for crystallization. So, indeed, we may have a higher level of crystallinity in this material. I cannot comment on the molecular weight distribution. We did not measure it.

M. Lambla: There is also a second possibility. You showed very good wetting of the filler. You use γ-aminopropylsilane for the sizing of the glass beads. This may produce co-crystallinity at the surface, which would also enhance the properties.

L. A. Goettler: Some of the scanning electron micrographs which I showed suggest the presence of a modified, perhaps transcrystalline, layer at the interfaces.

C. L. Beatty: Have you measured crystallinity and compared its level in filled and unfilled systems?

L. A. Goettler: No, we have not.

L. A. Utracki: Lloyd, some years ago you published a paper plotting the strength of glass fiber composites against the dipole moment of the matrix. The polyamides were right in the upper right-hand corner. If you place a point for your new system on that graph, is it going to be above the line or on the line?

L. A. Goettler: The data you are referring to were literature data for injection molded specimens containing 30 volume percent of a commercial fiberglass compound. The new system would fit at the upper right where the points for nylon-6,6 and nylon-6 were located. But it is difficult to make a direct comparison due to differences in fiber length. For example, the tensile strengths of 24 volume percent composites reported here vary from 84 MPa for bead fillers to 175 MPa for planar random reinforcement with 13 mm chopped fiberglass. These bracket the results you reference.

L. A. Utracki: During the ring opening polymerization of ϵ-caprolactam, the volume expands or contracts?

L. A. Goettler: Reaction is exothermic, and in general, ring opening polymerizations should produce small volume change. Thus, the net effect upon return to room temperature should be a small linear contraction of 2 to 3 percent.

L. A. Utracki: Some ring monomers are known to expand on polymerization generating excellent adhesion to filler. Mike Piggott published several papers on the subject. Finally, during your presentation, several times you stressed sensitivity to moisture. But is the sensitivity for your product higher than for any other glass fiber nylon-6 composite?

L. A. Goettler: No. In general moisture sensitivity for activated anionic nylon-6 is lower than that for both nylon-6 produced by hydrolytic condensation as well as nylon-6,6. I probably overemphasized the one obvious detraction from an otherwise exemplary set of properties.

Reaction Injection Molding of Mica Reinforced Polyurethane

B. RÉMILLARD, T. VU-KHANH, *and* B. FISA*

Industrial Materials Research Institute
National Research Council Canada
Boucherville, Quebec, Canada J4B 6Y4

and

S. NAIK
Marietta Resources International
Boucherville, Québec, Canada J4B 6A1

Reaction injection molded polyurethanes are reinforced with inorganic materials to improve stiffness and structural integrity at elevated temperatures and to reduce the coefficient of thermal expansion. This work describes the reinforcement obtained with an experimental grade of mica designed to achieve low viscosity of mica suspensions in polyol. The effect of mica on properties is essentially identical to that of glass flake (i.e., improved stiffness at the cost of reduced impact strength). Compared to hammer milled glass fiber, mica and glass flakes yield more isotropic, albeit weaker, materials. The study of unreinforced polyurethane shows that mechanical properties (tensile and impact strength, flexural modulus) are approximately proportional to the square of foam density.

INTRODUCTION

Reaction injection molding (RIM) is one of the fastest growing processes for production of large complicated plastic parts. Initially limited to polyurethanes (1), which are still dominating the market, recent years have seen RIM to be used with nylon (2), dicyclopentadiene (3) and other systems. In reaction injection molding, low viscosity monomers or prepolymers are injected into a low pressure mold where the polymerization takes place. Constant progress led to the introduction of fast curing systems and internal mold release agents (4). These developments dramatically improved the mass production utility of the process.

For many applications, the stiffness, structural integrity at elevated temperatures, and the coefficient of linear thermal expansion (CLTE) of the base system are insufficient and use of reinforcing fillers is required. Several fillers including milled (5, 6) or chopped (7, 8) glass fibers, wollastonite (9), glass spheres (10), glass (11), and mica (12, 13) flakes were evaluated. A survey of the literature appears to indicate that glass fibers impart the best mechanical properties to the system. However, the well known flow-induced fiber orientation gives materials with undesirable anisotropy, while flake materials give essentially isotropic materials (in 2 dimensions). In addition, due to their impermeable nature, flakes reduce moisture penetration (14), hence lower—dimensional changes during humidity cycling.

Two classes of flake reinforcement are currently available: glass and mica. Mica has been used primarily in thermoplastics—polypropylene and high-density polyethylene (PP, HDPE)—whereas glass flakes are principally used in reaction injection molding. Mica has seen little use in RIM for two reasons: difficult processing due to high viscosities of mica-polyol suspensions and lower impact strength of mica reinforced systems (15). This work describes properties of a high modulus polyurethane elastomer reinforced with an experimental grade of mica, which was developed to achieve better processability.

EXPERIMENTAL

Materials

Polyurethane

A high modulus (80,000 psi at room temperature) polyurethane elastomer Bayflex 110-80

* To whom all correspondence should be addressed.

(Mobay Chemical Corp. Pittsburg) was used throughout this work.

Mica

Several commercial and experimental grades of phlogopite mica (Marietta Resources International, Boucherville, Canada) that were used are described in the text.

Glass

Glass flakes (1/64") were obtained from Owens Corning Fiberglass. Except for a small amount of calcium carbonate to prevent caking, the glass flakes are not surface treated. Milled glass fibers (1/16"—grade 737BB) were also used from the same supplier.

Molding

An Accuratio MICRO RRIM II machine was used to mold all samples. The mold dimensions and the gating arrangement are illustrated in *Fig. 1*. The industrial practice of incorporating all filler into the polyol was followed. Filler concentration in polyol was adjusted to yield 0, 5, 10, and 20 weight percent of the filler in the final molded product. Both the isocyanate and polyol sides were maintained under constant agitation, at 40 °C and 0.35 MPa air pressure. The injection pressure was 11 MPa; mold temperature was set at 65 °C.

The product density and the void volume fraction were varied by controlling the amount of liquid injected. In the event of a short shot, the dissolved gases (liberated as a result of the pressure drop between the reservoir and the mold) formed bubbles which expanded to form a microcellular structure filling the mold. Following a 3-minute molding period, the molded panel was postcured in an oven for one hour at 125 °C.

Viscosity

The apparent viscosities of filler/polyol slurries were measured with a Brookfield HBT viscometer mounted on the Helipath Stand, which automatically lowers a rotating spindle (T-B type) into the slurry. This procedure is recommended for high viscosity pastes with yield. Results reported here were obtained at a 30 weight percent concentration, 2 rpm, and 30 °C.

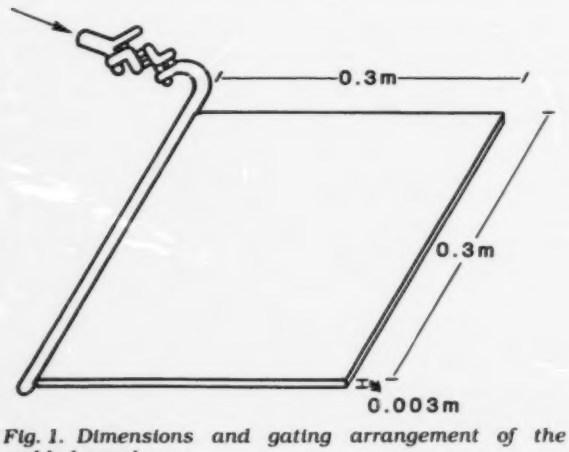

Fig. 1. Dimensions and gating arrangement of the molded panel.

Void Volume Fraction

The void volume fraction of the matrix, ϕ_v was calculated using the relation

$$\phi_v = 1 - \frac{\rho_c \rho_r (1 - w_r)}{\rho_m (\rho_r - \rho_c w_r)} \quad (1)$$

where: ρ_r and ρ_m are the densities of the filler and the matrix respectively, while w_r is the weight fraction of the filler. The apparent density of the composite, ρ_c, was determined with a direct reading, water displacement densimeter. The filler concentration was determined by burning away the resin and weighing the residue using the procedure described in ref. 16. For ρ_m and ρ_r, values of 1125 and 2860 kg/m^3 were used.

Mechanical Properties

Specimens (ASTM D638-type 4) were cut out from molded panels in flow and cross-flow directions using the same predetermined pattern for all samples. Tests were performed on an Instron, Model 1125 tester at a crosshead speed of 0.05 m/min. The flexural modulus was measured according to the ASTM D-790 method. Sample dimensions were 76 by 13 by 3 mm with supports fixed at a 51 mm distance. The crosshead speed was 5 mm/min. Impact strength was determined using notched samples following the ASTM D-256 method. Sample size was 76 by 13 by 3 mm. Reported results are average values from 10 specimens (5 in flow, 5 in cross-flow direction).

Coefficient of Linear Thermal Expansion (CLTE)

The CLTE was measured following the ASTM D-696 method using a Multicool system. The temperature range was −30 to 70°C. Sample size was 76 by 13 by 3 mm. All reported results are average values from 4 tests.

Microscopy

Fracture surfaces were examined in a scanning electron microscope (JEOL 35 CF). An optical microscope was used to observe flake geometry.

Particle Size Analysis

The particle size distribution was determined by a HIAC-PA 720 (Pacific Scientific Co., Montclair, CA.) using a method described previously (16).

The volume average flake diameter, d_v, was calculated as follows (16):

$$d_v = \frac{\sum n_i d_i^4}{\sum n_i d_i^3} \quad (2)$$

where n_i is the number of particles having a Feret's diameter of d_i. The shape factor, ψ, was computed from the following relation:

$$\psi = \frac{\sum n_i V_{H,i}}{V_r} \quad (3)$$

where $V_{H,i}$ is the spherical (encompassed) volume of the particle "i", and V_r is the total volume of the sample. The shape factor, ψ, is closely related to the aspect ratio, p. For monodispersed circular flakes, $\psi = 2p/3$.

RESULTS AND DISCUSSION

Mica/Polyol Viscosity

The relatively disappointing experience with currently available mica grades appears to be linked to the high viscosities of mica/polyol suspensions. It was felt, therefore, that methods of reducing the viscosity should be investigated first. At a given concentration, flow of suspensions is primarily influenced by three factors: state of dispersion, shape of suspended particles, and size distribution (17, 18). In general, poor dispersion increases the viscosity. The presence of aggregates having interstitial spaces filled with immobilized fluid makes the system behave as if the filler concentration was higher than what was actually added. Dispersion can be promoted by treatments with coupling or sizing agents that reduce particle-particle cohesion. In some cases, in particlar involving suspensions of fine particles (~1 μm), very dramatic reductions in viscosity can be obtained (19).

For monodispersed particles, the shape determines the maximum packing volume fraction, ϕ_m (20). This parameter is related to the zero shear suspension viscosity by the well known Mooney equation (21):

$$\ln (\eta/\eta_1) = \frac{k_e \phi}{1 - \phi/\phi_m} \quad (4)$$

where k_e is the Einstein coefficient; ϕ is the volume fraction of the filler; η and η_1 are respectively the viscosity of suspension and suspending liquid. The shape of a particle can be described in terms of its aspect ratio p, which is the ratio of the longest and shortest dimensions (length over diameter for fibers, diameter over thickness for flakes). In a recently proposed empirical equation derived for crushed glass fiber, ϕ_m was related to p by (22):

$$\frac{1}{\phi_m} = 1.38 + 0.0376 p_w^{1.4} \quad (5)$$

where p_w is the weight average aspect ratio. Suspensions of anisometric particles in which the filler volume fraction $\phi > \phi_m$ can flow only if the particles become oriented.

Both approaches, i.e., improving the dispersion and reducing the aspect ratio, were investigated. Various grades of mica were surface treated with silanes and other compounds and reduction of viscosity was recorded. All viscosities were measured at 30 weight percent mica concentration in polyol. This concentration is required to give 20 weight percent of mica in the final product. The first four lines of *Table 1* illustrate typical results produced by this approach. Silane treated micas, 60SN and 200SN, indeed have lower viscosities than their untreated counterparts, but the reduction in η is small. Other surface treatments produced similar results. This indicates the untreated mica is relatively easy to disperse in the polyol, and gains in dispersion provided by surface treatments are small.

Results obtained with three untreated mica grades (60HK, 200HK, and 325HK) indicate the magnitude of the effect of the shape factor, ψ, on the viscosity, and they confirm that it is the single most important factor affecting the viscosity of mica suspensions in polyol. Following these preliminary experiments, the flake delamination stage in the mica processing plant was modified to yield flakes with lower ψ. One experimental grade with a suspension viscosity similar to that of glass flakes was selected for further work. This grade is identified as 50R. It is worth noting that only suspensions of 50R mica and of glass flakes could be easily processed on the RRIM machine at concentrations of 30 weight percent in polyol. Optical micrographs of the 50R mica and of glass flakes are shown in the *Fig. 2*. Differences in flake geometry and size distribution reflect different manufacturing methods for these two materials.

Properties of Unreinforced Resin

Morphology

Figure 3 illustrates the foam structure for densities corresponding to void volume fractions, $\phi_v = 0.05$ (*Fig. 3A*), 0.10 (*Fig. 3B*), and 0.15 (*Fig. 3C*). *Figure 3D* ($\phi_v = 0.15$) illustrates the differences between the structure in an area close to the skin and in the core (*Fig. 3C*). The voids are present throughout the sample thickness. Despite the fact that the voids are very close to the surface, the skin is smooth and continuous. The very large density gradients characteristic of thermoplastic structural foams (23) are absent here.

Table 1. Apparent Viscosity of 30 Weight Percent Suspensions in Polyol (Volume Fraction $\phi = 0.153$).

Type	Surface Treatment	d_i (μm)	ψ	η (Pa.s)	ϕ_m*
60HK	None	505	66	100	0.040
60SN	Silane			96	
200HK	None	138	54	93	0.053
200SN	Silane			87	
325HK	None	54	37	33	0.098
50R	None	486	29	19	0.114
Glass Flake	—	—	—	21	—

* Calculated using *Eq 5* and assuming that $p_w = 3\psi/2$.

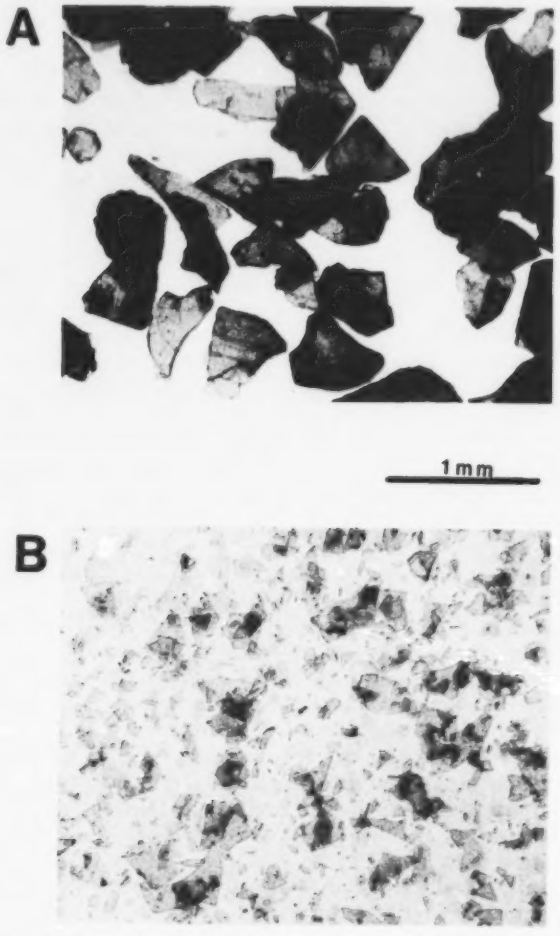

Fig. 2. Optical micrographs of: A—mica 50R and B—glass flakes.

The size and number of voids in samples of different densities indicate that the formation of microcellular structure is nucleation controlled. With increasing void fraction (*Figs. 3A, B,* and *C*), the number of voids, rather than their size, increases. One can visualize a mechanism whereby void nuclei are formed as a result of the thermodynamic instability that occurs when the reacting system, which is saturated with dissolved gas, is suddenly exposed to a lower pressure following injection into the mold. The initial void size growth rate must be relatively fast compared to the rate of nucleation and is slowed down due to the local depletion of dissolved gas in the void vicinity. When the mold is completely filled, both void nucleation and growth are arrested because of the pressure rise.

Mechanical Properties

Interpretation of mechanical behavior of foamed polymers in terms of foam density using theoretical models has had limited success. For example, Progelhof and Throne (24) compared experimental values of the zero strain Young's modulus of uniform density thermoplastic foams with several theoretical and semi-empirical models. The best correlation was obtained with the simple, entirely empirical relation:

$$E_f = E_o[1 - \phi_v]^n \qquad (6)$$

where $n = 2$. E_f and E_o are Young's moduli of the foam and solid polymer respectively; $(1 - \phi_v)$, is the reduced density of the foam, ϕ_v being the void volume fraction. This relationship (*Eq 6*), which was verified for a variety of polymers (25, 26), is now commonly used as a basis in stiffness calculations of structural foams (23). For other properties, expressions similar to *Eq 6* have been proposed. For impact strength, for example, values of exponent, n, close to 3 were found (23, 27).

The tensile stress-strain curves of unfilled resin are shown in *Fig. 4* for the solid resin ($\phi_v = 0$) and the foam ($\phi_v = 0.15$), elongation, ϵ, being expressed as $\epsilon = 100\ (l - l_o)/l_o$, where l and l_o are sample lengths at $\epsilon = \epsilon$ and $\epsilon = 0$ respectively. Both curves are similarly shaped. The initial elastic region is followed by large scale homogeneous yielding starting at $\epsilon \sim 5$ percent. The presence of bubbles does not have a significant effect on the elongation at break. *Figure 5* illustrates the effect of the void volume fraction, ϕ_v, on the ultimate strength, σ_u, yield strength, σ_y, and on elongation at break. The apparently high scatter in some of these results is due to a relatively small range of densities studied. Empirical equations fitted to the experimental points are also given. The value of the exponent n is close to $n = 2$.

The notched impact strength, σ_i, and flexural modulus, E_f, of unreinforced foam as functions of void volume fraction follow the same pattern (*Fig. 6*). The electron micrograph of a fracture surface produced during the impact test is shown in *Fig. 7*. Many microcracks usually connecting two or more voids are seen. In addition, the void distribution in the fracture surface does not appear to be entirely random. In many places short rows consisting of several voids are visible. It remains to be seen whether this phenomenon is a result of a crack following the path of least resistance, or whether the voids in the foam are partially ordered following some sort of row nucleation during the foam growth.

Figures 5 and *6* confirm the importance of the effect of the void volume fraction on properties of microcellular polyurethanes. It follows that when reinforced reaction injection molded systems are studied, the void fraction should be carefully considered. In several recently published papers (15, 28) on the merits of different reinforcements for RIM, the reported densities indicate that the void volume fractions varied widely with the type or concentration of reinforcement. Such results are obviously of limited value. In this work, the void fraction was kept constant at $\phi_v \sim 0.07$.

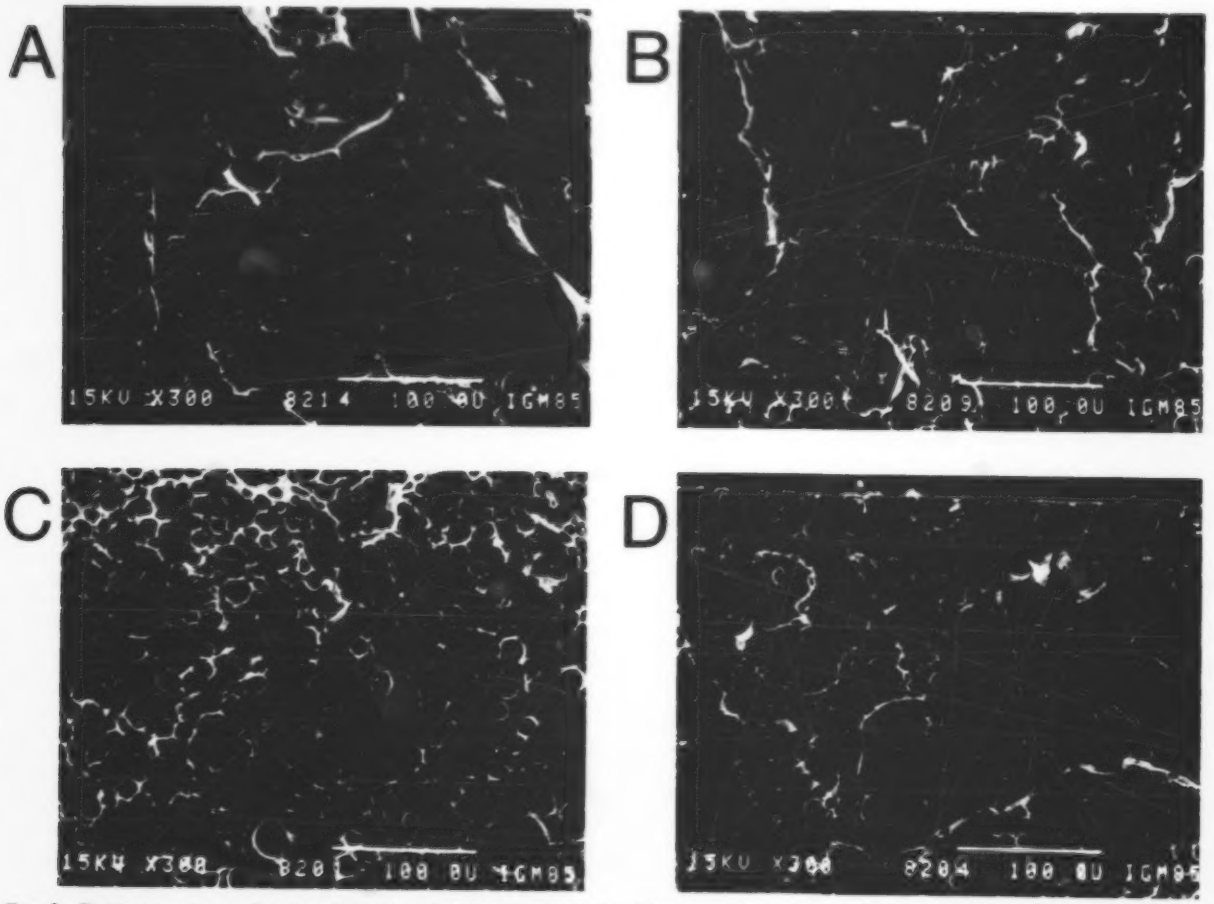

Fig. 3. Foam structure of unreinforced resin (fractured in liquid nitrogen): A) $\phi_v \approx 0.05$, core; B) $\phi_v = 0.10$, core; C) $\phi_v = 0.15$, core; D) $\phi_v = 0.15$, skin.

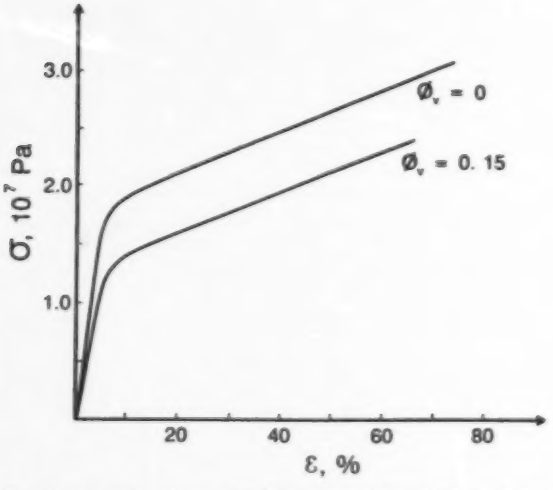

Fig. 4. Tensile stress-strain curves of unreinforced resin for void volume fractions, $\phi_v = 0$ and 0.15.

Mica Reinforced Resin

Morphology

A typical flake orientation in the cured plate containing 20 weight percent of mica is shown in *Fig. 8*. Throughout the thickness of the plate, the flakes are oriented in directions that are close to parallel to the plate surface. In injection molded, flake filled thermoplastics, in particular those of high melt viscosity, the flakes tend to orient parallel to the flow direction close to the surface and perpendicular in the core (29). Such effects are not observed here. In fact, the flake orientation is reminiscent of mica filled nylon 66—a polymer with low melt viscosity (30).

Estimating the value of the Reynolds number during the mold filling stage, one obtains a value of $Re < 1$ (assuming the density, $\rho = 1000$ kg/m^3, fluid velocity during the mold filling $v = 0.25$ m/s, mold thickness $l = 0.003$ m and the fluid viscosity $\eta > 1$Pa.s). It follows that the mold filling occurs in the laminar regime. Consequently, ideas and models developed initially for injection molding of thermoplastics (31) can be used, with appropriate modifications, to interpret the mold filling stage in the RRIM process. A striking confirmation of this is offered in *Fig. 9* where the mica concentration in the molding, as a function of the distance from the gate, is recorded. Despite a relatively short distance (0.25 m), a very significant increase in the mica concentration is observed. It should be noted

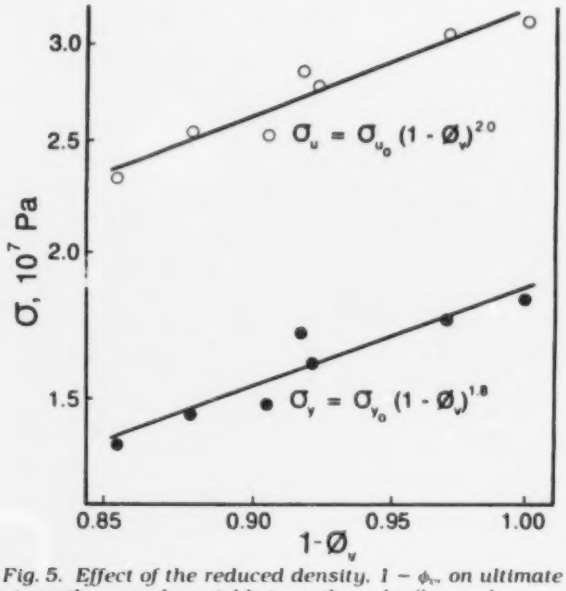

Fig. 5. Effect of the reduced density, $1 - \phi_v$, on ultimate strength, σ_u, and on yield strength, σ_y; log/log scale.

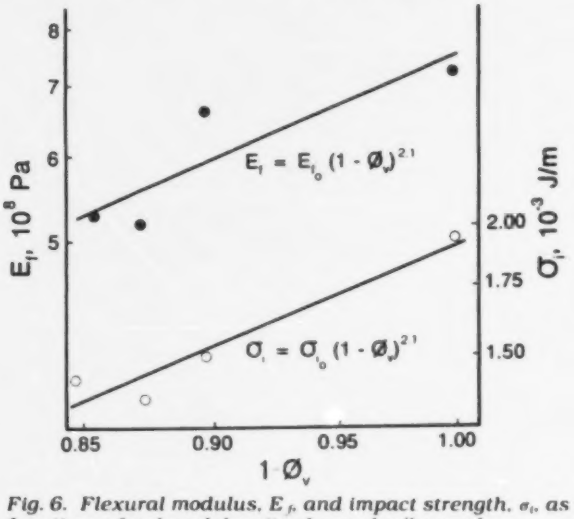

Fig. 6. Flexural modulus, E_f, and impact strength, σ_i, as functions of reduced density, $1 - \phi_v$; log/log scale.

that across the plate, perpendicular to the flow, the mica concentration was constant for a given distance from the gate. The concentration gradient is a consequence of a well-known phenomenon of particle migration in laminar shear flow (32 to 34). The tendency of particles to migrate towards the center, i.e., to a region of higher fluid velocity, is transformed into a concentration gradient along the flow direction. *Figure 10* shows the data of *Fig. 9* expressed in terms of reduced concentration, $c/\bar{c}$, where c is the local mica concentration and $\bar{c}$ is the overall average concentration in the plate. For low concentration $\bar{c}$ = 4 weight percent, the concentration increases linearly with the distance from the gate. For higher mica concentrations ($\bar{c}$ = 12 percent and 20 percent), the rate of change of $c/\bar{c}$ increases with the distance from the gate.

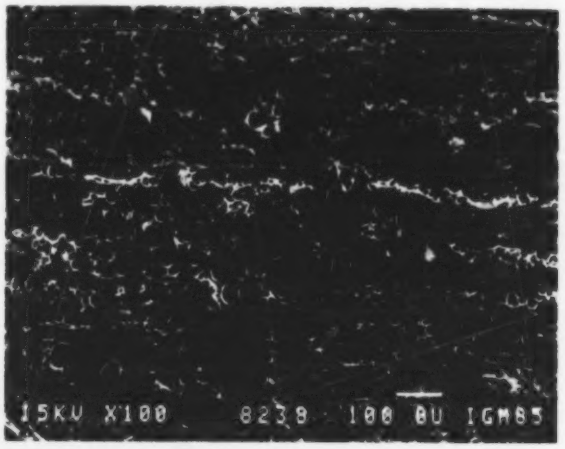

Fig. 7. Scanning electron micrograph of the impact fracture surface of unreinforced resin.

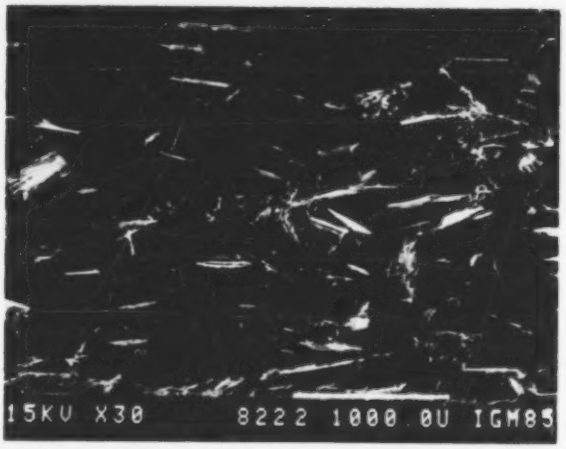

Fig. 8. Scanning electron micrograph of 20 weight percent mica reinforced polyurethane: typical flake orientation, ϕ_v = 0.07.

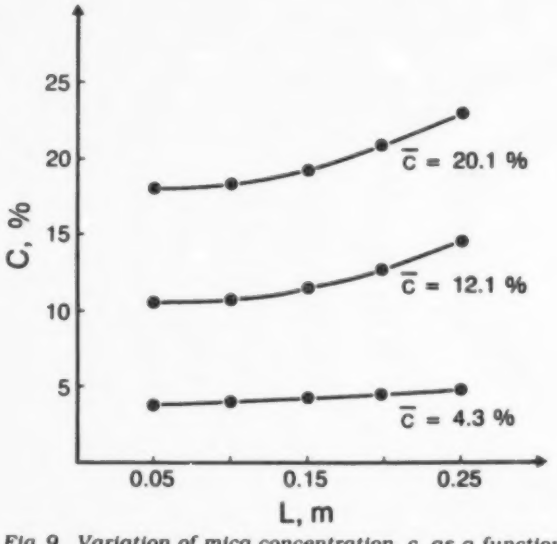

Fig. 9. Variation of mica concentration, c, as a function of the distance from the gate, L, for 3 different average mica concentrations.

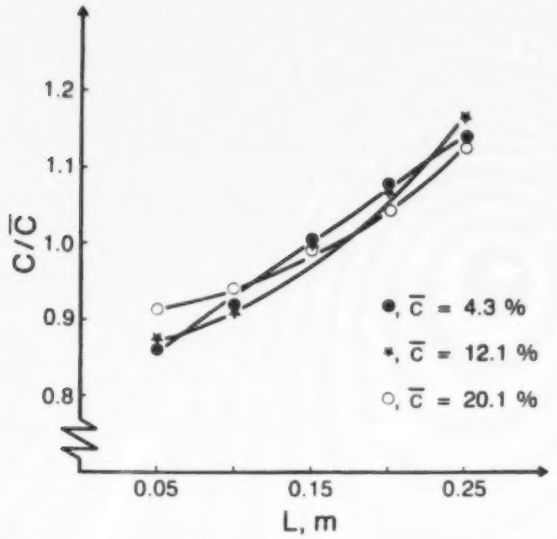

Fig. 10. Variation of the reduced concentration, c/c̄, as a function of the distance from the gate, L, for 3 different average mica concentrations.

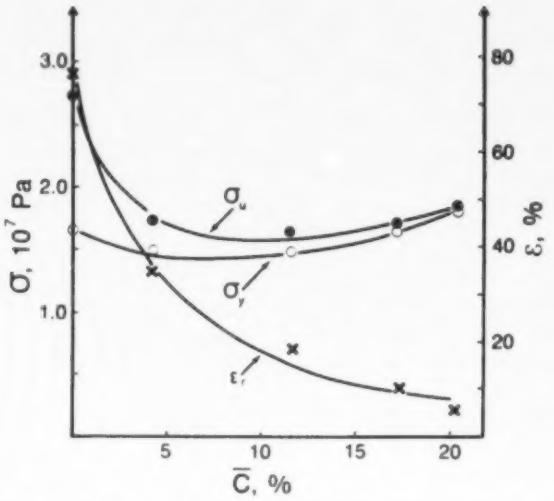

Fig. 11. Effect of the average mica concentration, c̄, on ultimate strength, σ_u, yield strength, σ_y, and elongation at break, ϵ_f.

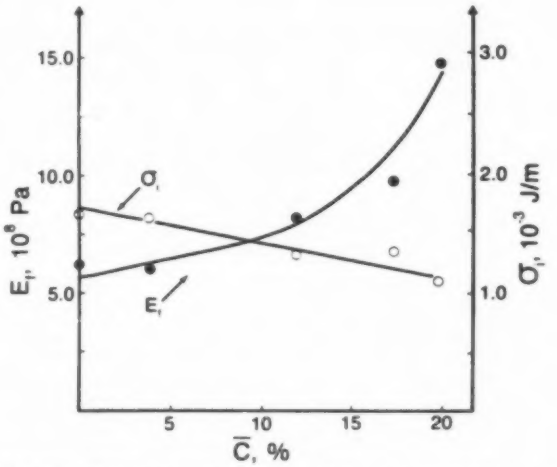

Fig. 12. Flexural modulus, E_f, and impact strength, σ_i, as a function of average mica concentration, c̄.

Surprisingly, little attention was paid to this phenomenon in polymer processing (32 to 34). It is clear that in processes such as reaction injection molding of large parts, where the distances from the gate are substantially longer than 0.25 m, more substantial concentration gradients may occur. This in turn would lead to property variations throughout the molding. In addition, a more systematic study of longitudinal gradients generated in intermittent flow should give much new information about the flow of concentrated suspensions.

Mechanical Properties

The introduction of mica flakes into the elastomeric matrix severely limits the material's ability to yield. This is illustrated in *Fig. 11* showing the effect of mica content on tensile behavior. At 20 weight percent of mica, elongation at break is reduced to about 5 percent compared to 75 percent for an unfilled elastomer. For this reason, the ultimate strength is seriously affected by even small amounts of mica. On the other hand, the yield strength declines up to a mica concentration of about 5 percent, remains constant between 5 and 10 percent, and increases beyond 10 percent. However, the variations of σ_y with mica content are relatively small.

The effect of mica on stiffness and impact strength is shown in *Fig. 12*. At 20 percent of mica, about 100 percent improvement of the flexural modulus is obtained at the expense of a 30 percent reduction in impact strength. This is similar to what was observed for other reinforced materials (1, 2, 15). Mica flakes seen in fracture surfaces are clean without any visible evidence of strong filler matrix adhesion (*Fig. 13*). Both flake pullout and flake fracture were

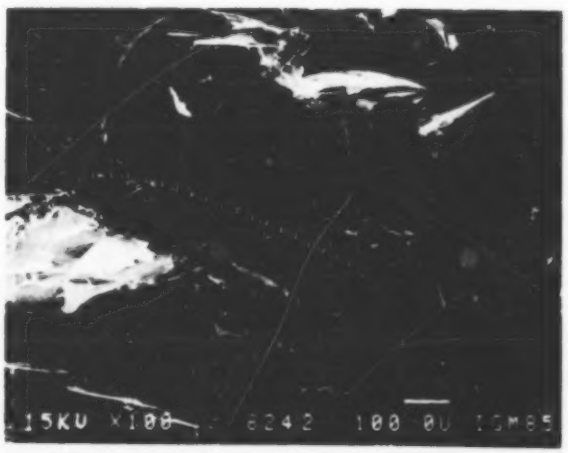

Fig. 13. Scanning electron micrograph of tensile fracture surface polyurethane at c̄ = 20 weight percent of mica 50R.

observed. The latter phenomenon occurs primarily via flake cleavage, which is due to the low interlayer cohesion in flakes (35).

Mica Versus Glass Flakes and Fibers

Other reinforcements, namely glass flakes and hammer milled glass fibers, were also processed using the same conditions as for mica 50R. Only those results obtained at 20 weight percent of reinforcement are shown here (*Table 2*). In addition, composites containing 10 percent of 50R and 10 percent of 200HK were also produced. The viscosity of this sample (15 percent of 50R plus 15 percent of 200HK in the polyol) was about the highest that could be handled by our machine. Properties obtained with mica 50R strongly resemble those of a glass flake reinforced system. The highest tensile and impact strengths were shown by glass fiber. However, the anisotropy in both stiffness, E_f, and CLTE were also higher. The fact that the 50R and 200HK blend produced higher E_f than the 50R sample is not surprising because of the higher average aspect ratio. However, the reduced impact strength is disappointing and is likely due to structural heterogeneities caused by inefficient mixing (consider the very high difference of viscosities of components—polyol/mica and diisocyanate).

Tensile fracture surfaces of mica and glass flake reinforced resin, as well as those with glass fiber are shown in the *Fig. 14*. Both mica and glass flake samples (*Fig. 14A* and *14B*) reveal that the tensile deformation was accom-

Table 2. Comparison of the Mechanical and Physical Properties of Different Reinforced RIM Polyurethanes, 20 Weight Percent.

		E_f, (10) Pa		σ_m, (10) Pa		σ_i, (10) J/m		CLTE (10) °C^{-1}	
	ϕ_v	∥	⊥	∥	⊥	∥	⊥	∥	⊥
Mica 50R	0.060	15.31	13.86	1.83	1.80	1.05	0.94	8.6	9.5
Mica 50R/Mica 200HK (50%/50%)	0.050	18.62	16.90	2.19	1.94	0.75	0.64	—	—
Glass Flake	0.053	13.33	12.34	2.42	2.18	0.96	0.94	7.0	8.6
Glass Fiber	0.038	18.62	11.38	3.05	2.54	1.33	1.18	5.2	12.5

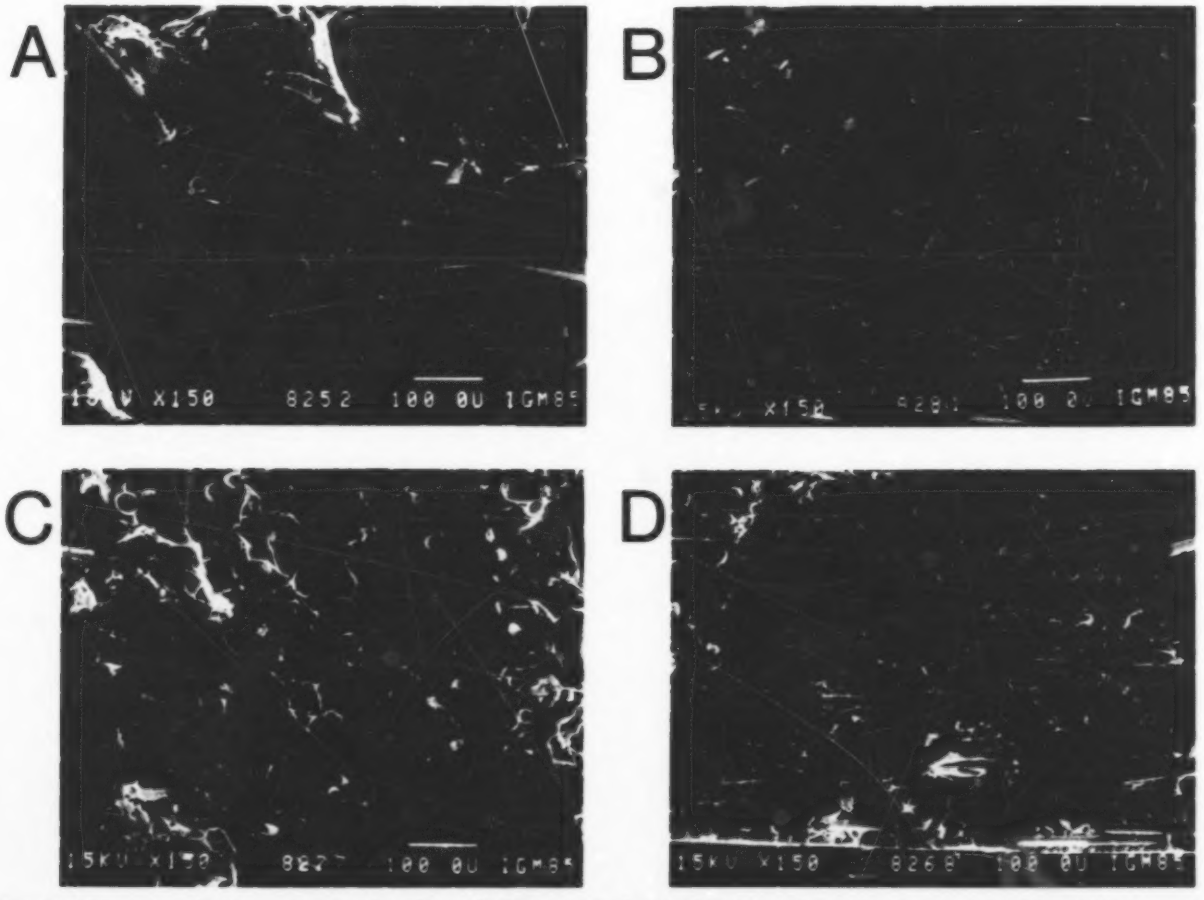

Fig. 14. Scanning electron micrographs of tensile fracture surfaces of reinforced polyurethane at $\dot{c}$ = 20 weight percent. A) Mica 50R. B) Glass flakes. C) Glass fibers—flow direction. D) Glass fibers—cross-flow direction.

panied by a debonding effect at the filler/polymer matrix interface. Given the particle size of both glass and mica flakes and the absence of a strong matrix-filler bond, one could expect to see a significant number of pulled out flakes at the fracture surface. The number of such flakes is surprisingly small. Careful examination of both fracture surfaces from the same fractured specimen side by side shows that only smaller flakes, or those with one end close to the fracture plane, would be pulled out. Large flakes with both ends embedded far from the fracture plane break. Considering the irregular shape of the flakes as well as their orientation (close to but not perfectly parallel to the applied stress), one can understand the tendency of some flakes to break. Glass fibers (*Figs. 14C* and *14D*) are preferentially oriented in the flow direction. In addition, these silane treated fibers have good adhesion to the matrix. In *Fig. 14C* most of the fibers broke very close to the fracture plane.

CONCLUSIONS

The viscosity of mica/polyol suspensions is very high when currently available mica grades are used. This renders processing on the RRIM polyurethane machine difficult and may affect impingement mixing efficiency. Surface treatment of mica to improve dispersion reduced the viscosity very slightly. Significantly lower viscosity can be obtained by a reduction of the average flake aspect ratio. Properties of unreinforced microcellular polyurethane are strongly affected by the void volume fraction. Mechanical properties are approximately proportional to the square of the density. Introduction of mica into the polymer matrix strongly increases the stiffness with some loss of impact strength. Reinforcement obtained with mica is essentially identical to that observed with glass flakes. On the other hand, glass fibers generate the best mechanical properties. However, the anisotropy due to fiber orientation is also highest.

ACKNOWLEDGMENTS

The contributions of Mr. G. Chouinard, Mr. M. Thibodeau, and Mr. M. Carmel to the experimental part of this work are gratefully acknowledged.

REFERENCES

1. F. M. Sweeney, "Introduction to Reaction Injection Molding," Technomic Pub. Co., Westport (1979).
2. R. Hedrick, J. D. Gabbert, and M. H. Wol, *ACS Symp. Ser.*, **270**, 136 (1985).
3. N. R. Newburg, *U. S. Pat.*, 4481344 (1984).
4. A. S. Wood, *Mod. Plast.*, **61** (10), 48 (1984).
5. A. Anderson, *Mod. Plast.*, **55** (4), 66 (1978).
6. P. M. Tarin, B. Prokai, and E. G. Schwarz, SPE ANTEC *Tech. Papers*, **25**, 668 (1979).
7. B. C. Chisnall, and D. Thorpe, 35th Annual Technical Conference, Reinf. Plast. Compos. Inst., Soc. Plast. Ind., Preprints, Section 22 A (1980).
8. M. M. Girgis, B. Das, and J. A. Harvey, 36th Annual Technical Conference, Reinf. Plast. Compos. Inst., Soc. Plast. Ind., Preprints, Section 6-C, (1981).
9. W. A. Gill, and R. M. Gerkin, S.P.E./S.P.I. Conf. Proceedings, Philadelphia, (June 21–23, 1984)
10. N. S. Strand, *Plast. Eng.*, **36**, 35 (1980).
11. C. M. Hall, *Plast. Rubb. Proc. Appl.*, **3**, 373 (1983).
12. S. H. Metzger Jr., and K. Seel, *J. Cell. Plast.*, **17**, 268 (1981).
13. R. L. McBrayer, *Elastomerics*, **112**, 33 (1980).
14. M. Fenton, and G. Hawley, *Polym. Compos.*, **3**, 218 (1982).
15. C. J. McGregor, and R. A. Parker, *Plast. Compound.*, **2** (5), 53 (1979).
16. B. Fisa, B. Sanschagrin, and B. Favis, *Polym. Compos.*, **5**, 264 (1985).
17. L. A. Utracki, and B. Fisa, *Polym. Compos.*, **3**, 193 (1982).
18. L. A. Utracki, *Rubb. Chem. Technol.*, **57**, 507 (1984).
19. E. P. Plueddeman, and G. L. Stark, "Additives for Plastics," R. B. Seymour ed., Vol. 2, p. 48, Academic Press, New York (1977).
20. J. V. Milevski, *Plast. Compound.*, **1**, 26 (1978).
21. L. E. Nielsen, "Polymer Rheology," Marcel Dekker, New York (1977).
22. M. M. Cross, A. Kaye, J. L. Stanford, and R. F. T. P. Stepto, *ACS Polym. Mat. Sci. Eng. Div., Prepr.*, **49**, 531 (1983).
23. A. A. Ahmadi, and P. R. Hornsby, *Plast. Rubb. Proc. Appl.*, **5**, 35 (985).
24. R. C. Progelhof, and J. L. Throne, *Polym. Eng. Sci.*, **19**, 493 (1979).
25. D. R. Moore, and M. J. Iremorger, *J. Cell. Plast.*, **10**, 230 (1974).
26. P. F. Pramuk, *Polym. Eng. Sci.*, **16**, 559 (1976).
27. R. C. Progelhof, and J. L. Throne, SPE ANTEC Tech. Papers, **27**, 863 (1981).
28. A. E. Johnson, and J. R. Jackson, *Plast. Rubb. Proc. Appl.*, **1**, 245 (1981).
29. B. Sanschagrin, B. Favis, and B. Fisa, SPE ANTEC Tech. Papers, **30**, 683 (1984).
30. F. Bataille, T. Vu-Khanh, and B. Fisa, SPE ANTEC Tech. Papers, **31**, 1174 (1985).
31. Z. Tadmor, *J. Appl. Polym. Sci.*, **18**, 1753 (1973).
32. J. Kubat, and A. Szalanczi, *Polym. Eng. Sci.*, **14**, 873 (1974).
33. L. Böröcz, and J. Kubat, *Plast. Rubb., Process.*, **4**, 82 (1979).
34. R. P. Hegler, and G. Menning, *Polym. Eng. Sci.*, **25**, 395 (1985).
35. K. Okuno, *Kobunshi Ronbunshu*, **38**, 53 (1981).

SI METRIC UNITS

The following list shows the names, symbols, and equivalence of the more common quantities allowed in the SI metric system. The prefixes and symbols for the more common multiple units are also shown. Neither list is complete. Full details are given by F. S. Conant, Polym. Eng. Sci., **17,** 222 (1977). A table of the more frequently needed conversion factors required to use the SI system is also shown. This journal prefers that SI metric units be employed in manuscripts submitted for publication.

Units and Symbols

Quantity	Name	Symbol	Equivalent to:
Length	metre	m	—
Time	second	s	—
	minute	min	—
	hour	h	—
Mass	kilogram	kg	—
Electric current	ampere	A	—
Plane angle	radian	rad	—
Capacity	litre	L	$10^{-3}m^3$
Frequency	hertz	Hz	s^{-1}
Force	newton	N	$m \cdot kg \cdot s^{-2}$
Pressure, Stress	pascal	Pa	$N \cdot m^{-2}$
Energy, Work, Heat	joule	J	$N \cdot m$
Power	watt	W	$J \cdot s^{-1}$
Viscosity, dynamic	pascal second	Pa·s	$N \cdot s \cdot m^{-2}$

(The following units should ***not*** be used: micron, angstrom, dyne, erg, calorie, poise, or stoke.)

Multiple Units

Prefix	Symbol	Equivalent to:
giga	G	10^9
mega	M	10^6
kilo	k	10^3
deci	d	10^{-1}
centi	c	10^{-2}
milli	m	10^{-3}
micro	μ	10^{-6}
nano	n	10^{-9}

Conversion Factors

Force: $1N = 10^5$ dynes $= 1.02 \times 10^{-1}$ kgf $= 2.248 \times 10^{-1}$ lbf.

Pressure, Stress: 1 Pa = 10 dyne $cm^{-2} = 7.5 \times 10^{-3}$ mm Hg $= 10^{-5}$ bar $= 1.02 \times 10^{-5}$ kg $cm^{-2} = 1.45 \times 10^{-4}$ psi.

Energy: $1 J = 2.387 \times 10^{-1}$ cal.

Viscosity: 1 Pa·s = 10 poise.

INFORMATION FOR AUTHORS

Submission of original and review articles is encouraged. There is no limit on length. Three copies of the manuscript should be submitted, which should be typed, one side only, double space, with at least a 1-inch margin. Submission will be taken to imply that the paper has not been previously published, that it is not being considered elsewhere for publication, and that if accepted it will not be published elsewhere in the same form, in any language, without the consent of the editor or publisher. Authors must agree to transfer copyright to the publisher when an article is accepted for publication. Unless notified to the contrary by the authors, the publisher assumes that the act of submitting the article signifies the author's agreement to such copyright transfer to the publisher. The journal carries a voluntary page charge. Each manuscript should include:

A separate title page, headed by a concise, meaningful title (avoid abbreviations) for the paper. This page should provide:

- The name and affiliations of each contributing author at the time the paper was prepared.
- Indicate by asterisk any changes of address for each author since article preparation.
- Acknowledgment of any prior oral presentation and original source of the material.

A separate abstract page, consisting of a single paragraph of 100–200 words to include the title and the names and addresses of the authors. Define any abbreviations for substances or methods (such as ABS, SAXS, etc.).

A list of references, on a separate page at the end of the text, numbered in order of text citation. The references are to be abbreviated in the form used in Chemical Abstracts using the names of all authors preceded by initials; see Bibliographic Guide for Editors and Authors, American Chemical Society, Washington, D.C.

- Within the text, the reference citations are typed in parentheses in line with the main copy (no superscripts or subscripts), thus:

  According to Young, et al. (1) . . .

- In the list of references the general style is as follows:

  For periodicals:

  1. S. S. Young, J. L. White, E. S. Clark and Y. Oyanogi, Polym. Eng. Sci., 20, 798 (1980).

  The journal name and volume are to be underlined and the year is placed in parentheses. The issue number is given only when needed for identification. The article name is eliminated unless the reference is unclear without it.

  For books: The title to be spelled out in full.
  5. H.-G. Elias, "Macromolecules," Ch. 1, Vol. 2, Plenum Press, New York (1977). (Include the state when the city is not identifiable.)

A list of nomenclature, identifying symbols and abbreviations, commonly desirable at the end of the text. Footnotes are to be avoided.

Equations, numbered and typed in the appropriate place in the text. Where symbols cannot be typed, write them neatly in ink.

Tables, each typed on a separate page, with a heading, and numbered with arabic numerals that correspond to the order in which they are cited in the text. The tables should be inserted in the manuscript after the references and before the figures.

Figures, assembled at the end of the manuscript and preceded by a typed list of captions that explain them. Please also supply a set of original figures or sharp glossy photos thereof, on 8½ × 11 paper or attached to sheets of this size, one sheet for each figure. Each should be identified on the front edge or on the back (photographs) with the name of the first author and the figure number (e.g., Smith, Fig. 1). Originals are to be prepared with high contrast India ink and to bear uniformly stencilled notations. Line drawings and photos should be of a quality suitable for good photographic reproduction and retained legibility upon size reduction to one quarter. Manuscript transmittal letter should indicate if the figures need be returned.

Send manuscripts to:
Roger S. Porter, Editor
POLYMER COMPOSITES
% Polymer Science & Engineering
University of Massachusetts
Amherst, Massachusetts 01003

For information concerning publication dates, page charges and reprint orders contact:
Editorial Department
Society of Plastics Engineers
14 Fairfield Drive
Brookfield Center, Connecticut 06805

Continued From Front Cover

355 L. PICHÉ and A. HAMEL/Ultrasonic Evaluation of Filled Polymers: I. Techniques and Models for the Elastic Moduli of a Resin Filled With Iron Spherical Inclusions

363 P. OUELLETTE, S.V. HOA, and T.S. SANKAR/Buckling of Composite Cylinders Under External Pressure

375 T. VU-KHANH and B. FISA/Impact Fracture of Glass-Flake Reinforced Polypropylene

383 L.A. GOETTLER and W.J. NEFF/Mechanical Performance of Various Nylon 6 Composites Formed by *In-Situ* Polymerization of Caprolactam

395 B. RÉMILLARD, T. VU-KHANH, B. FISA, and S. NAIK/Reaction Injection Molding of Mica Reinforced Polyurethane

SOCIETY OF PLASTICS ENGINEERS, 14 Fairfield Drive, Brookfield Center, CT 06805